2007

Rigorous Analysis Of Wave Guiding And Diffractive Integrated Optical Structures

Andrew Greenwell
University of Central Florida

RIGOROUS ANALYSIS OF WAVE GUIDING AND DIFFRACTIVE INTEGRATED OPTICAL STRUCTURES

by

ANDREW BERNARD GREENWELL
B.A. Transylvania University, 2001
M.S. University of Central Florida, 2003

A dissertation submitted in partial fulfillment of the requirements
for the degree of Doctor of Philosophy
in the College of Optics and Photonics
at the University of Central Florida
Orlando, Florida

Spring Term
2007

Major Professor: M.G. Moharam

ABSTRACT

The realization of wavelength scale and sub-wavelength scale fabrication of integrated optical devices has led to a concurrent need for computational design tools that can accurately model electromagnetic phenomena on these length scales. This dissertation describes the physical, analytical, numerical, and software developments utilized for practical implementation of two particular frequency domain design tools: the modal method for multilayer waveguides and one-dimensional lamellar gratings and the Rigorous Coupled Wave Analysis (RCWA) for 1D, 2D, and 3D periodic optical structures and integrated optical devices. These design tools, including some novel numerical and programming extensions developed during the course of this work, were then applied to investigate the design of a few unique integrated waveguide and grating structures and the associated physical phenomena exploited by those structures.

The properties and design of a multilayer, multimode waveguide-grating, guided mode resonance (GMR) filter are investigated. The multilayer, multimode GMR filters studied consist of alternating high and low refractive index layers of various thicknesses with a binary grating etched into the top layer. The separation of spectral wavelength resonances supported by a multimode GMR structure with fixed grating parameters is shown to be controllable from coarse to fine through the use of tightly controlled, but realizable, choices for multiple layer thicknesses in a two material waveguide; effectively performing the simultaneous engineering of the wavelength dispersion for multiple waveguide grating modes. This idea of simultaneous dispersion band tailoring is then used to design a multilayer, multimode GMR filter that possesses broadened angular acceptance for multiple wavelengths incident at a single angle of incidence.

The effect of a steady-state linear loss or gain on the wavelength response of a GMR filter is studied. A linear loss added to the primary guiding layer of a GMR filter is shown to produce enhanced resonant absorption of light by the GMR structure. Similarly, linear gain added to the guiding layer is shown to produce enhanced resonant reflection and transmission from a GMR structure with decreased spectral line width.

A combination of 2D and 3D modeling is utilized to investigate the properties of an embedded waveguide grating structure used in filtering/reflecting an incident guided mode. For the embedded waveguide grating, 2D modeling suggests the possibility of using low index periodic inclusions to create an embedded grating resonant filter, but the results of 3D RCWA modeling suggest that transverse low index periodic inclusions produce a resonant lossy cavity as opposed to a resonant reflecting mirror.

A novel concept for an all-dielectric unidirectional dual grating output coupler is proposed and rigorously analyzed. A multilayer, single-mode, high and graded-index, slab waveguide is placed atop a slightly lower index substrate. The properties of the individual gratings etched into the waveguide's cover/air and substrate/air interfaces are then chosen such that no propagating diffracted orders are present in the device superstrate and only a single order is present outside the structure in the substrate. The concept produces a robust output coupler that requires neither phase-matching of the two gratings nor any resonances in the structure, and is very tolerant to potential errors in fabrication. Up to 96% coupling efficiency from the substrate-side grating is obtained over a wide range of grating properties.

For my parents, whose unconditional and limitless love and support have allowed me to pursue my dreams wherever they might take me.

ACKNOWLEDGMENTS

I would like to thank my dissertation advisor, Dr. Jim Moharam, for providing me with a challenging computational science problem on which to study and to write, and for providing answers to my many, many questions over my five and a half years at CREOL. Even in the times when the answers were not always clear cut, being able to work through those questions has helped me grow significantly. Thank you.

I would also like to thank all of the faculty members that were a part of my committee over the course of my graduate career. While the membership may have changed considerably over time, everyone asked valuable questions that helped improve this work.

Thanks also go out to the members of my research group both past and present. Specifically, I would like to thank Don Jacob for welcoming me in to his office as a new student and for introducing me to MATLAB, as well as George Siganakis and Sakoolkan Boonruang for being pleasant and enjoyable officemates.

The formatting tips that were provided by the UCF thesis and dissertation editor, Matt Waller, as well as his sidekick in the Office of Instructional Resources, Rebecca Yost, were of immense help in finalizing this document. I am especially grateful for the help both of you provided.

Additional thanks go to some of my fellow graduate students here at CREOL. To Joel, Mike, Will, and Rich, the pick-up basketball games were always competitive and a lot of fun. To Alok, Pete, Ricky, Heidi, Claudiu, Grady, Tipper, and others, I really enjoyed getting to know all of you….keep in touch.

To my dearest Elizabeth, thank you for being my number one cheerleader. You really did bring the life back to my life.

Finally, I would like to thank my family for always supporting me in everything I have ever pursued. Without your unconditional love and encouragement I would never have been able to make it this far.

TABLE OF CONTENTS

LIST OF FIGURES

LIST OF TABLES

LIST OF ACRONYMS/ABBREVIATIONS

1D	One-dimensional
2D	Two-dimensional
3D	Three-dimensioal
∇	Multi-dimensional spatial partial derivative operator – "del"
$\frac{\partial}{\partial t}$	Partial derivative operator with respect to time
θ	Polar incident angle
ϕ	Azimuthal incident angle
γ	Transverse component of the propagation constant
γ'	Transverse component of the propagation constant divided by ε_x or μ_x
$\delta_{x,y,z}$	Absorption coefficient in x, y, or z direction
$s_{x,y,z}$	$1 - j\delta_{x,y,z}$
δ	Kronecker delta function/vector
ρ	Electric charge density
ε	Electric permittivity
ε_0	Electric permittivity of free space
μ	Magnetic permeability
μ_0	Magnetic permeability of free space
η_0	Impedance of free space
ξ	Non-orthogonal periodicity tilt angle
$\sigma_{x,y}$	Group theoretic class for reflection symmetry about x or y plane

C_{2v}	Group theoretic class for reflection symmetry about x and y plane
β	Longitudinal component of the propagation constant
ω	Angular frequency
κ	Gain or loss coefficient of the complex refractive index
λ	Free space wavelength
χ_e	Electric Susceptibility
χ_m	Magnetic Susceptibility
$\Delta\lambda_{FWHM}$	Full width half maximum wavelength line width
$\Delta\theta_{FWHM}$	Full width half maximum angular line width
$\Lambda_{x,y}$	Grating periodicity in x or y direction
$\Lambda_{sub,\sup}$	Grating periodicity for the substrate or superstrate grating
j	Square root of -1, $\sqrt{-1}$
k_0	Free space wavenumber, $\frac{2\pi}{\lambda}$
$k_{x,y}$	Tangential harmonic component of the periodic wavevector
c_p	Cover side phase constant for multilayer waveguide dispersion problem
s_p	Substrate side phase constant for multilayer waveguide dispersion problem
x', y', z'	Spatial coordinate multiplied by the free space wavenumber
$d\vec{s}$	Differential surface of a surface integral
$d\vec{l}$	Differential length of contour integral
dV	Differential volume of a volume integral

Δs	Cross-sectional area of a finite cylinder
Δh	Finite height of test loop across an interface between two media
Δl	Finite length of test loop across an interface between two media
ΔA	Area contained in loop of size Δl by Δh
h	Height of a material layer for a waveguide or grating
d	Thickness of a lamellar layer
b	Backward propagating field harmonic amplitude
f	Forward propagating field harmonic amplitude
ff	Grating fill factor
n_{eff}	Effective modal index
$n_{cladding}, n_{core}$	Refractive index in the cladding or core region
$n_{sub}, n_{\sup}$	Refractive index in the substrate or superstrate region
n'_{mode}	Real part of the modal index
n''_{mode}	Imaginary part of the modal index
$n_{\perp}, \varepsilon_{\perp}$	Refractive index and permittivity in direction normal to grating interface
$n_{\|\|}, \varepsilon_{\|\|}$	Refractive index and permittivitn in direction parallel to grating interface
$\varepsilon_{low}, \varepsilon_{high}$	Permittivity for low and high valued regions respectively
$\vec{r}$	Spatial position vector
$r^{b,f}, R^{b,f}$	Reflection submatrices of asymmetric scattering matrices
$t^{b,f}, T^{b,f}$	Transmission submatrices of asymmetric scattering matrices
r, R	Reflection submatrices of symmetric scattering matrices

t, T	Transmission submatrices of symmetric scattering matrices
S_L, S_R	Left and right hand side scattering matrices
$r_{E,\perp}$	Reflection coefficient of the electric field harmonics for rotated perpendicular component in a 2D periodic problem
$r_{H,\perp}$	Reflection coefficient of the magnetic field harmonics for rotated perpendicular component in a 2D periodic problem
$r_{E,\parallel}$	Reflection coefficient of the electric field harmonics for rotated parallel component in a 2D periodic problem
$r_{H,\parallel}$	Reflection coefficient of the magnetic field harmonics for rotated parallel component in a 2D periodic problem
$t_{E,\perp}$	Transmission coefficient of the electric field harmonics for rotated perpendicular component in a 2D periodic problem
$t_{H,\perp}$	Transmission coefficient of the magnetic field harmonics for rotated perpendicular component in a 2D periodic problem
$t_{E,\parallel}$	Transmission coefficient of the electric field harmonics for rotated parallel component in a 2D periodic problem
$t_{H,\parallel}$	Transmission coefficient of the magnetic field harmonics for rotated parallel component in a 2D periodic problem
$\vec{F}$	Generic field vector
S	Reference surface for a contour or volume integral
C	Reference line for a contour integral
$\vec{T}$	Unit tangent vector along a contour integral
$\hat{n}$	Unit normal vector across a surface S
$\hat{u}_z$	Unit vector in longitudinal direction
$Q(\vec{r},t)$	Energy dissipated in a medium per unit volume

$\mathrm{P}(\vec{r},t)$	Instantaneous complex Poynting vector
$\vec{E}$	Electric field vector
$\vec{H}$	Magnetic field vector
$\vec{D}$	Electric displacement vector
$\vec{B}$	Magnetic flux density vector
$\vec{M}$	Magnetization vector
$\vec{P}$	Electric polarization vector
$\vec{J}$	Electric current density vector
$S_{x,y,z}$	Electric field harmonic amplitude in a periodic grating layer in x, y, or z
$U_{x,y,z}$	Magnetic field harmonic amplitude in a periodic grating layer in x, y, or z
$S_{\parallel}$	Electric field harmonic amplitude rotated parallel to the plane of incidence
$S_{\perp}$	Electric field harmonic amplitude rotated perpendicular to the plane of incidence
$U_{\parallel}$	Magnetic field harmonic amplitude rotated parallel to the plane of incidence
$U_{\perp}$	Magnetic field harmonic amplitude rotated perpendicular to the plane of incidence
$S_{\tan}$	Tangential electric field harmonic amplitude in a periodic grating layer
$U_{\tan}$	Tangential magnetic field harmonic amplitude in a periodic grating layer
$K_{x,y,z}$	Grating vector component in the x, y, or z direction
Y_{I}, Y_{II}	Longitudinal direction component of the input or output homogeneous eigenvalues normalized by k_0

Z_I, Z_{II}	Longitudinal direction component of the input or output homogeneous eigenvalues normalized by k_0 and divided by the product of the permittivity and permeability
I	Identity matrix
R_m	Reflection coefficient of the m^{th} reflected order/mode
T_m	Transmission coefficient of the m^{th} reflected order/mode
$DE_{m,reflected}$	Diffraction efficiency of the m^{th} reflected order
$DE_{m,transmitted}$	Diffraction efficiency of the m^{th} transmitted order
q	Grating harmonic eigenvalues
W	Electric (Magnetic) field eigenvector for TE or 2D (TM) problems
V	Magnetic (Electric) field eigenvector for TE or 2D (TM) problems
AR	Anti-Reflective
TE	Transverse Electric
TM	Transverse Magnetic
RCWA	Rigorous Coupled Wave Analysis
FMM	Fourier modal method
PML	Perfectly matched layer
FDTD	Finite difference time-domain method
FEM	Finite element method
CAMFR	Cavity modeling framework [174]
DtN	Dirichlet to Neumann boundary condition
T-Matrix	Transmittance matrix
S-Matrix	Scattering matrix

R-Matrix	Impedance matrix
H-Matrix	Hybrid matrix
GMR	Guided mode resonance

CHAPTER 1 INTRODUCTION

As micro-scale and then nano-scale fabrication techniques have been introduced and refined, the promise of optical devices having feature sizes on the same scale as or smaller than the wavelength of light has gone from pure theoretical conceptualization to physical reality. This miniaturization of device size has made possible the potential duplication of the successes that have been achieved in integrated electronic circuits, where numerous functionalities are provided by devices on a single chip, with integrated photonic devices possessing similar capabilities.

As society pushes towards wavelength scale and subwavelength scale optical components, there has been a concurrent need for design tools that accurately represent the physical phenomena occurring at these diminishing length scales. While all of classical electromagnetism can be described by Maxwell's famous set of equations [1], it is the sources and materials (with their respective geometries) which are to be modeled using these equations that determine the complexity needed and difficulty level in building the mathematical tools necessary for useful designs. Whereas classical lens design may only require a geometrical ray tracing for an acceptable design solution or a weakly guiding waveguide or a phase grating may only require a scalar approximation of the wave equation [2-4], nano-scale optical devices often require a full rigorous treatment of Maxwell's equations for an acceptably accurate solution to the wave propagation design problem.

Traditionally, two of the main building blocks for passive integrated optical devices have been piecewise continuous index-guided waveguides, consisting of two or more materials where light is guided by a core with a relatively high-magnitude permittivity surrounded by a material having lower magnitude permittivity, and diffraction gratings, consisting of structures having

periodic variations of high and low permittivity materials. Devices consisting of a combination of these building blocks provide for a wide variety of functionalities ranging from simple light pipes and channels, to wavelength filters, to dispersion compensators and enhancers, to interferometers, to beam shapers/splitters/combiners, to sensors of all kinds, and many other devices [4-8].

While the development of both waveguide theory and grating theory share common roots, namely in Maxwell's equations of electromagnetism, differences in device geometries and differences in required boundary conditions between the two types of structures have led to a variety of techniques for determining modal/homogeneous solutions and wave propagation/particular solutions for the corresponding systems of equations. Despite the variety, it was not until this decade, apart from generic methods that do not fully exploit device geometry, that techniques were developed which specifically linked waveguide and grating modeling in a single method that could reliably and efficiently handle either type of device [9]. While it has been pointed out that there is no "silver bullet", no "one size fits all" technique [10], for efficiently modeling all types of integrated optical devices, the enhancement of the Rigorous Coupled Wave Analysis (RCWA) technique [7, 11-15] with the inclusion of Perfectly Matched Layer (PML) boundary conditions [16] has extended what is probably the most extensively used tool for modeling infinitely periodic diffraction gratings into a tool for efficiently modeling many types of problems involving finite waveguides.

In the course of this work, some recently extended numerical techniques were implemented for modeling finite waveguides using a bi-directional eigenmode expansion method, which in this case involved using RCWA/PML as the eigenmode solver, and either an enhanced transmittance matrix [13] or a scattering matrix method [17, 18] for mode matching

and wave propagation. Further enhancements and extensions to the implementation of these methods [19] developed during the course of this work were added for modeling some new variations on integrated waveguides and gratings that were the physical focus of our study. This dissertation provides a thorough description of the mathematical and numerical development needed to model integrated waveguides and gratings in one, two, or three dimensions using RCWA as well as an explanation of how to go about translating the derived equations for numerical solutions into efficient and flexible computer codes that can be used for a variety of different material property distributions and input sources. These tools are then applied to some unique nano-scale integrated waveguide/grating devices whose overriding themes are enhanced functionality over conventional devices due to integration of components on a single platform, and material geometries that provide a realistic potential for fabrication using current fabrication techniques. For each of the devices studied, the desired functionality of the device is described in terms of the relevant physics involved in device operation and relevant geometric and material tolerances required for desired device performance.

As much of the design work undertaken in this study revolves around understanding and manipulating the properties of a waveguide or grating's eigenmodes, Chapter 2 provides the development of the transcendental equations which may be used to solve for the eigenmodes of a simple three layer slab waveguide, an anisotropic multilayer slab waveguide, and binary lamellar diffraction gratings. This chapter also provides a discussion of the various types of modes that can be supported by these structures, as well as the effects that the choice of boundary conditions, and solution method has on the solutions to these systems of equations.

Chapter 3 describes the Rigorous Coupled Wave Analysis (RCWA) method for modeling transversely infinite diffraction gratings and finite waveguides. A development is presented of

the equations necessary for using RCWA in determining eigenmodes in homogeneous regions of space, as well as one, two, and three dimensionally periodic regions of space. Use of these modes for determining diffraction efficiencies from one and two dimensional infinite gratings are discussed, as well as the means for incorporating Perfectly Matched Layer (PML) boundary conditions for modeling transversely finite waveguides.

Chapter 4 develops the tools necessary for modeling wave propagation in layered media. The concept of mode matching between layers having differing eigenmodes is discussed as well as four separate means of relating input and output waves at an interface between two distinct layers. The two methods utilized during the course of this work are then discussed more thoroughly, the enhanced transmittance matrix and the scattering matrix. The means of modeling the propagating energy between separate layer's eigenmodes as well as through a generic multilayer system are presented in detail. For the scattering matrix technique, in particular, use of the Redheffer star-product operation [16, 19, 20] allows for a numerically stable means of calculating the field harmonic amplitudes either internal or external to the multilayered system. This chapter concludes with a novel computational enhancement to the RCWA/Scattering-Matrix technique introduced during the course of this work, zero thickness homogeneous layers [19].

In the following chapters, the numerical tools that are developed in Chapters 2 through 4, as well as Appendices B through E, are used to design a few unique waveguide/grating structures as well as study the physical phenomena governing their operation. In Chapter 5, the concept of a multilayer, multimode, guided mode resonance filter is studied. This inquiry begins with a brief discussion of the history of resonant gratings and the theory of their operation. This historical introduction leads into a discussion of the fundamental physics involved in resonant

gratings, their mode structure and coupling properties. Next, a mixture of effective medium theory [21] and the multilayer waveguide theory from Chapter 2 is utilized for modeling the real-valued properties of the eigenmodes in a multilayer, multimodal resonant grating structure, and is utilized for studying the control of resonance separation in a multilayer multimode GMR filter. Making use of scattering matrix methods [22, 23] for modeling the complex-valued dispersion properties of resonant grating structures, the concept of coupling an input plane wave to two modes at a dispersion band edge resulting in broadened angular acceptance is expanded to the case of multiple wavelengths and oblique incidence. In Chapter 6, the effects of incorporating a linear gain or linear loss within the primary guiding layer of a waveguide grating guided mode resonance filter are studied. Chapter 7 explores the potential for integrating transverse, low-index, periodic inclusions as an embedded waveguide grating filter/mirror. In Chapter 8, the concept of an all dielectric, unidirectional, dual grating output coupler is proposed and rigorously analyzed in terms of its separate components as well as a unified whole device. The output coupling performance of this structure is shown to be very robust in that it does not depend on any grating resonances and is tolerant to potential fabrication errors in numerous grating parameters. Conclusions and potential for future work is then presented in Chapter 9.

Appendix A provides some of the electromagnetic background upon which eigenmode expansion modeling is grounded. Appendix B through D provide some of the implementation details needed for setting up the coupled wave modal matrix equations described in Chapter 3. Appendix B describes the creation of spatial harmonic grids in one, two, and three dimensionally periodic systems [24]. Appendix C presents various means of determining the permittivity and permeability dependent coupling coefficient matrices in one, two, and three dimensions [10, 25-32]. Appendix D discusses the exploitation of symmetries present in one and two dimensionally

periodic systems [33-35] that can decrease the numerical size, and hence increase the computational efficiency, of certain eigenmode problems. Appendix E ties the entire computational process together by describing the workflow of an RCWA computation from the initial definition of geometry, material, and input wave properties through to post-processing of output data.

CHAPTER 2 MODAL SOLUTIONS IN SLAB WAVEGUIDES AND DIFFRACTION GRATINGS

In order to go about the process of designing integrated optical components, it is first necessary to develop the fundamentals of electromagnetic wave propagation in continuous or discrete, and uniform or periodic media. In this chapter, a review is provided for the equations describing how light propagates through materials having these varied geometries. By starting from a derivation of the time harmonic Maxwell's equations, boundary conditions, and Poynting Theorem , from Appendix A, an analytical derivation is provided for the transcendental equations governing the eigenmodes of simple three-layer TE and TM slab waveguides [36] in section 2.1.1, and for an arbitrary anisotropic multilayer TE and TM slab waveguides are presented in section 2.1.2. Orthogonality of the modes within a slab waveguide is established in section 2.1.3. Section 2.2 provides a similar development of solving for the eigenmodes in a diffraction grating, with the Rayleigh expansion of plane waves in a homogeneous medium [37] presented in section 2.2.1 and the one-dimensional grating modal problem presented in Section 2.2.2. Section 2.3 discusses the issue of how complex boundary conditions can be helpful in solving for the properties of all the various types of modes that can be determined using these transcendental equations. Section 2.4 discusses how to obtain direct numerical solutions to these transcendental eigenvalue equations by means of root-searching algorithms, whose positive and negative issues are discussed, and finally, the alternative approach utilized in this study is introduced.

2.1 Eigenmodes in Slab Waveguides

Electromagnetic waveguides are formed by a spatial variation of material properties (permittivity, permeability, conductivity) that cause energy to be concentrated in, and bound by, a certain region of space [6, 36, 38]. While this spatial variation may be continuous or discrete, in this section we consider only discrete spatial variations in electromagnetic material properties.

Having properly derived the governing forms of Maxwell's equations at an interface between two separate media, an extension of these concepts to two or more interfaces allows for the possibility of confining energy within the bounds of those interfaces and for the creation of a waveguide. This section provides a development of the eigenmodes within a passive dielectric/magnetic waveguide, and the orthogonality relationships between these modes.

2.1.1 Eigenmode Expansion in Three-layer Slab Waveguides

One of the simplest types of wave guiding structures consists of a finite thickness slab of permittivity ε_{film} and permeability μ_{film} encased by semi-infinite substrate and superstrate layers having permittivities, $\varepsilon_{substrate}$ and $\varepsilon_{superstrate}$, and permeabilities, $\mu_{substrate}$ and $\mu_{superstrate}$, as shown in Figure 2-1.

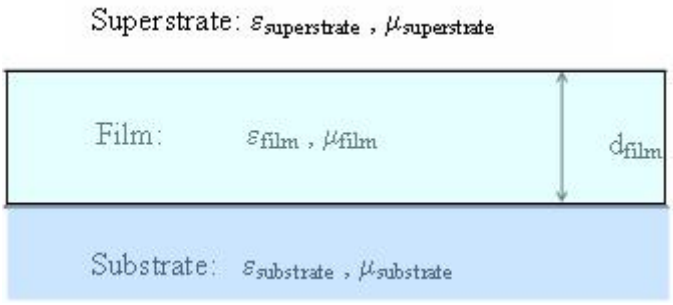

Figure 2-1 A sketch showing a 3-layer asymmetric slab waveguide.

Expanding the time-harmonic Maxwell's Equations (A.1.19) and (A.1.20) in terms of Cartesian components:

(A.1.19) (a)	(A.1.20) (b)	
$\frac{\partial E_y}{\partial z} - \frac{\partial E_z}{\partial y} = -j\omega\mu_0\mu_x H_x$	$\frac{\partial H_y}{\partial z} - \frac{\partial H_z}{\partial y} = j\omega\varepsilon_0\varepsilon_x E_x$	(2.1.1a) (2.1.1b)
$\frac{\partial E_x}{\partial z} - \frac{\partial E_z}{\partial x} = -j\omega\mu_0\mu_y H_y$	$\frac{\partial H_x}{\partial z} - \frac{\partial H_z}{\partial x} = j\omega\varepsilon_0\varepsilon_y E_y$	(2.1.2a) (2.1.2b)
$\frac{\partial E_y}{\partial x} - \frac{\partial E_x}{\partial y} = -j\omega\mu_0\mu_z H_z$	$\frac{\partial H_y}{\partial x} - \frac{\partial H_x}{\partial y} = j\omega\varepsilon_0\varepsilon_z E_z$	(2.1.3a) (2.1.3b)

the component fields within a z- and y- invariant slab waveguide for TE and TM waveguides may be expressed in terms of simplified Maxwell relationships:

TE (a)	TM (b)	
$\frac{\partial E_y}{\partial z} = -j\omega\mu_0\mu_x H_x$	$\frac{\partial H_y}{\partial z} = j\omega\varepsilon_0\varepsilon_x E_x$	(2.1.4a) (2.1.4b)
$H_y = 0$	$E_y = 0$	(2.1.5a) (2.1.5b)
$\frac{\partial E_y}{\partial x} = -j\omega\mu_0\mu_z H_z$	$\frac{\partial H_y}{\partial x} = j\omega\varepsilon_0\varepsilon_z E_z$	(2.1.6a) (2.1.6b)
$E_x = 0$	$E_x = 0$	(2.1.7a) (2.1.7b)
$\frac{\partial H_x}{\partial z} - \frac{\partial H_z}{\partial x} = j\omega\varepsilon_0\varepsilon_y E_y$	$\frac{\partial E_x}{\partial z} - \frac{\partial E_z}{\partial x} = -j\omega\mu_0\mu_y H_y$	(2.1.8a) (2.1.8b)
$E_z = 0$	$H_z = 0$	(2.1.9a) (2.1.9b)

For this z-invariant slab waveguide, the time-harmonic electric and magnetic fields may be expressed as follows:

$$\begin{aligned} \vec{E}(\vec{r},t) &= \vec{E}(x,y)e^{j(\omega t-\beta z)} \\ \vec{H}(\vec{r},t) &= \vec{H}(x,y)e^{j(\omega t-\beta z)} \end{aligned} \tag{2.1.10}$$

Determining the TE and TM eigenvalues, β, for this slab waveguide, involves properly expressing the x-components of the electric and magnetic fields of (2.1.10) in each region and

properly handling the boundary conditions between fields at the two interfaces of the film. For the substrate and the superstrate, the equations in (2.1.10) may be rewritten as:

$$\begin{aligned} \vec{E}_{substrate}(\vec{r},t) &= \vec{E}^{-}_{substrate} e^{+\gamma_{substrate} x} e^{j(\omega t-\beta z)} \quad TE \\ \vec{H}_{substrate}(\vec{r},t) &= \vec{H}^{-}_{substrate} e^{+\gamma_{substrate} x} e^{j(\omega t-\beta z)} \quad TM \end{aligned} \tag{2.1.11}$$

$$\begin{aligned} \vec{E}_{superstrate}(\vec{r},t) &= \vec{E}^{+}_{superstrate} e^{-\gamma_{superstrate} x} e^{j(\omega t-\beta z)} \quad TE \\ \vec{H}_{superstrate}(\vec{r},t) &= \vec{H}^{+}_{superstrate} e^{-\gamma_{superstrate} x} e^{j(\omega t-\beta z)} \quad TM \end{aligned} \tag{2.1.12}$$

where the sign on the decay constant γ properly represents a decaying of the fields towards positive or negative infinity. For fields within the film layer, Equation (2.1.10) may be expressed as:

$$\begin{aligned} \vec{E}_{film}(\vec{r},t) &= \left(\vec{E}^{-}_{film} e^{\gamma_{film}(x-d_{film})} + \vec{E}^{+}_{film} e^{(-\gamma_{film} x)}\right) e^{j(\omega t-\beta z)} \quad TE \\ \vec{H}_{film}(\vec{r},t) &= \left(\vec{H}^{-}_{film} e^{\gamma_{film}(x-d_{film})} + \vec{H}^{+}_{film} e^{(-\gamma_{film} x)}\right) e^{j(\omega t-\beta z)} TM \end{aligned} \tag{2.1.13}$$

where the origin of the x-axis is located along the substrate-film interface for a film of thickness d_{film}. In all of these equations, the following dispersion relations hold between the wavelength λ, the eigenvalues, β, the decay constants, γ, and the individual layer permittivities, ε, and permeabilities, μ:

TE (a) TM (b)

$$\left(\frac{2\pi}{\lambda}\right)^2 \varepsilon_{y,substrate} = -\frac{\gamma^2_{substrate}}{\mu_{x,substrate}} + \frac{\beta^2}{\mu_{z,substrate}} \tag{2.1.14a}$$

$$\left(\frac{2\pi}{\lambda}\right)^2 \mu_{y,substrate} = -\frac{\gamma^2_{substrate}}{\varepsilon_{x,substrate}} + \frac{\beta^2}{\varepsilon_{z,substrate}} \tag{2.1.14b}$$

$$\left(\frac{2\pi}{\lambda}\right)^2 \varepsilon_{y,superstrate} = -\frac{\gamma^2_{superstrate}}{\mu_{x,superstrate}} + \frac{\beta^2}{\mu_{z,superstrate}} \tag{2.1.15a}$$

$$\left(\frac{2\pi}{\lambda}\right)^2 \mu_{y,superstrate} = -\frac{\gamma^2_{superstrate}}{\varepsilon_{x,superstrate}} + \frac{\beta^2}{\varepsilon_{z,superstrate}} \tag{2.1.15b}$$

$$\left(\frac{2\pi}{\lambda}\right)^2 \varepsilon_{y,film} = -\frac{\gamma^2_{film}}{\mu_{x,film}} + \frac{\beta^2}{\mu_{z,film}} \tag{2.1.16a}$$

$$\left(\frac{2\pi}{\lambda}\right)^2 \mu_{y,film} = -\frac{\gamma^2_{film}}{\varepsilon_{x,film}} + \frac{\beta^2}{\varepsilon_{z,film}} \tag{2.1.16b}$$

Upon inserting Equations (2.1.11) – (2.1.13) into Equations (2.1.4) – (2.1.9) for TE and TM waveguides, equating tangential field components, and solving the determinant of the resulting

homogeneous matrix equation, the dispersion relation for the three layer slab waveguide can be expressed as the following transcendental equation:

$$\tanh\left(\gamma_{film} d_{film}\right) = \frac{\gamma'_{film}\left(\gamma'_{sup} - \gamma'_{sub}\right)}{\gamma'^{2}_{film} + \gamma'_{sub}\gamma'_{sup}} \tag{2.1.17}$$

where for TE waveguides $\gamma' = \frac{\gamma}{\mu_x}$ and for TM waveguides $\gamma' = \frac{\gamma}{\varepsilon_x}$. Once the eigenvalues of the waveguide have been determined, using the orthogonality properties of the eigenmodes to be established in section 2.1.3, any field distribution within the waveguide can be expressed as a weighted sum of the set of eigenmodes supported by that waveguide.

2.1.2 Eigenmode Expansion in Anisotropic Multilayer Slab Waveguides

In order to extend the dispersion relation derived in the previous section to an arbitrary multilayer slab waveguide, the field equations (2.1.11) and (2.1.12) and dispersion relations (2.1.14) and (2.1.15) remain unchanged, but an equation of the form (2.1.13) and dispersion relation of the form (2.1.16) are added for each layer in the slab. In order to derive the dispersion relation of the multilayered slab, once again a homogeneous matrix equation is created involving the electric and magnetic field boundary condition equations at each interface of the slab. Establishing the eigenvalues of this homogeneous equation involves finding the roots of the homogeneous determinant polynomial. As this is also a transcendental equation, any solutions must be determined numerically.

Upon inserting equations of the form (2.1.11) – (2.1.13) into the TE and TM sets of z, y, and time-invariant Maxwell's equations in (2.1.4) – (2.1.9), and equating tangential field components, the matrix equation for the multilayer slab waveguide takes a similar form to following (which is given for a 6 region waveguide):

$$\begin{bmatrix} +1 & -X_1 & -1 & 0 & 0 & 0 & 0 & 0 & 0 & 0 \\ +\frac{\gamma'_{sup}}{\gamma'_1} & -X_1 & +1 & 0 & 0 & 0 & 0 & 0 & 0 & 0 \\ 0 & +1 & +X_1 & -X_2 & -1 & 0 & 0 & 0 & 0 & 0 \\ 0 & +\frac{\gamma'_1}{\gamma'_2} & -\frac{\gamma'_1}{\gamma'_2}X_1 & -X_2 & +1 & 0 & 0 & 0 & 0 & 0 \\ 0 & 0 & 0 & +1 & +X_2 & -X_3 & -1 & 0 & 0 & 0 \\ 0 & 0 & 0 & +\frac{\gamma'_2}{\gamma'_3} & -\frac{\gamma'_2}{\gamma'_3}X_2 & -X_3 & +1 & 0 & 0 & 0 \\ 0 & 0 & 0 & 0 & 0 & +1 & +X_3 & -X_4 & -1 & 0 \\ 0 & 0 & 0 & 0 & 0 & +\frac{\gamma'_3}{\gamma'_4} & -\frac{\gamma'_3}{\gamma'_4}X_3 & -X_4 & +1 & 0 \\ 0 & 0 & 0 & 0 & 0 & 0 & 0 & +1 & +X_4 & -1 \\ 0 & 0 & 0 & 0 & 0 & 0 & 0 & +\frac{\gamma'_4}{\gamma'_{sub}} & -\frac{\gamma'_4}{\gamma'_{sub}}X_4 & +1 \end{bmatrix} \begin{bmatrix} F^+_{sup} \\ F^-_1 \\ F^+_1 \\ F^-_2 \\ F^+_2 \\ F^-_3 \\ F^+_3 \\ F^-_4 \\ F^+_4 \\ F^-_{sub} \end{bmatrix} = \begin{bmatrix} 0 \\ 0 \\ 0 \\ 0 \\ 0 \\ 0 \\ 0 \\ 0 \\ 0 \\ 0 \end{bmatrix} \quad (2.1.18)$$

where $X_n = e^{-\gamma_n d_n}$ is the exponential decay of a wave propagating through a layer, F_n^+ and F_n^- are either the electric field (TE) or magnetic field (TM) amplitudes for waves propagating toward the superstrate or substrate respectively, and $\gamma' = \frac{\gamma}{\mu_x}$ or $\gamma' = \frac{\gamma}{\varepsilon_x}$ for TE or TM waveguides respectively. The eigenvalues, β, of this matrix equation are found by solving for the roots of the polynomial created by setting the matrix determinant equal to zero, or equivalently solving for the roots of a polynomial created by Gaussian elimination of the matrix equation.

A second means of solving this system of equations, and the one utilized in this study, involves determining the proper phase shifts at each interface for a wave propagating within a single layer of the multilayer structure as laid out in the notes by Moharam [39], but similar means of solving these equations have been derived elsewhere [40, 41]. Here we restate the equations for the electric and magnetic fields for TE polarized waves propagating in a multilayer slab structure:

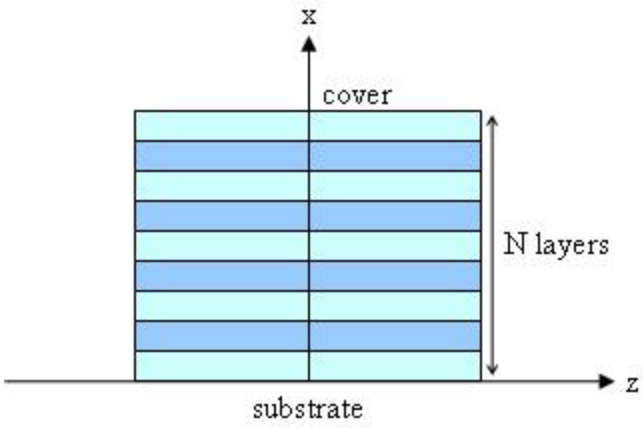

Figure 2-2 A sketch of a multilayer slab waveguide where the origin of the coordinate system is located at the substrate interface.

Substrate: $x \le 0$

$$\vec{E}_{substrate} = F_0^- e^{+\gamma_0 x} e^{-j\beta z} \hat{y}$$
$$\vec{H}_{substrate} = F_0^- \left(-\frac{\beta}{\omega\mu_{x,0}} \hat{x} + j\frac{\gamma_0}{\omega\mu_{z,0}} z \right) e^{+\gamma_{sub} x} e^{-j\beta z} \tag{2.1.19}$$

Cover: $x \ge \sum_{i=1}^{N} d_i$

$$\vec{E}_{superstrate} = F_{N+1}^+ e^{-\gamma_{N+1} x} e^{-j\beta z} \hat{y}$$
$$\vec{H}_{superstrate} = F_{N+1}^+ \left(-\frac{\beta}{\omega\mu_{x,N+1}} \hat{x} - j\frac{\gamma_{N+1}}{\omega\mu_{z,N+1}} \hat{z} \right) e^{-\gamma_{N+1} x} e^{-j\beta z} \tag{2.1.20}$$

N layers: $\sum_{i=1}^{p-1} d_i \le x \le \sum_{i=1}^{p} d_i \qquad 0 \le x_{from\_substrate\_side,p} \le d_{from\_substrate\_side,p}$

$$\vec{E}_{film,p} = \left(F_p^- e^{\gamma_p (x - d_p)} + F_p^+ e^{(-\gamma_p x)} \right) e^{-j\beta z} \hat{y}$$
$$\vec{H}_{film,p} = \left[\frac{\beta}{\omega\mu_x} \left(F_p^- e^{\gamma_p (x - d_p)} + F_p^+ e^{-\gamma_p x} \right) \hat{x} + j\frac{\gamma_p}{\omega\mu_z} \left(F_p^- e^{\gamma_p (x - d_p)} - F_p^+ e^{-\gamma_p x} \right) \hat{z} \right] e^{-j\beta z} \tag{2.1.21}$$

The equations in 2.1.21 for the electric and magnetic fields within internal layers are expressed in terms of two unknown amplitude coefficients. Within any particular layer *p*, the following relationship holds between the counter-propagating field amplitude coefficients:

$$F_p^- = F_p^+ c_p X_p \quad F_p^- = F_p^+ c_p X_p \quad X_p = e^{-\gamma_p d_p} \quad \gamma'_p = \gamma_p / \mu_{z,p} \tag{2.1.22}$$

Using these relationships, the electric and magnetic fields in equation 2.1.21 can be expressed in one of two manners as follows:

$$\begin{aligned} \vec{E}_{film,p} &= F_p^- \left(e^{\gamma_p (x-d_p)} + s_p X_p e^{(-\gamma_p x)} \right) e^{-j\beta z} \hat{y} \\ \vec{H}_{film,p} &= F_p^- \left[\frac{\beta}{\omega \mu_x} \left(e^{\gamma_p (x-d_p)} + s_p X_p e^{-\gamma_p x} \right) \hat{x} + j \frac{\gamma'_p}{\omega} \left(e^{\gamma_p (x-d_p)} - s_p X_p e^{-\gamma_p x} \right) \hat{z} \right] e^{-j\beta z} \end{aligned} \tag{2.1.23}$$

$$\begin{aligned} \vec{E}_{film,p} &= F_p^+ \left(c_p X_p e^{\gamma_p (x-d_p)} + e^{(-\gamma_p x)} \right) e^{-j\beta z} \hat{y} \\ \vec{H}_{film,p} &= F_p^+ \left[\frac{\beta}{\omega \mu_x} \left(c_p X_p e^{\gamma_p (x-d_p)} + e^{-\gamma_p x} \right) \hat{x} + j \frac{\gamma'_p}{\omega} \left(c_p X_p e^{\gamma_p (x-d_p)} - e^{-\gamma_p x} \right) \hat{z} \right] e^{-j\beta z} \end{aligned} \tag{2.1.24}$$

The y and z components of the field are tangential to the interfaces, as shown in Figure 2-2, and are utilized to determine the overall system dispersion relation. By matching these components between two separate layers, the following relationships between the field amplitudes in the separate layers are determined:

Substrate Side	Cover Side	
$F_{p-1}^- \left(1 + s_{p-1} X_{p-1}^2\right) = F_p^- X_p \left(1 + s_p\right)$	$F_{p+1}^- \left(1 + c_{p+1} X_{p+1}^2\right) = F_p^- X_p \left(1 + c_p\right)$	(2.1.25)
$\gamma'_{p-1} F_{p-1}^- \left(1 - s_{p-1} X_{p-1}^2\right) = \gamma'_p F_p^- X_p \left(1 - s_p\right)$	$\gamma'_{p+1} F_{p+1}^- \left(1 - c_{p+1} X_{p+1}^2\right) = \gamma'_p F_p^- X_p \left(1 - c_p\right)$	(2.1.26)

Using Equations 2.1.25, the following similar relationships hold between forward propagating waves amplitudes in adjacent layers and between backward propagating wave amplitudes in adjacent layers.

Substrate Side	Cover Side	
$F_{p-1}^- = F_p^- \dfrac{X_p \left(1 + s_p\right)}{\left(1 + s_{p-1} X_{p-1}^2\right)}$	$F_{p+1}^+ = F_p^+ \dfrac{X_p \left(1 + c_p\right)}{\left(1 + c_{p+1} X_{p+1}^2\right)}$	(2.1.27)

Inserting Equations 2.1.27 into Equations 2.1.26, the following definitions can be made for the unknown coefficients s_p and c_p:

Substrate Side	Cover Side	
$s_p \equiv \frac{\gamma'_p\left(1+s_{p-1}X_{p-1}^2\right)-\gamma'_{p-1}\left(1-s_{p-1}X_{p-1}^2\right)}{\gamma'_p\left(1+s_{p-1}X_{m-1}^2\right)+\gamma'_{m-1}\left(1-s_{p-1}X_{p-1}^2\right)}$	$c_p \equiv \frac{\gamma'_p\left(1+c_{p+1}X_{p+1}^2\right)-\gamma'_{p+1}\left(1-c_{p+1}X_{p+1}^2\right)}{\gamma'_p\left(1+c_{p+1}X_{p+1}^2\right)+\gamma'_{p+1}\left(1-c_{p+1}X_{p+1}^2\right)}$	(2.1.28)

Rearranging this equation, we can express these quantities in the following manner:

Substrate Side	Cover Side	
$s_p = \frac{\gamma'_p - \gamma^s_{p-1}}{\gamma'_p + \gamma^s_{p-1}}$ and $s_0 = 0$	$c_p = \frac{\gamma'_p - \gamma^c_{p+1}}{\gamma'_p + \gamma^c_{p+1}}$ and $c_{N+1} = 0$	(2.1.29)

where

$\gamma^s_{p-1} = \gamma'_{p-1}\frac{\left(1-s_{p-1}X_{p-1}^2\right)}{\left(1+s_{p-1}X_{p-1}^2\right)}$	$\gamma^c_{p+1} = \gamma'_{p+1}\frac{\left(1-c_{p+1}X_{p+1}^2\right)}{\left(1+c_{p+1}X_{p+1}^2\right)}$	(2.1.30)

In the current reference layer of the multilayer stack, the transverse decay constant, γ_p, can be expressed as purely imaginary number ($\gamma_p = j\kappa$). In this case, Equations 2.1.25 – 2.1.29 can be written as follows:

Substrate Side	Cover Side	
$F^-_{ref-1}\left(1+s_{ref-1}X^2_{ref-1}\right) = F^-_{ref}X_{ref} + F^+_{ref}$	$F^-_{ref+1}\left(1+c_{ref-1}X^2_{ref+1}\right) = F^+_{ref}X_{ref} + F^-_{ref}$	(2.1.31)
$\gamma'_{ref-1}F^-_{ref-1}\left(1-s_{ref-1}X^2_{ref-1}\right) = j\kappa'\left(F^-_{ref}X_{ref} - F^+_{ref}\right)$	$\gamma'_{ref+1}F^-_{ref+1}\left(1-c_{ref+1}X^2_{ref+1}\right) = j\kappa'\left(F^+_{ref}X_{ref} - F^-_{ref}\right)$	(2.1.32)
$F^+_{ref} = e^{-j\kappa d_{ref}}s_{ref}F^-_{ref}$	$F^-_{ref} = e^{-j\kappa d_{ref}}c_{ref}F^+_{ref}$	(2.1.33)
$s_{ref} = \frac{\kappa'_{ref}\left(1+s_{ref-1}X^2_{ref-1}\right)+j\gamma'_{ref-1}\left(1-s_{ref-1}X^2_{ref-1}\right)}{\kappa'_{ref}\left(1+s_{ref-1}X^2_{ref-1}\right)-j\gamma'_{ref-1}\left(1-s_{ref-1}X^2_{ref-1}\right)}$	$c_{ref} = \frac{\kappa'_{ref}\left(1+c_{ref+1}X^2_{ref+1}\right)+j\gamma'_{ref+1}\left(1-c_{ref+1}X^2_{ref+1}\right)}{\kappa'_{ref}\left(1+c_{ref+1}X^2_{ref+1}\right)-j\gamma'_{ref+1}\left(1-c_{ref+1}X^2_{ref+1}\right)}$	(2.1.34)
$s_{ref} = \frac{j\kappa' - \gamma^s_{ref-1}}{j\kappa' + \gamma^s_{ref-1}} = e^{j2\phi_s}$	$c_{ref} = \frac{j\kappa' - \gamma^c_{ref+1}}{j\kappa' + \gamma^c_{ref+1}} = e^{j2\phi_c}$	(2.1.35)

With the construction of the phase shift terms (analogous to the Goos-Hanchen shift for a three-layer slab waveguide [2]), ϕ_s and ϕ_c, by propagating from the substrate and cover respectively

toward the reference layer, the following dispersion equation can be used to determine the propagation constants supported by the waveguide:

$$e^{j2\left(\kappa d_{ref}-\phi_c-\phi_s\right)}=1 \tag{2.1.36}$$

This equation holds true when the term in parentheses is equal to a multiple of π as follows:

$$\kappa d_{ref}-\phi_c-\phi_s=m\pi \tag{2.1.37}$$

This method is used for solving the dispersion relation in a single reference layer of a multilayer system surrounded by two media of lower refractive index. In a system that contains many such identical high/low index layer pairings, solving this particular dispersion relation in many separate reference layers allows for greater certainty that all modes will be determined for a given sampling tolerance of the dispersion relation being solved. The value of repeating the modal solver in separate reference layers is that the slope of the dispersion relation near any given solution can be significantly different depending on the particular reference layer chosen in a multilayer slab. By solving the system in each reference layer separately, solutions that may have been missed at one reference layer may be more likely to be found in one of the other reference layers for the same initial sample spacing and tolerance. The implementation of these equations used in this study used a vectorized bracket bisection method [42] where the locations of individual eigenmodes were initially located for a given propagation constant sampling. The function was then re-sampled in a vectorized manner near the location of any solution in order narrow down the location of the root and check for nearly degenerate roots. Other methods of solving the transcendental equations (2.1.18) and (2.1.37) will be discussed briefly in section 2.4.

2.2 Eigenmodes in Lamellar Diffraction Gratings

Diffraction gratings consist of a spatially periodic variation of electromagnetic material properties [37]. As with a waveguide, this spatial variation may also be continuous or discrete, but in either case the interaction of electromagnetic waves with a spatially periodic media this variation causes diffraction and interference effects that result in the energy being redirected in discrete directions, or diffracted orders.

The electromagnetic theory of diffraction gratings has a long history that encompasses a full range continuous geometries and discrete geometries for the spatial distribution of material properties describing surface-relief gratings [15] and holographic gratings [7], as well as a wide variety of methods for solving Maxwell's Equations in these various geometries [7, 11, 14, 43, 44]. In this study, the structures in which we were interested consisted of both continuous and discrete surface-relief gratings, but we limited ourselves to solution methods that involved only stratified lamellar layers. In such cases, the homogeneous solutions to the time-harmonic Maxwell's Equations lead to the possibility of modal expansions in both spatially periodic regions, as well as spatially homogeneous regions [12, 23, 45]. By performing mode-matching at the interfaces between layers, the reflected and transmitted energy distribution that results from an input plane-wave or spectral decomposition of plane-waves can be determined.

In this section, modal expansions of spatially periodic fields due to interaction with a two-material spatially periodic layer are derived for both homogeneous media in Section 2.2.1 and one-dimensional spatially periodic media in Section 2.2.2. In a similar manner to the discussion presented for waveguides, the concepts of Lorentz reciprocity and modal orthogonality are useful concepts for justifying the representation of any field distribution as a

weighted sum of eigenmodes. Derivations of these concepts for diffraction gratings may be found elsewhere [37].

2.2.1 Rayleigh Expansion in Homogeneous Media and the Grating Equation

In an effort to explain the nature of the diffracted orders produced from a diffraction grating, and the diffraction anomalies in previously observed by Wood [46], Lord Rayleigh introduced in 1907 the concept of expanding an electric field in a homogeneous region above a spatially periodic grating in terms of a plane wave expansion [47, 48]. Spatially periodic boundary conditions imposed on the tangential components of the electric and magnetic fields the homogeneous region adjacent to the grating lead to a mathematical description of the diffracted orders that can be physically observed.

The notion of transverse spatial periodicity of the diffracted field imposes the following conditions on the supported spatial field distribution in a homogeneous region of space [12, 37]:

$$\begin{aligned}\vec{E}(\vec{r},t) &= \vec{E}(x,y)e^{j(\omega t-\beta z)} = \vec{E}\left(x+\Lambda_x, y+\Lambda_y\right)e^{j(\omega t-\beta z)} \\ \vec{H}(\vec{r},t) &= \vec{H}(x,y)e^{j(\omega t-\beta z)} = \vec{H}\left(x+\Lambda_x, y+\Lambda_y\right)e^{j(\omega t-\beta z)}\end{aligned} \tag{2.2.1}$$

where Λ_x and Λ_y are the spatial periods in the x and y directions. This spatial periodicity condition has been previously shown to be satisfied by multiplying the original field expression by an appropriate spatially periodic phase function as follows:

$$\vec{F}e^{j(\omega t-\beta z)}e^{-j\left(k_x x+k_y y\right)} = \vec{F}e^{j(\omega t-\beta z)}e^{-j\left(k_x x+k_y y\right)}e^{-j\left(k_x\Lambda_x+k_y\Lambda_y\right)} \tag{2.2.2}$$

where k_x and k_y represent the tangential components of the wave vector for a generic field vector $\vec{F}$. To create a plane wave series expansion, we create an infinite summation of terms that differ from one another by phases incorporating integer multiples of the grating vector.

$$\begin{aligned}\vec{F}_{diffracted} &= e^{-j(k_x x+k_y y)}\sum_{m=-\infty}^{\infty}\sum_{n=-\infty}^{\infty}\vec{F}e^{-j(mK_x x+nK_y y)}e^{j(\omega t-\beta_{m,n}z)} \\ &= \sum_{m=-\infty}^{\infty}\sum_{n=-\infty}^{\infty}\vec{F}e^{-j((k_x+mK_x)x+(k_y+nK_y)y)}e^{j(\omega t-\beta_{m,n}z)} \\ &= \sum_{m=-\infty}^{\infty}\sum_{n=-\infty}^{\infty}\vec{F}e^{-j(k_{xm}x+k_{yn}y)}e^{j(\omega t-\beta_{m,n}z)}\end{aligned} \tag{2.2.3}$$

The terms k_{xm} and k_{yn} can be considered to be the tangential components of the wave vectors associated with each spatial harmonic/diffracted order, and K_x and K_y are the grating vector amplitudes in the x and y directions. The definitions of k_{xm} and k_{yn} as $k_{xm} = k_x + mK_x$ and $k_{ym} = k_y + nK_y$ are the famous grating equations in the x and y directions. The normal component of the wavevector for each spatial harmonic/diffracted order can be expressed in terms of the tangential wavevector components as follows:

$$\beta_{m,n} = \begin{cases} k_0\sqrt{\mu\varepsilon - \left(\frac{k_{x,(m,n)}}{k_0}\right)^2 - \left(\frac{k_{y,(m,n)}}{k_0}\right)^2} & if \quad k_0^2\mu\varepsilon > k_{x,(m,n)}^2 + k_{y,(m,n)}^2 \\ -jk_0\sqrt{\left(\frac{k_{x,(m,n)}}{k_0}\right)^2 + \left(\frac{k_{y,(m,n)}}{k_0}\right)^2 - \mu\varepsilon} & if \quad k_0^2\mu\varepsilon < k_{x,(m,n)}^2 + k_{y,(m,n)}^2 \end{cases} \tag{2.2.4}$$

2.2.2 Eigenmode Expansion in Transversely Periodic Dielectric/Magnetic z-Invariant Media

Performing an explicit modal expansion in a transversely periodic medium involves a development similar to that provided for waveguides in sections 2.1.1 and 2.1.2 for slab waveguides with a few slight exceptions. In the case of a slab waveguide, the boundary conditions in the substrate and superstrate regions were such that the fields decay towards infinity. Solving the modal problem in a lamellar grating layer requires periodic transverse boundary conditions. Consequently, there are no semi-infinite transverse layers, and a boundary

condition is added matching layer 1 and layer N. The second difference involves the imposition of longitudinal boundary conditions that take into account an input plane wave in an adjacent homogeneous region as well as all diffracted waves in the Rayleigh expansion.

For a one-dimensional, two-material lamellar diffraction grating in TE, TM, or conical mounts, the full derivation of the transcendental eigenvalue equation is presented by Li [43]. Using definitions of the decay constants within each layer similar to those defined in Equations (2.1.14) – (2.1.16), this eigenvalue equation is given as follows:

$$\cosh(\gamma_1 d_1)\cosh(\gamma_2 d_2)+\frac{1}{2}\left(\frac{\gamma_1'}{\gamma_2'}+\frac{\gamma_2'}{\gamma_1'}\right)\sinh(\gamma_1 d_1)\sinh(\gamma_2 d_2)=\cos(k_x \Lambda_x) \tag{2.2.5}$$

Real propagating modes may be found by searching the real axis of β^2, whereas complex, leaky, or evanescent modes are found by searching the entire complex plane.

2.3 Properties of Various Waveguide/Grating Eigenmodes

In previous sections of this chapter, various types of analytical boundary conditions were utilized in determining the modes that are supported by waveguides and diffraction gratings. This section expands on these analytical boundary conditions and the properties of modes that can be most easily determined for systems of equations having each of these types of boundaries. While the types of modes present in any given physical structure depend only on the nature of the device itself, the ease or difficulty in modeling the properties of those modes depends on the computational methods utilized.

2.3.1 Analytical Boundary Conditions

When solving any system of differential equations, the solution to that system depends on both the differential equation itself as well as the manner in which the equation is handled on the

boundary of the solution's domain. For the linear systems of equations normally utilized in a computational environment, the eigenmodes that can be determined by solving the system depend significantly upon the choice of boundary conditions. Common types of analytical boundary conditions used for solving a system of Partial Differential Equations [49, 50] include Dirichlet boundary conditions, where the field is homogeneous/constant on the boundary, Neumann boundary conditions, where the derivative of the field is homogeneous/constant on the boundary, Robin boundary conditions, where the sum of the field and its derivative are homogeneous/constant on the boundary, periodic boundary conditions, where the fields are cyclical within the boundary and multiple boundaries become adjacent, and open boundary conditions, such as Dirichlet to Neumann [51-53] where an outward propagating field decays to infinity without reflection.

2.3.2 Eigenmodes in Open and Closed Domains

A thorough description of the various types of eigenmodes that can be supported by optical waveguides on bounded and unbounded domains is given in the dissertation by Bienstman [54], and this section restates much of the excellent description given in that work. For a reciprocal lossless dielectric slab waveguide, a mode supported by that waveguide can be described by its propagation constant β_{eff}, or by dividing by the free space wavenumber, k_0, the mode can be represented by a complex effective index, n_{eff}.

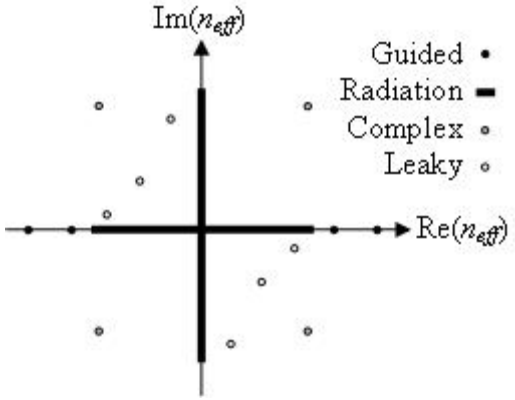

Figure 2-3 Plot showing the discrete and continuous spectra of modes supported by an open waveguide structure.

By plotting the complex plane for n_{eff}, as seen in Figure 2-3, there can be seen four separate types of modes that can be supported by a slab waveguide in an open domain:

1. Guided modes take on discrete values and are located solely on the real axis. These modes correspond to energy concentration in the core of a waveguide that decays into the cladding.

2. Radiation modes are located found along both the real and imaginary axes, and can take on a continuum of values. The field profiles of these modes oscillate in the cladding and extend to infinity. A real, propagative, radiation mode maintains its amplitude as it moves along the axis of a waveguide, whereas an imaginary, evanescent, radiation mode decreases in amplitude with movement along the waveguide axis.

3. Leaky modes are located in the complex plane and may be considered as a continuation of the guided modes at low frequencies. The field profile of a leaky mode increases exponentially in the cladding, and consequently are not physical, but can still be useful for describing the field in certain situations [55]. A leaky mode may arise from a guided mode when a periodic perturbation is introduced as part of the supporting waveguide.

4. Complex modes are also found in the complex plane and always occur in quartets. These modes are very rare, and are only found when resonant transfer occurs between TE and TM modes [56].

In a closed domain, when the boundary conditions are of the Dirichlet, Neumann, Robin or periodic type, the radiation modes that can be determined no longer form a continuum, but are limited by the boundary conditions to take only discrete values, as seen in Figure 2-4.

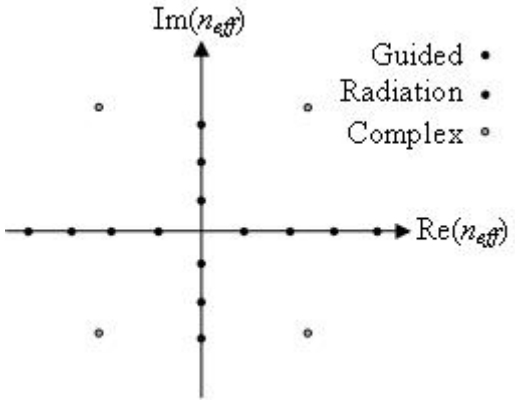

Figure 2-4 Plot showing the possible discrete spectra of modes supported within a multilayer slab waveguide structure with Dirichlet, Neumann, or Robin type boundary conditions. Also representative of the possible longitudinal modes present in a system having only transverse periodicity.

Consequently, there is no difference mechanically between determining a guided mode or a radiation mode, but the standard convention is to treat those modes having a real effective index, Real(n_{eff}), which is greater than the cladding index, $n_{cladding}$, and less than the core index, n_{core}, are said to be guided modes, while those modes have a real effective index less than the index of the cladding are said to be radiation modes. When open and close boundary conditions are mixed [22, 23], for example in a multilayer periodic structure, leaky modes may also be determined as shown in Figure 2.9.

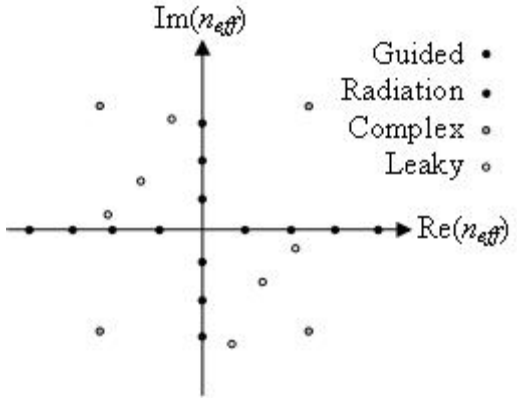

Figure 2-5 Plot showing the possible discrete spectra of modes present in a multilayer system having Dirichlet, Neumann, Robin, or periodic boundary conditions where absorbing layer boundary conditions (i.e. PML BC's) are utilized in the computational window. Leaky modes were found to be present in this study when solving generalized eigenvalue problems in longitudinally periodic systems.

When using eigenmodes to represent a field, the completeness of the basis set, i.e. the ability to represent any given field using the modes in that set, is important for producing an accurate and reliable numerical model. For lossless waveguides that do not support complex modes, the guided modes along with the radiation modes can be rigorously proven to form a complete basis. While for structures containing lossy materials or supporting complex modes, there has been no formal proof of completeness. The use of guided and radiation modes as a basis set in the presences of lossy materials often give results that appear to be complete within any desired numerical accuracy, and with the addition of complex modes to the basis set, near effective completeness has been shown for structures supporting complex modes as well [57]. Leaky modes have not been shown to be useful in producing a complete basis set in any setting [58].

2.3.3 Eigenmode Orthogonality

Establishing an orthogonal set of eigenmodes for a waveguide creates a set of basis functions that can be weighted to represent any field distribution within that waveguide. To establish this orthogonality, we begin with the electric and magnetic field distributions, ($\vec{E}_m, \vec{H}_m$) and ($\vec{E}_n, \vec{H}_n$) associated with two eigenmodes:

Mode *m* (a)	Mode *n* (b)	
$\vec{E}_m(\vec{r}) = \vec{E}_m(x,y)e^{-j\beta_m z}$	$\vec{E}_n(\vec{r}) = \vec{E}_n(x,y)e^{-j\beta_m z}$	(2.3.1a)
$\vec{H}_m(\vec{r}) = \vec{H}_m(x,y)e^{-j\beta_m z}$	$\vec{H}_n(\vec{r}) = \vec{H}_n(x,y)e^{-j\beta_m z}$	(2.3.1b)

To show that any two eigenmodes of a waveguide are orthogonal to one another, we begin by utilizing the Lorentz reciprocity theorem for longitudinally invariant media:

$$\iint_S \frac{\partial}{\partial z}\left(\vec{E}_m \times \vec{H}_n - \vec{E}_n \times \vec{H}_m\right)\cdot \hat{u}_z dS = \iint_S \left(\vec{J}_m \cdot \vec{E}_n - \vec{J}_n \cdot \vec{E}_m\right)\cdot dS \tag{2.3.2}$$

As the establishment of these eigenmodes is the result of solving a homogenous equation, they exist in source-less media, and consequently the currents $\vec{J}_m$ and $\vec{J}_n$ are equal to zero. Inserting equations (2.3.1) into the resulting homogeneous equation involving the left-hand side of (2.3.2), results in the following equation:

$$(\beta_m + \beta_n)\iint_S \left(\vec{E}_m(x,y)\times \vec{H}_n(x,y) - \vec{E}_n(x,y)\times \vec{H}_m(x,y)\right)\cdot \hat{u}_z dS = 0 \tag{2.3.3}$$

Next, by considering a similar relationship between a mode *m* propagating in the same z-direction as before and a mode *n* that is propagating in the opposite z-direction, the following expression can be obtained:

$$(\beta_m - \beta_n)\iint_S \left(\vec{E}_m(x,y)\times \vec{H}_n(x,y) + \vec{E}_n(x,y)\times \vec{H}_m(x,y)\right)\cdot \hat{u}_z dS = 0 \tag{2.3.4}$$

Assuming that β_m and β_n are not degenerate, the addition of (2.3.5) and (2.3.6) provides the following orthogonality relationship between modes *m* and *n*:

$$\iint_S \left(\bar{E}_m(x,y)\times \bar{H}_n(x,y)\right)\cdot \hat{u}_z dS = 0 \tag{2.3.7}$$

2.4 Discussion of Direct Numerical Solutions to Modal Expansion Methods

Numerical solutions to transcendental eigenvalue equations of the type found in Equations (2.1.17), (2.1.18), (2.1.37), and (2.2.4) require root-searching algorithms, which, depending on the properties of the modes to be determined, search either the real number line or the entire complex plane. For searching exclusively along the real number line, examples of simple root-searching algorithms include the bracketing and bisection method, the Newton-Raphson method, the secant-method, and various hybrid root-finding methods [59]. For multimodal systems, root-searching algorithms generally involve separate iterations or the branching of separate threads for determining each individual mode of the system. Root searching algorithms can potentially run into problems for systems having nearly degenerate eigenmodes, or in cases where the slope of the transcendental function close to a root is nearly infinite, especially for methods that involve the derivative of a function. In such cases, sampling of the real line or complex plane must be very fine in order to distinguish between separate eigenmodes or even to find what may be multiple eigenmodes that are nearly degenerate. As an alternative to exact modal expansions and root-searching algorithms, in this study we made use of a method that approximates the modes of a spatially periodic material via an orthogonal function expansion. By doing so, problems with sampling transcendental functions are transferred to the relatively more straightforward problem of convergence in a finite series expansion and solution of a matrix eigenvalue problem.

CHAPTER 3 RIGOROUS COUPLED WAVE ANALYSIS OF DIFFRACTION GRATINGS AND FINITE WAVEGUIDES

As a member of the family of differential modal methods for solving Maxwell's equations (and more broadly as a member of the family of spectral modal methods), RCWA now has a long history as a robust and flexible tool for the analysis of wave propagation in periodic optical media [7, 9, 11-15, 19, 25, 27, 28, 31, 60-64]. RCWA is a frequency-domain method for determining the modal properties of the electric and magnetic fields within a transversely periodic longitudinally-invariant lamellar layer. The method rigorously solves Maxwell's equations by decomposing the electric and magnetic fields, as well as the material properties, within a lamellar layer in terms of spatial harmonics on a pseudo-periodic Fourier basis set. As the technique has matured through the years, it has been applied successfully in modeling the diffractive properties of volume gratings, as well as binary and multilevel surface relief gratings composed of isotropic or anisotropic dielectric, metallic and magnetic materials. At the turn of the new millennium, the range of the technique's usefulness was extended by the incorporation of absorbing boundary conditions [9, 16], most notably PML boundary conditions [65, 66], within the unit cell of the periodic media. By incorporating this absorbing boundary condition, RCWA could then be utilized as a modal solver for finite transverse waveguides. This chapter intends to provide a full development of the RCWA as a modal solver for one, two, or three dimensional infinitely periodic media.

3.1 Coupled Wave Modal Expansion of Periodic Maxwell's Equations

3.1.1 Homogeneous Rayleigh Expansion in Cartesian or Skewed Coordinates

For homogeneous material layers, the plane wave expansion utilized for determining eigenmodes in a Rayleigh expansion is performed in exactly the same manner as that presented in Section (2.3.1). Unlike the modal method presented in Chapter 2, which currently has only been implemented in regular Cartesian, cylindrical, or spherical axes for one-dimensional modal problems, RCWA allows for the use of periodicity in non-orthogonal coordinate multi-dimensional systems as well.

For periodicity on a two-dimensional non-orthogonal lattice, having an angle, ξ, between directions of periodicity, the corresponding homogeneous region Rayleigh expansion for a generic field vector may be expressed as follows:

$$\vec{F}_{diffracted} = \sum_{m=-\infty}^{\infty} \sum_{n=-\infty}^{\infty} A_{m,n} e^{-j\left(\left(k_x + m\frac{2\pi}{\Lambda_b}\sec(\xi) + n\frac{2\pi}{\Lambda_a}\tan(\xi)\right)x + \left(k_y + n\frac{2\pi}{\Lambda_a}\right)y\right)} e^{j(\omega t - \beta_{m,n} z)} \tag{3.1.1}$$

3.1.2 Three-dimensional Coupled-Wave Modal Expansion

Over the last two decades, there has been an increased interest in optical structures having multi-dimensional periodicity. Theoretically, infinite three-dimensional photonic crystals possess the ability to completely forbid the propagation of certain wavelengths of light from traveling in particular directions through the crystal [32, 67-69], analogous to the forbidden band-gaps of electrons in solid-state electronics [70]. Realistically, infinitely periodic structures are not possible in practice, but if the size of the structure is much larger than the wavelength of the light and periodicity length within the structure, then the assumption of infinite periodicity describes well the performance of a structure away from its boundaries. Determination of these

photonic band-gaps for crystals of any material and geometry depend upon finding solutions to a three dimensional eigenvalue problem. The use of three-dimensional periodicity models can also be useful in determining the properties of certain two-dimensionally periodic structures when proper boundary conditions are utilized [71]. Exploiting three-dimensional models for determining the modal properties of two-dimensionally periodic structures requires the use of absorbing boundary conditions similar to those explained in section 2.4.2, but in doing so one must utilize an orthogonal function expansion in all three dimensions and may require many thousands of basis functions to obtain modal convergence.

Starting from Maxwell's Equations as expressed in Equations (2.2.1) – (2.2.3), the Cartesian, three-dimensional, homogeneous equation to be solved can be expressed as:

$$\begin{bmatrix} 0 & -\frac{\partial}{\partial z'} & \frac{\partial}{\partial y'} & \mu_x & 0 & 0 \\ \frac{\partial}{\partial z'} & 0 & -\frac{\partial}{\partial x'} & 0 & \mu_y & 0 \\ -\frac{\partial}{\partial y'} & \frac{\partial}{\partial x'} & 0 & 0 & 0 & \mu_z \\ -\varepsilon_x & 0 & 0 & 0 & -\frac{\partial}{\partial z'} & \frac{\partial}{\partial y'} \\ 0 & -\varepsilon_y & 0 & \frac{\partial}{\partial z'} & 0 & -\frac{\partial}{\partial x'} \\ 0 & 0 & -\varepsilon_z & -\frac{\partial}{\partial y'} & \frac{\partial}{\partial x'} & 0 \end{bmatrix} \begin{bmatrix} E_x \\ E_y \\ E_z \\ j\eta_0 H_x \\ j\eta_0 H_y \\ j\eta_0 H_z \end{bmatrix} = \begin{bmatrix} 0 \\ 0 \\ 0 \\ 0 \\ 0 \\ 0 \end{bmatrix} \tag{3.1.2}$$

where $x' = k_0 x$, $y' = k_0 y$, $z' = k_0 z$, and $\eta_0 = \sqrt{\frac{\mu_0}{\varepsilon_0}}$. By applying periodic series expansions of the fields in all three-dimensions, as in Equation (3.1.1), and taking the necessary partial-derivatives, the above homogeneous equation can be expressed as:

$$\begin{bmatrix} 0 & -K_z & K_y & \mu_x & 0 & 0 \\ K_z & 0 & -K_x & 0 & \mu_y & 0 \\ -K_y & K_x & 0 & 0 & 0 & \mu_z \\ -\varepsilon_x & 0 & 0 & 0 & -K_z & K_y \\ 0 & -\varepsilon_y & 0 & K_z & 0 & -K_x \\ 0 & 0 & -\varepsilon_z & -K_y & K_x & 0 \end{bmatrix} \begin{bmatrix} E_x \\ E_y \\ E_z \\ j\eta_0 H_x \\ j\eta_0 H_y \\ j\eta_0 H_z \end{bmatrix} = \begin{bmatrix} 0 \\ 0 \\ 0 \\ 0 \\ 0 \\ 0 \end{bmatrix} \tag{3.1.3}$$

which can be put in the form of a matrix eigenvalue problem as follows:

$$\begin{bmatrix} \varepsilon_x^{-1}\left(K_z\mu_y^{-1}K_z + K_y\mu_z^{-1}K_y\right) & -\varepsilon_x^{-1}\left(K_y\mu_z^{-1}K_x\right) & -\varepsilon_x^{-1}\left(K_z\mu_y^{-1}K_x\right) \\ -\varepsilon_y^{-1}\left(K_x\mu_z^{-1}K_y\right) & \varepsilon_y^{-1}\left(K_z\mu_x^{-1}K_z + K_x\mu_z^{-1}K_x\right) & -\varepsilon_y^{-1}\left(K_z\mu_x^{-1}K_y\right) \\ -\varepsilon_z^{-1}\left(K_x\mu_y^{-1}K_z\right) & -\varepsilon_z^{-1}\left(K_y\mu_x^{-1}K_z\right) & \varepsilon_z^{-1}\left(K_x\mu_y^{-1}K_x + K_y\mu_x^{-1}K_y\right) \end{bmatrix} \begin{bmatrix} E_x \\ E_y \\ E_z \end{bmatrix} = \begin{bmatrix} E_x \\ E_y \\ E_z \end{bmatrix} \tag{3.1.4}$$

where K_x, K_y, K_z are diagonal matrices containing the x, y, and z components of the wave vector ($k_{x,(l,m.n)}$, $k_{y,(l,m.n)}$, $k_{z,(l,m.n)}$) for each spatial harmonic, divided the free space angular wavenumber, k_0.

While the above development has addressed the spatial periodicity of the field, it has not yet addressed the spatial periodicity of the materials. The matrices defined by ε_x, ε_y, ε_z, μ_x, μ_y, and μ_z are full matrices created by performing Fourier series expansions of the spatially periodic functions representing material permittivity and permeability components. The matrices are full since the involve coupling every spatial harmonic in the electric and magnetic field series expansions to every other spatial harmonic in that series. Explicit derivations and discussions of these coupling matrices can be found in Appendix A.

3.1.3 Two-dimensional Coupled-Wave Modal Expansion

Solutions to the coupled-wave equations for systems involving two-dimensional transverse periodicity and longitudinal invariance can be useful for modeling infinite crossed diffraction grating devices [25, 27, 31] as well as finite-sized integrated guided wave structures [72]. Solving this set of equations begins with the same set of Maxwell's Equations as expressed in Equation (3.1.2), but in this case Fourier expansion of the electric and magnetic fields using pseudo-periodic boundary conditions are only taken for the transverse (x and y) directions with the longitudinal fields solved as a matrix eigenvalue problem. Applying the pseudo-periodic Fourier series expansions in Equation (3.1.1) to the transverse fields in Equation (3.1.2), and taking derivatives for the transverse coordinates results in the following relationships between the transverse electric and magnetic field harmonic expansions:

$$\begin{bmatrix} \frac{\partial E_y}{\partial z'} \\ \frac{\partial E_x}{\partial z'} \end{bmatrix} = \begin{bmatrix} K_y \varepsilon_z^{-1} K_x & \mu_x - K_y \varepsilon_z^{-1} K_y \\ K_x \varepsilon_z^{-1} K_x - \mu_y & -K_x \varepsilon_z^{-1} K_y \end{bmatrix} \begin{bmatrix} H_y \\ H_x \end{bmatrix} \tag{3.1.5}$$

$$\begin{bmatrix} \frac{\partial H_y}{\partial z'} \\ \frac{\partial H_x}{\partial z'} \end{bmatrix} = \begin{bmatrix} K_y \mu_z^{-1} K_x & \varepsilon_x - K_y \mu_z^{-1} K_y \\ K_x \mu_z^{-1} K_x - \varepsilon_y & -K_x \mu_z^{-1} K_y \end{bmatrix} \begin{bmatrix} E_y \\ E_x \end{bmatrix} \tag{3.1.6}$$

Upon taking the derivative of Equation (3.1.5) with respect to z' and inserting Equation (3.1.6) into the result of this derivative, we obtain the following matrix eigenvalue equation for the transverse electric field harmonic expansions:

$$\begin{bmatrix} \frac{\partial^2 E_y}{\partial z'^2} \\ \frac{\partial^2 E_x}{\partial z'^2} \end{bmatrix} = \begin{bmatrix} K_y \varepsilon_z^{-1} K_y \varepsilon_y + \mu_x K_x \mu_z^{-1} K_x - \mu_x \varepsilon_y & K_y \varepsilon_z^{-1} K_x \varepsilon_x - \mu_x K_x \mu_z^{-1} K_y \\ K_x \varepsilon_z^{-1} K_y \varepsilon_y - \mu_y K_y \mu_z^{-1} K_x & K_x \varepsilon_z^{-1} K_x \varepsilon_x + \mu_y K_y \mu_z^{-1} K_y - \mu_y \varepsilon_x \end{bmatrix} \begin{bmatrix} E_y \\ E_x \end{bmatrix} \tag{3.1.7}$$

A similar equation may be obtained by solving the system as a magnetic field eigenvalue problem. By solving Equation (3.1.7), not only can the vector of eigenvalues, q, (the modal indices) be determined, but an eigenvector matrix, W, (the modal matrix) can be determined where each column is a spatial harmonic decomposition of each individual mode in the system. The corresponding magnetic field eigenvector can be expressed as follows:

$$V = \begin{bmatrix} K_y \mu_z^{-1} K_x & \varepsilon_x - K_y \mu_z^{-1} K_y \\ K_x \mu_z^{-1} K_x - \varepsilon_y & -K_x \mu_z^{-1} K_y \end{bmatrix} [W] diag\left(\begin{bmatrix} 1 \\ \overline{q} \end{bmatrix} \right) \tag{3.1.8}$$

Utilizing these eigenvalues and eigenvectors, the spatial harmonic expansions of the transverse electric and magnetic field components can be expressed as follows:

$$\begin{bmatrix} S_y \\ S_x \\ U_y \\ U_x \end{bmatrix} = \begin{bmatrix} W & W \\ V & -V \end{bmatrix} \begin{bmatrix} \exp(k_0 q(z-d)) & 0 \\ 0 & \exp(-k_0 qz) \end{bmatrix} \begin{bmatrix} b \\ f \end{bmatrix} \tag{3.1.9}$$

where b and f are the unknown field harmonic amplitudes in this lamellar layer. The normal components of the electric and magnetic field can be determined by inserting Equation (3.1.9) into Equations (2.2.6a), isolating the normal field harmonic components, and taking the proper derivatives.

$$\begin{aligned} S_z &= -j\eta_0 \varepsilon_z^{-1} \left[K_x U_y - K_y U_x \right] \\ U_z &= -j\eta_0^{-1} \mu_z^{-1} \left[K_x S_y - K_y S_x \right] \end{aligned} \tag{3.1.10}$$

The actual electric and magnetic fields within the layer can then be determined by multiplying the spatial harmonic expansions by appropriate phase terms for each harmonic at any point on a predetermined spatial grid as follows:

$$E_{x,y,z}(x,y,z) = \sum_m \sum_n S_{x,y,z,(m,n)}(z) e^{-j\left(k_{x,(m,n)}x + k_{y,(m,n)}y\right)}$$
$$H_{x,y,z}(x,y,z) = \sum_m \sum_n U_{x,y,z,(m,n)}(z) e^{-j\left(k_{x,(m,n)}x + k_{y,(m,n)}y\right)} \quad (3.1.11)$$

3.1.4 One-dimensional Coupled-Wave Modal Expansion

In a similar vein, one-dimensionally periodic coupled wave equations may also be used to model systems that have one dimension of transverse periodicity, one dimension of longitudinal invariance, but also have one dimension of transverse invariance [11, 12]. The structures that can be modeled also include diffraction gratings having infinite transverse periodicity as well as waveguides with finite transverse dimensions. In one-dimensional systems though, the approach taken to solve the eigenvalue problem for a lamellar layer depends upon the polarization of the input light. For systems whose input wavevector is coplanar with the grating vector and the surface normal vector, only a single eigenvalue equation need be solved involving a second order differential equation for a single field component. However, in the case of conical diffraction [12, 62] from a purely isotropic dielectric grating, where the incident wave vector is not coplanar with the grating vector and surface normal vector, two decoupled polarizations are present in the system. Consequently, the system may be solved either as a single eigenvalue equation involving both polarizations, or as two separate sets of eigenvalue equations involving separate field components. In the latter case, portions of the fields involving each polarization are combined upon field matching with outer homogeneous layers to produce proper reflection and transmission coefficients for each diffracted order.

For one-dimensionally periodic structures having TE polarized incident light, the electric field is in the y-direction, which is parallel to the grating grooves and perpendicular to the grating vector. Components of the electric field parallel to the grating vector and in the

longitudinal direction are null, as is the component of the magnetic field in the y-direction. Starting from Maxwell's Equations in (3.1.2), and then inserting an x-direction, pseudo-periodic series expansion for the non-null components of the field, results in the following matrix eigenvalue equation for the transverse electric field harmonic expansion:

$$\left[\frac{\partial^2 E_y}{\partial z'^2}\right] = \left[\mu_x K_x \mu_z^{-1} K_x - \mu_x \varepsilon_y\right]\left[E_y\right] \tag{3.1.12}$$

With the resulting vector of eigenvalues, q, and electric field eigenvector matrix, W, the corresponding magnetic field eigenvector can be expressed as $V = \mu_x W diag\left(\left[1/q\right]\right)$. The transverse electric and magnetic field harmonic expansions can be expressed as follows:

$$\begin{bmatrix} S_y(z) \\ U_x(z) \end{bmatrix} = \begin{bmatrix} W & W \\ V & -V \end{bmatrix}\begin{bmatrix} \exp(k_0 q(z-d)) & 0 \\ 0 & \exp(-k_0 qz) \end{bmatrix}\begin{bmatrix} b \\ f \end{bmatrix} \tag{3.1.13}$$

where b and f are the unknown field harmonic amplitudes in this lamellar layer. The normal components of the electric and magnetic field can be determined by inserting Equation (3.1.9) into Equations (2.2.6a) isolating the normal component magnetic field expansion, and taking the proper spatial derivatives.

$$U_z = -j\eta_0^{-1}\mu_z^{-1} K_x S_y \tag{3.1.14}$$

The actual electric and magnetic fields within the layer can then be determined by multiplying the spatial harmonic expansions by appropriate phase terms for each harmonic at any point on a predetermined spatial grid as follows:

$$E_y(x,y,z) = \sum_m \sum_n S_{y,(m,n)}(z) e^{-j\left(k_{x,(m,n)}x + k_{y,(m,n)}y\right)}$$
$$H_{x,z}(x,y,z) = \sum_m \sum_n U_{x,z,(m,n)}(z) e^{-j\left(k_{x,(m,n)}x + k_{y,(m,n)}y\right)} \tag{3.1.15}$$

Following similar logic for a one-dimensional, transversely periodic system having a transverse magnetic field, the matrix eigenvalue problem to be solved takes the following form:

$$\left[\frac{\partial^2 H_y}{\partial z'^2}\right] = \left[\varepsilon_x K_x \varepsilon_z^{-1} K_x - \varepsilon_x \mu_y\right][H_y] \tag{3.1.16}$$

where the electric and magnetic fields are calculated in a similar manner to the TE problem.

For one-dimensionally periodic systems in a conical mount, the y-component of the incident, reflected, and transmitted wavevectors is a constant, non-zero value. Consequently, the derivative matrix, K_y, is an identity matrix multiplied by the incident wavevector's y-component, normalized by the free-space angular wavenumber. In solving the modal problem for the case of a purely dielectric grating composed of isotropic materials in a conical mount, the most efficient manner is to start with Maxwell's Equations as given in (3.1.2), insert the proper series expansions containing the pseudo-periodic phase terms into the electric and magnetic field terms, take the necessary derivatives, and then simplify the system in to two separate eigenvalue problems. The resulting electric and magnetic field matrix eigenvalue equations are the following:

$$\frac{\partial^2 E_x}{\partial z'^2} = \left[K_x \varepsilon^{-1} K_x \varepsilon + K_y^2 - \varepsilon\right] E_x \tag{3.1.17}$$

$$\frac{\partial^2 H_x}{\partial z'^2} = \left[I + K_x^2 - \varepsilon\right] H_x \tag{3.1.18}$$

where once again the electric and magnetic fields can be calculated using the eigenvalues and eigenvectors resulting from the above equations, and performing summations over the spatial harmonic expansions.

3.2 Diffraction Grating Efficiency Calculations

Having determined the modal expansions in all homogenous and spatially periodic regions through the use of Rayleigh expansions as well as Fourier series approximations of spatially periodic modes, diffraction efficiency calculations can be performed via a mode matching of proper tangential components for the fields in each region and the selection of a particular mode(s)/diffracted order(s) into which the input energy is placed, which allows for the determination of all spatial harmonic field amplitudes.

3.2.1 One-Dimensional Diffraction Efficiency Calculations

Matching the tangential components of the electric and magnetic field harmonic expansions in the input and output homogenous layers to the grating layer results in the following homogenous system of equations:

$$\begin{bmatrix} -I & -I & W & WX & 0 & 0 \\ -jY_I & jY_I & V & -VX & 0 & 0 \\ 0 & 0 & WX & W & -I & -I \\ 0 & 0 & VX & -V & -jY_{II} & jY_{II} \end{bmatrix} \begin{bmatrix} \delta \\ R \\ f \\ b \\ T \\ 0 \end{bmatrix} = \begin{bmatrix} 0 \\ 0 \\ 0 \\ 0 \end{bmatrix} \tag{3.2.1}$$

where $X = \exp(-k_0 qd)$ for both TE and TM systems, $Y_I = (\beta_{m,input} / k_0)$, $Y_{II} = (\beta_{m,output} / k_0)$ for TE systems, and $Y_I = (\beta_{m,input} / (k_0 \mu_{input} \varepsilon_{input}))$, $Y_{II} = (\beta_{m,output} / (k_0 \mu_{output} \varepsilon_{output}))$ for TM systems.

By initially eliminating the reflection and transmission coefficients, Equation (3.2.1) can be rearranged to solve for the unknown forward and backward propagating spatial harmonic amplitudes as follows:

$$\begin{bmatrix} f \\ b \end{bmatrix} = \begin{bmatrix} \left(jY_I W + V\right) & \left(jY_I W - V\right)X \\ -\left(jY_{II} W - V\right)X & -\left(jY_{II} W + V\right) \end{bmatrix}^{-1} \begin{bmatrix} j2Y_I \delta \\ 0 \end{bmatrix} \tag{3.2.2}$$

The reflection and transmission coefficients can then be solved using the following matrix equations:

$$R = Wf + WXb - \delta \tag{3.2.3}$$

$$T = WXf + Wb \tag{3.2.4}$$

Finally, the diffraction efficiency for each diffracted order can then be determined using the above reflection and transmission coefficients.

$$DE_{m,reflected} = \left(R_m R_m^*\right)\mathrm{Re}\left(\frac{Y_{I,m}}{Y_{I,0}}\right) \tag{3.2.5}$$

$$DE_{m,reflected} = \left(T_m T_m^*\right)\mathrm{Re}\left(\frac{Y_{II,m}}{Y_{I,0}}\right) \tag{3.2.6}$$

Diffraction efficiency calculations for purely dielectric gratings in conical mountings require the rotation of the eigenvector spatial harmonic decompositions into planes that are perpendicular and parallel to the plane of incidence of the input wavevector. After rotation of the eigenvectors, the procedure for determining the diffraction efficiency for each diffracted order follows essentially the same procedure as for TE and TM mounts (presented above) and for two-dimensional gratings (presented below) [39].

3.2.2 Two-Dimensional (Crossed) Gratings

To calculate the diffraction efficiency for two-dimensional gratings, tangential components of the spatial harmonic field expansions in the grating layer first need to be rotated into planes that are perpendicular and parallel to the incident wavevector's plane of incidence. Rotation of the field harmonic expansions involves the following rotation matrices:

$$\begin{bmatrix} S_{\perp} \\ S_{//} \end{bmatrix} = \begin{bmatrix} K'_x & -K'_y \\ K'_y & K'_x \end{bmatrix} \begin{bmatrix} S_y \\ S_x \end{bmatrix} \qquad \begin{bmatrix} U_{\perp} \\ U_{//} \end{bmatrix} = \begin{bmatrix} K'_x & -K'_y \\ K'_y & K'_x \end{bmatrix} \begin{bmatrix} U_y \\ U_x \end{bmatrix} \tag{3.2.7}$$

$$\begin{bmatrix} S_y \\ S_x \end{bmatrix} = \begin{bmatrix} K'_x & K'_y \\ -K'_y & K'_x \end{bmatrix} \begin{bmatrix} S_{\perp} \\ S_{//} \end{bmatrix} \qquad \begin{bmatrix} U_y \\ U_x \end{bmatrix} = \begin{bmatrix} K'_x & K'_y \\ -K'_y & K'_x \end{bmatrix} \begin{bmatrix} U_{\perp} \\ U_{//} \end{bmatrix} \tag{3.2.8}$$

where the rotation sub-matrices are defined as follows:

$$K'_x = diagonal\left[\frac{k_{x,(m,n)}}{\sqrt{k^2_{x,(m,n)} + k^2_{y,(m,n)}}} \right] \tag{3.2.10}$$

$$K'_y = diagonal\left[\frac{k_{y,(m,n)}}{\sqrt{k^2_{x,(m,n)} + k^2_{y,(m,n)}}} \right] \tag{3.2.11}$$

These rotation operations are effectively linear transformations that are performed on the eigenvector matrices W and V.

Matching the tangential components of the electric and magnetic field harmonic expansions in the input and output homogenous layers to the grating layer results in the following homogenous system of equations:

$$\begin{bmatrix} -I & 0 & -I & 0 & W_{11} & W_{12} & W_{11}X_1 & W_{12}X_1 & 0 & 0 & 0 & 0 \\ 0 & -jZ_I & 0 & jZ_I & W_{21} & W_{22} & W_{21}X_2 & W_{22}X_2 & 0 & 0 & 0 & 0 \\ -jY_I & 0 & jY_I & 0 & V_{21} & V_{22} & -V_{21}X_1 & -V_{22}X_1 & 0 & 0 & 0 & 0 \\ 0 & -I & 0 & -I & V_{11} & V_{12} & -V_{11}X_2 & -V_{12}X_2 & 0 & 0 & 0 & 0 \\ 0 & 0 & 0 & 0 & W_{11}X_1 & W_{12}X_1 & W_{11} & W_{12} & -I & 0 & -I & 0 \\ 0 & 0 & 0 & 0 & W_{21}X_2 & W_{22}X_2 & W_{21} & W_{22} & 0 & -jZ_{II} & 0 & jZ_{II} \\ 0 & 0 & 0 & 0 & V_{21}X_1 & V_{22}X_1 & -V_{21} & -V_{22} & -jY_{II} & 0 & jZ_{II} & 0 \\ 0 & 0 & 0 & 0 & V_{11}X_2 & V_{12}X_2 & -V_{11} & -V_{12} & 0 & -I & 0 & -I \end{bmatrix} \begin{bmatrix} \delta_{0,0}\sin\psi \\ \delta_{0,0}\cos\psi \\ r_{E,\perp} \\ r_{H,\perp} \\ f_1 \\ f_2 \\ b_1 \\ b_2 \\ t_{E,\perp} \\ t_{H,\perp} \\ 0 \\ 0 \end{bmatrix} = \begin{bmatrix} 0 \\ 0 \\ 0 \\ 0 \\ 0 \\ 0 \\ 0 \\ 0 \end{bmatrix} \tag{3.2.12}$$

where $X = \exp(-k_0 qd)$ and is divided into two equal sized sub-matrices X_1 and X_2,

$Y_I = (\beta_{m,input} / k_0)$, $Y_{II} = (\beta_{m,output} / k_0)$, $Z_I = (\beta_{m,input} / (k_0 \mu_{input} \varepsilon_{input}))$, and

$Z_{II} = (\beta_{m,output} / (k_0 \mu_{output} \varepsilon_{output}))$.

By eliminating the reflection and transmission coefficients, Equation (3.2.12) can be rearranged to solve for the forward and backward propagating spatial harmonic amplitudes:

$$\begin{bmatrix} f_1 \\ f_2 \\ b_1 \\ b_2 \end{bmatrix} = \begin{bmatrix} (jY_I W_{11} - V_{21}) & (jY_I W_{12} - V_{22}) & (jY_I W_{11} - V_{21})X_1 & (jY_I W_{12} - V_{22})X_1 \\ (W_{21} - jZ_I V_{11}) & (W_{22} - jZ_I V_{12}) & (W_{21} - jZ_I V_{11})X_2 & (W_{22} - jZ_I V_{12})X_2 \\ (jY_{II} W_{11} - V_{21})X_1 & (jY_{II} W_{12} - V_{22})X_1 & (jY_{II} W_{11} - V_{21}) & (jY_{II} W_{12} - V_{22}) \\ (W_{21} - jZ_{II} V_{11})X_2 & (W_{22} - jZ_{II} V_{12})X_2 & (W_{21} - jZ_{II} V_{11}) & (W_{22} - jZ_{II} V_{12}) \end{bmatrix}^{-1} \begin{bmatrix} j2Y_I \sin\psi\delta_{0,0} \\ j2Z_I\sqrt{\mu_I \varepsilon_I}\cos\psi\delta_{0,0} \\ 0 \\ 0 \end{bmatrix} \tag{3.2.13}$$

$$\begin{bmatrix} r_{E,\perp,TE} \\ jZ_I r_{H,\perp,TE} \end{bmatrix} = Wf + WXb - \begin{bmatrix} \delta_{0,0} \\ jZ_I \delta_{0,0} \end{bmatrix} \tag{3.2.14}$$

$$\begin{bmatrix} t_{E,\perp,TE} \\ jZ_{II} t_{H,\perp,TE} \end{bmatrix} = WXf + Wb \tag{3.2.15}$$

The diffraction efficiency for each diffracted order can then be determined using the above reflection and transmission coefficients.

$$DE_{m,reflected} = \sin^2\psi \left| r_{E,\perp,(m,n)} \right|^2 \mathrm{Re}\left(\frac{Y_{I,(m,n)}}{Y_{I,(0,0)}} \right) + \cos^2\psi \left| r_{H,\perp,(m,n)} \right|^2 \mathrm{Re}\left(\frac{Z_{I,(m,n)}}{Y_{I,(0,0)}} \right) \tag{3.2.16}$$

$$DE_{m,transmitted} = \sin^2\psi \left| t_{E,\perp,(m,n)} \right|^2 \mathrm{Re}\left(\frac{Y_{II,(m,n)}}{Y_{I,(0,0)}} \right) + \cos^2\psi \left| t_{H,\perp,(m,n)} \right|^2 \mathrm{Re}\left(\frac{Z_{II,(m,n)}}{Y_{I,(0,0)}} \right) \tag{3.2.17}$$

3.3 Use of RCWA in Integrated Optics

As cleverly introduced by Lalanne and Silberstein [9, 16], the RCWA modal method can be extended to the modeling of transversely finite-sized waveguides through the incorporation of artificial absorbing material layers or non-linear, complex coordinate transforms [73] within the system's transverse unit cell. Proper selection of these absorbing parameters can numerically isolate the materials and propagating modes within a unit cell from its neighboring cell and will dampen any and all energy scattered from guided modes in the unit cell due to mode matching between layers. The most effective absorbing boundary layers are the Perfectly Matched Layer (PML) type boundaries described in Section 2.4.2. Incorporation of PML materials in this study were implemented in the manner of an anisotropic material as described by Sacks [66]. Using RCWA/PML expansions, the modes determined by the truncated Fourier series are no longer strictly orthogonal to one another, but for practical purposes the modes have been found to be "nearly-orthogonal" as discussed in Section 2.4.2. The origins of the PML concept and the definition of a PML as an anisotropic material are presented in section 3.3.1, and the incorporation of a PML into a periodic unit cell, as implemented in RCWA, is discussed in section 3.3.2.

3.3.1 Artificial Absorbing Boundary Materials and Perfectly Matched Layers

When modeling an object in any system of differential equations using a purely closed or periodic system creates a problem for attempting to model finite sized structures. The presence of "hard walls" associated with purely Dirichlet or Neumann boundary conditions or strongly coupled unit cells with periodic boundary conditions means that any scattered energy will be reflected or coupled back into the region of interest upon interacting with the boundaries.

Attempting to alleviate this problem while maintaining purely Dirichlet, Neumann, or periodic boundary conditions often means that the size of the computational window must be increased dramatically and a centrally located object of interest then only occupies a small percentage of the entire computational window. Increasing the size of the computational window utilized, regardless of boundary condition or modeling technique utilized, usually increases the expense of performing the computation in both time and memory requirements. Consequently, finding methods of minimizing the size of a computational window for a given problem is very important.

One approach that is often taken to approximate an open, Dirichlet to Neumann (DtN) boundary condition is to place an absorbing material within a computational window that will collect all of the energy from the primary object being studied. Application of this idea in the electromagnetics community developed through a number of different iterations starting with a "radiating boundary condition," [74, 75] followed by the matched layer where the computational domain is encased in an absorbing media matched to free space [65, 76], as well as a "one-way" approximation of the wave equation at a boundary [77]. A dramatic improvement in the convergence of most widely used computational methods (finite-difference, finite-element, spectral methods) can be obtained through the use of so-called Perfectly Matched Layer (PML) boundary conditions. As originally proposed by Berenger for the truncation of two-dimensional FDTD meshes [65], a PML boundary condition is a material which is impedance matched to the computational region of interest's outer boundary such that the interface is reflection-less for energy propagating at all angles, polarizations, and wavelengths. Consequently, all power is transmitted into and absorbed by the PML. Berenger's formulation of the PML boundary condition required a "split-field" modification of Maxwell's equations on the Yee grid [78]

utilized in FDTD calculations. A second interpretation of the PML boundary condition was proposed by Sacks et. al. [66], which does not require a significant modification of Maxwell's equations. This approach treats the PML region as an anisotropic material having complex permittivity and permeability properties. This anisotropic material interpretation of the PML is utilized in this work. Further equivalent interpretations of the PML concept include the idea of utilizing a complex coordinate stretching of the spatial variable included in the argument of a wave's phase term in certain regions of space [79, 80], as well as the concept of a non-linear coordinate stretching that maps infinite boundaries to finite locations [73]. This last interpretation comes closest to the idea of a true DtN boundary condition, which itself has also recently been added to the list of boundary conditions that have been utilized within a computational electromagnetics setting [81].

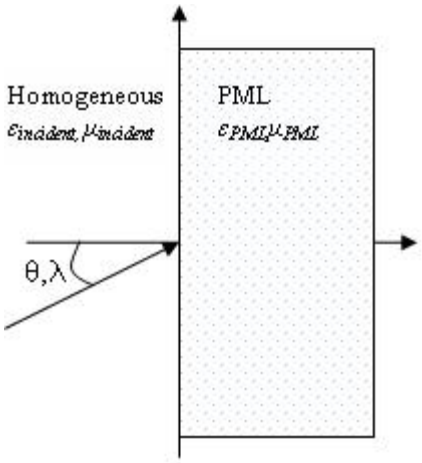

Figure 3-1 A sketch showing an interface between a homogeneous material half-space and a Perfectly Matched Layer material half-space that absorbs, without reflection, a plane wave traveling with any wavelength in any direction.

Explaining the concept of a PML as an anisotropic dielectric/magnetic material begins with considering two material layers that are impedance matched as follows:

$$\sqrt{\frac{[\mu]_{incident}}{[\varepsilon]_{incident}}} = \sqrt{\frac{[\mu]_{PML}}{[\varepsilon]_{PML}}} \Rightarrow [\mu]_{incident}[\varepsilon]_{PML} = [\varepsilon]_{incident}[\mu]_{PML} \tag{3.3.1}$$

For energy incident from a non-magnetic material upon a PML material as shown in Figure 3-1, $\mu_{incident}$ is an identity matrix and μ_{PML} is the following matrix:

$$[\mu]_{PML} = \begin{bmatrix} 1/s_x & 0 & 0 \\ 0 & s_x & 0 \\ 0 & 0 & s_x \end{bmatrix} \qquad s_x = 1 - j\delta_x \tag{3.3.2}$$

where δ_x is an absorption/gain coefficient of the material. For a PML to be truly as effective as designed here, it must be of a semi-infinite spatial extent. In most computational settings, this is rarely the case. As a result, the PML implemented within a computational environment must be of a finite spatial extent and must be truncated with a Dirichlet, Neumann, or a periodic boundary condition, as in the RCWA approach. Perfect absorption is not analytically possible within a finite PML region, but by properly choosing both the layer thickness and the value of the absorption/gain parameter δ_x, any wave incident upon the PML region can be effectively absorbed without undergoing any further interaction with the scattering object of interest . The PML absorption profile utilized in most of this study is one that was developed by our research group, and was found to be effective in most cases. Studies of varying PML properties or computational window sizes have been performed [9, 16, 22], and has shown that given an

adequate initial choice for a PML's absorbing properties, the performance of that PML is fairly robust to changes in wavelength and layer thickness.

For three dimensional systems, the PML material utilized can be either a uniaxial or a biaxial material depending on its location with the computational window. The most general material would allow for light to be perfectly absorbed along any of the three Cartesian axes and would have a permeability matrix as follows:

$$[\mu]_{PML} = \begin{bmatrix} 1/s_x & 0 & 0 \\ 0 & s_x & 0 \\ 0 & 0 & s_x \end{bmatrix} \begin{bmatrix} s_y & 0 & 0 \\ 0 & 1/s_y & 0 \\ 0 & 0 & s_y \end{bmatrix} \begin{bmatrix} s_z & 0 & 0 \\ 0 & s_z & 0 \\ 0 & 0 & 1/s_z \end{bmatrix} = \begin{bmatrix} \frac{s_y s_z}{s_x} & 0 & 0 \\ 0 & \frac{s_x s_z}{s_y} & 0 \\ 0 & 0 & \frac{s_x s_y}{s_z} \end{bmatrix} \tag{3.3.3}$$

$$s_x = 1 - j\delta_x \quad s_y = 1 - j\delta_y \quad s_z = 1 - j\delta_z$$

For absorption along any desired direction, the value of δ corresponding to that particular direction is non-zero. For the computational techniques utilized in this study, the value of δ_z is always chosen to be zero within the lamellar layers utilized for eigenmode computation. The assumption of input and output half spaces that are utilized in this study allow any light scattered into the PML material traveling in a longitudinal direction to continue propagating infinitely without contaminating the fields near the device of interest. Figure 3-2 shows the permittivity layout for a ridge waveguide structure that represents a 2D lamellar layer which can be used within a 3D eigenmode expansion computation.

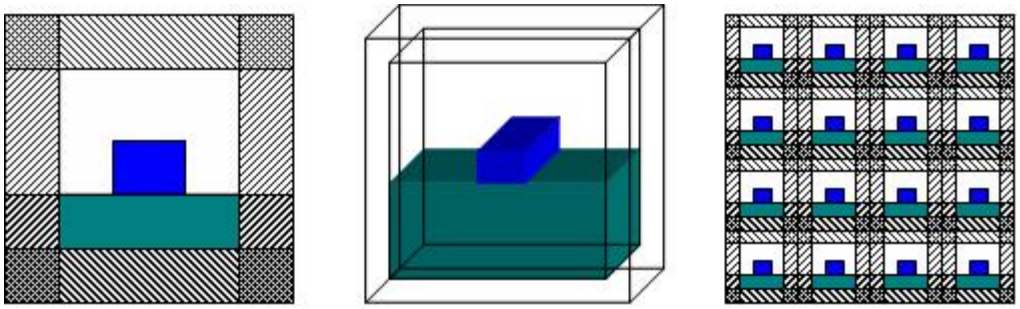

(a) (b) (c)

Figure 3-2 (a) A figure showing the transverse computational window of a ridge waveguide device with PML boundaries in the window. (b) A 3D-view of a ridge waveguide structure with PML boundaries, also showing the depth of a layer slice. (c) A transversely periodic structure where each unit supercell contains a single ridge waveguide structure. In solving for the modes of the ridge waveguide using RCWA, this structure is truly representative of the problem solved.

The ridge waveguide is surrounded by an air region, and the entire structure is surrounded by PML materials. For three dimensional structures, the PML material in this case is chosen to match its neighboring dielectric material. This choice creates the scenario of having different PML materials adjacent to one another, which generates the possibility for spurious reflections, but for a robustly designed total PML region, these interfaces usually do not present a significant problem for determining fundamental eigemode solutions given the overall absorption of the total PML regions. Robustness of an eigenmode solution for a given PML can normally be checked by varying the computational window size or by the number of spatial harmonic basis functions in an RCWA calculation (or similarly by varying the grid sampling in a FDTD or FEM computation).

3.3.2 Use of PML in RCWA

Use of PML layers in RCWA involves incorporating layers with PML properties at the borders of the computational window. To model anything except a simple slab waveguide (1D eigenmodes) or ridge waveguide (2D eigenmodes), requires the use of longitudinal mode-

matching techniques between separate layers having different eigenmodes. The actual routines for performing wave propagation through these differing layers will be explained in the next chapter, but here we will concern ourselves with methods for determining a system's reflection and transmission coefficients as well as a means for approximating conservation of energy in our finite waveguide problem.

By performing mode matching and wave propagation through a layered system, the reflection and transmission coefficients associated with each mode (each column of the modal matrices W and V) can be determined. In order to determine the actual reflection and transmission efficiencies into each mode, an overlap integral must be performed between the spatial profile of the input mode from the input half-space region and the spatial profile of each mode of the input and output half-spaces weighted by their corresponding reflection and transmission coefficients. These overlap integrals are then normalized by the magnitude of the power contained in the input mode. Given that the overlap integrals are performed on spatial modes that have been decomposed in terms of spatial harmonics, these overlap integrals can be performed as inner products between the spectral decompositions of each pair of modes. Compact expressions of the reflection efficiency for a mode m in the input half-space and a mode n in the output half-space are given as follows:

$$R_m = \left| r_m^{input} \right|^2 \frac{\left\langle W_m^{input}, V_m^{input} \right\rangle}{\left\langle W_0^{input}, V_0^{input} \right\rangle} \tag{3.3.4}$$

$$T_m = \left| t_m^{output} \right|^2 \frac{\left\langle W_m^{output}, V_m^{output} \right\rangle}{\left\langle W_0^{input}, V_0^{input} \right\rangle} \tag{3.3.5}$$

As the modes calculated using the RCWA/PML method are not truly orthogonal, energy balance between the incident, reflected, and transmitted waves does not hold identically due to

absorption of energy within the PML materials, and the non-hermitian nature of the matrix operators involved.

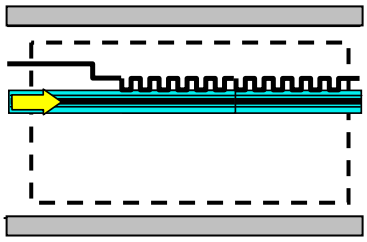

Figure 3-3 A single surface waveguide grating coupler with sampling box drawn interior to absorbing boundaries within a transverse unit cell and over the length of the structure.

By calculating the power flow around a box that is external to the PML boundary layers, it has been shown empirically that conservation of energy can be obtained to any desired accuracy by proper spatial sampling of both the transverse and longitudinal computational windows [19]. Figure 3.1 shows an example of a spatial sampling box that may be utilized for calculating conservation of energy around a simple waveguide grating coupler.

CHAPTER 4 WAVE PROPAGATION IN LAYERED MEDIA

In modeling the propagation of light through multilayered stratified media, or through structures with continuously varying surface geometries, it is often convenient, and necessary, to represent the geometry via layer stair casing. For numerical modeling techniques utilizing eigenmode expansion in longitudinally-invariant media, approximating these various geometries using stratified layered media is normally required. Any continuous or discrete variation of a structure's longitudinal material property distributions (permittivity, permeability, conductivity) require that the structure be approximated by a stack of uniform thickness layers each having distinct solutions to separate eigenvalue problems. This chapter aims to present various methods of modeling wave propagation in layered media, to discuss the strengths and weaknesses of each technique that determine when one technique is more appropriate than another, and to discuss how the building blocks of single layers may be pieced together for accurate and efficient modeling of various device geometries.

For completeness, Section 4.1 briefly introduces four separate matrix propagation methods for layered media (the transfer matrix [13, 82], the scattering matrix [16, 17, 19, 20, 83], the impedance matrix [84-86], and the hybrid matrix [87]), discusses the potential numerical instability present in two of the methods, as well as the strengths and weaknesses of each propagation method. Section 4.2 discusses the standard transfer matrix formalism in more depth, and derives the enhanced transfer matrix that properly eliminates this numerical instability. Section 4.3 presents the scattering matrix formalism, and discusses its strengths in modeling longitudinally periodic layered media as well as numerically stable calculations of internal field amplitudes, and its relationship to the longitudinal eigenmodes of a cavity.

4.1 Mode/Field Matching and Wave Propagation

For any type of eigenmode expansion technique, the propagation of light within a layer, or transmission and reflection of light between layers involves coupling between all of the modes within a layer or between adjacent layers. Expression of the field harmonic expansion within a single layer of thickness *d* was given in Equation (3.1.13) in terms of the layer's eigenvalues and eigenvectors and is restated here as follows:

$$\begin{bmatrix} S_{\tan}(z) \\ U_{\tan}(z) \end{bmatrix} = \begin{bmatrix} W & W \\ V & -V \end{bmatrix} \begin{bmatrix} \exp(k_0 q(z-d)) & 0 \\ 0 & \exp(-k_0 qz) \end{bmatrix} \begin{bmatrix} b \\ f \end{bmatrix} \tag{4.1.1}$$

Propagation of light within a layer or between layers can be expressed by the interaction of two sets of Equations based on (4.1.1). The use of mode matching methods have a long history in areas of applied mathematics, science and engineering ranging from network transmission line wave propagation [88-90], to seismic wave propagation [91-98], to atmospheric radio wave propagation [99], and quantum wave propagation [100]. For transmission and reflection between two layers, 1 and 2, the tangential components of electric and magnetic field harmonic expansions ($S_{\tan}^{(1)}(0), S_{\tan}^{(2)}(d), U_{\tan}^{(1)}(0), U_{\tan}^{(2)}(d)$) are set equal and a relationship can be determined between the field harmonic amplitudes, *b* and *f*, in each layer.

$$\begin{bmatrix} S_{\tan}^{(1)}(0) \\ U_{\tan}^{(1)}(0) \end{bmatrix} = \begin{bmatrix} W_1 X_1 & W_1 \\ V_1 X_1 & -V_1 \end{bmatrix} \begin{bmatrix} b_1 \\ f_1 \end{bmatrix} \quad \begin{bmatrix} S_{\tan}^{(2)}(d) \\ U_{\tan}^{(2)}(d) \end{bmatrix} = \begin{bmatrix} W_2 & W_2 X_2 \\ V_2 & -V_2 X_2 \end{bmatrix} \begin{bmatrix} b_2 \\ f_2 \end{bmatrix} \tag{4.1.2}$$

When determining propagation within a layer, the field harmonic amplitudes, *b* and *f*, are constant allowing for a relationship between the field expansions at both ends of a layer, ($S_{\tan}^{(1)}(0), S_{\tan}^{(1)}(d), U_{\tan}^{(1)}(0), U_{\tan}^{(1)}(d)$).

$$\begin{bmatrix} S_{\tan}^{(1)}(0) \\ U_{\tan}^{(1)}(0) \end{bmatrix} = \begin{bmatrix} W_1 X_1 & W_1 \\ V_1 X_1 & -V_1 \end{bmatrix} \begin{bmatrix} b_1 \\ f_1 \end{bmatrix} \quad \begin{bmatrix} S_{\tan}^{(1)}(d) \\ U_{\tan}^{(1)}(d) \end{bmatrix} = \begin{bmatrix} W_1 & W_1 X_1 \\ V_1 & -V_1 X_1 \end{bmatrix} \begin{bmatrix} b_1 \\ f_1 \end{bmatrix} \tag{4.1.3}$$

The four methods utilized for solving Equations (4.1.2) and (4.1.3) are generally referred to as the Transfer Matrix (T-Matrix), the Scattering Matrix (S-Matrix), the Impedance Matrix (R-Matrix), and the Hybrid Matrix (H-Matrix).

$$\begin{bmatrix} b_2 \\ f_2 \end{bmatrix} = \begin{bmatrix} \frac{1}{2}\left(W_2^{-1}W_1 + V_2^{-1}V_1\right)X_1 & \frac{1}{2}\left(W_2^{-1}W_1 - V_2^{-1}V_1\right) \\ \frac{1}{2}X_2^{-1}\left(W_2^{-1}W_1 - V_2^{-1}V_1\right)X_1 & \frac{1}{2}X_2^{-1}\left(W_2^{-1}W_1 + V_2^{-1}V_1\right) \end{bmatrix} \begin{bmatrix} b_1 \\ f_1 \end{bmatrix} \quad \text{(T-Matrix)} \quad (4.1.4)$$

$$\begin{bmatrix} b_2 \\ f_1 \end{bmatrix} = \begin{bmatrix} 2\left[W_1^{-1}W_2 + V_1^{-1}V_2\right]^{-1}X_1 & -\left[W_1^{-1}W_2 + V_1^{-1}V_2\right]^{-1}\left[W_1^{-1}W_2 - V_1^{-1}V_2\right]X_2 \\ -\left[W_2^{-1}W_1 + V_2^{-1}V_1\right]^{-1}\left[W_2^{-1}W_1 - V_2^{-1}V_1\right]X_1 & 2\left[W_2^{-1}W_1 + V_2^{-1}V_1\right]^{-1}X_2 \end{bmatrix} \begin{bmatrix} b_1 \\ f_2 \end{bmatrix} \quad \text{(S-Matrix)} \quad (4.1.5)$$

$$\begin{bmatrix} S_{\tan}(0) \\ S_{\tan}(d) \end{bmatrix} = \begin{bmatrix} -W_1\left(1+X_1^2\right)\left(1-X_1^2\right)^{-1}V_1^{-1} & 2W_1X_1\left(1-X_1^2\right)^{-1}V_1^{-1} \\ -2W_1X_1\left(1-X_1^2\right)^{-1}V_1^{-1} & W_1\left(1+X_1^2\right)\left(1-X_1^2\right)^{-1}V_1^{-1} \end{bmatrix} \begin{bmatrix} U_{\tan}(0) \\ U_{\tan}(d) \end{bmatrix} \quad \text{(R-Matrix)} \quad (4.1.6)$$

$$\begin{bmatrix} S_{\tan}(0) \\ U_{\tan}(d) \end{bmatrix} = \begin{bmatrix} 2W_1X_1\left(1+X_1^2\right)^{-1}W_1^{-1} & -W_1\left(1-X_1^2\right)\left(1+X_1^2\right)^{-1}V_1^{-1} \\ V_1\left(1-X_1^2\right)\left(1+X_1^2\right)^{-1}W_1^{-1} & 2V_1X_1\left(1+X_1^2\right)^{-1}V_1^{-1} \end{bmatrix} \begin{bmatrix} S_{\tan}(d) \\ U_{\tan}(0) \end{bmatrix} \quad \text{(H-Matrix)} \quad (4.1.7)$$

Upon an initially analyzing Equations (4.1.4) – (4.1.7), the T-Matrix and the R-Matrix can be seen to possess potential numerical instabilities due to matrix inversion. For the standard T-Matrix, numerical instability occurs when either the eigenvalues or the thickness of layer 2 are large enough to cause the exponential terms to be near zero. For the R-Matrix, numerical instability occurs when the thickness of the layer approaches zero. For modeling of diffraction grating efficiencies, where the field harmonic amplitudes and field amplitudes internal to the structure are not necessary, the cascading of these matrix methods have been reformulated in such a manner to eliminate these numerical instabilities [13, 84]. The definitions of the S-Matrix and the H-Matrix, as well as their respective recursive algorithms for cascading matrices are both numerically stable for any value of layer thickness values. The H-Matrix definition and recursive algorithm provide a relationship between the field expansions at two separate planes, whereas the S-Matrix definition and recursive algorithm provide relationships between the field harmonic amplitudes in separate layers. The choice of when to use one method over the other

depends upon the initial system information that is present and the final information that is desired. Use of the H-Matrix is more beneficial when the specific spatial profile of the input fields of a generic field distribution is known, and system response to that known distribution is desired. The S-Matrix is more beneficial when all initial energy is placed into specific modes of the input layers and the modal reflection and transmission coefficients are desired. The S-Matrix is also the most straightforward method for determining the complex modal indices of periodically layered media. In either case, the internal field expansions and field harmonic amplitudes are easily obtained in a numerically stable manner through the use of recursive propagation algorithms. In this study, only the enhanced T-Matrix algorithm and the S-Matrix algorithm were utilized for diffraction grating efficiency and integrated optical waveguide studies and will be presented in more detail in the following sections.

4.2 Enhanced Transfer Matrix Method

As presented in Equation (4.1.4), the transfer matrix relates known forward and backward propagating field harmonics in layer 1 to unknown forward and backward propagating field harmonics in layer 2. In order to make use of the transfer matrix in a numerically stable manner, the instability present due to the inversion of the exponential eigenvalue matrix X_2 must be properly handled [13]. To gain an understanding of how to properly handle this instability, it is enlightening for first expand Equation (4.1.4) into a series of block 2x2 matrix multiplications as follows:

$$\begin{bmatrix} b_2 \\ f_2 \end{bmatrix} = \begin{bmatrix} 1 & 0 \\ 0 & X_2^{-1} \end{bmatrix} \begin{bmatrix} W_2 & W_2 \\ V_2 & -V_2 \end{bmatrix}^{-1} \begin{bmatrix} W_1 & W_1 \\ V_1 & -V_1 \end{bmatrix} \begin{bmatrix} X_1 & 0 \\ 0 & 1 \end{bmatrix} \begin{bmatrix} b_1 \\ f_1 \end{bmatrix} \tag{4.2.1}$$

Cascading the transfer matrix between layers 1 and N produces the following matrix relationship:

$$\begin{bmatrix} b_N \\ f_N \end{bmatrix} = \begin{bmatrix} 1 & 0 \\ 0 & X_N^{-1} \end{bmatrix} \begin{bmatrix} W_N & W_N \\ V_N & -V_N \end{bmatrix}^{-1} \begin{bmatrix} W_{N-1} & W_{N-1} \\ V_{N-1} & -V_{N-1} \end{bmatrix} \begin{bmatrix} X_{N-1} & 0 \\ 0 & 1 \end{bmatrix} \begin{bmatrix} 1 & 0 \\ 0 & X_{N-1}^{-1} \end{bmatrix} \begin{bmatrix} W_{N-1} & W_{N-1} \\ V_{N-1} & -V_{N-1} \end{bmatrix}^{-1} \begin{bmatrix} W_{N-2} & W_{N-2} \\ V_{N-2} & -V_{N-2} \end{bmatrix} \begin{bmatrix} X_{N-2} & 0 \\ 0 & 1 \end{bmatrix} \cdots \begin{bmatrix} 1 & 0 \\ 0 & X_3^{-1} \end{bmatrix} \begin{bmatrix} W_3 & W_3 \\ V_3 & -V_3 \end{bmatrix}^{-1} \begin{bmatrix} W_2 & W_2 \\ V_2 & -V_2 \end{bmatrix} \begin{bmatrix} X_2 & 0 \\ 0 & 1 \end{bmatrix} \begin{bmatrix} 1 & 0 \\ 0 & X_2^{-1} \end{bmatrix} \begin{bmatrix} W_2 & W_2 \\ V_2 & -V_2 \end{bmatrix}^{-1} \begin{bmatrix} W_1 & W_1 \\ V_1 & -V_1 \end{bmatrix} \begin{bmatrix} X_1 & 0 \\ 0 & 1 \end{bmatrix} \begin{bmatrix} b_1 \\ f_1 \end{bmatrix} \tag{4.2.2}$$

For determining the reflection and transmission coefficients in diffraction grating problems, the exponential decay terms in the input and output regions can be disregarded without affecting the physical correctness of the solution, and the backward propagating waves in the output region are null.

$$\begin{bmatrix} R \\ \delta \end{bmatrix} = \begin{bmatrix} W_N & W_N \\ V_N & -V_N \end{bmatrix}^{-1} \begin{bmatrix} W_{N-1} & W_{N-1} \\ V_{N-1} & -V_{N-1} \end{bmatrix} \begin{bmatrix} X_{N-1} & 0 \\ 0 & 1 \end{bmatrix} \begin{bmatrix} 1 & 0 \\ 0 & X_{N-1}^{-1} \end{bmatrix} \begin{bmatrix} W_{N-1} & W_{N-1} \\ V_{N-1} & -V_{N-1} \end{bmatrix}^{-1} \begin{bmatrix} W_{N-2} & W_{N-2} \\ V_{N-2} & -V_{N-2} \end{bmatrix} \begin{bmatrix} X_{N-2} & 0 \\ 0 & 1 \end{bmatrix} \cdots \begin{bmatrix} 1 & 0 \\ 0 & X_3^{-1} \end{bmatrix} \begin{bmatrix} W_3 & W_3 \\ V_3 & -V_3 \end{bmatrix}^{-1} \begin{bmatrix} W_2 & W_2 \\ V_2 & -V_2 \end{bmatrix} \begin{bmatrix} X_2 & 0 \\ 0 & 1 \end{bmatrix} \begin{bmatrix} 1 & 0 \\ 0 & X_2^{-1} \end{bmatrix} \begin{bmatrix} W_2 & W_2 \\ V_2 & -V_2 \end{bmatrix}^{-1} \begin{bmatrix} W_1 \\ V_1 \end{bmatrix} T \tag{4.2.3}$$

The process of avoiding numerical instability then proceeds by introducing some intermediary variables:

$$\begin{bmatrix} F_1 \\ G_1 \end{bmatrix} = \begin{bmatrix} W_1 \\ V_1 \end{bmatrix} \tag{4.2.4}$$

$$\begin{bmatrix} a_2 \\ b_2 \end{bmatrix} = \begin{bmatrix} W_2 & W_2 \\ V_2 & -V_2 \end{bmatrix}^{-1} \begin{bmatrix} F_1 \\ G_1 \end{bmatrix} \tag{4.2.5}$$

which then allows for the stack of transfer matrices to be expressed as follows:

$$\begin{bmatrix} R \\ \delta \end{bmatrix} = \begin{bmatrix} W_N & W_N \\ V_N & -V_N \end{bmatrix}^{-1} \begin{bmatrix} W_{N-1} & W_{N-1} \\ V_{N-1} & -V_{N-1} \end{bmatrix} \begin{bmatrix} X_{N-1} & 0 \\ 0 & 1 \end{bmatrix} \begin{bmatrix} 1 & 0 \\ 0 & X_{N-1}^{-1} \end{bmatrix} \begin{bmatrix} W_{N-1} & W_{N-1} \\ V_{N-1} & -V_{N-1} \end{bmatrix}^{-1} \begin{bmatrix} W_{N-2} & W_{N-2} \\ V_{N-2} & -V_{N-2} \end{bmatrix} \begin{bmatrix} X_{N-2} & 0 \\ 0 & 1 \end{bmatrix} \cdots \begin{bmatrix} 1 & 0 \\ 0 & X_3^{-1} \end{bmatrix} \begin{bmatrix} W_3 & W_3 \\ V_3 & -V_3 \end{bmatrix}^{-1} \begin{bmatrix} W_2 & W_2 \\ V_2 & -V_2 \end{bmatrix} \begin{bmatrix} X_2 a_2 T \\ X_2^{-1} b_2 T \end{bmatrix} \tag{4.2.6}$$

The substitution which effectively handles the numerical instability defines the following temporary variable:

$$T = b_2^{-1} X_2 T_2 \tag{4.2.7}$$

which upon inserting into (4.1.8) creates the following expression:

$$\begin{bmatrix} R \\ \delta \end{bmatrix} = \begin{bmatrix} W_N & W_N \\ V_N & -V_N \end{bmatrix}^{-1} \begin{bmatrix} W_{N-1} & W_{N-1} \\ V_{N-1} & -V_{N-1} \end{bmatrix} \begin{bmatrix} X_{N-1} & 0 \\ 0 & 1 \end{bmatrix} \begin{bmatrix} 1 & 0 \\ 0 & X_{N-1}^{-1} \end{bmatrix} \begin{bmatrix} W_{N-1} & W_{N-1} \\ V_{N-1} & -V_{N-1} \end{bmatrix}^{-1} \begin{bmatrix} W_{N-2} & W_{N-2} \\ V_{N-2} & -V_{N-2} \end{bmatrix} \begin{bmatrix} X_{N-2} & 0 \\ 0 & 1 \end{bmatrix} \cdots \begin{bmatrix} 1 & 0 \\ 0 & X_3^{-1} \end{bmatrix} \begin{bmatrix} W_3 & W_3 \\ V_3 & -V_3 \end{bmatrix}^{-1} \begin{bmatrix} F_2 \\ G_2 \end{bmatrix} T_2 \tag{4.2.8}$$

where

$$\begin{bmatrix} F_2 \\ G_2 \end{bmatrix} = \begin{bmatrix} W_2 \left(I + X_2 a_2 b_2^{-1} \right) \\ V_2 \left(I - X_2 a_2 b_2^{-1} \right) \end{bmatrix} \tag{4.2.9}$$

This process can be repeated until a final expression is obtained involving the incidence and reflection coefficients:

$$\begin{bmatrix} W_N & W_N \\ V_N & -V_N \end{bmatrix} \begin{bmatrix} R \\ \delta \end{bmatrix} = \begin{bmatrix} F_{N-1} \\ G_{N-1} \end{bmatrix} T_{N-1} \tag{4.2.10}$$

where

$$T_{N-1} = 2 \left[W_N^{-1} F_{N-1} - V_N^{-1} G_{N-1} \right]^{-1} \delta \tag{4.2.11}$$

$$R = W_N^{-1} F_{N-1} T_{N-1} - \delta \tag{4.2.12}$$

$$T = b_2^{-1} X_2 T_2 b_3^{-1} X_3 T_3 \cdots b_l^{-1} X_l T_l \cdots b_{N-2}^{-1} X_{N-2} T_{N-2} b_{N-1}^{-1} X_{N-1} T_{N-1} \tag{4.2.13}$$

4.3 Scattering Matrix Method

The scattering matrix represents what is essentially a 4 port system that separates the information that is known initially on one-side of the matrix equation (system inputs for field harmonic amplitudes) from what is unknown on the opposite side of the equality (system outputs for field harmonic amplitudes). As was stated previously, through recursive application of scattering matrices within a stack of lamellar layers, a numerically stable method of determining the field harmonic amplitudes and field amplitudes can be obtained. In this study, the scattering

matrix technique for wave propagation was utilized to build a flexible and efficient tool for the modeling of passive waveguide and diffractive optical devices.

4.3.1 Scattering Matrix Definition

Starting from our definition of the scattering matrix in Equation (4.1.5), the sub-matrices of the scattering matrix could be defined as follows:

$$\begin{bmatrix} t_1^b & r_1^f \\ r_1^b & t_1^f \end{bmatrix} = \begin{bmatrix} 2\left[W_1^{-1}W_2 + V_1^{-1}V_2\right]^{-1} X_1 & -\left[W_1^{-1}W_2 + V_1^{-1}V_2\right]^{-1}\left[W_1^{-1}W_2 - V_1^{-1}V_2\right]X_2 \\ -\left[W_2^{-1}W_1 + V_2^{-1}V_1\right]^{-1}\left[W_2^{-1}W_1 - V_2^{-1}V_1\right]X_1 & 2\left[W_2^{-1}W_1 + V_2^{-1}V_1\right]^{-1} X_2 \end{bmatrix} \tag{4.3.1}$$

but this definition of the S-Matrix is not the most convenient definition for handling the exponential terms from various layers. By renormalizing the longitudinal coordinate system in the stack of layers, a single layer scattering matrix can be defined as following manner. As shown in Figure 4.1, the layered media is defined such that the origin is placed at the output.

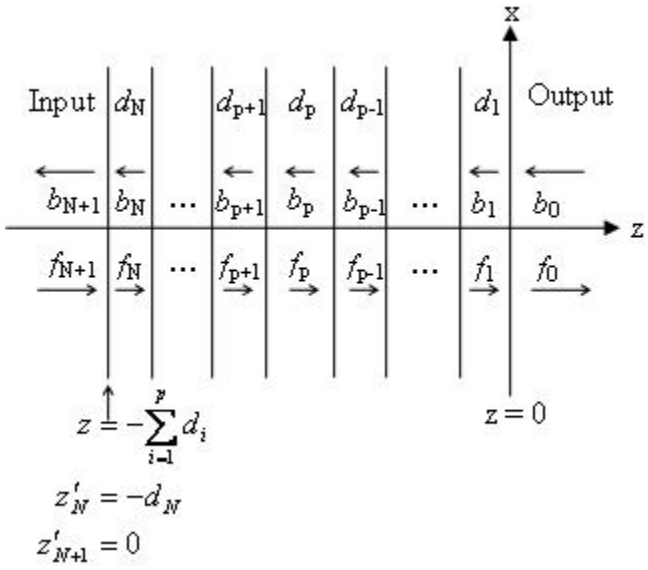

Figure 4-1 Sketch showing a stack of layers and the associated coordinate system, distances, layer labels, and field harmonic labels used in the scattering matrices developed in this section.

The overall distance from the origin within any layer is defined to be a negative quantity, but the thickness value utilized in the exponential eigenvalue matrices correspond to a negatively valued distance measured from the input side of a particular layer, $z'_p = z + \sum_{i=1}^{p=1} d_i < 0$. Given these definitions for the longitudinal coordinate system, the amplitudes of the field expansions within a single layer can be expressed as follows:

$$\begin{bmatrix} S_{\tan,p}(z) \\ U_{\tan,p}(z) \end{bmatrix} = \begin{bmatrix} W_p \exp(k_0 q_p z'_p) & W_p \exp(-k_0 q_p z'_p) \\ V_p \exp(k_0 q_p z'_p) & -V_p \exp(-k_0 q_p z'_p) \end{bmatrix} \begin{bmatrix} b_p \\ f_p \end{bmatrix} \tag{4.3.2}$$

At the interface between the pth and pth + 1 layers, the location in the pth layer is $z'_p = -d_p$ and the location in the pth + 1 layer is $z'_{p+1} = 0$. Setting equal the tangential fields in these two layers leads to the following equality:

$$\begin{bmatrix} W_p X_p & W_p X_p^{-1} \\ V_p X_p & -V_p X_p^{-1} \end{bmatrix} \begin{bmatrix} b_p \\ f_p \end{bmatrix} = \begin{bmatrix} W_{p+1} & W_{p+1} \\ V_{p+1} & -V_{p+1} \end{bmatrix} \begin{bmatrix} b_{p+1} \\ f_{p+1} \end{bmatrix} \tag{4.3.3}$$

The interface scattering matrix between two layers can then be expressed in the following manner:

$$\begin{bmatrix} b_{p+1} \\ f_p \end{bmatrix} = \begin{bmatrix} 2\left[W_p^{-1}W_{p+1} + V_p^{-1}V_{p+1}\right]^{-1} X_p & -\left[W_p^{-1}W_{p+1} + V_p^{-1}V_{p+1}\right]^{-1}\left[W_p^{-1}W_{p+1} - V_p^{-1}V_{p+1}\right] \\ -X_p\left[W_{p+1}^{-1}W_p + V_{p+1}^{-1}V_p\right]^{-1}\left[W_{p+1}^{-1}W_p - V_{p+1}^{-1}V_p\right]X_p & 2X_p\left[W_{p+1}^{-1}W_p + V_{p+1}^{-1}V_p\right]^{-1} \end{bmatrix} \begin{bmatrix} b_p \\ f_{p+1} \end{bmatrix} \tag{4.3.4}$$

$$\begin{bmatrix} t_p^b & r_p^f \\ r_p^b & t_p^f \end{bmatrix} = \begin{bmatrix} 2\left[W_p^{-1}W_{p+1} + V_p^{-1}V_{p+1}\right]^{-1} X_p & -\left[W_p^{-1}W_{p+1} + V_p^{-1}V_{p+1}\right]^{-1}\left[W_p^{-1}W_{p+1} - V_p^{-1}V_{p+1}\right] \\ -X_p\left[W_{p+1}^{-1}W_p + V_{p+1}^{-1}V_p\right]^{-1}\left[W_{p+1}^{-1}W_p - V_{p+1}^{-1}V_p\right]X_p & 2X_p\left[W_{p+1}^{-1}W_p + V_{p+1}^{-1}V_p\right]^{-1} \end{bmatrix} \tag{4.3.5}$$

4.3.2 Redheffer's Star Product

Propagation of energy through a stack of layers requires the cascading of scattering matrices using the Redheffer star product [16, 17, 19, 20, 89, 90, 101]. This star product is a type of linear fractional transformation that maintains the relationship between the system inputs

and outputs on opposite sides of the resulting matrix expression. The Redheffer star product and resulting scattering matrix between the interface scattering matrices for interfaces p – p+1 and p+1 – p+2 can be expressed as follows:

$$\begin{bmatrix} b_{p+2} \\ f_p \end{bmatrix} = \begin{bmatrix} T_{p+1}^b & R_{p+1}^f \\ R_{p+1}^b & T_{p+1}^f \end{bmatrix} \begin{bmatrix} b_p \\ f_{p+2} \end{bmatrix} \tag{4.3.6}$$

$$\begin{bmatrix} T_{p+1}^b & R_{p+1}^f \\ R_{p+1}^b & T_{p+1}^f \end{bmatrix} = \begin{bmatrix} t_{p+1}^b & r_{p+1}^f \\ r_{p+1}^b & t_{p+1}^f \end{bmatrix} * \begin{bmatrix} t_p^b & r_p^f \\ r_p^b & t_p^f \end{bmatrix} \tag{4.3.7}$$

$$T_{p+1}^b = t_{p+1}^b \left[I - r_p^f r_{p+1}^b \right]^{-1} t_p^b \tag{4.3.8}$$

$$R_{p+1}^b = r_p^b + t_p^f r_{p+1}^b \left[I - r_p^f r_{p+1}^b \right]^{-1} t_p^b \tag{4.3.9}$$

$$R_{p+1}^f = r_{p+1}^f + t_{p+1}^b r_p^f \left[I - r_{p+1}^b r_p^f \right]^{-1} t_p^f \tag{4.3.10}$$

$$T_{p+1}^f = t_p^f \left[I - r_{p+1}^b r_p^f \right]^{-1} t_p^f \tag{4.3.11}$$

By cascading star products for all layers in a stack, a relationship can be determined between the input and output infinite half-space modes.

The inverted matrix $\left[I - rr \right]^{-1}$, is known as the reverberation operator, and can be considered as an infinite summation of reflections between two interfaces. The reverberation operator is intimately related to the modes of a longitudinal cavity as well as the gain threshold required for laser resonators. This infinite summation is one reason that in the presence of evanescent waves, the scattering matrix does not possess a numerically stable inverse operation.

4.3.3 Internal Field Harmonic Amplitudes

Once the field harmonic amplitudes are known for the input and output half-spaces, the field harmonic amplitudes for internal layers can then be determined in a numerically stable manner. By knowing the two scattering matrices (S_L and S_R) representing all layers on each side of a plane of interest, as well as the forward and backward field harmonic amplitudes on the

input and output sides of the region of interest (b_L, f_L, b_R, f_R), the internal field harmonics at this plane of interest can be determined as follows:

$$\begin{bmatrix} b_L \\ f_M \end{bmatrix} = \begin{bmatrix} T_L^b & R_L^f \\ R_L^b & T_L^f \end{bmatrix} \begin{bmatrix} b_M \\ f_L \end{bmatrix} \qquad \begin{bmatrix} b_M \\ f_R \end{bmatrix} = \begin{bmatrix} T_R^b & R_R^f \\ R_R^b & T_R^f \end{bmatrix} \begin{bmatrix} b_R \\ f_M \end{bmatrix} \tag{4.3.12}$$

$$f_M = \left[I - R_L^b R_R^f \right]^{-1} \left[R_L^b T_R^b b_R + T_L f_L \right] \tag{4.3.13}$$

$$b_M = T_R^b b_R + R_R^f f_M \tag{4.3.14}$$

4.3.4 Incorporating Homogeneous Zero-Thickness Layers

Within an isotropic, homogeneous layer, solving of the necessary eigenvalue problem results in eigenvector matrices that are diagonal matrices. When the eigenvalue problem solved is for the tangential electric fields, the electric field eigenvector matrix is an identity matrix, and the corresponding magnetic field eigenvector matrix is a diagonal matrix containing the layer's eigenvalues (normal direction propagation constants). In this case, the electric field expansion amplitudes can be determined as the simple sum of the forward and backward field harmonic amplitudes in the layer, and the magnetic field expansion amplitudes can be determined as the difference of these forward and backward field harmonic amplitudes multiplied by this diagonal magnetic field eigenvector matrix.

$$\begin{bmatrix} S_{\tan} \\ U_{\tan} \end{bmatrix} = \begin{bmatrix} I & I \\ Q & -Q \end{bmatrix} \begin{bmatrix} b_{uniform} \\ f_{uniform} \end{bmatrix} = \begin{bmatrix} b_{uniform} + f_{uniform} \\ Q\left(b_{uniform} - f_{uniform}\right) \end{bmatrix} \tag{4.3.14}$$

$$Q_{m,n} = \begin{cases} diagonal\left[\sqrt{k_{x(m,n)}^2 + k_{y(m,n)}^2 - \mu\varepsilon}\right] & TE \\ diagonal\left[\sqrt{k_{x(m,n)}^2 + k_{y(m,n)}^2 - \mu\varepsilon} / \mu\varepsilon\right] & TM \\ \begin{bmatrix} \sqrt{k_{x(m,n)}^2 + k_{y(m,n)}^2 - \mu\varepsilon} & 0 \\ 0 & \mu\varepsilon / \sqrt{k_{x(m,n)}^2 + k_{y(m,n)}^2 - \mu\varepsilon} \end{bmatrix} & 2D \end{cases} \tag{4.3.15}$$

Utilizing Equations (4.3.2) and (4.3.14), the tangential fields in a periodic layer surrounded by identical homogenous, isotropic layers may be set equal as follows:

$$\begin{bmatrix} I & I \\ Q & -Q \end{bmatrix} \begin{bmatrix} b_{uniform,L} \\ f_{uniform,L} \end{bmatrix} = \begin{bmatrix} WX & WX^{-1} \\ VX & -VX^{-1} \end{bmatrix} \begin{bmatrix} b \\ f \end{bmatrix}$$
$$\begin{bmatrix} W & W \\ V & -V \end{bmatrix} \begin{bmatrix} b \\ f \end{bmatrix} = \begin{bmatrix} I & I \\ Q & -Q \end{bmatrix} \begin{bmatrix} b_{uniform,R} \\ f_{uniform,R} \end{bmatrix} \tag{4.3.16}$$

The composite scattering matrix for these two interfaces takes the following form:

$$\begin{bmatrix} b_{uniform,L} \\ f_{uniform,R} \end{bmatrix} = \begin{bmatrix} t & r \\ r & t \end{bmatrix} \begin{bmatrix} b_{uniform,R} \\ f_{uniform,L} \end{bmatrix} \tag{4.3.17}$$

where the sub-matrices can be defined as follows:

$$r = D^{-1}C + 4D^{-1}XA^{-1}BX\left[I - A^{-1}BXA^{-1}BX\right]^{-1}A^{-1} \tag{4.3.18}$$
$$t = 4D^{-1}X\left[I - A^{-1}BXA^{-1}BX\right]^{-1}A^{-1} \tag{4.3.19}$$
$$A^{-1} = \left[V + QW\right]^{-1}Q \tag{4.3.20}$$
$$A^{-1}B = \left[V + QW\right]^{-1}\left[V - QW\right] \tag{4.3.21}$$
$$D^{-1} = W\left[V + QW\right]^{-1}V \tag{4.3.22}$$
$$D^{-1}C = -W\left[V + QW\right]^{-1}\left[V - QW\right]W^{-1} \tag{4.3.23}$$

By analyzing Equations (4.3.14) and (4.3.17), the advantages of surrounding all transversely periodic lamellar layers with zero-thickness homogeneous layers becomes apparent. These additions to the system do not change the physical nature of the problem being studied, but they

create symmetry in the single layer scattering matrix that can reduce memory storage requirements by half for a single layer and they allow for the field calculations throughout the internal layers of a structure to be obtained as a simple sum and difference of plane waves (as opposed to a full matrix-vector product). The usefulness of longitudinal symmetry also extends beyond a single layer. When a stack of layers is longitudinally symmetric, the composite scattering matrix shares these same properties. Furthermore, a binary-based application of the Redheffer star-product [19, 20], which will be explained in Appendix D, can be executed far more efficiently in the presence of longitudinal symmetry.

Once the field harmonic amplitudes are known within the homogeneous layers surrounding a transversely periodic lamellar layer, the field harmonic amplitudes within that lamellar layer can then be calculated without using interface scattering matrices as follows:

$$\begin{bmatrix} b \\ f \end{bmatrix} = \begin{bmatrix} \frac{1}{2}W^{-1}\left(b_{uniform,R} + f_{uniform,R}\right) - \frac{1}{2}V^{-1}Q\left(b_{uniform,R} - f_{uniform,R}\right) \\ \frac{1}{2}W^{-1}\left(b_{uniform,L} + f_{uniform,L}\right) - \frac{1}{2}V^{-1}Q\left(b_{uniform,L} - f_{uniform,L}\right) \end{bmatrix} \tag{4.3.24}$$

The corresponding field amplitudes within the layer can then be determined as follows:

$$\begin{aligned} S_{\tan}(z) &= W\left[\exp\left(k_0 q\left(z-d\right)\right)b + \exp\left(-k_0 qz\right)\right] \\ U_{\tan}(z) &= V\left[\exp\left(k_0 q\left(z-d\right)\right)b + \exp\left(-k_0 qz\right)\right] \end{aligned} \tag{4.3.25}$$

CHAPTER 5 MULTILAYER MULTIMODE GUIDED MODE RESONANT FILTERS

Resonant grating structures are devices that utilize spatial periodicity and energy storage to provide narrowband spectral and spatial filtering of a free-space or guided optical wave [45, 102]. The narrowband filtering provided by a transversely periodic grating structure can be either a reflection [45, 102-111] or a transmission filter [112, 113]. In either case, the transverse periodicity that gives rise to the diffraction process utilized for filtering is often not wholly sufficient for producing an acceptable optical filter since it alone does not address the broadband behavior of the device. A desirable narrowband optical filter is a device providing for full reflection or transmission of energy over a predefined spectral or angular range, whereas outside of that range the device performs in the completely opposite manner. To accomplish this contrasting behavior, it has been noted [113, 114] that by partially decoupling the diffraction process from the energy storage/wave guiding process, narrowband filters having nearly 100% reflection or transmission that also have nearly 0% out-of-band reflection or transmission respectively can be designed more easily than through use of a single periodic layer alone.

A single grating layer with a single separate wave guiding layer is usually designed to support a single leaky mode that produces resonant filtering over a single spectral or angular range. While the design of resonant grating devices that support multiple leaky modes producing multiple resonances has received some attention in the literature [108, 115, 116], there are varied methods of exploiting multiple leaky modes. This chapter aims to briefly discuss these various means of exploiting multiple leaky mode resonant grating devices, and then present in more detail the structure under study in this work: the multilayer, multimode guided mode resonant filter.

The chapter begins with a brief discussion of the history of diffraction grating anomalies and the theory of resonant gratings. Then the physical and mathematical underpinnings of guided mode resonance are presented. Next, effective medium theory and dielectric waveguide theory are utilized to explore the nature of resonance separation for multimode guided mode resonant structures. Using these tools, the real-valued dispersion properties of multilayer structures are studied and an initial approach for designing resonance separations is presented. Then, through the use of diffraction grating theory and explicit numerical tools like RCWA, the complex band structures of multilayer, multimode resonant gratings are presented. By using these complex band structures, a multi-parameter design/optimization approach is developed for modeling multilayer, multimode guided mode resonant reflection filters that produce multiple narrowband spectral resonances with broadened angular acceptance at normal and obliquely incident angles.

5.1 Historical Background of Resonant Gratings

The study of resonant grating devices has a long history beginning with R.W. Wood's experimental observations of "anomalous" behavior present in the intensity variations of diffraction orders over narrow frequency ranges [46]. From this initial set of observations, the explanation for this observed anomalous behavior of diffraction gratings has been continually developed over the past century, and can now be readily explained by two separate phenomena; the redistribution of energy associated with the passing off of a diffracted order and the coupling of energy to leaky modes supported by the grating structure. While a thorough historical account of the development of resonant grating theory, and guided mode resonant devices, has been provided elsewhere [117], a few of the major highlights of this development are restated here.

Following the work of Wood, Lord Rayleigh ascribed the presence of grating anomalies to the passing off of diffracted orders with a change in wavelength or incident angle, arguing that as a diffracted order reaches its cut-off condition the energy must be redistributed among diffracted orders [47, 48]. Fano was the first to connect the presence of grating anomalies to the coupling to surface waves in metallic gratings as well as describe the spectral shape of these anomalies nearly twenty-five years later [118, 119]. The next major development was presented by Hessel and Oliner when they implemented a model involving a periodically variation in surface impedance that was approximated using a Fourier series expansion [120]. By coupling this model with a Rayleigh expansion external to the grating, the resulting linear systems treatment of the grating problem was able to identify both the redistribution of energy with the passing off of a diffracted order and the coupling to leaky modes supported by a grating-waveguide. Through further refinement of the ideas presented by Hessel and Oliner, Nevière further explained the presence of grating anomalies as the coupling to resonant modes supported by the grating [106, 121]. He later showed how the complex modal index associated with a grating mode describes the Lorentzian shape of the grating resonances [45]. During this same period, Peng and Tamir developed an explicit Fourier-series expansion, scattering matrix method for calculating the complex modal indices associated with a periodically modulated waveguide [23]. With much of the physics of grating resonance explained, Mashev and Popov [105], and shortly thereafter Magnusson and Wang [102], began to investigate the use of resonant gratings as narrowband optical filters, as well as use for performing a variety of other functionalities. With the physical explanation grating resonances, as well as numerical and phenomenological modeling tools in place, much of the theoretical work of the last twenty five years surrounding the study of grating resonances has gone into developing an understanding of the means of

controlling resonance properties (spectral/spatial location, bandwidth) and total system response (reflection/transmission contrast) to a variety of input conditions.

5.2 Fundamentals of Grating Resonances

As stated in the previous section, the "anomalous" behavior that can be observed in the spectral and/or angular reflection or transmission response of a diffraction grating to an incident wave can be explained as either the redistribution of energy with the passing-off of a diffracted order or the coupling to a complex valued leaky mode supported by a grating-waveguide. It is the latter of these two mechanisms that lends itself to the engineering of spatial and spectral filtering devices. By properly controlling the structural parameters of a grating waveguide, optical filters can be designed that possess a narrowband spectral response, a broadband angular response, and a nearly 100% contrast between in-band and out-of-band reflection and transmission.

An explicit explanation of the resonant grating phenomena utilized in resonant grating filters begins with a definition of the complex mode supported by a periodic system. A grating's leaky mode tangential propagation constant is defined as follows:

$$k_{\text{mode}} = k_{\text{mode,real}} - j\alpha_{\text{mode}} \tag{5.2.1}$$

$$\frac{k_{\text{mode}}}{k_0} \equiv n_{\text{mode}} = n'_{\text{mode}} - jn''_{\text{mode}} \qquad k_0 = \frac{2\pi}{\lambda} \tag{5.2.2}$$

For a plane wave incident upon the grating, the tangential component of the wave can be expressed using the grating equation. For TE incident light on a one-dimensional periodicity, the tangential x-component of the propagation constant can be expressed as follows:

$$k_{x,p} = k_{incident} - pK \tag{5.2.3}$$

$$\frac{k_{x,p}}{k_0} = n_{incident} \sin\theta_{incident} - p\frac{\lambda}{\Lambda_x} \tag{5.2.4}$$

Coupling between an incident wave and grating's leaky mode determines the spectral and spatial location of the resonance, and it occurs when the real part of the tangential propagation constants defined in Equations (5.2.2) and (5.2.4) are approximately equal.

$$n'_{\text{mode}} \cong n_{incident} \sin\theta_{incident} - p\frac{\lambda}{\Lambda_x} \tag{5.2.5}$$

As was shown by Nevière [45], when coupling occurs between an incident plane wave and a single complex mode, the spectral and spatial bandwidth of the grating's Lorentzian shaped resonant response is directly proportional to the imaginary part of the leaky mode index. The relationships between the spectral and spatial bandwidths and the imaginary leaky mode index are the following:

$$\Delta\lambda_{FWHM} = 2n''_{\text{mode}}\Lambda \tag{5.2.6}$$

$$\Delta\theta_{FWHM} = 2n''_{\text{mode}} \tag{5.2.7}$$

At normal incidence, the tangential components of both the +1 and -1 diffracted orders are phase-matched to equal magnitude leaky mode propagation constants traveling in opposing directions. In this situation, it has now been often noted that while the spectral bandwidth of the resonant grating can remain very narrow, on the order of a few Angstroms, the angular bandwidth can often become quite broad, many angular degrees [117]. Studying the manner in which to control this pair of properties for normal incidence has now been widely studied [117, 122-126], and has also been extended to the idea of increased angular tolerance for obliquely incident waves as well [117, 125, 127]. In the case of oblique incidence, the phase matching occurs when two diffracted orders become phase matched to two counter-propagating complex

grating modes of differing magnitudes. It is this idea that we exploit in this study to design, multilayer, multimode resonant grating filters that have narrow spectral resonances, and broadened angular resonances at nearly a single angle of incidence, be it normal or oblique.

5.3 Effective Medium Theory and Waveguide Theory for Modeling Multilayer Grating Waveguides

While the concept of resonant coupling to grating leaky modes is valid for gratings of almost any periodicity, in practice a grating periodicity that produces multiple diffracted orders in either the reflected or transmitted regions, for reflection or transmission filters respectively, is not very practical. As the main purpose of most optical filters is to either fully reflect or fully transmit waves of a specific frequency band in a specific range of directions, the presence of higher order diffraction can reduce the amount of energy passed to a desired diffraction order. Consequently, resonant gratings are often configured with "sub-wavelength gratings" that cut-off all but the zero order from propagating.

For modeling the properties of sub-wavelength periodicity it can often be sufficient to consider the grating layer as an effective homogeneous medium, making use of approximate methods to model both the grating resonance and broadband behavior. The means by which this approximation of a homogenous medium can be made varies in complexity from simplistic to rigorous. Although in any plausible model, the results reflect the fact that a sub-wavelength grating made of isotropic materials will behave as an anisotropic material with varying refractive indices between the grating's tangential and normal directions.

In the most simplistic approach, the tangential component of a grating's permittivity is modeled as a weighted sum of the two materials comprising the grating layer, where the weights are the fractional composition of each material in the layer.

$$n_{\perp}^2 = \varepsilon_{\perp} = \varepsilon_{high}(f) + \varepsilon_{low}(1-f) \tag{5.3.1}$$

where f is fractional part of the grating period occupied by the high index material. Similarly, the normal component of a grating's impermittivity is modeled as a weighted sum of the two materials in the grating layer.

$$\frac{1}{n_{\parallel}^2} = \frac{1}{\varepsilon_{\parallel}} = \frac{f}{\varepsilon_{high}} + \frac{1-f}{\varepsilon_{low}} \tag{5.3.2}$$

These relationships are equivalent to keeping only the 0^{th} order term in a Fourier harmonic expansion of the permittivity and impermittivity respectively. Consequently, as the index contrast of the two materials increases, this approximation becomes less accurate.

A more accurate approach to an effective medium theory of binary gratings was presented by Rytov [21]. In this approach, a rigorous evaluation of the dispersion relation is derived which is equivalent to Equation (2.3.5) except that the tangential component of the input wave is parallel to the grating interface. Consequently, cosine term in (2.3.5), which contains information about the tangential phase of the input wave, is equal to zero.

$$\cosh(\gamma_1 d_1)\cosh(\gamma_2 d_2) + \frac{1}{2}\left(\frac{\gamma_1'}{\gamma_2'} + \frac{\gamma_2'}{\gamma_1'}\right)\sinh(\gamma_1 d_1)\sinh(\gamma_2 d_2) = 0 \tag{5.3.3}$$

where the transverse propagation constant, γ, is related to the waveguide modal propagation constant, β, within a single layer as follows:

$$\left(\frac{2\pi}{\lambda}\right)^2 \mu_{layer}\varepsilon_{layer} = -\gamma_{layer}^2 + \beta^2 \tag{5.3.4}$$

and $\gamma'_{layer} = \dfrac{\gamma_{layer}}{\mu_{layer}}$ for TE waveguides and $\gamma'_{layer} = \dfrac{\gamma_{layer}}{\varepsilon_{layer}}$ for TM waveguides.

Upon applying various trigonometric identities, the dispersion relation in (5.3.3) can be expressed as follows:

$$\gamma'_2 \tanh\left(\frac{\gamma_2 d}{2}\right) + \gamma'_1 \tanh\left(\frac{\gamma_1 d}{2}\right) = 0 \tag{5.3.5}$$

Rytov's approximation then consists of taking a power series approximation to Equation (5.3.5). If only the 0^{th} order term is kept, then the Equations in (5.3.1) or (5.3.2) are obtained for TE or TM respectively. As with any power series expansion, the accuracy of the approximation increases by retaining more terms in the series. By keeping the second order terms, one obtains the following expressions for TE and TM respectively:

$$n_{\perp}^2 = \varepsilon_{\perp} = \varepsilon_{low} + \left(\varepsilon_{high} - \varepsilon_{low}\right) f + \left(\varepsilon_{high} - \varepsilon_{low}\right)^2 \frac{\pi}{3} f^2 (1-f)^2 \left(\frac{\Lambda}{\lambda}\right)^2 \tag{5.3.6}$$

$$n_{\parallel}^2 = \varepsilon_{\parallel} = \frac{\varepsilon_{high}\varepsilon_{low}}{\varepsilon_{high} + \left(\varepsilon_{low} - \varepsilon_{high}\right) f} + \frac{\varepsilon_{high}\varepsilon_{low}\left(\varepsilon_{high} - \varepsilon_{low}\right)^2 \left(\varepsilon_{low} + \left(\varepsilon_{high} - \varepsilon_{low}\right) f\right)}{\left(\varepsilon_{high} + \left(\varepsilon_{low} - \varepsilon_{high}\right) f\right)^3} \frac{\pi^2}{3} f^2 (1-f)^2 \left(\frac{\Lambda}{\lambda}\right)^2 \tag{5.3.7}$$

It has been previously shown that as the index contrast, grating period to wavelength ratio, and grating thickness to wavelength ratio increase, the effectiveness of effective medium theories for modeling resonant gratings decreases [128-130]. While no homogenous thin-film approximations produce rigorous solutions to the resonant grating problem, the most accurate means of using an effective medium theory is to solve the transcendental dispersion problem in Equation (5.3.3) or (5.3.5) directly for the fundamental modal propagation constant, β. The modal index can be derived from this modal propagation constant and this quantity is then utilized as the refractive index of the homogeneous thin-film representing the grating.

By incorporating this homogeneous thin-film into the multilayer waveguide, a solution to the multilayer dispersion relation similar to Equation (2.2.37) provides an approximate value for the real-modal indices of the multilayered grating waveguide. To determine the location of the resonances for a multilayered grating waveguide using an effective medium approximation, the transcendental modal solution of Equation (2.3.5) must be determined over a range for a parameter of interest (wavelength, period). The grating equation is then solved for each diffraction order present in the multilayer waveguide. As the concept of refractive index and angle of propagation are only truly defined within a single material layer, only the solution to the grating equation at normal incidence is determined for each diffracted order. The intersection of the multilayer modal index spectral curves with the spectral curves associated with the diffraction orders satisfy the requirements of Equation (5.2.5) and approximate the spectral location of the multilayer waveguide grating resonances. This approach to using an effective medium in the approximation of multilayer multimode grating resonances was introduced in Liu et al [115], but in this paper they utilized both the 0^{th} order effective medium approximation and separate waveguide dispersion relations for two separate high index regions surrounding a grating layer, as opposed to single dispersion relation for the multilayer waveguide stack used here. Using the solution to transcendental dispersion relations for both a grating layer to approximate an effective medium and a multilayer waveguide provides a more accurate approximation of all modal indices within a multimode structure.

5.4 Real-Valued Dispersion Tailoring for the Design of Multiple Resonance Locations

5.4.1 Single Layer, Multimode Structures

One of the simplest manners for creating a resonant grating structure supporting multiple resonances is to couple a diffraction grating layer with a single optically thick layer of material. The single layer of material is thick enough to support multiple waveguide modes, each of which can be coupled to a diffracted order having a proper tangential wavevector component. Figure 5-1 shows the two modes supported by a multilayer waveguide grating composed of only three materials as well as the modal index curves and 0^{th} order reflection for this waveguide grating calculated using RCWA. The structure is composed of an infinite substrate of index $n_{sub} = 1.47$, an infinite superstrate of index $n_{sup} = 1$, a high index film layer of index $n_{film} = 2.5$, and a grating layer with refractive indices $n_{high} = 1.47$ and $n_{low} = 1$. The grating periodicity is chosen to be 220 nm with a 50% high index fill factor.

While the fabrication complexity of a single material layer for the waveguide is minimal, this configuration also provides the least flexibility for tailoring the shape of the modal index curves, and hence the separation of resonances. Figures 5-2 through 5-4 show how the modal index curves and reflection efficiencies supported by the multimode waveguide change as the thickness of the high index film increases.

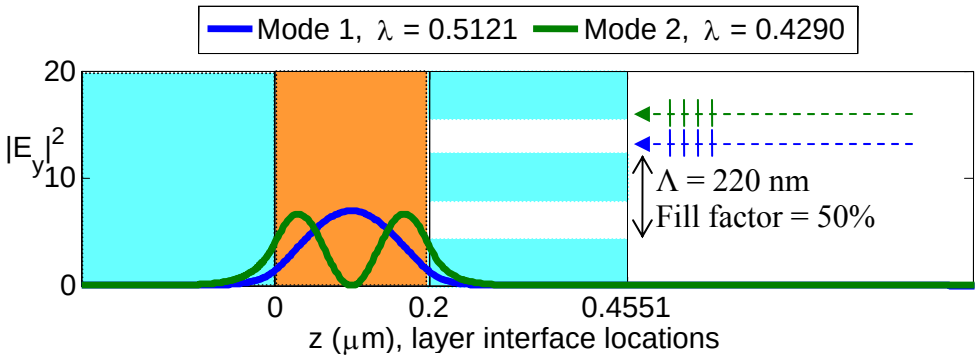

(a)

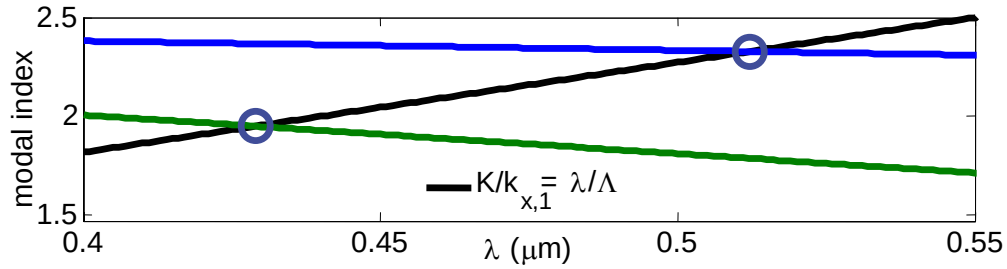

(b)

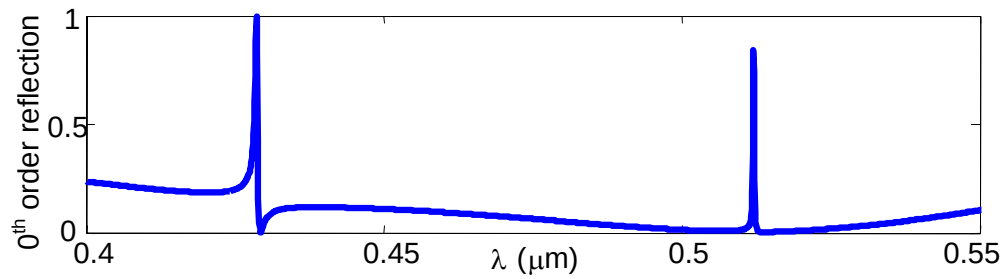

(c)

Figure 5-1 (a) Figure showing both the index distribution and spatial mode profile for the two modes supported by the single waveguiding layer GMR structure. (b) The real modal index distribution of the two modes supported by the structure as well as the modal index of the ±1 tangential diffracted order in free space, whose intersection indicates the location of a resonance. (c) The 0^{th} order reflection response for the structure calculated using RCWA showing the spectral resonance response.

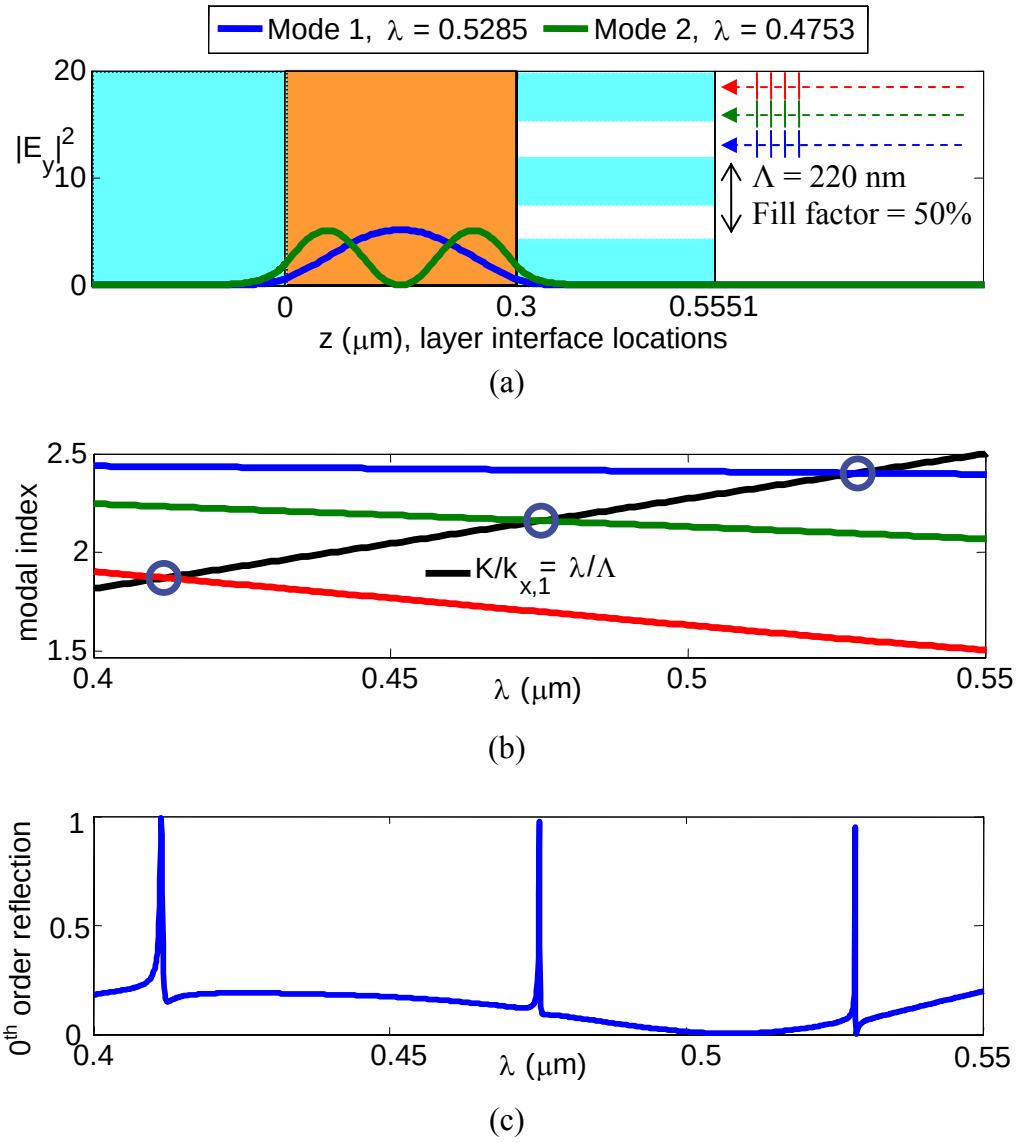

Figure 5-2 (a) Figure showing both the index distribution and spatial mode profile for the first two modes supported by the single waveguiding layer GMR structure. (b) The real modal index distribution of the three modes supported by the structure as well as the modal index of the ±1 tangential diffracted order in free space, whose intersection indicates the location of a resonance. (c) The 0^{th} order reflection response for the structure calculated using RCWA showing the spectral resonance response.

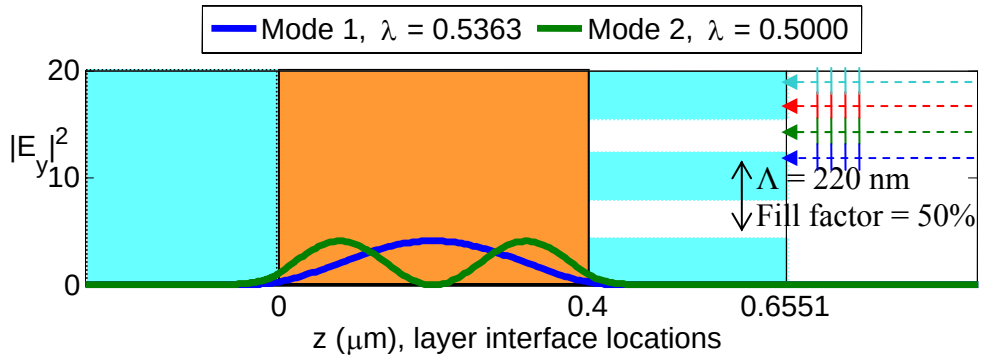

(a)

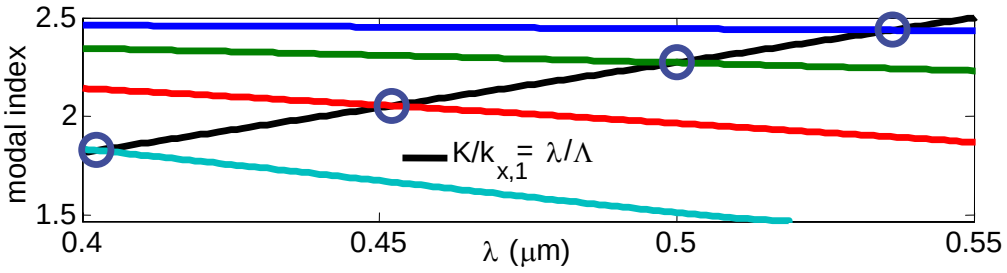

(b)

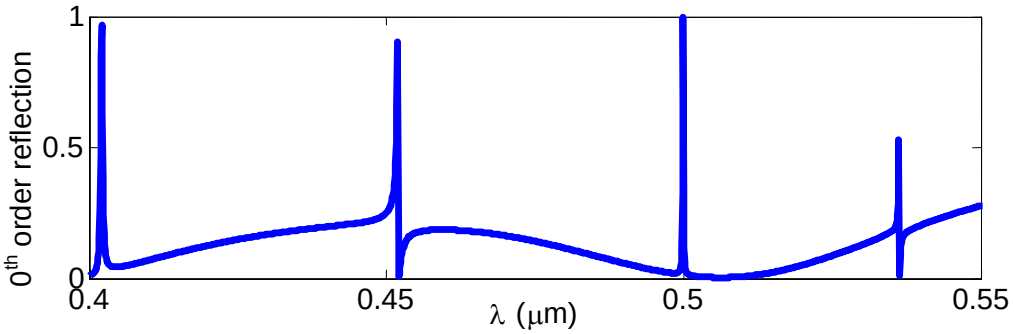

(c)

Figure 5-3 (a) Figure showing both the index distribution and spatial mode profile for the first two modes supported by the single waveguiding layer GMR structure. (b) The real modal index distribution of the four modes supported by the structure as well as the modal index of the ±1 tangential diffracted order in free space, whose intersection indicates the location of a resonance. (c) The 0^{th} order reflection response for the structure calculated using RCWA showing the spectral resonance response.

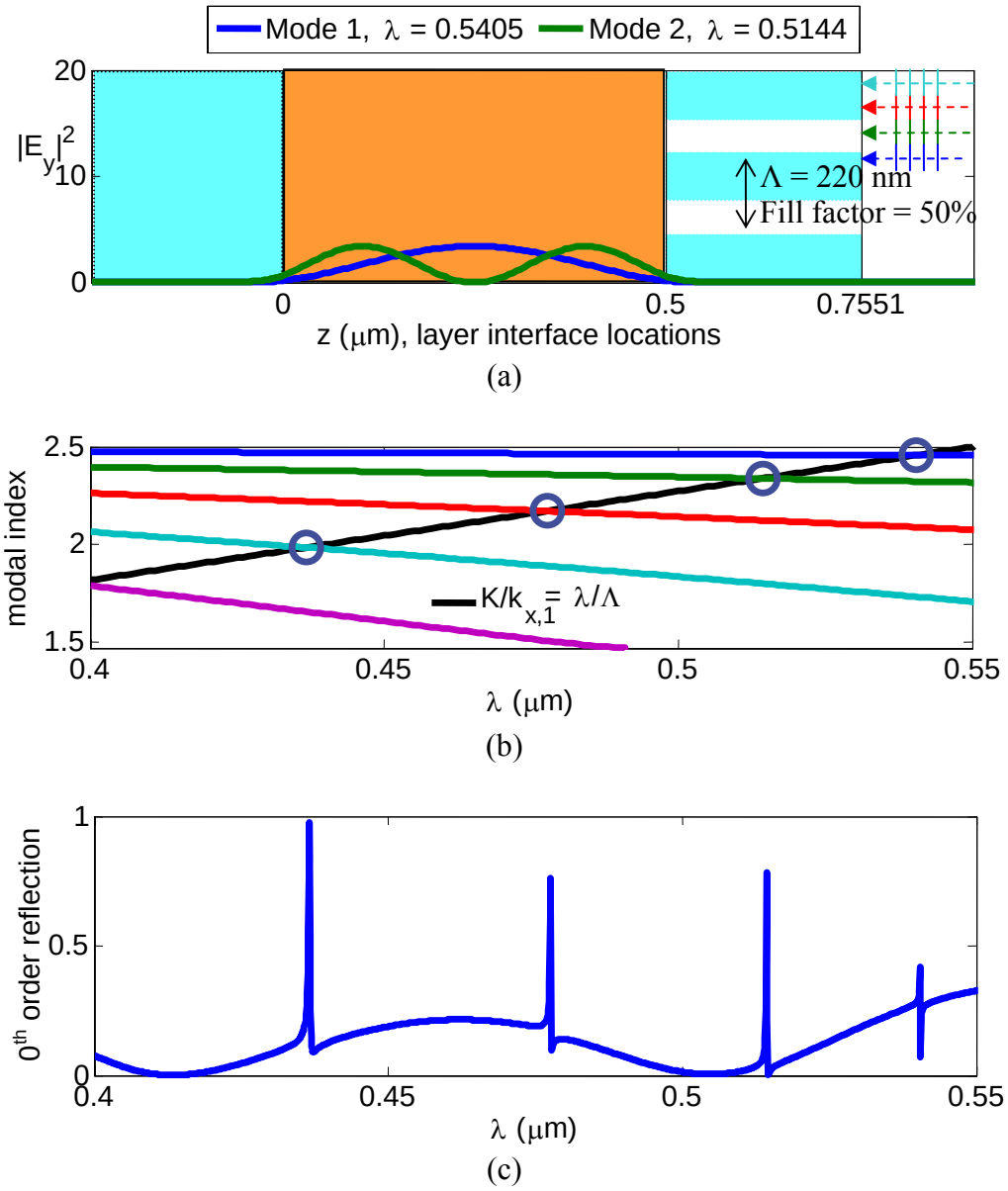

Figure 5-4 (a) Figure showing both the index distribution and spatial mode profile for the first two modes supported by the single waveguiding layer GMR structure. (b) The real modal index distribution of the five modes supported by the structure as well as the modal index of the ±1 tangential diffracted order in free space, whose intersection indicates the location of a resonance. (c) The 0^{th} order reflection response for the structure calculated using RCWA showing the spectral resonance response.

Increasing the thickness of the film layer not only changes the location of, and separation between, the original resonances, but also introduces more resonances into the spectral range of interest.

5.4.2 Single Layer, Single Mode Structures with Multiple Periodicities

Having the ability to tailor the spectral location of, and separation between multiple resonances is a desirable property for multi-line filters. The most direct means of controlling a two-line filter is to introduce multiple directions of periodicity as presented by Boonruang [131]. In this scenario, the modes supported by a vertical slab waveguide can have energy coupled into them by diffracted orders along two separate dimensions of transverse periodicity. Since the periodicity of each transverse dimension can be controlled separately during design and fabrication, the location of two separate resonances can be controlled independently.

5.4.3 Multiple Layer, Multimode Structures

A separate method for providing more control over multiple grating resonances, involves the introduction of multiple layers within the vertical waveguide stack. While the fabrication complexity involved in growing multiple layers is more difficult than using a single wave guiding layer, thin-film filters have long been grown with tens or hundreds of alternating layers of high and low refractive indices [5]. In the multilayer, multimode resonant grating filter, the variation of thickness for multiple layers of two or more refractive index values allows for a wide range of flexibility in tailoring the dispersion properties of super-modes in a multilayer structure. While the dispersion properties (spectral slope, spectral separation) of every mode in the system are changed when any variable in the system changes, having the ability to alter the vertical spatial distribution of material properties provides far more control over the dispersion properties

of each mode than does having only a single layer of one material. Figures 5-5 to 5-8 show how the separation between two resonances can be altered from course to fine over a given spectral range by changing only the thicknesses of the layers. Design of a multi-line filter with any desired spectral separation, within the limits of the materials present in the structure, then becomes a multi-parameter numerical optimization problem.

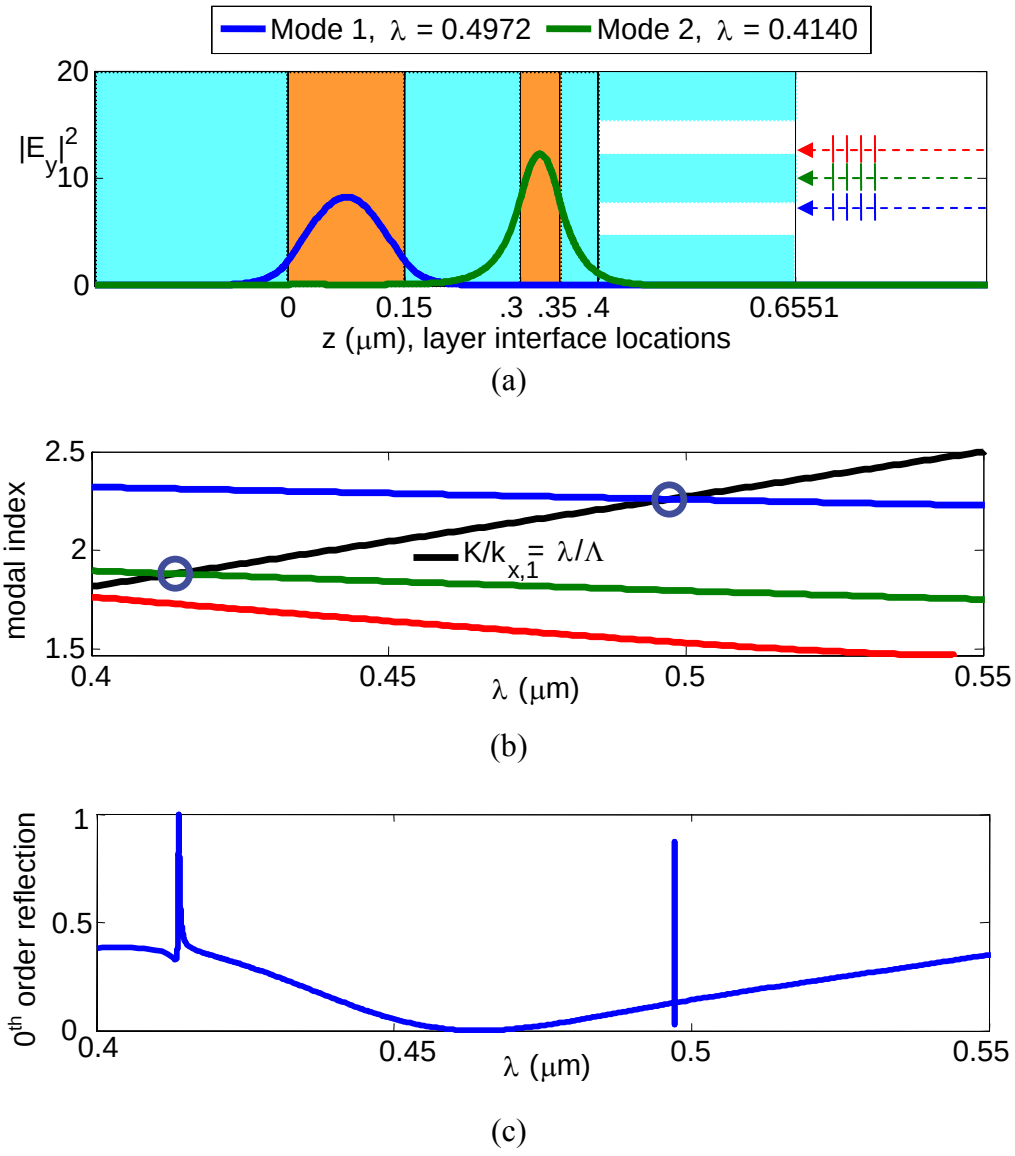

Figure 5-5 (a) Figure showing both the index distribution and spatial mode profile for the first two modes supported by the multilayer waveguiding layer GMR structure. (b) The real modal index distribution of the three modes supported by the structure as well as the modal index of the ±1 tangential diffracted order in free space, whose intersection indicates the location of a resonance. (c) The 0^{th} order reflection response for the structure calculated using RCWA showing the spectral resonance response.

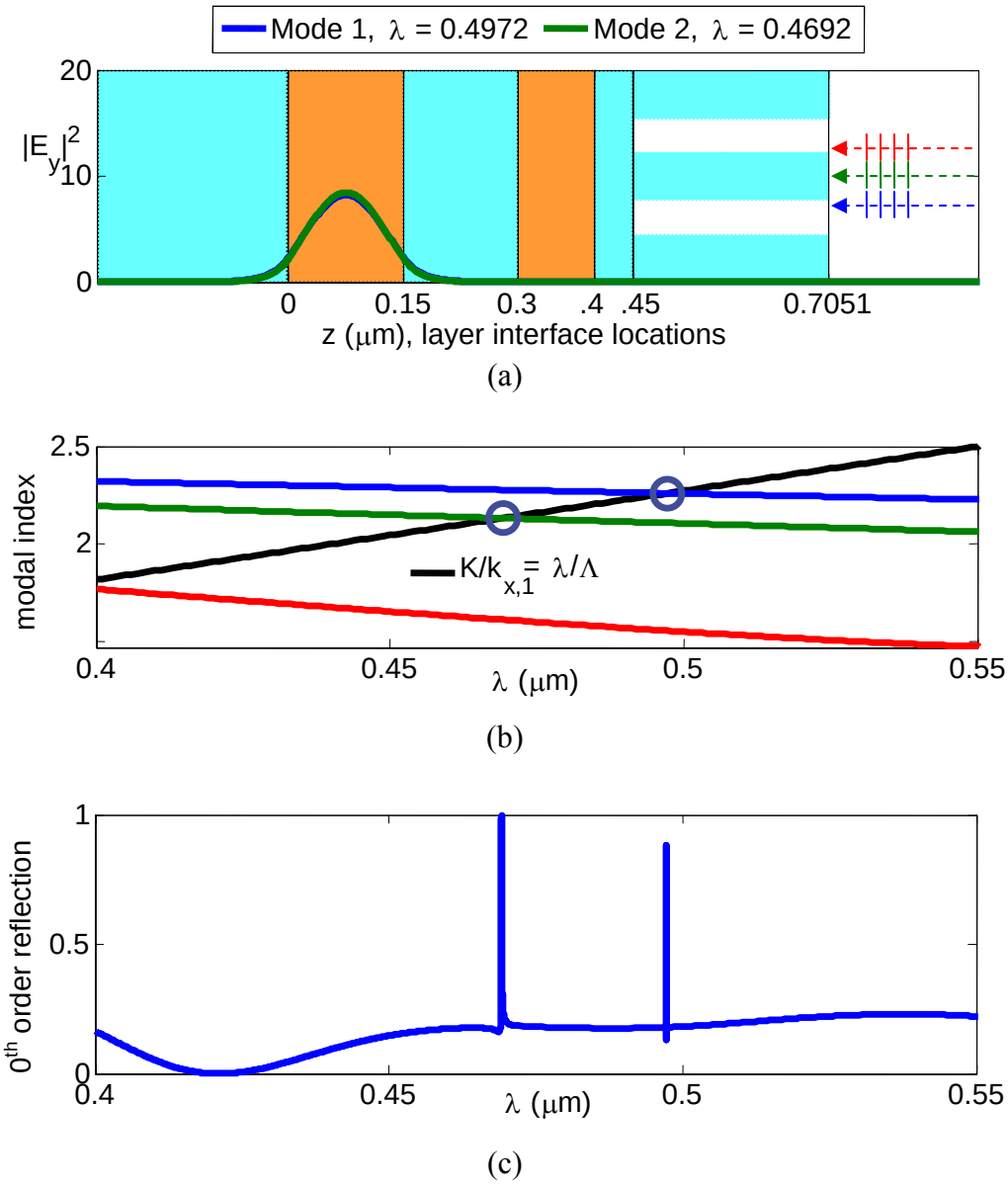

Figure 5-6 (a) Figure showing both the index distribution and spatial mode profile for the first two modes supported by the single waveguiding layer GMR structure. (b) The real modal index distribution of the three modes supported by the structure as well as the modal index of the ±1 tangential diffracted order in free space, whose intersection indicates the location of a resonance. (c) The 0^{th} order reflection response for the structure calculated using RCWA showing the spectral resonance response.

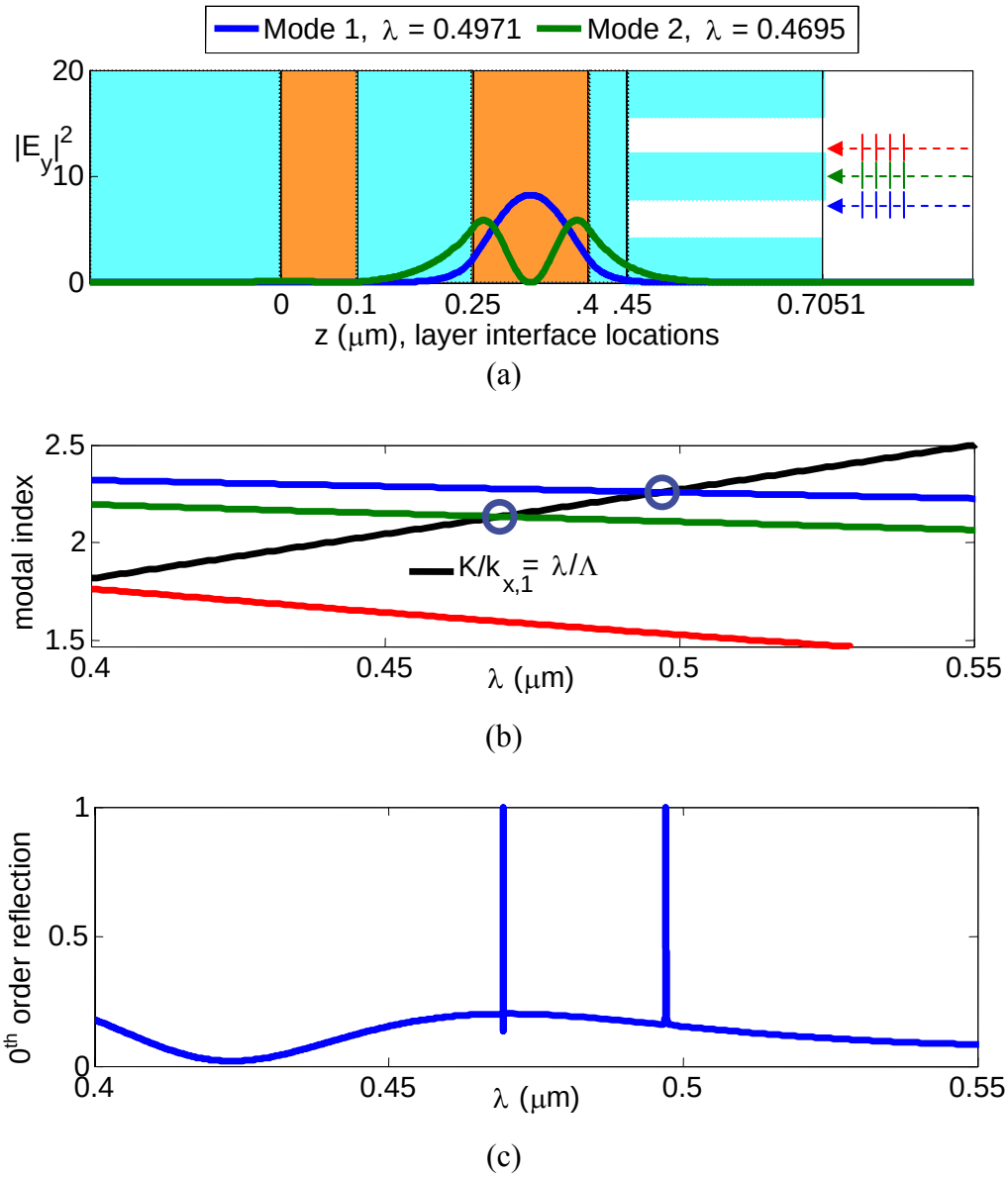

Figure 5-7 (a) Figure showing both the index distribution and spatial mode profile for the first two modes supported by the single waveguiding layer GMR structure. (b) The real modal index distribution of the three modes supported by the structure as well as the modal index of the ±1 tangential diffracted order in free space, whose intersection indicates the location of a resonance. (c) The 0^{th} order reflection response for the structure calculated using RCWA showing the spectral resonance response.

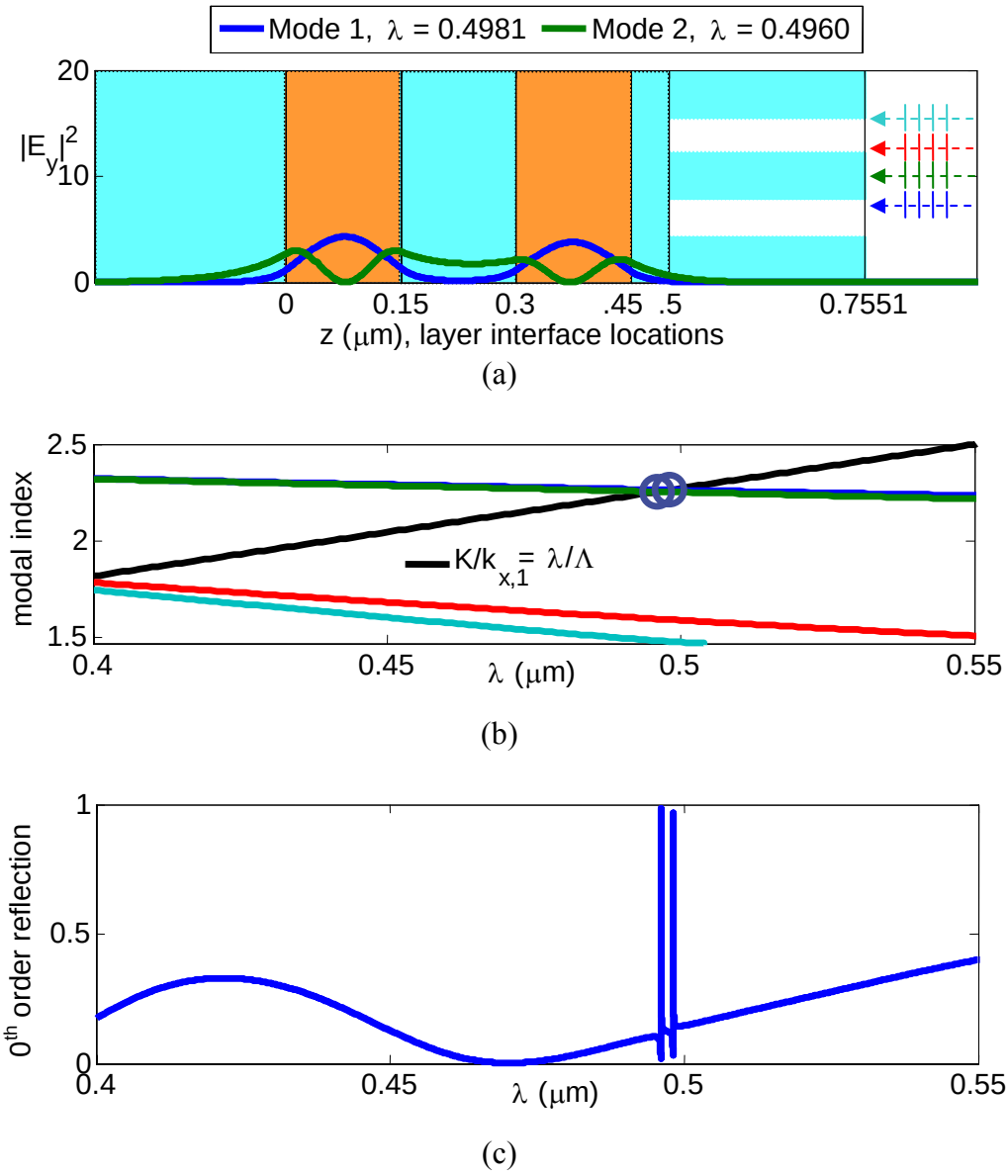

Figure 5-8 (a) Figure showing both the index distribution and spatial mode profile for the first two modes supported by the single waveguiding layer GMR structure. (b) The real modal index distribution of the four modes supported by the structure as well as the modal index of the ±1 tangential diffracted order in free space, whose intersection indicates the location of a resonance. (c) The 0^{th} order reflection response for the structure calculated using RCWA showing the spectral resonance response.

5.5 Use of Grating Theory and the "Homogeneous Problem" for Modeling Multilayer, Multimode GMR Devices

Exact solutions for the complex modal indices of a resonant grating structure require the use of a rigorous Maxwell equation solver, like RCWA. The method by which the complex modal indices of the multilayer diffraction grating can be extracted from the eigenmode solutions and layer propagation matrices of RCWA can be accomplished in two different manners. The original method by which these values were obtained involves a solution to the "homogeneous" problem [45, 122, 132]. In this method [23], the eigenmodes of a transversely periodic lamellar diffraction grating are combined with the plane wave expansions in a structure's uniform homogenous layers to produce a single "transverse" scattering matrix as shown in Figure 5-9.

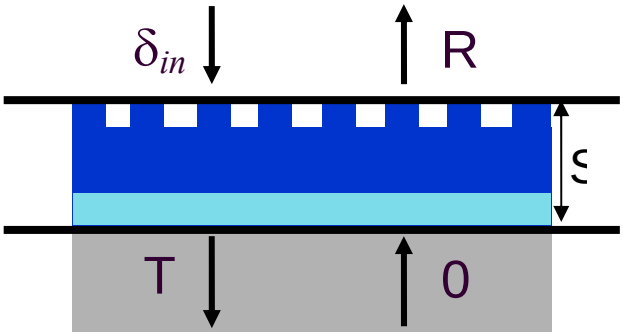

Figure 5-9 (a) A drawing of a multilayer grating structure showing the relationship between the incoming and outgoing waves for a "transverse" scattering matrix.

For a single incident plane wave, the relationship between the incident, reflected and transmitted waves can be expressed as follows:

$$\begin{bmatrix} R \\ T \end{bmatrix} = \begin{bmatrix} S_{11}^{t} & S_{12}^{t} \\ S_{21}^{t} & S_{22}^{t} \end{bmatrix} \begin{bmatrix} 0 \\ \delta_{input} \end{bmatrix} \tag{5.5.1}$$

The homogeneous problem involves determining non-trivial solutions to Equation (5.5.1) when $\delta_{input} = 0$.

$$\begin{bmatrix} S_{11}^t & S_{12}^t \\ S_{21}^t & S_{22}^t \end{bmatrix}^{-1} \begin{bmatrix} R \\ T \end{bmatrix} = \begin{bmatrix} 0 \\ 0 \end{bmatrix} \tag{5.5.2}$$

Such non-trivial solutions are only possible if the determinant of the inverse matrix in (5.5.2) equals zero.

$$\det\left(\begin{bmatrix} S_{11}^t & S_{12}^t \\ S_{21}^t & S_{22}^t \end{bmatrix}^{-1} \right) = 0 \tag{5.5.3}$$

The complex roots of this determinant correspond to the poles of the original scattering matrix, where these poles are the complex modes of the grating waveguide. Solving this determinant equation requires an iterative numerical process that searches the entire complex plane similar to that described in Section 2.5, but whereas that process only described a root search performed in one dimension, two dimensions are necessary here. A number of different methods have been developed for determining the complex roots of transcendental equations [59], but regardless off the method chosen, each complex mode that is to be found must be searched for in a separate iterative process.

A second method of determining the complex modal indices, which was utilized in this study, involves the use of a "longitudinal" scattering matrix [22]. In this approach, RCWA is utilized where PML boundary conditions are matched to the superstrate and substrate regions and contained within an artificial transversely periodic unit-cell as described in Section 3.3. The scattering matrix for a single grating unit cell is then created by cascading the scattering matrices of the slices that represent the high and low grating index sections.

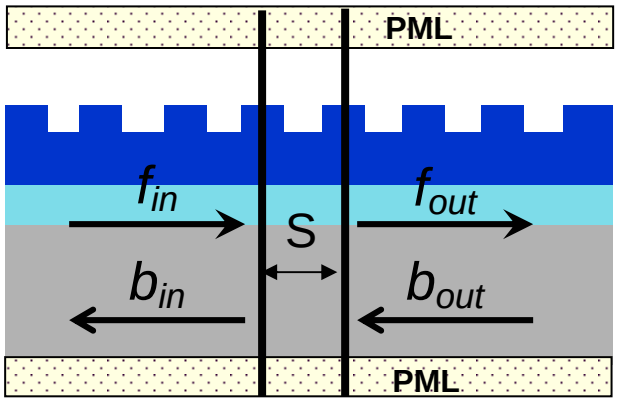

Figure 5-10 A drawing of a multilayer grating structure showing the relationship between the incoming and outgoing waves for a "longitudinal" scattering matrix.

The relationships between the incoming and outgoing modes to this unit cell are shown in Figure 5-10 and are related through this longitudinal scattering matrix as follows:

$$\begin{bmatrix} b_{in} \\ f_{out} \end{bmatrix} = \begin{bmatrix} S_{11}^{l} & S_{12}^{l} \\ S_{21}^{l} & S_{22}^{l} \end{bmatrix} \begin{bmatrix} b_{out} \\ f_{in} \end{bmatrix} \tag{5.5.4}$$

The complex modal indices can then be determined by applying longitudinal periodic boundary conditions, $b_{out} = e^{j\beta_{\text{mode}}\Lambda} b_{in}$ and $f_{out} = e^{j\beta_{\text{mode}}\Lambda} f_{in}$, and solving the following generalized eigenvalue problem:

$$\begin{bmatrix} I & -S_{12}^{l} \\ 0 & S_{22}^{l} \end{bmatrix} \begin{bmatrix} b_{in} \\ f_{in} \end{bmatrix} = e^{j\beta_{\text{mode}}\Lambda} \begin{bmatrix} S_{11}^{l} & 0 \\ -S_{21}^{l} & I \end{bmatrix} \begin{bmatrix} b_{in} \\ f_{in} \end{bmatrix} \tag{5.5.5}$$

Unlike the "transverse" scattering matrix approach, the solution of Equation (5.5.5) determines all complex modes supported by the waveguide grating system in a single matrix operation. By solving Equation (5.5.5) over a range of wavelengths or grating periods, complex-valued modal dispersion curves can be determined. Figure 5-11 shows the material and

structural parameters for a grating-waveguide structure supporting single leaky mode whose corresponding complex band structure is shown in Figure 5-12.

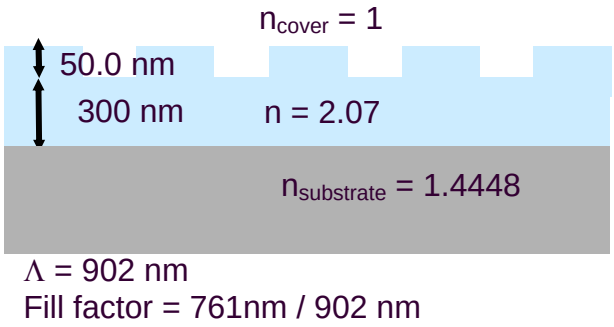

Figure 5-11 A drawing a grating waveguide structure that supports a single leaky mode, as well as the material and structural parameters for the grating waveguide.

In a manner similar to that described in Section 5.3, the intersection of the grating modal dispersion curves with the tangential component of the diffracted waves satisfies the conditions in Equation (5.2.5) and indicates the presence of a resonance. Figure 5-12 shows the complex band structure diagrams and 0^{th} order reflection spectra for this single-mode as well as the angular spectrum associated with the each of the resonances at normal incidence and at a 1º angle of incidence respectively.

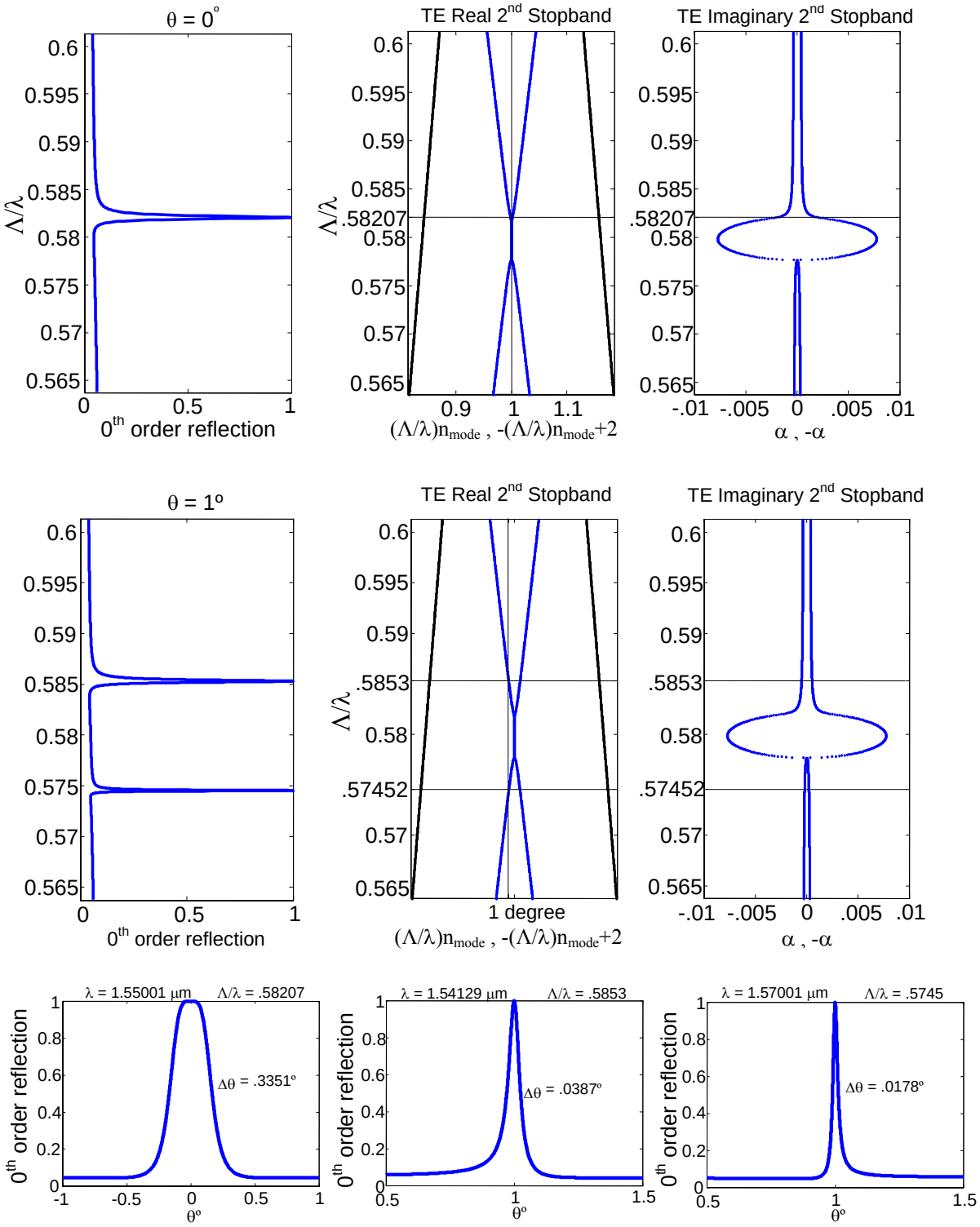

Figure 5-12 The complex band structure, as well as the 0th order reflection response for all of the resonances of the system at 0º and 1º angles of incidence for the single leaky mode resonant grating structure.

Table 5.1 Numerical values for the spectral and spatial resonance properties associated with the single leaky mode grating structure in Figure 5-11 and plots in Figure 5-12. The table shows the central resonance wavelengths, spectral bandwidths, angular bandwidths, and complex modal indices associated with resonances at normal incidence and 1º.

q	0°	1°	
resonance	1	1	2
$\lambda_{resonance}$ (μm)	1.55001	1.54129	1.57001
Δλ (nm)	.934	.653	.281
Δθ (mrad) (degrees)	5.848 .33509	.6747 .03866	.3115 .01785
n’	1.7363	1.7262	1.7231
n’’	.000336	.000364	.000159
$2n''\Lambda \cong \Delta\lambda$ (nm)	N/A	.6567	.2868
$2n'' \cong \Delta\theta$ (mrad)	N/A	.7281	.3182

Table 5.1 shows the quantitative relationship between the resonance wavelength, spectral and angular bandwidths, and complex modal index values for the structure at normal and 1º angles of incidence. The angular bandwidth for this structure is nearly 100 times broader at normal incidence than at oblique incidence due to the coupling of symmetric diffracted orders into counter-propagating complex modes. The coupling of these two modes causes a flattening of the dispersion relation and the creation of a "band-edge." Between the upper band-edge and lower band-edge is the "photonic band-gap" where coupling between free-space and periodic modes is considerably suppressed.

5.6 Complex-Valued Dispersion Tailoring for Design of Multilayer, Multimode GMR Devices

Using the concepts and numerical methods introduced in the previous sections, the band structures of multilayer, multimode resonant grating devices can be rigorously calculated. By proper design of the material and structural parameters of a two-mode resonant grating, Sentenac et. al [127] showed how the concept of dual mode coupling and grating asymmetry can be used to broaden the angular line width of not only normally incident filters but obliquely incident filters as well. Figure 5-13 shows the structural and material parameters of the dual mode grating waveguide studied in their work.

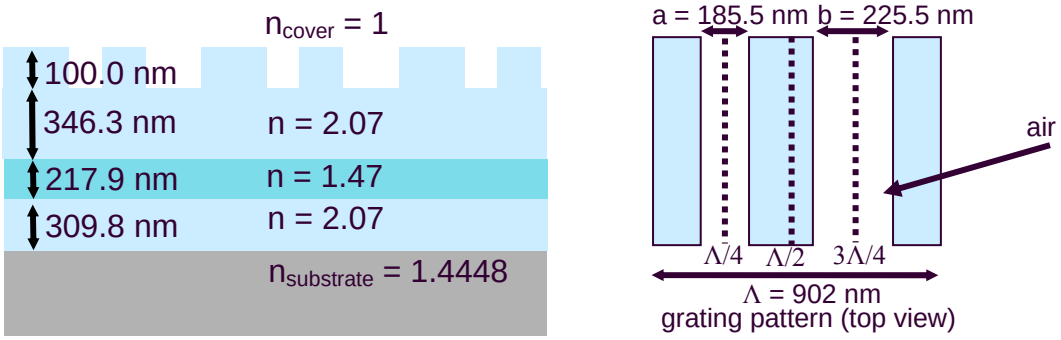

Figure 5-13 A drawing of a grating waveguide structure that supports two leaky modes, as well as the material and structural parameters for the grating waveguide.

At normal incidence, their structure supports two resonances. The complex band structure, spectral reflection, and angular acceptance of each resonance can be seen in Figure 5-14.

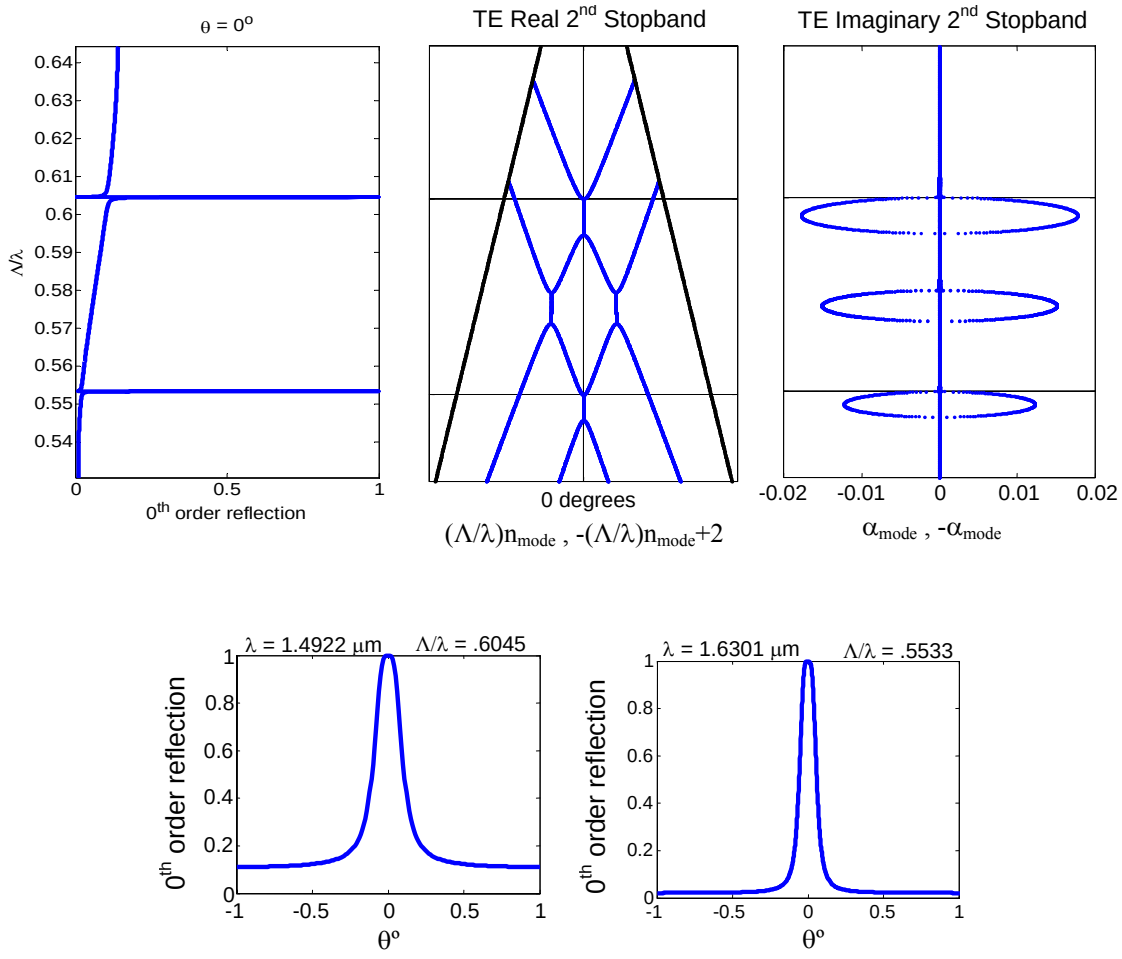

Figure 5-14 The complex band structure, as well as the 0th order reflection response for all of the resonances of the system at a 0º angle of incidence for the dual leaky mode resonant grating structure.

By changing the angle of incidence to 1º, as shown in Figure 5-15, the angular line width associated with the each of the four resonances produced is considerably narrowed.

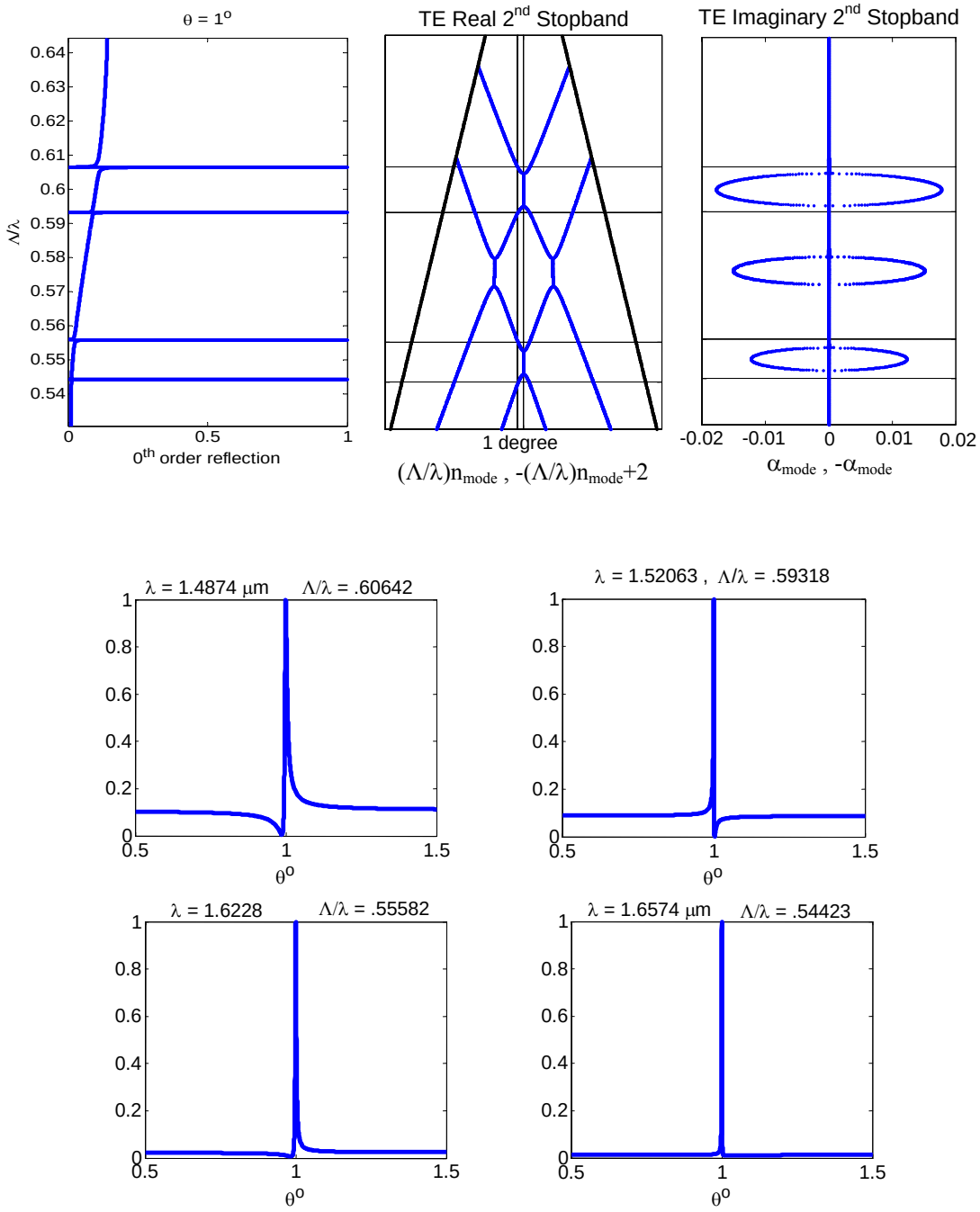

Figure 5-15 The complex band structure, as well as the 0th order reflection response for all of the resonances of the system at 1° angles of incidence for the dual leaky mode resonant grating structure.

Figure 5-16 shows the reflection spectrum and band structure diagrams at an angle of incidence of 4.986º, which is the location of the band-edge between the TE_0 and TE_1 modes. By examining the angular spectrum of each resonance shown in Figure 5-16, the angular line width of the resonance associated with the upper band-edge of central band-gap is shown to be considerably broadened.

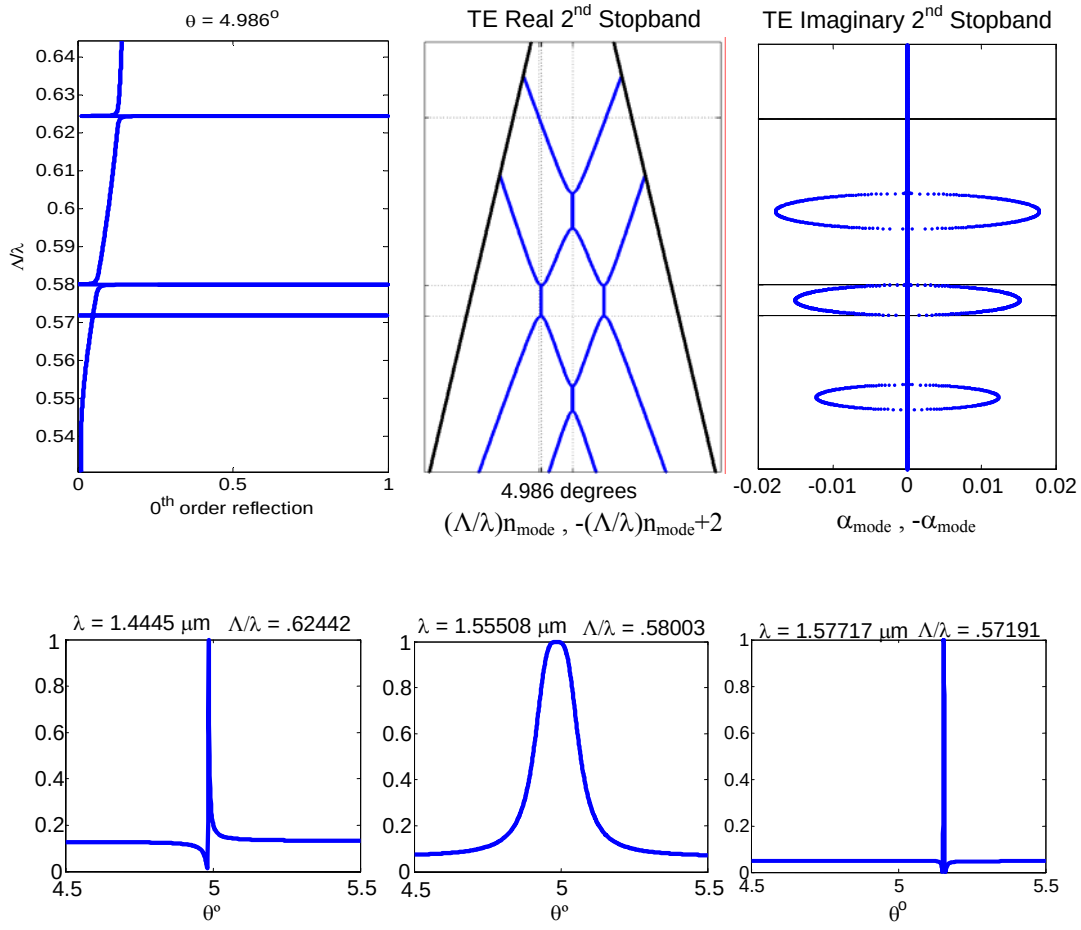

Figure 5-16 The complex band structure, as well as the 0th order reflection response for all of the resonances of the system at a 4.986º angle of incidence for the dual leaky mode resonant grating structure.

Due to the curvature of the modal band diagram in this band-gap, as can be seen more closely in Figure 5-17, the central portions of the upper and lower band-edges are not aligned with one another.

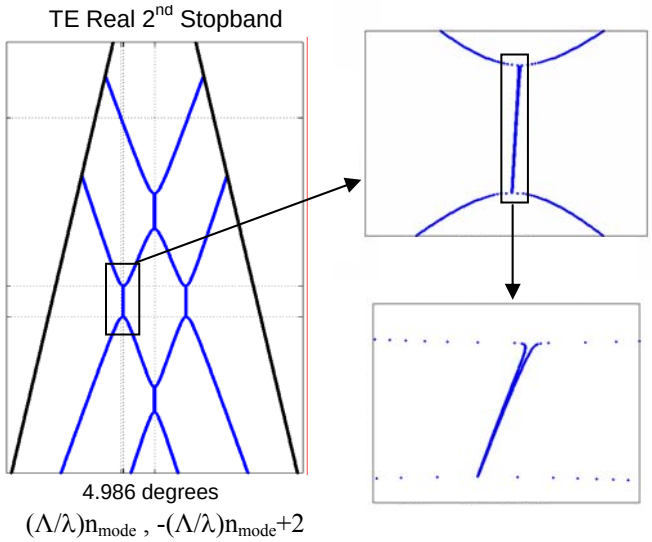

Figure 5-17 The complex band structure for the dual leaky mode resonant grating structure showing the non-alignment of the upper and lower band edges at oblique incidence.

Consequently, the spectral response of the 0^{th} order reflection includes resonances for both the upper and lower band-edges, but in this case only the upper band-edge produces a broadened angular response.

The original contribution of our work performs a slight variation on this idea of multimode coupling. In order to produce an N-line resonant filter that has broadened angular acceptance for each resonance at an oblique angle of incidence requires a wave-guide grating that supports N+1 complex modes, where N band-edges are aligned in the angular domain for separate spectral resonance.. Figure 5-18 shows a slightly altered version of the structure studied by Sentenac, where the new structure supports three complex modes.

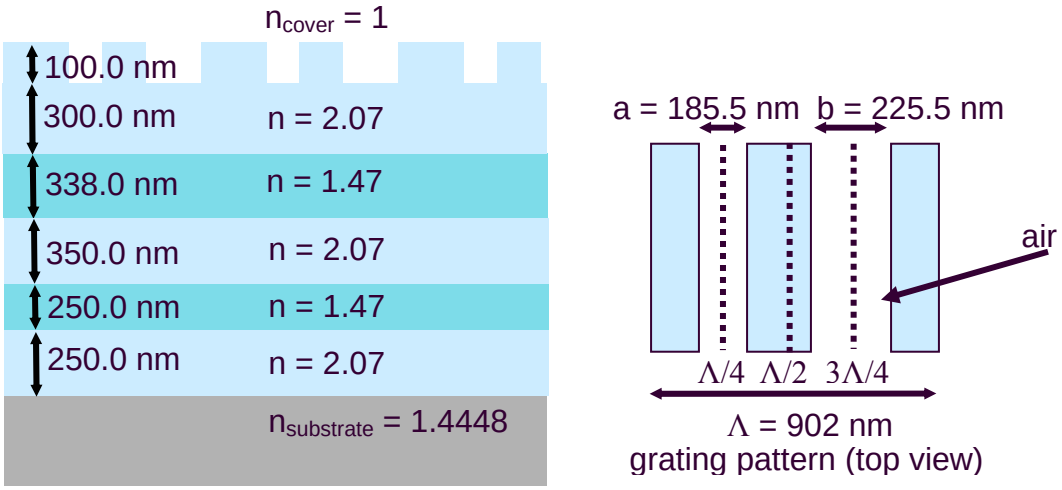

Figure 5-18 A drawing of a grating waveguide structure that supports three leaky modes, as well as the material and structural parameters for the grating waveguide.

The grating properties of this new structure at the same as for the Sentenac structure, but two additional layers have been added to the waveguide and the thickness of each layer in the waveguide has been varied. Figure 5-19 shows the 0^{th} order reflection spectrum and the complex band diagram for the three mode system at normal incidence, as well as the angular acceptance of each of the three resonances. Figures 5-20 to 5-22 show the same information at 1º, 2.455º, and 5.374º.

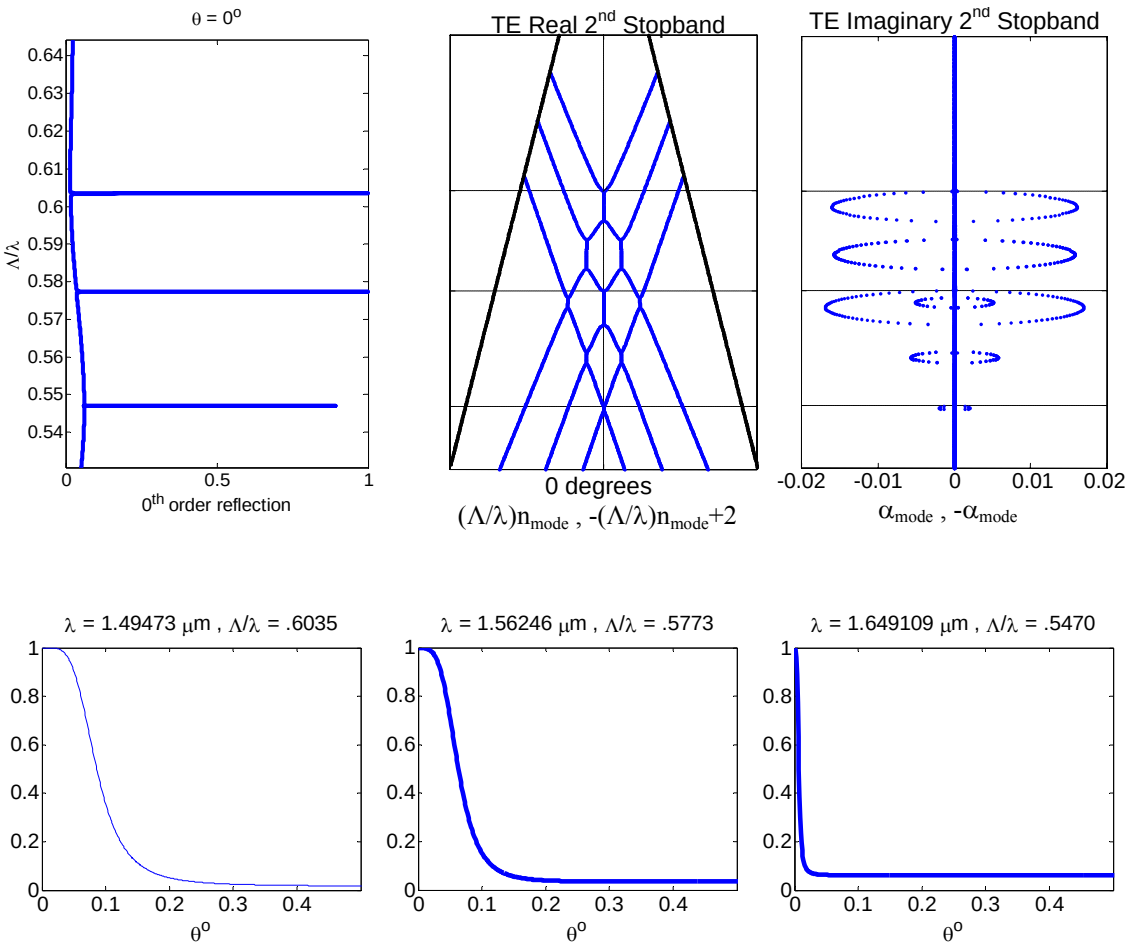

Figure 5-19 The complex band structure, as well as the 0th order reflection response for all of the resonances of the system at a 0º angle of incidence for the dual leaky mode resonant grating structure.

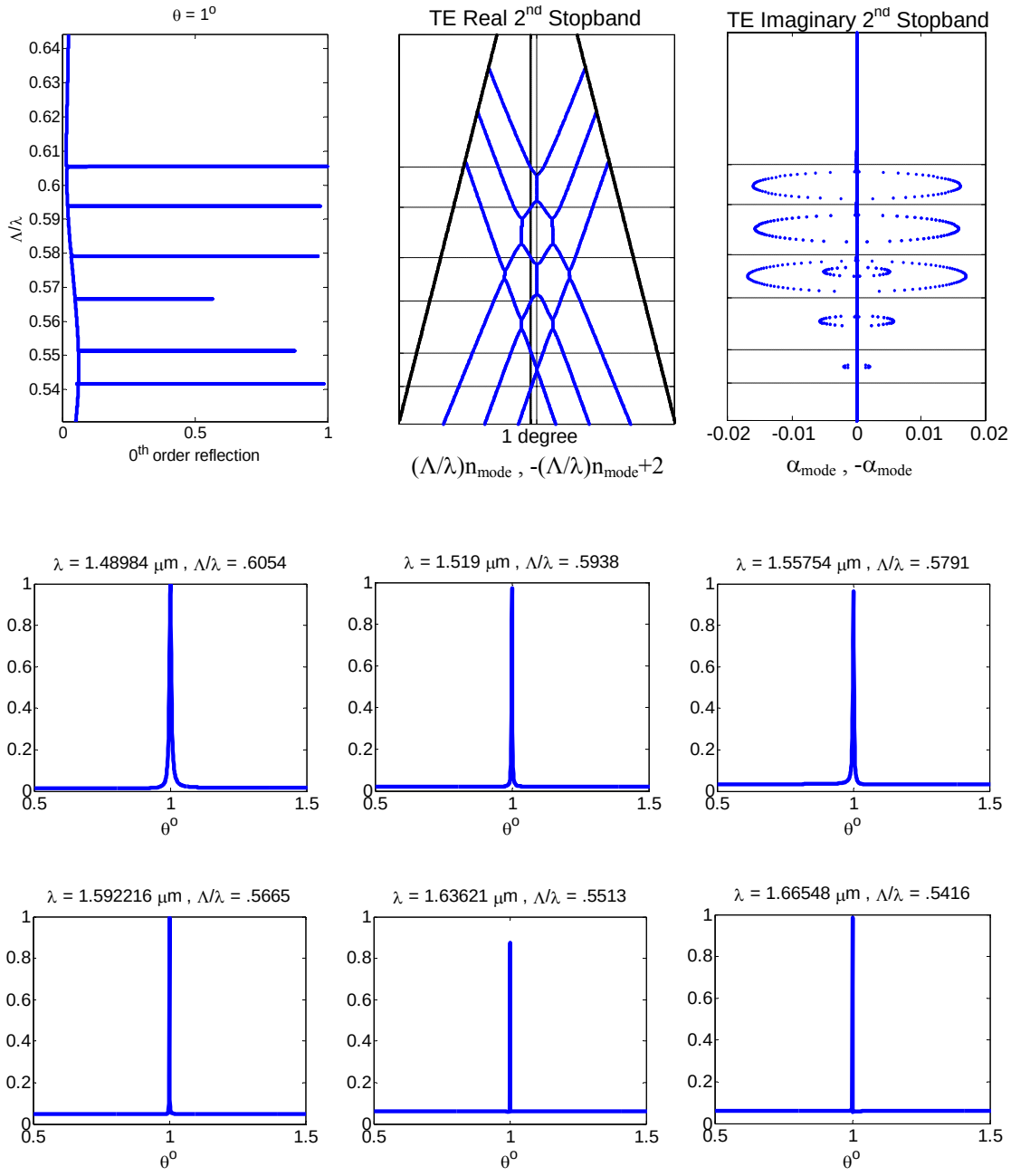

Figure 5-20 The complex band structure, as well as the 0th order reflection response for all of the resonances of the system at a 1° angle of incidence for the three leaky mode resonant grating structure.

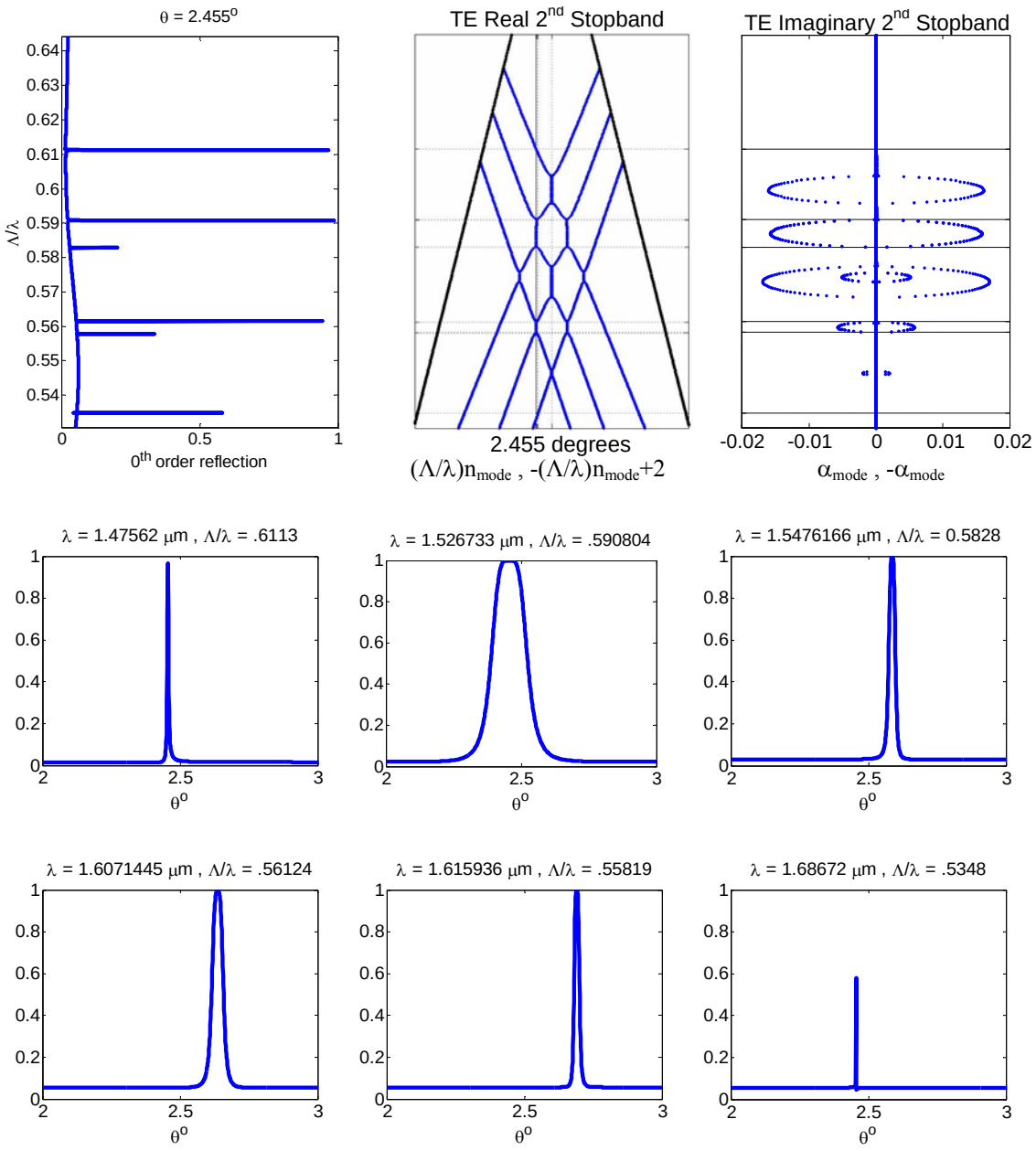

Figure 5-21 The complex band structure, as well as the 0th order reflection response for all of the resonances of the system at a 2.455º angle of incidence for the three leaky mode resonant grating structure. At this angle of incidence, the broadened resonances are nearly aligned in their central angle.

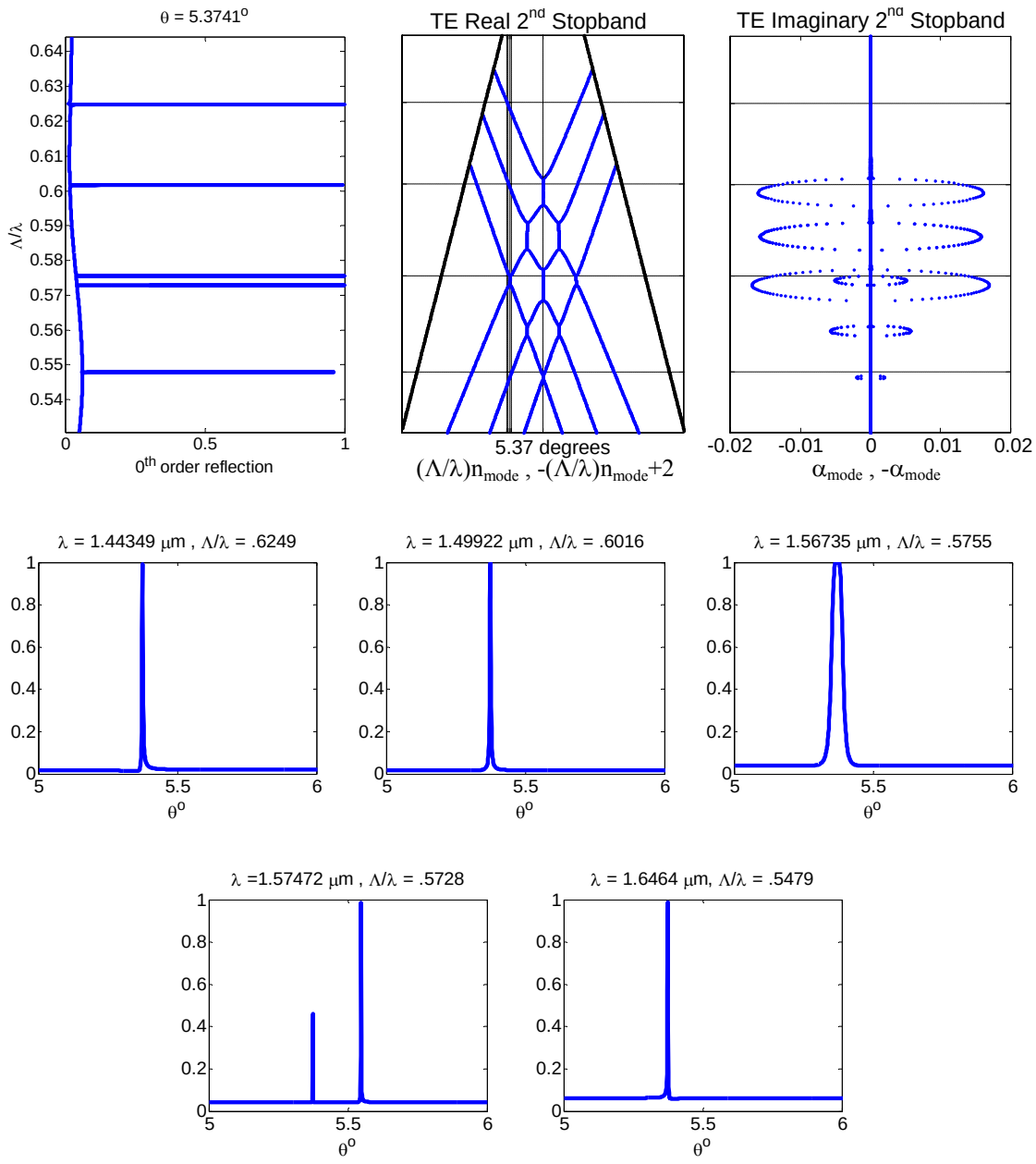

Figure 5-22 The complex band structure, as well as the 0th order reflection response for all of the resonances of the system at a 5.37º angle of incidence for the three leaky mode resonant grating structure.

While this design does not possess polarization independence, as can be seen in Figure 5-23 showing the real part of the band diagrams associated with TE and TM polarizations for this structure, there is no theoretical reason why a structure with these properties could not be designed.

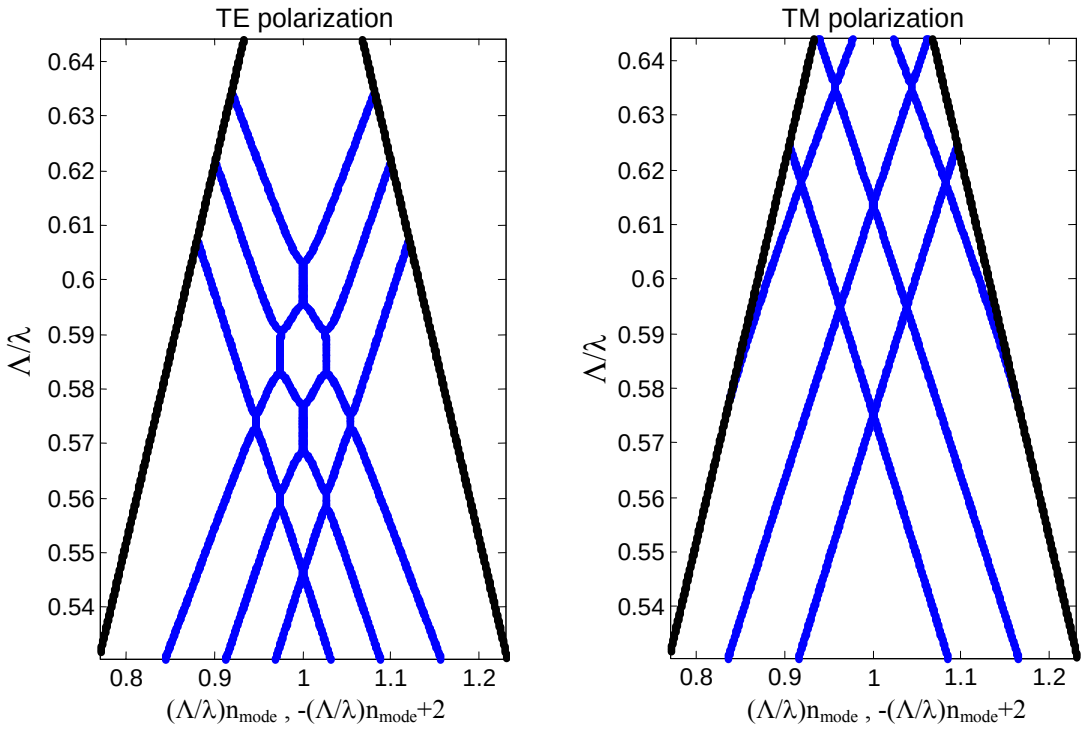

Figure 5-23 The real part of the band structure diagram for the three leaky mode resonant grating structure for both TE and TM polarizations. These diagrams show the obvious polarization dependence for this resonant grating structure.

Attempting to create a specific design for a polarization independent multi-line resonant filter with broad angular acceptance for all resonances operating at oblique incidence would double the number of conditions to be met in an optimization problem, and would therefore increase the level of difficulty in performing the optimization.

While the angular alignment of resonances is not fully present in the previous figures, the graphs for a 2.455º angle of incidence show broadened angular resonances that are nearly aligned

to the same angle of incidence. In order obtain angular alignment of the resonances; a numerical search/scan and optimization can be performed over any combination of grating parameters one so chooses. Changing any single parameter or combination of parameters affects the slope and shape of all of the dispersion curves in the band structure diagrams. As an example of how this process can be performed, the thickness of the bottom two layers of the structure were varied in tandem, as shown in Figure 5-24, maintaining a constant overall structure thickness.

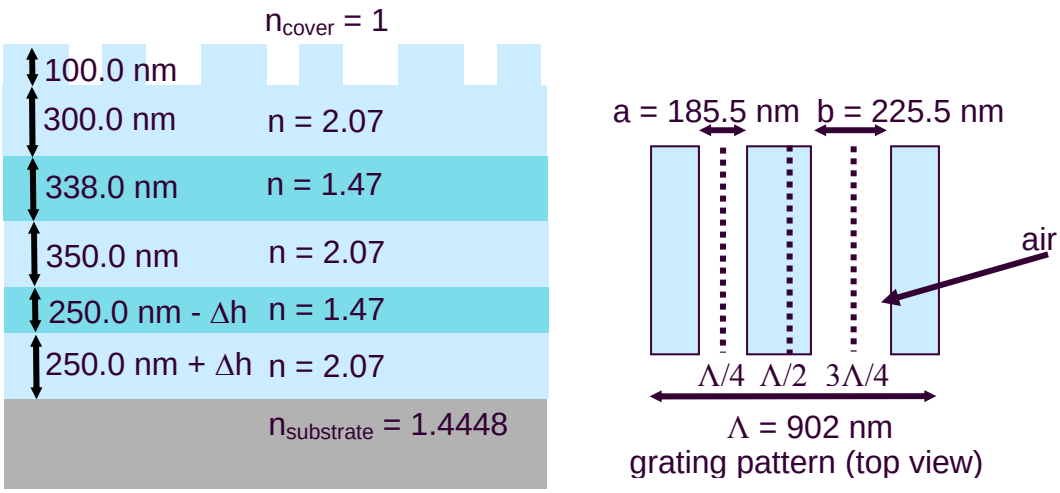

Figure 5-24 A drawing of a grating waveguide structure that supports three leaky modes, as well as the material and structural parameters for the grating waveguide and the two layers that were varied in tandem to modify the overall dispersion properties of the structure.

By varying Δh from -100 nm to +100 nm, the relative locations of the two upper band-edge dispersion curves vary significantly. Figure 5-25 shows three-dimensional plots of the real and the imaginary parts of the band structure diagrams over this entire range, as well as two-dimensional plots of these same band structure diagrams superimposed.

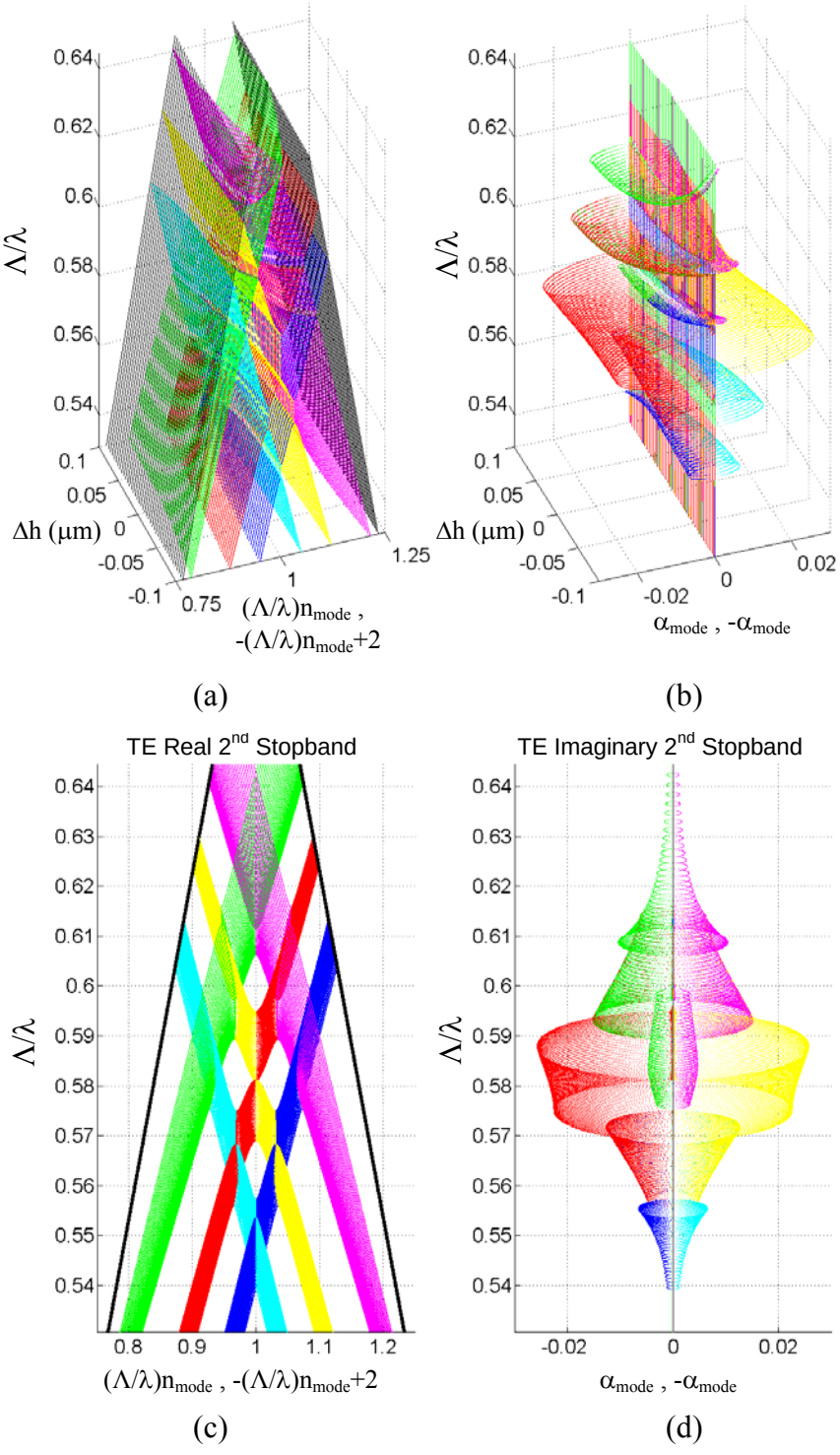

Figure 5-25 Plots showing the changing nature of the real (a) & (c) and imaginary (b) & (d) parts of the band structure diagram as a function of Δh.

The changing nature of the resonances involved can also be seen by directly observing the reflection from the structure, as shown in Figure 5-26 for normal incidence.

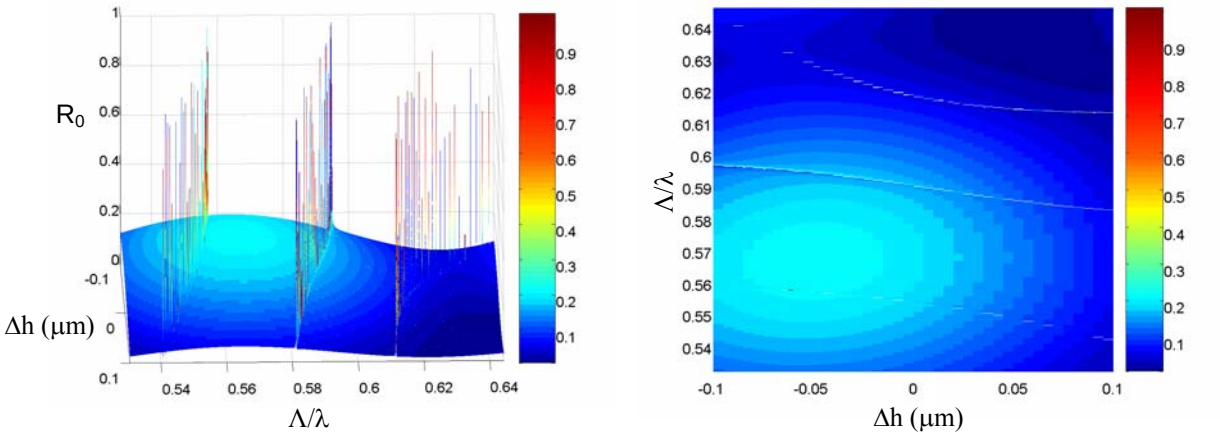

Figure 5-26 Plots of the 0th order reflection spectrum for the multilayer resonant grating structure as a function of the period/wavelength ratio and change in layer height.

In investing the two upper band edges involved in the targeted simultaneous broadened angular acceptance at oblique incidence, it is instructive to zoom-in on this section of the band diagram plot, as shown in Figure 5-27.

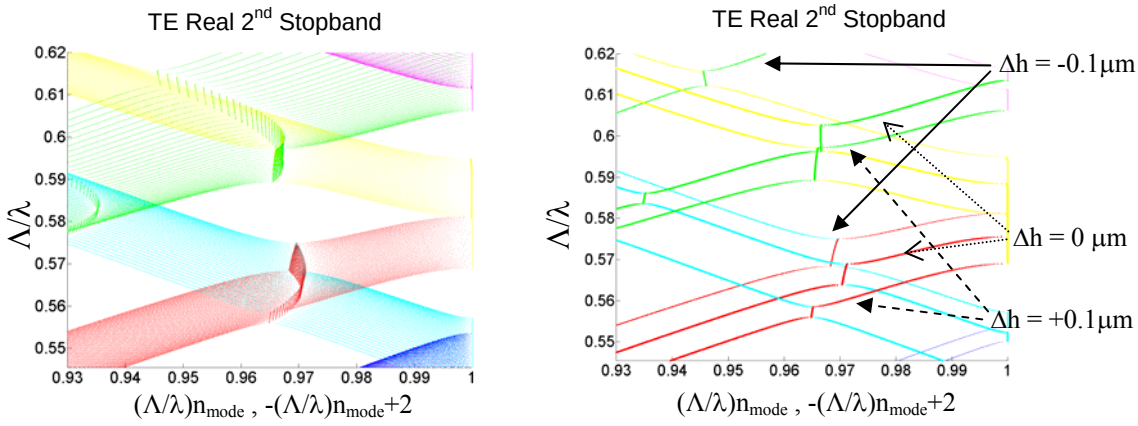

Figure 5-27 Plots showing the dispersion band edges involved in the angular alignment problem. (a) Plot showing the dispersion curves for the entire range of Δh. (b) Plot showing the dispersion curves at Δh = -100 nm, 0 nm, and 100 nm.

This figure shows that negative values of Δh (which decreases the amount of high index material) alter the band structure appreciably, and causes serious angular misalignment of the resonance locations. On the other hand, positive values of Δh (which increases the amount of high index material) have a smaller affect on resonance separation and a small positive value (Δh = 63.7 nm) actually brings about the angular alignment being sought. Figure 5-28 shows the reflection spectrum and complex band structure for the structure with an optimized angular resonance alignment at an input angle of 3.165º.

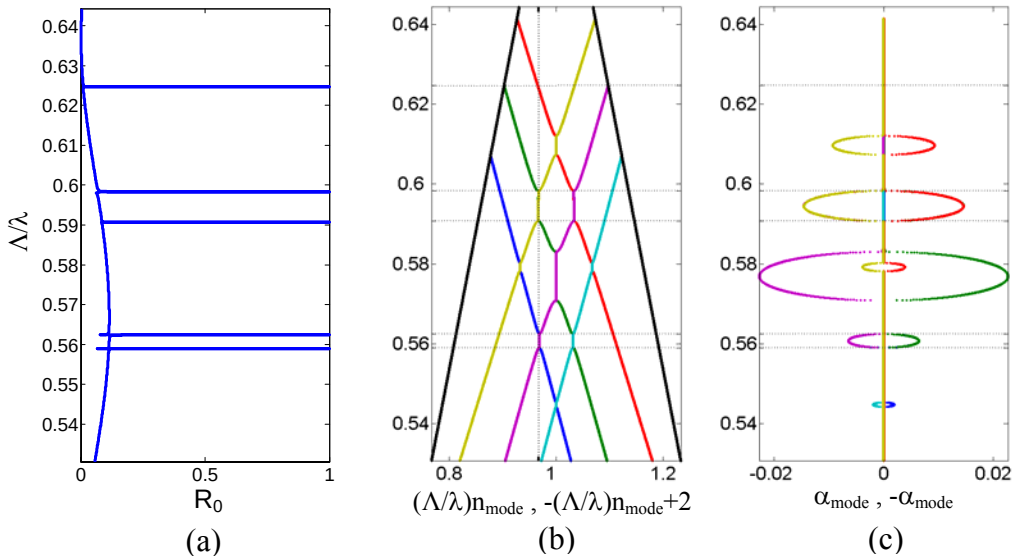

Figure 5-28 Reflection spectrum and complex dispersion band diagram for the optimized multilayer structure (Δh = 63.7 nm) having two collocated, angular spectrum resonances at separate wavelengths. The vertical lines in (b) represent the value of the expression $1 - \Lambda / \lambda \sin\theta$, while the horizontal lines represent the value of Λ / λ for the same resonance.

The plot of the angular spectrum at the peak wavelength of each spectral resonance can be seen in Figure 5-29 along with an image of the real part of the dispersion band diagram for

this aligned structure tightened to show only the two dispersion band edges contributing to the angular resonances of interest. The resonance properties of each resonance are in Table 5-2.

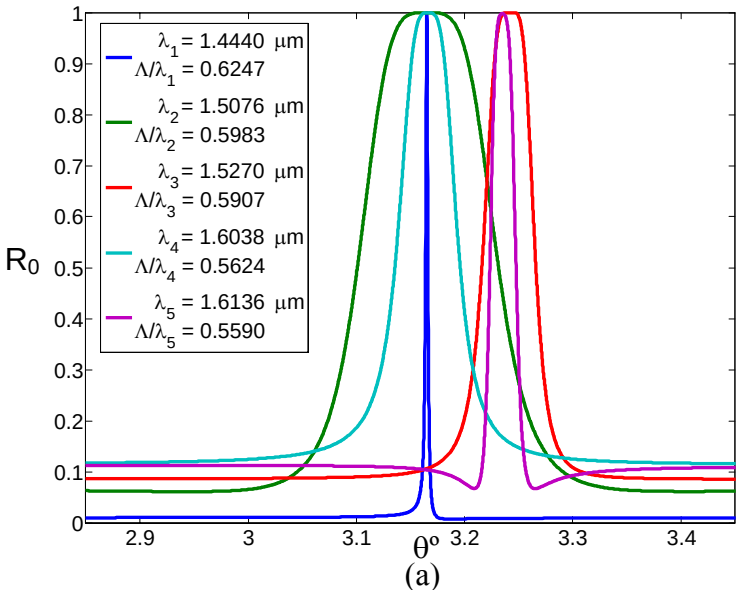

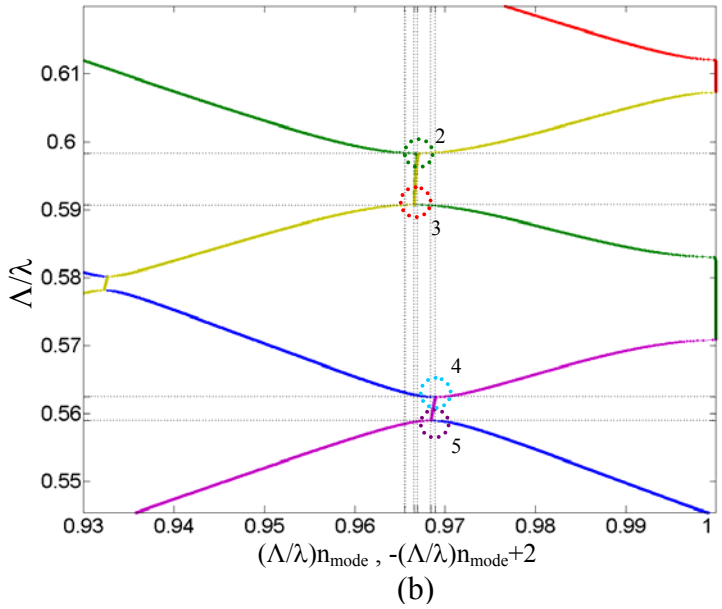

Figure 5-29 (a) Plot showing the angular resonances associated with the optimized multilayer guided mode resonance structure. The resonances at wavelengths of 1.5076 μm and 1.6038 μm are both centered at an input angle of 3.165° and have broad angular bandwidth due to the simultaneous interactions of separate pairs of leaky modes. (b) The real band structure diagram showing the band edges of interest. The circles are numbered and color-matched to the resonance curves from part (a).

Table 5.2 Numerical values for the spectral and spatial resonance properties associated with the optimized multilayer multimode guided mode resonance filter having two collocated broadened angular resonances for two separate wavelengths. The table shows the central resonance wavelengths, spectral bandwidths, angular bandwidths, and complex modal indices associated with resonances at a 3.165º angle of incidence.

resonance	1	2	3	4	5
$\lambda_{resonance}$ (μm)	1.44396	1.50761	1.52704	1.60381	1.61370
$\Delta\lambda$ (nm)	.025144	.065396	.010290	.026894	.004839
$\Delta\theta$ (mrad)	.003982	.227848	.087816	.105519	.042296
(degrees)	.002281	.130547.	.050028	.060458	.024234

5.7 Multilayer Multimode Guided Mode Resonance Filter Conclusions

This chapter discussed the concept of a multilayer multimode guided mode resonance filter by initially discussing the background and history of the resonant grating concept, then presenting various means of modeling the real and complex parts of the modal indices associated with a multilayer resonant grating, and finally specific examples of multilayer, multimode GMR filters were investigated. The multilayer, multimode GMR filter was shown to possess the ability to control spectral resonance separations from coarse to fine depending on only the (very controllable) properties of multilayer thicknesses for a pair of alternating material layers, given set grating parameters. The angular resonances associated with a multilayer, multimode GMR filter were then investigated, and it was shown that a multilayer, multimode GMR filter could be designed to have broadened angular acceptance for multiple wavelengths at a single angle of incidence by properly tailoring the structure's complex modal dispersion bands.

CHAPTER 6 EFFECT OF LOSS OR GAIN ON GUIDED MODE RESONANT DEVICES

As described in the previous chapter, guided mode resonant (GMR) devices couple an input optical wave to a leaky mode via diffraction from a grating. Utilizing the GMR effect, a variety of narrow bandpass and bandstop devices have been designed previously for tailoring the spectral and angular response of an optical filter, as discussed in the previous and following chapters, but to date most work has focused either on modeling dielectric materials having purely real permittivity values or metallic structures having significant conductivity. The idea of incorporating a GMR structure as a resonant mirror interacting with a gain medium has been proposed previously, but the effect of the gain itself on the resonance was not investigated [133]. Spectrally selective grating waveguide absorbers have been proposed as well by incorporating metallic layers with significant conductivity [134-136]. The purpose of this chapter is to investigate the effect of incorporating a slight gain or loss within the high refractive index layer that primarily contains the leaky mode. The incorporation of an appropriate amount of gain or loss is shown to produce an enhanced reflection/transmission or absorption resonance respectively.

6.1 Definition of Physical Parameters Studied and Device Structure

In terms of a material's complex refractive index, $n - j\kappa$, with n defined as a purely positive value, the imaginary part of the refractive index corresponds to either a gain or loss depending on whether κ is negative or positive. Figure 6.1 shows the geometric structure of the device under study as well as the layer whose absorption/gain parameter is varied.

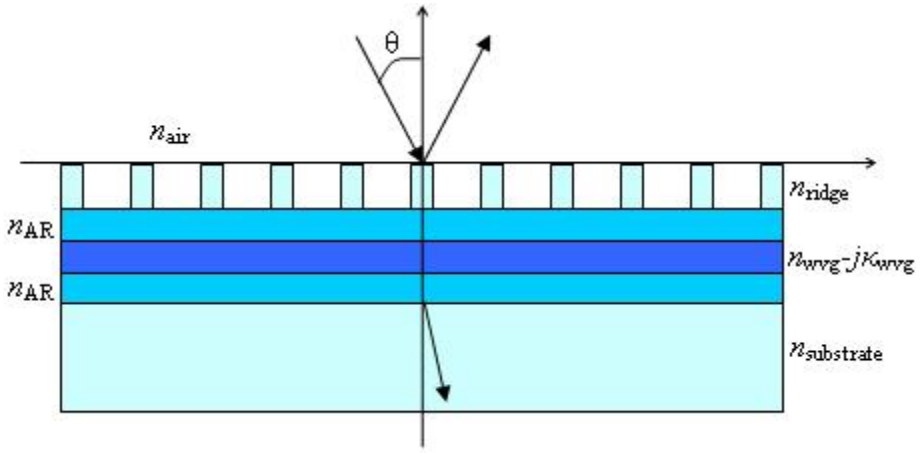

Figure 6-1 Guided Mode Resonance Structure with gain/loss layer integrated

Using RCWA, a GMR structure without gain or loss is designed initially to produce a narrowband reflection peak at a design wavelength (in this case λ = 1.55 μm). The multilayer structure under study consists of a high index substrate ($n_{substrate}$ = 3.24), a quarter wave – half wave – quarter wave thickness stack with refractive indices of n_{AR} = 3.37, n_{wvg} = 3.5, and n_{AR} = 3.37, and a grating layer with high and low refractive indices of n_{ridge} = 3.24 and n_{groove} = n_{air} = 1 respectively. The input half space is assumed to be air. For normally incident having TE polarization, a grating period of 469 nm is chosen such that a resonance is produced at the design wavelength and non-zero order diffraction is not present in either the input or output half-spaces. The fill factor (.1705) and the thickness of the grating (230 nm) are chosen such that the broadband Fresnel reflection of the structure is minimized.

6.2 Results and Discussion

As shown in Figure 6.2 and Figure 6.3, the addition of loss or gain to the system is investigated by varying the imaginary part of the refractive index for the wave guiding layer. Figure 6.2 shows the spectral response of the structure's absorption, reflection, and transmission

as the imaginary part of the refractive index is varied over positive values, i.e. loss in our definition.

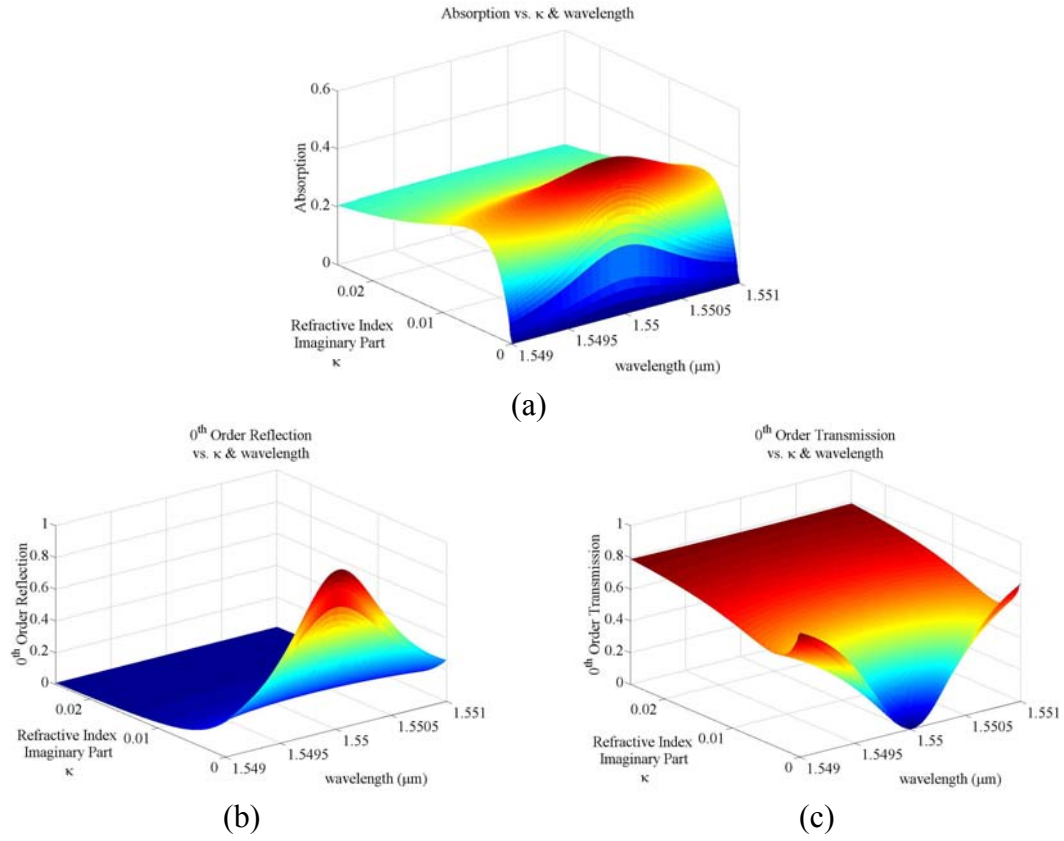

Figure 6-2 (a) GMR absorption wavelength spectra plotted for varying imaginary refractive index. (b) Corresponding 0^{th} order reflection spectra. (c) Corresponding 0^{th} order transmission spectra.

Initially, a peak absorption of approximately 50% with an absorption line width of 2.5 nm is found at the design wavelength when $\kappa_{wvg} = .0027$. By further varying the grating thickness at this value of κ_{wvg}, the peak absorption is increased to 64% and the absorption line width is 1.9 nm when the grating thickness is equal to 296 nm. This increased absorption peak results from an improved phase matching between the diffracted wave and the guided leaky mode. A further increase in the loss coefficient of the material reduces the absorption peak, causing most of the

energy to shift into the 0th transmitted order. This effect is due to the fact that as the loss is increased, the phase matching condition no longer holds between the tangential component of the diffracted wave and the modal index of the leaky mode.

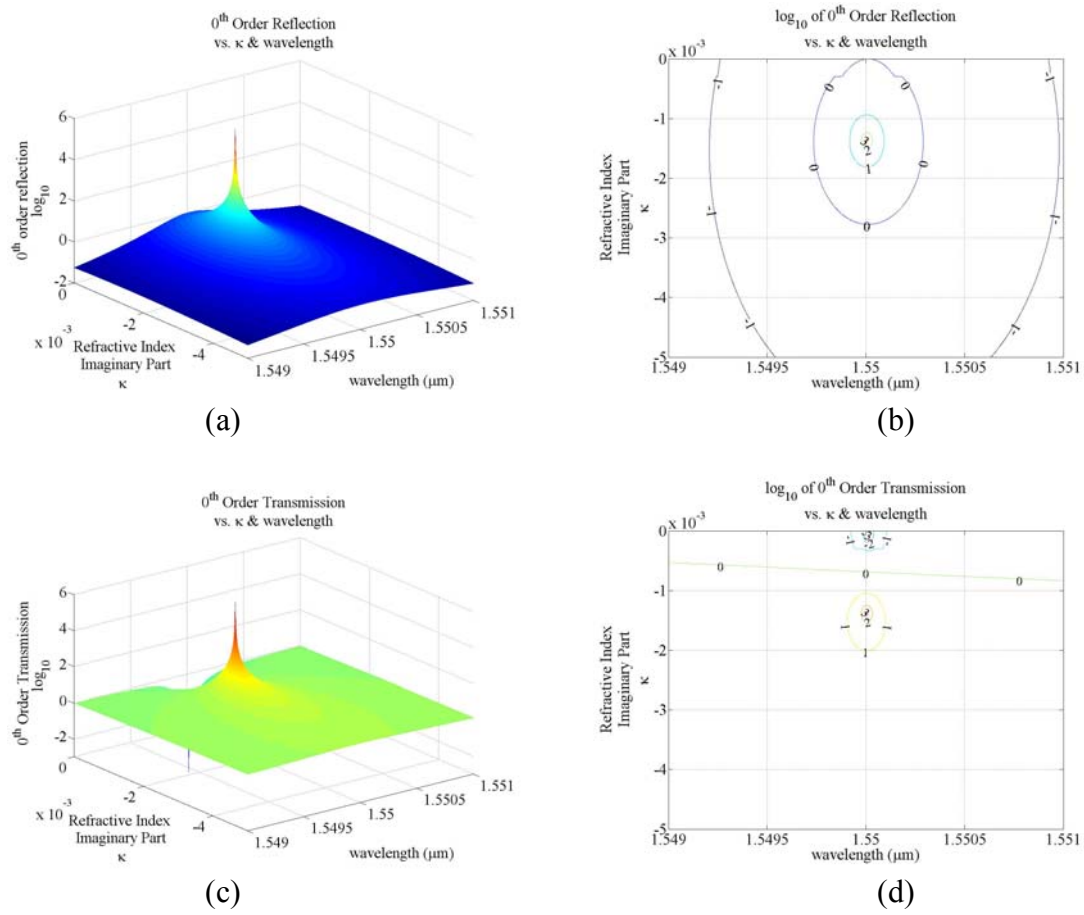

Figure 6-3 (a) 0th order reflection plotted with change in wavelength and imaginary part of refractive index for the guiding layer. (b) Contour plot of 0th order reflection. (c) 0th order transmission plotted with change in wavelength and imaginary part of refractive index for the guiding layer. (d) Contour plot of 0th order transmission.

Similarly, Figure 6.3(a) through Figure 6.3(d) show the spectral response of the 0th order reflection and 0th order transmission as κ_{wvg} is varied over negative values, i.e. gain in our definition. While feedback is not pertinent to this numerical model, in a practical system utilizing optical pumping, feedback into the pumping source is not desirable. To eliminate any

feedback along the direction of the incident wave, the angle of incidence is set to 10º. While the issues of the previous chapter involving the interaction of multiple modes at oblique incidence would be relevant to increasing the angular tolerance of this model, multiple modes were not considered in this example. The grating period is adjusted to 446 nm to maintain resonance at the design wavelength, and the fill factor (.179) and the grating thickness (220 nm) are adjusted to minimize broadband reflection.

Upon varying the gain, a peak reflection occurs at a value of κ_{wvg} = -.00137. At this value of κ_{wvg}, the peak reflection is increased by a factor of greater than 2.6 x 10^5 versus a gain-less resonator, while the level of the sidebands changes considerably less. As shown in Figure 6.3(b), the existence of a resonant reflection is very tolerant to a change in the amount of gain present in the wave guiding layer, but the substantial increase in resonant reflection that occurs near the peak value of the gain occurs within a narrower range. The resonant response takes on a Lorentzian line shape in both wavelength and gain. Near the gain resonance, the 0^{th} order transmission of the structure increases significantly, with a peak transmission having the same order of magnitude as the peak reflection. For both the reflection and transmission responses, increasing the gain beyond an optimal value decreases the effectiveness of the resonator. As with the absorption response, an increase in the gain causes the phase matching condition to breakdown, eventually eliminating the resonance entirely.

As previously suggested [133], use of a gain material within a GMR device could be useful as an integrated mirror/resonator/amplifier for either a vertical cavity laser or as a means of altering an incident free space optical wave in an optical pumping regime, but the gain level must be kept within a specific, albeit wide, range to maintain resonant reflection. Similarly, the addition of a lossy material to a GMR structure could also be useful as a narrowband, current

producing spectral sensor [134], but the amount of loss included within the GMR structure will affect the shape, or even the presence, of the resonant absorption spectral profile. As with all GMR devices, finite beam size and finite grating size will affect the resonant performance of the structure. Furthermore, the effects presented above are for steady-state gain or loss of the system. In summary, this chapter shows that incorporation of gain or loss within a defined range for a specific GMR device geometry can be expected to enhance resonant reflection/transmission or absorption.

CHAPTER 7 EMBEDDED WAVEGUIDE GRATINGS AND WAVEGUIDE GRATING FILTERS/MIRRORS

In the same manner that a periodic structure can be used as a means of spatially and spectrally filtering a free-space optical wave, gratings may also be utilized to filter and reflect guided waves. Over the past decade, there has been a considerable amount of research in the area of planar photonic crystal waveguides which make use of this idea [68, 137-142]. In a planar photonic crystal waveguide, a spatially periodic array of holes is etched into waveguide that vertically confines a guided mode. By varying the periodicity, removal factor, and index contrast of the holes, as well as creating "defects" in areas where holes are not present, photonic crystal waveguides exploit Bragg diffraction from multiple rows of embedded layered gratings to guide light within the defect regions. An embedded resonant grating performs in a slightly different manner from a standard planar photonic crystal mirror. In an embedded resonant grating, the vertically guided mode is incident on what can be a single row periodic structure. Transverse diffraction occurs at the site of this periodicity, and when the mode is phase-matched to the periodic region, energy is stored in the periodic layer and either resonant reflection or resonant transmission can occur.

A principal problem in planar photonic crystal waveguides and embedded gratings is that of vertical confinement. When a waveguide mode is tightly confined to the waveguide core, due to a vertical core/cladding refractive index contrast, the presence a lower index inclusion, such as an air hole, causes vertical scattering of light. The strength of this vertical scattering depends on all properties of the holes (periodicity, removal factor, index contrast, depth). If the removal of material can be replaced by the addition of material of a higher refractive index than all other

materials within the waveguide, then vertical scattering from a planar periodic structure can be eliminated.

This chapter explains how the design of an embedded resonant grating structure was attempted, using two separate two-dimensional models. The first two-dimensional is a horizontal-direction + longitudinal-direction model that uses an effective index for the vertical direction. This model can show transverse diffraction, but assumes the vertical direction is infinitely invariant. The second two-dimensional model is a vertical-direction + longitudinal-direction model that determines the modal index of the confined vertical mode. This model can also take into account vertical scattering from low index inclusions, but does not include transverse diffraction. By comparing the results of the initial two-dimensional model with a fully three-dimensional model, the assumption of a vertical effective index made in the horizontal + longitudinal two-dimensional model is shown to ignore vertical scattering and eliminates (or at least severely reduces) the possibility of properly designing an embedded resonant grating with low index periodic inclusions. Finally, the incorporation of high refractive index periodic inclusions within the waveguide is shown to solve the problem of vertical scattering and allow for the design of embedded resonant grating structures.

7.1 Two-Dimensional Embedded Grating Models

7.1.1 Determination of the Waveguide's Modal Index

In order to determine the modal index of a vertical slab waveguide, a multilayer modal solver was utilized. Both the transcendental dispersion equation approach described in Chapter 2 and the RCWA/PML method described in Chapter 3 can be utilized to determine the modal index of a slab waveguide. In both this chapter and the next, the base structure considered is a

high refractive index device representing an AlGaAs multi-quantum well core, surrounded by a graded index cladding, with a GaAs substrate, a GaAs cover layer, and an air superstrate. Figure 7.1 shows the index distribution and spatial modal profile of the single mode waveguide considered.

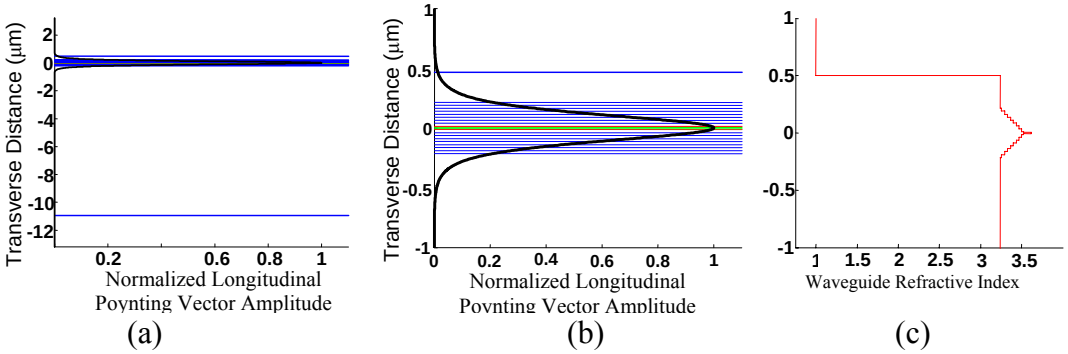

Figure 7-1 The normalized longitudinal Poynting vector component and refractive index distribution of the single mode waveguide showing both location and size of the graded index section relative to the substrate and the power distribution within the graded index section.

The modal index of this single mode waveguide is 3.355. Variations in the cover layer thickness, and to an even lesser extent in the substrate thickness, have a small effect on this modal index.

7.1.2 Two-Dimensional Horizontal + Longitudinal Model

A two-dimensional model of the transverse diffraction was implemented using the standard infinitely periodic grating implementation of RCWA where the high refractive index regions were assigned the modal index of the single mode waveguide and the low refractive index regions were assigned to be air. As the incident light is confined within the waveguide, the input region of the model is assigned the value of the high refractive index material. Since the original concept to be studied called for a waveguide mirror, the output region was assigned to be that of air, as would be present in a cleaved end-facet. In order to create the conditions for

both transverse diffraction and a resonator cavity, a single row of air holes was placed within the high index region as shown in Figure 7.2.

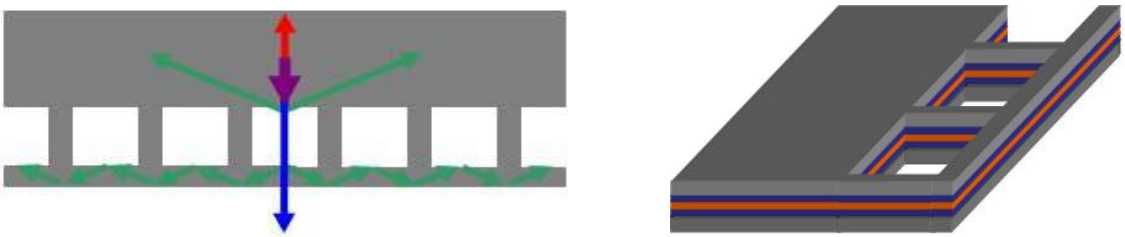

(a) (b)

Figure 7-2 (a) A top view of an waveguide with an embedded periodicity of low-index inclusions (air holes) and a thin resonator cavity layer, as well as arrows representing the incident, reflected and diffracted plane wave directions in the structure. (b) A three-dimensional view of the waveguide with embedded air holes.

The periodicity of the grating was chosen such that upon normal incidence, an input plane wave produces both +1 and -1 diffracted orders within the high index regions but produces no higher order diffraction within the output air region. Since the presence of this transverse diffraction could potentially degrade the performance of an input light source, the grating should be designed to minimize the amount of energy diffracted into these orders. This same diffraction mechanism also occurs within the resonator cavity, but upon resonance of the +1 and -1 diffracted orders in this region, nearly all of the input energy would be retro-reflected into the input 0^{th} order. Figure 7-3 shows the reflection response for a system of square low index inclusions.

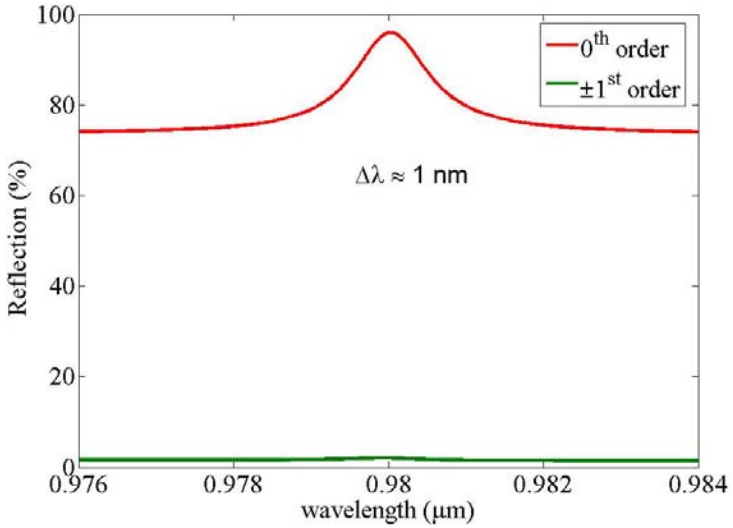

Figure 7-3 The reflection response of the 0^{th} order and $\pm 1^{st}$ order diffracted plane waves in the 1D grating RCWA model.

While this structure does produce a nearly 100% reflection response on resonance, the presence of a high index contrast output causes a significant broadband reflection response as well. In order to decrease the level of this broadband reflection without having to introduce extra material layers, the addition of subwavelength gratings acting as artificial optical materials can be introduced [143, 144] as shown in Figure 7-4.

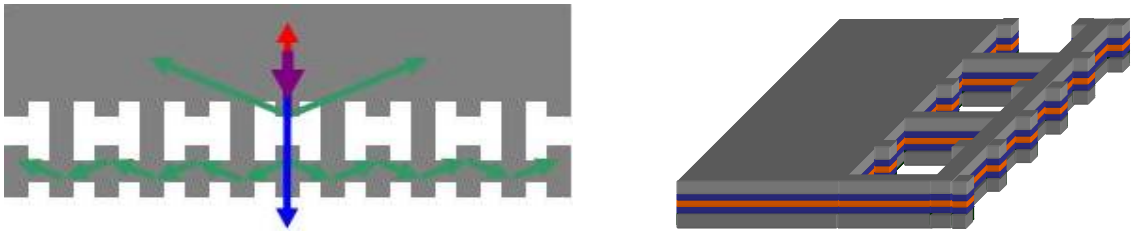

(a) (b)

Figure 7-4 (a) A top view of an waveguide with an embedded periodicity of low-index inclusions (H-shaped air holes) and a thin resonator cavity layer, as well as arrows representing the incident, reflected and diffracted plane wave directions in the structure. (b) A three-dimensional view of the waveguide with embedded H-shaped air holes.

At each interface of the homogeneous high index material, a subwavelength grating is added in order to decrease the impedance mismatch between that high index material and either the adjacent grating layer or the output air region. For the two subwavelength AR layers surrounding the diffraction grating, mechanical stability and fabrication issues for the resulting structure would limit the periodicity of these layers to be half that of the actual diffractive grating layer. This geometry produces what from the top-down view would look like a row of "H" shaped holes. On the output side of the structure the periodicity of the subwavelength grating can take any periodicity that does not produce higher order diffraction in the air regions or +2 or -2 diffraction in the high index region, but for simplicity in the computations this period was chosen to be the same as the other two AR layers. Figure 7-5 shows the 0^{th} order reflection response of this structure.

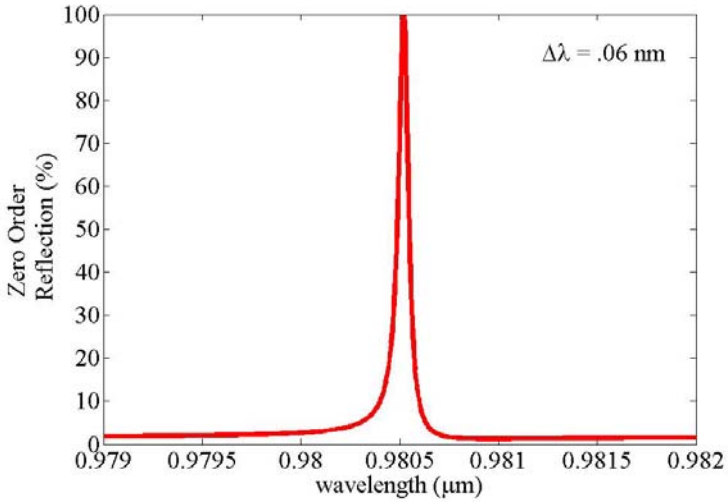

Figure 7-5 The reflection response of the 0^{th} order and ±1st order diffracted plane waves in the 1D grating RCWA model for the structure with H-shaped air holes.

As is desired for any resonant grating reflection filter, the broadband reflection response of this structure is almost non-existent, whereas the narrowband reflection response is nearly 100%.

7.1.3 Two-Dimensional Vertical + Longitudinal Model

In order to estimate the amount of loss due to vertical scattering from longitudinal holes, the two-dimensional, RCWA/PML eigenmode expansion, scattering matrix model was utilized. A single low index inclusion was set to represent an air hole that has been fully etched through the graded index waveguide down to the level of the substrate.

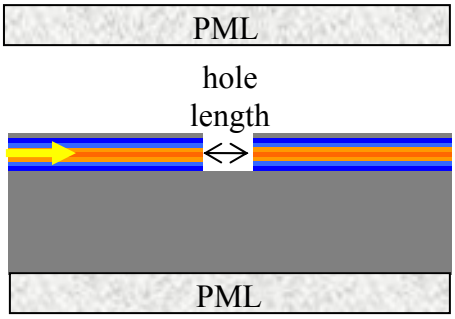

Figure 7-6 A sketch showing the graded index waveguide with a fully etched hole (etched to the substrate) where the length of the hole is set to be the maximum hole length considered in the H-shaped holes of the previous section. The sum of the spectral reflection and transmission into the fundamental mode was used to estimate vertical losses from the etched waveguide.

By setting the length of this hole to be the same as the length of the holes used in the previous section, the difference between the incident energy and the sum of the reflection and transmission coefficients of the fundamental mode in the input and output waveguides can be used to estimate the amount of loss due to vertical scattering. In the wavelength range from 970 nm to 990 nm, the vertical loss from the structure with a hole length of 400 nm ranged from 23.4% to 23.7%.

7.2 Three-Dimensional Embedded Grating Models

A full three dimensional model of an embedded grating was implemented using RCWA with incorporated PML boundary conditions in the vertical direction, purely periodic boundary

conditions in the horizontal direction, and identical infinite waveguides in the input and output half-spaces. The two-dimensional modal problem to be solved in each longitudinal slice makes use of the coupled wave expansion as described in Section 3.1.3 as well as the Fourier harmonic expansions for 2D systems described in Appendix C with horizontal symmetry considerations as derived in Appendix D. The propagation of energy was calculated using the scattering matrix method of Section 4.3, with the reflection coefficients of each mode determined using the methods described in Section 3.3. Due to the large number of Fourier harmonics used to obtain convergence of the eigenvalue problem (1059 harmonics on a diamond shaped grid) for each transverse slice, the determination of spectral modal reflection and transmission coefficients resulted in rather long computational run times.

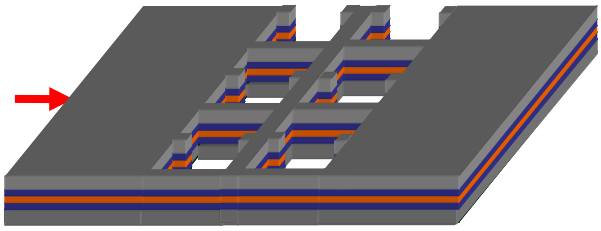

Figure 7-7 A sketch of the longitudinally symmetric 3D structure considered in the computation having an output half-space waveguide as opposed to a half space air region.

Using the final grating geometries presented in the previous section, two rows of "H" shaped holes are embedded in the waveguide structure. This structure was tested for the longitudinally symmetric three-dimensional model shown in Figure 7-7 using an output waveguide as opposed to an output air half-space, due to concerns about the accuracy of representing the system as having a purely homogeneous output air half space that would involve longitudinal interfaces between vertical PML layers and complete air regions (as well as concerns about numerical contamination between previously isolated unit cells), or having an

output air region with vertical PML layers whose mode structure was not clearly understood. Figure 7-8 shows both the reflection and transmission response of this structure.

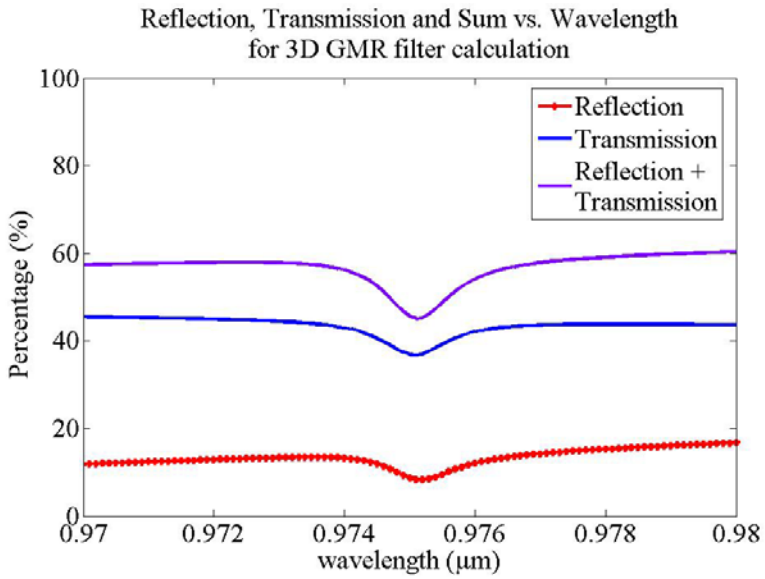

Figure 7-8 Reflection and transmission response of the fundamental mode associated with the longitudinally symmetric structure with two rows of H-shaped holes. The sum of the reflection and transmission clearly indicate that on resonance this structure has enhanced scattering (either vertical or longitudinal but out of the fundamental mode).

The location of the resonance for this structure can be seen, but the performance of the structure on resonance is not as desired. On resonance both the transmission and reflection of the device in the fundamental mode have decreased, which can be interpreted as an increase in the amount of vertical scattering that occurs in the device on resonance. Consequently, the inclusions of these low-index holes in no way act as a narrowband resonant mirror for a vertically confined waveguide mode.

Upon conclusion of this work involving low index inclusions, it was found in the patent by Grann [145], a means of resolving this vertical scattering issue. The concept presented requires that the transverse periodic inclusions in a vertical waveguide must possess a higher refractive index than all of the other materials comprising the vertical slab waveguide. When the

periodic inclusions are the highest index in the material, transverse diffraction of the input waveguide mode can occur without excessive vertical scattering. Energy diffracted by the embedded grating is both vertically and horizontally concentrated in the regions near the high index inclusions and a true resonator cavity can then be created. Fabrication of such a device structure in a semiconductor waveguide is a considerable challenge due to the need to either backfill material into holes or grow material around pillars in a controlled and precise manner.

Testing of both the low index inclusion and high index inclusion device structures are both very costly computational problems. While code capable of modeling the device structure was written and debugged, a definitive answer as to the feasibility of a low index inclusion structure operating as an embedded resonant waveguide grating device could not be determined satisfactorily given the present computational resources. The one 3D calculation produced in this study made use of C_{2v} symmetry considerations and ignored the substrate altogether. The reasoning behind this assumption was that the fundamental mode is confined primarily to the graded index waveguide, with little impact from the substrate itself. Any scattering from that input fundamental mode would then result in energy lost that could not be fed back into that mode through a resonant cavity. Even with these symmetry considerations, the 101 iterations utilized to produce Figure 7-8 took 2 weeks of run-time, and several previously failed trials due to out of memory errors, to produce. As the price/performance ratio of computational hardware decreases, and the use of parallel algorithms in photonics becomes more prevalent (or at least the ability of the present author and potential readers to write effective parallel algorithms increases), the ability to tackle computational problems of the size and scope considered in this chapter will become much more common place. So in conclusion, the concept of an embedded waveguide grating guided mode resonant filter having low index inclusions remains an open problem.

CHAPTER 8 ALL-DIELECTRIC UNIDIRECTIONAL DUAL GRATING OUTPUT COUPLER

8.1 Introduction

Traditionally, the out coupling of light guided within a planar waveguide has been achieved in one of four manners: end facet couplers, prism couplers, tapered couplers and grating couplers [146]. End facet coupling creates the problems of reflection from a cleaved facet back into the input waveguide mode that can affect the stability of the light source generating the guided wave, the presence of an elliptical spot size created by planar waveguides that normally have vastly different horizontal and vertical dimensions, and the potential for catastrophic end facet damage in high power configurations. Prism coupling eliminates the issues of reflection into an input mode and end facet damage by the use of vertical surface coupling, but the necessity for a prism to have a denser refractive index than the materials comprising the waveguide also precludes the use of prism coupling for high refractive index semiconductor waveguides. Vertically tapered couplers normally consist of an adiabatic variation of the modal index of a waveguide by means of a gradual geometric variation, similar to a prism coupler, but normally results in a large beam divergence. Transversely tapered couplers can be either adiabatic transverse variations [147] or a numerically optimized series of end facet couplings that utilize multilayer resonance effects [148]. In either case, the use of a final end facet coupling retains the same potential for end-facet damage in high power configurations. The use of a surface grating as a means of out coupling from a planar waveguide addresses the weaknesses of both end facet and prism coupling by minimizing reflection into the input waveguide mode and providing a means of surface coupling for any type of material, while also spreading power over a larger surface area and providing numerous degrees of freedom for shaping the output beam.

Grating coupler surface emitting devices tend to have deep grooves in order to interact with the guided mode. This results in diffraction in both a low index superstrate, normally air, and a higher index substrate. Consequently, there is a splitting of the diffracted energy between the substrate and superstrate regions, an example of which can be seen in Figure 8-1.

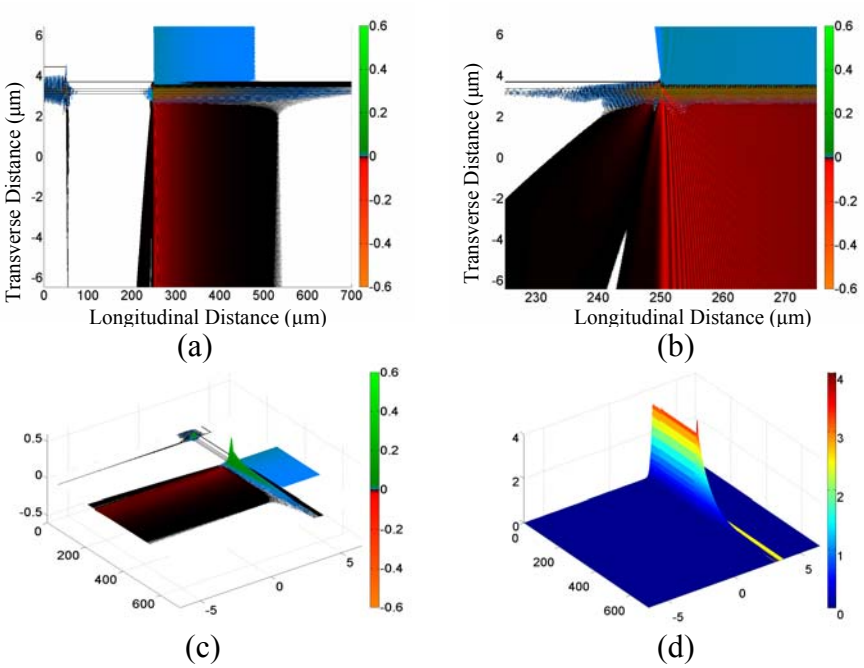

Figure 8-1 Power flow in a single surface grating with a 275 nm period, 250 nm depth, and 50% fill factor, which shows the splitting of diffracted energy between a substrate region (70%) and a superstrate region (30%). (a) Transverse power flow over the entire computational window. (b) Transverse power flow near the initial grating interface. (c)-(d) 3D view of transverse and normal power flow showing the power magnitude.

Attempts to force unidirectional coupling of the diffracted energy have previously involved the addition of either a metallic coating [149, 150] or a thin-film quarter-wave-stack coating to either the grating or the substrate [151]. Metallization of either the grating or the substrate introduces additional absorption and scattering losses which are also problems that should try to be minimized. The addition of a quarter wave stack mirror requires the deposition of additional

thin film layers having tight fabrication tolerances, which increases the structure's overall fabrication complexity.

In recent years, the concept of dual-side wafer processing for semiconductor waveguides has been introduced. By integrating a superstrate-side diffraction grating with either a substrate side refractive or diffractive element, numerous applications in spatial and spectral beam control have been introduced [149, 152]. In this work, we present a novel all-dielectric unidirectional grating coupler that avoids the need for any additional material deposition. A model for a unidirectional coupler with a 96% output coupling efficiency is obtained. The dual grating structure is shown to be tolerant to a variety of potential fabrication errors while maintaining a high output power coupling efficiency.

8.2 Proposed Structure and Device Design Methodology

8.2.1 Proposed Structure

The device considered consists of a single mode high index waveguide with a superstrate grating that does not produce diffraction in the superstrate air region and diffracts only a single order into the substrate, as well as a substrate side grating that diffracts a single order in the substrate side air region as shown in Figure 8-2.

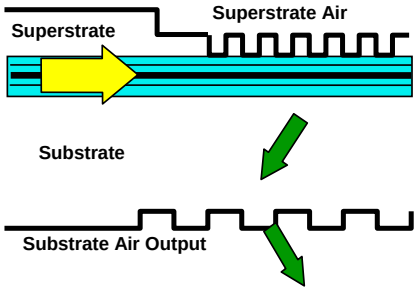

Figure 8-2 A simple drawing of the dual grating output coupler device considered in this study, as well as the principal directions of energy flow in the structure.

The periodicity for the superstrate side grating must result in that the guided mode diffraction by the grating produces no propagating diffracted orders in air and only produces a single diffracted order in the substrate region. This is determined from the grating equations:

$$k_{\text{tangential,diffracted}} = k_{\text{tangential,mode}} - pK_{\text{sup}}$$
$$n\sin\theta_{dif} = n_{\text{mode}} - p\frac{\lambda_0}{\Lambda_{\text{sup}}} \tag{8.2.1}$$

where λ_0 is light wavelength, Λ_{sup} is the periodicity of the superstrate grating, and n is the average refractive index of the region where the diffraction occurs. In order to restrict the propagation of diffracted orders in air, the upper bound on the superstrate periodicity is as follows:

$$\Lambda_{\text{sup}} < \lambda_0/(n_{\text{mode}}+1) \tag{8.2.2}$$

To ensure the propagation of at least a single diffracted order in the substrate region (n_{sub}), the lower bound on the superstrate periodicity obeys the following inequality:

$$\Lambda_{\text{sup}} > \lambda_0/(n_{\text{mode}}+n_{sub}) \tag{8.2.3}$$

For the grating on the substrate side, the grating equation is as follows:

$$\sin\theta_{dif,out} = \left(n_{\text{mode}} + \frac{\lambda_0}{\Lambda_{\text{sup}}}\right) - p\frac{\lambda_0}{\Lambda_{\text{sub}}} \tag{8.2.4}$$

To ensure that the substrate grating will produce only a single diffracted order in air, its periodicity is determined by the following inequalities:

$$\lambda_0/(n_{\text{mode}} - \sin\theta_{air} + \lambda_0/\Lambda_{\text{sup}}) < \Lambda_{sub} < 2\lambda_0/(n_{\text{mode}} - \sin\theta_{air} + \lambda_0/\Lambda_{\text{sup}}) \tag{8.2.5}$$

To investigate the properties and behavior of the proposed dual grating structure, the properties of each individual grating are rigorously studied by means of the Rigorous Coupled Wave Analysis (RCWA), using both its original form for infinite transverse gratings [12, 13] and its

application to finite-sized integrated optical structures [9, 16, 20, 153]. Finally, the integration of both gratings in a single device is studied using this same finite waveguide eigenmode expansion method. A similar approach to modeling an integrated dual grating directional coupler using a different eigenmode expansion technique has been used previously as well [154].

8.2.2 Single Mode Waveguide

The waveguide under consideration consists of a multi-quantum well $Al_xGa_{1-x}As$ region of tens of nanometer thickness surrounded by equivalent graded index Al_xGa_{1-x} regions of roughly 200nm in thickness on top of a GaAs substrate (n = 3.24). A superstrate GaAs cladding layer is added on top of the graded index layers. Using a modal solver with incorporated Perfectly Matched Layer (PML) boundary conditions, the modal index of this TE single mode waveguide considered at a 980 nm wavelength is determined to be 3.355. Figure 8-3 shows the longitudinal component of the time-averaged Poynting vector associated with this waveguide mode.

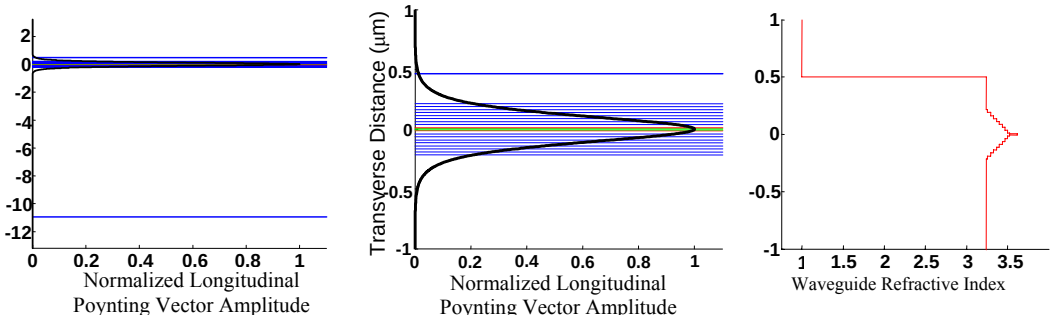

Figure 8-3 The normalized longitudinal Poynting vector component of the single mode waveguide showing both the location and size of the graded index section relative to the substrate and the distribution of power within the graded index section.

8.2.3 Bounds on Grating Periodicities

The modal index of the single mode waveguide is then used to determine the range of periodicities allowing for unidirectional output coupling from the substrate side of the device. For a modal index, n_{mode} = 3.355, the upper limit of the superstrate side grating periodicity is 225 nm (which ensures no diffraction in air). For a substrate region average index, n_{sub} = 3.24, the lower limit of the superstrate-side grating periodicity is 148 nm (which ensures the presence of diffraction into the substrate). As shown in Equation 8.2.5, the range on the substrate grating period depends upon the choice for the superstrate grating period, which determines the incident and exit angles for the substrate grating.

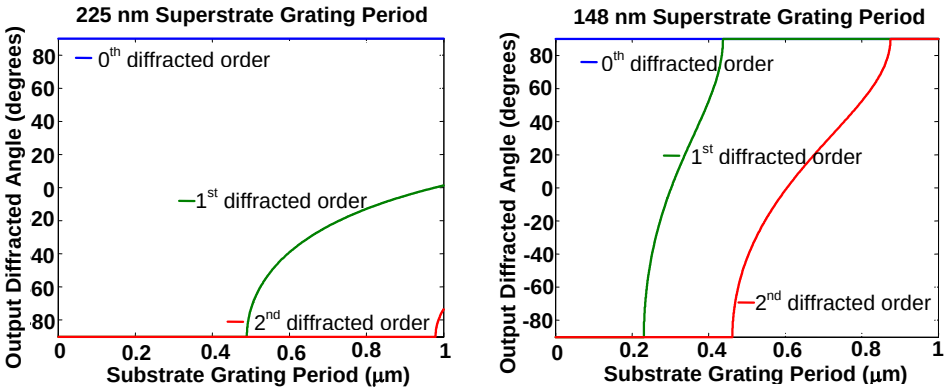

(a) (b)

Figure 8-4 The output diffracted angle in air vs. the substrate grating period, for substrate index of nsub = 3.24, and a superstrate grating period of (a) 225 nm. and (b) 148 nm.

As shown in Figure 8-4(a), for a superstrate grating period of 225 nm, the substrate grating period can take a value of anywhere from 490 nm (where the 1st order begins propagating) to 979 nm (where the 2nd order begins propagating). Similarly Figure 8-4(b) shows that for a superstrate grating period of 148 nm, the substrate grating period can range from 231 nm to 437 nm. With a choice of superstrate grating period between 148 nm and 225 nm, the potential periodicity range for the substrate grating moves accordingly, but as shorter

periodicities produce larger diffracted angles into the substrate, it is desirable to choose a period at the longer end of this range.

8.2.4 Determination of Proper Individual Grating Strengths

Once the ranges of potential superstrate and substrate grating periodicities are known, the gratings can then be evaluated on the basis of their diffractive strengths. For the superstrate and substrate gratings, properties such as the grating periodicity, depth, fill factor, and profile all contribute to how power is diffracted away from the input waveguide mode and out of the device substrate.

Since the superstrate grating affects the coupling loss from the input mode most significantly, its properties are investigated first. To analyze the superstrate grating in isolation, PML boundary conditions are placed adjacent to the superstrate air region and the GaAs substrate. A virtually semi-infinite grating coupler (length ~1 m) is used to ensure that all the energy is coupled out and no reflection occurs from a possibly mismatched output half-space waveguide. However, coupled energy was only collected over a finite length (~700 μm) which is found to be sufficient, in most cases, to collect all power that is scattered in the transverse direction by the structure as shown in Figure 8-5.

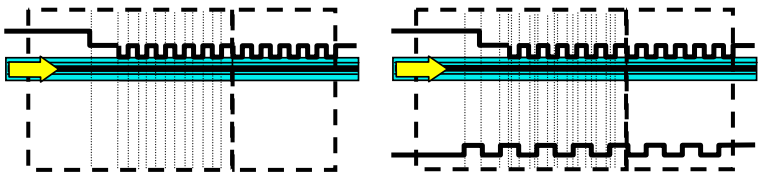

Figure 8-5 A sketch showing the computational and power collection windows for both a single surface grating with an "infinite" substrate and a dual grating coupler. Dotted lines represent interfaces used to define layer scattering matrices.

The selection of grating period, thickness, and fill factor for the superstrate grating involves a trade off between the coupling length of the complex grating mode, the modal mismatch between the input waveguide mode and the leaky waveguide-grating mode, and the reasonable ability to fabricate the chosen grating geometry.

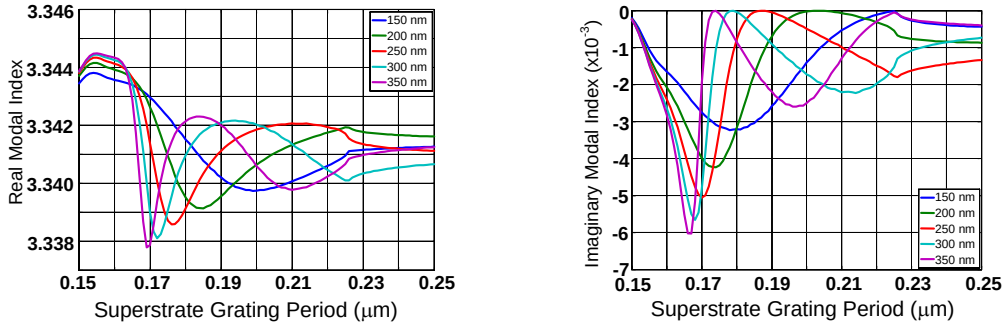

Figure 8-6 (a) Real part and (b) imaginary part of the Bloch mode index of the fundamental mode in the superstrate grating vs. superstrate grating period for various grating thicknesses.

Figures 8-6(a) and (b) show the real and imaginary Bloch mode index values vs. period associated with the superstrate grating for various grating thicknesses having a 50% fill factor calculated using the generalized eigenvalue approach described in Cao et. al [22]. While all values within the previously defined superstrate periodicity range will couple nearly all of the input power into the substrate, the variation in modal losses, seen in Figure 8-6(b), show that coupling length can vary significantly with grating period and grating depth. A grating period of 220 nm with a grating depth of 250 nm is chosen due to it having a relatively shallow diffraction angle in the substrate (~20º), a significant modal loss for our chosen 50% fill factor, a negligible reflection, and a reasonable depth from a fabrication point of view. Consequently, these parameters are utilized in the remainder of this work. Figures 8-7(a) through (d) show views of the transverse and normal components of the Poynting vector at a 220 nm period, with a 250 nm grating depth and 50% fill factor, which produce a 99.9% coupling efficiency into the substrate.

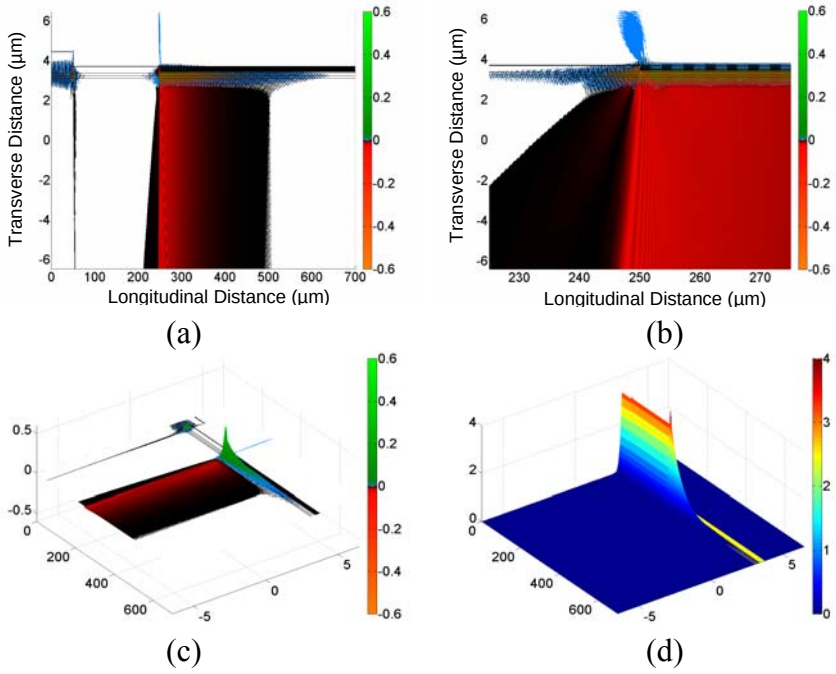

Figure 8-7 Power flow in a single surface grating (a) Transverse power flow over the length of the coupler (b) Transverse power flow near the initial grating interface. (c)-(d) 3D view of transverse and normal power flow showing the power magnitude.

Having analyzed properties for the superstrate grating, we then investigate the substrate grating properties. Using the infinitely periodic, grating form of RCWA, diffraction into the 1st diffracted order in air is calculated for the following set of parameters: a high index input half-space is assigned the refractive index of the GaAs substrate (n = 3.24), a low index output half-space is assigned that of air (n = 1), and the incident angle is assigned as the previously determined superstrate grating diffraction angle into the substrate (~20º). In performing a full parameter scan of the 3 dimensional space of grating period (400 nm to 700 nm), grating depth (25 nm to 525 nm), and fill factor (0 to 1), for the grating under consideration, it is found that a fill factor of 30% produced the highest diffraction efficiency over a wide range of grating periods and depths. The 2D contour plot of 1st order diffraction efficiency vs. grating depth and grating period at a fill factor of 30% is shown in Figure 8-8. The diffraction efficiency is calculated to

be above 85% within relative a wide range (570-595 nm for the grating period and 250-270 nm for the grating depth). Any grating period and grating depth within these ranges will produce nearly the maximum efficiency.

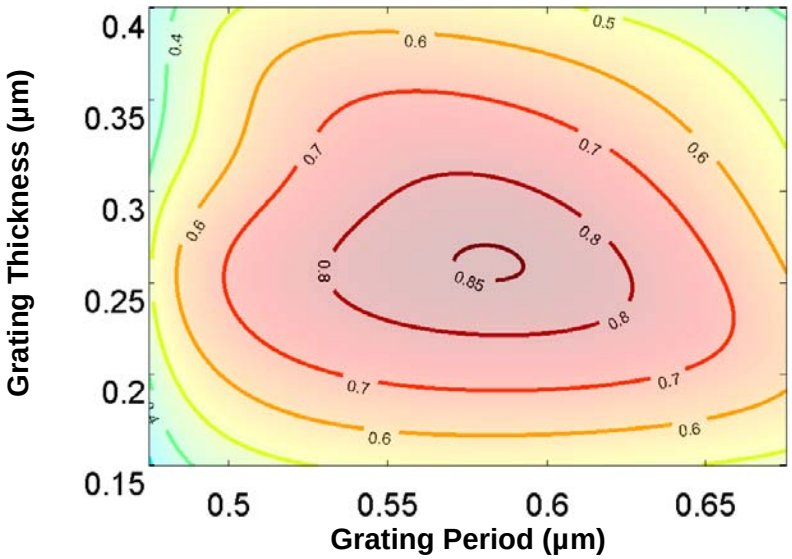

Figure 8-8 Contour plot showing the effects of varying grating period and grating depth on the 1st order Transmission efficiency for an infinite binary grating with an input refractive index, $n_{input} = 3.24$, an output refractive index, $n_{output} = 1$, a grating tooth refractive index of $n_{ridge} = 3.24$, a grating groove refractive index, $n_{groove} = 1$, an input angle, $\theta_{input} = -19.83°$, and a grating fill factor of 30%.

However, to reduce the computational effort it is important for the ratio between the periodicities of the superstrate side and substrate side gratings to have a ratio of two small integers. This reduces the length of the unit cell, as well as the number of layers needed to represent that unit cell. For example, a substrate grating period of 582 nm (peak of the range) would result in a grating period ratio of $\Lambda_{superstrate}/\Lambda_{substrate} = 110/291$ and over 800 distinct layers within the unit cell with a length of just over 64 microns. However, by choosing a grating period integer ratio of 3/8, resulting in a substrate grating period of 586 2/3 nm, the 1st order diffraction efficiency remains above 85%, but the length of the longitudinal unit cell (1.76 µm) and the

number of distinct layers (23 layers) within the unit cell are both significantly reduced. A more detailed discussion of the layer slicing necessary for modeling double grating structures in eigenmode expansion techniques can be found in Dong et. al [154].

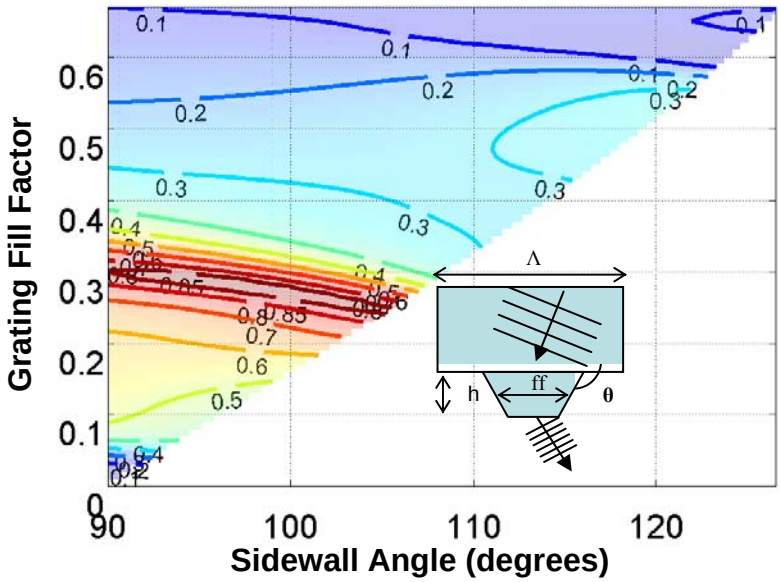

Figure 8-9 Contour plot showing the effects of varying the half-height grating fill factor and grating tooth sidewall angle on the 1st order Transmission efficiency for an infinite binary grating with an input refractive index, $n_{input} = 3.24$, an output refractive index, $n_{output} = 1$, a grating tooth refractive index of $n_{ridge} = 3.24$, a grating groove refractive index, $n_{groove} = 1$, an input angle, $\theta_{input} = -19.83^{\circ}$, a grating period of 586.66 nm, and a grating depth of 260 nm. Sloped sidewalls are approximated by an 8 level staircase profile. White background regions with a fill factor less than 67% represent gratings with triangular teeth which were not considered.

In Figure 8-9, we investigate the effect of the substrate grating profile by determining the 1st order diffraction efficiency of an infinitely periodic substrate grating as a function of the half height fill factor vs. outer sidewall angle for a grating depth of 260 nm. The tapered sidewall angle is approximated by an 8 level staircase profile. Angles that are greater than 90º represent a sloped grating tooth sidewall. Outside of the colored contour plot, the white background indicates grating tooth parameters that will produce a triangular shaped grating tooth and are not considered here. A slightly tapered sidewall angle of 92º at a fill factor of 30% is calculated to

have the best diffraction efficiency performance at nearly 86%, but as can be seen in Figure 8-9; in the neighborhood of a 25-30% fill factor there is a considerable amount of variation possible in the sidewall angle that maintains greater than 80% transmission efficiency.

8.2.5 Full Dual Grating Coupler Model

Building on the knowledge gained from investigating the superstrate and substrate grating properties, the performance of the full dual grating coupler device is then explored. For this dual grating structure, the two gratings are separated by a substrate of multiple wavelength thickness. In a real device this substrate is likely to be 100-500 μm in thickness, but to keep practical limits on the required amount of computation time we limited the size to about 10-20 μm such that the utilized number of spatial harmonics will maintain convergence in the eigenvalue problems. The superstrate and substrate gratings are then surrounded by air regions that are then adjacent to PML boundary layers. In order to collect all of the downward diffracted energy from the initial waveguide/superstrate grating interface, the length of the substrate grating is extended from the longitudinal location of the waveguide/superstrate grating interface toward the input interface by an arbitrary length of 150 μm. While this choice of length is more than enough to collect all of the scattered light for a substrate thickness of roughly 10 μm, for a realistic substrate of a few hundred microns a substrate grating extension of this length scale will be critical to collecting all of the scattered light. This length choice depends upon the substrate thickness and the angle of diffraction in the substrate. For the structure having simple binary superstrate and substrate gratings, the effect of grating separation on the model is initially tested. As can be seen in Figure 8-10(a), by changing the thickness of the substrate, relatively narrow resonances are produced, but by examining Figure 8-10(b), representing the reflection into the

input interface, as well as the reflection coefficients of all individual modes in the input half-space, these resonances can be attributed to coupling into higher order super-modes of the overall device.

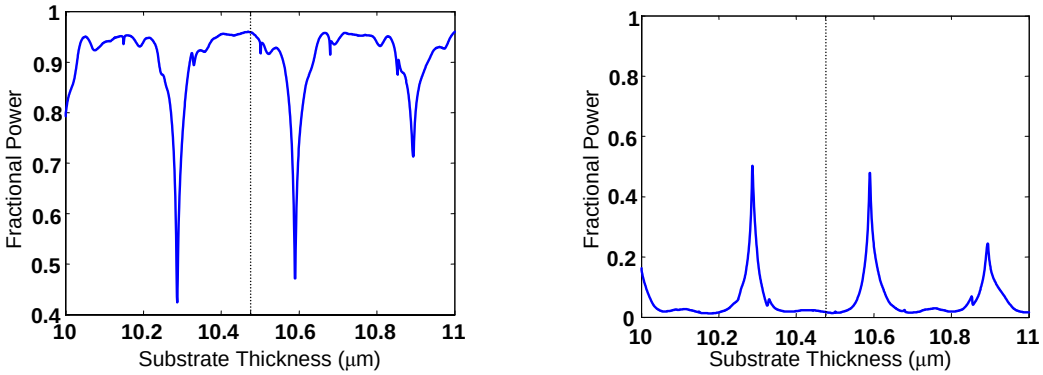

Figure 8-10 (a) Relationship between substrate thickness/grating separation and fractional substrate output coupling. Resonances indicate coupling to higher order super-modes of the entire waveguide stack. (b) Sum of the reflection into all individual modes at the computational window's input interface.

Given that a real device structure will have a slight amount of surface roughness and thickness variation over surface of the wafer; these resonances are most likely just an artifact of the model's "perfect geometry". To avoid this higher order mode coupling, a substrate thickness is chosen, as shown by the dotted line in Figure 8-10(a), in a relatively flat region between super-mode coupling resonances.

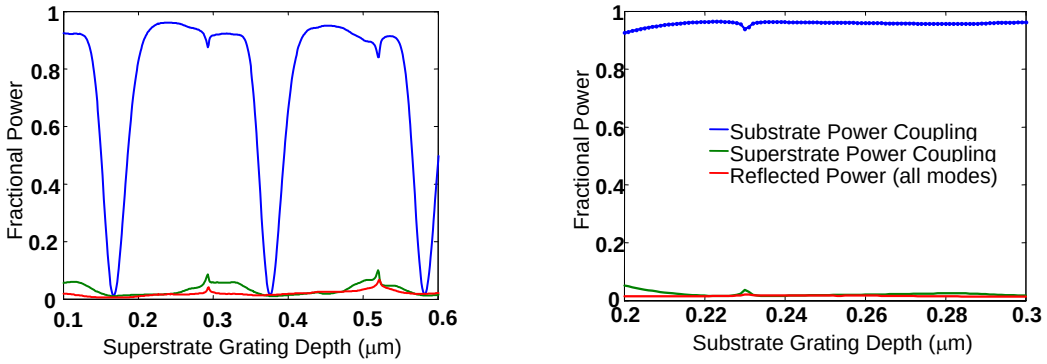

Figure 8-11 Substrate output power coupling vs. (a) the superstrate grating thickness and (b) the substrate grating thickness.

Figures 8-11(a) and (b) show the effects that varying superstrate grating thickness and substrate grating thickness in a dual grating structure have on substrate output power coupling efficiency. The narrow resonances in Figures 8-11(a) and (b) correspond to super-mode type resonances discussed earlier, while the broader resonances in Figure 8-11(a) correspond to increased coupling lengths (decreased modal leakage rates) that cause most of the energy to be guided beyond the 700 μm longitudinal window length.

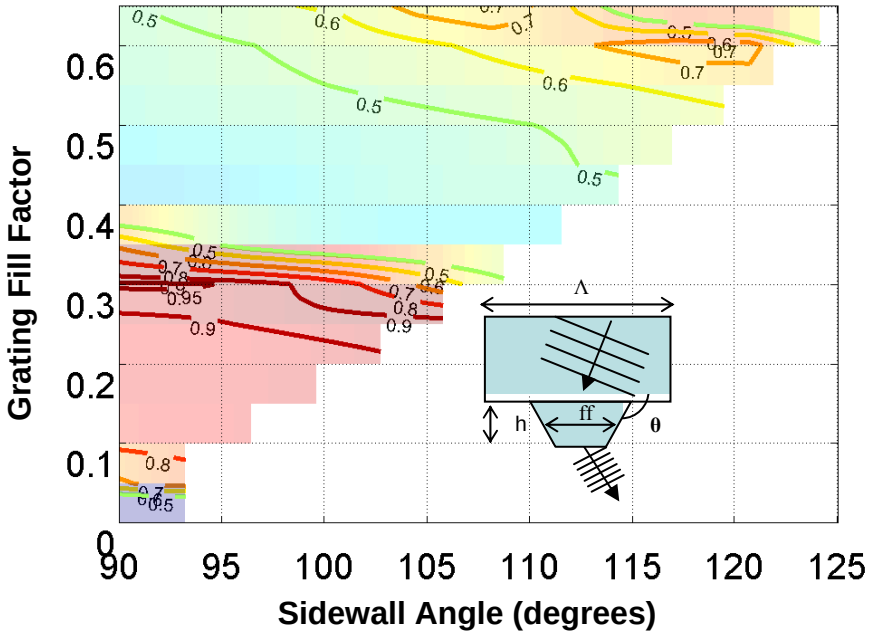

Figure 8-12 Map showing the effects of varying the half-height grating fill factor and grating tooth sidewall angle on the substrate output power coupling for the dual grating coupler. As in Figure 8-9, the white background regions with a fill factor less than 67% represent gratings with triangular teeth which were not considered.

Figure 8-12 shows the effects on substrate output power coupling for varying the substrate grating's half-height fill factor and outer side-wall angle. As in the infinite grating model, the peak substrate power coupling efficiency, which in this case is close to 96%, occurs near a fill factor of 30% and has a slightly sloped sidewall angle of 92º. As can be seen in Figure 8-12, there is a channel in the vicinity of a 25-30% fill factor, where the substrate power coupling efficiency remains above 90% from a sidewall angle of 90º to just over 105º. Both Figures 8-11 and 8-12 show that for the initial grating parameters determined in the previous section, a robust and tolerant output grating coupler having an output coupling efficiency around 96% can be achieved. As is the case with varying the grating period ratios, to perform sloped side-wall calculations for the dual grating device, stair-casing of the gratings increases the

number of layer interfaces, distinct eigenvalue problems, and scattering matrices required within a longitudinal unit cell.

Figure 8-13 shows the normal and transverse Poynting vector components for a dual grating coupler having a superstrate grating period, fill factor, and thickness of 220 nm, 50%, and 250 nm respectively, as well as a substrate grating period, fill factor and thickness of 586.66 nm, 30% and 260 nm respectively. Within the 700 μm longitudinal power collection window, the substrate power coupling efficiency is nearly 96%, with just over 2% coupled from the superstrate side of the device (primarily at the initial interface of the superstrate grating), and just under 2% coupled into all modes of the input interface. The substrate coupling efficiency can likely be improved upon even further by using a tapered transitional superstrate grating period similar to the approach used in Lalanne et. al [155]. Chirping the superstrate grating fill factor [150], depth, or period will also provide for the ability to shape the spatial distribution of output power, but will admittedly make the computational design process much more costly in time and memory requirements.

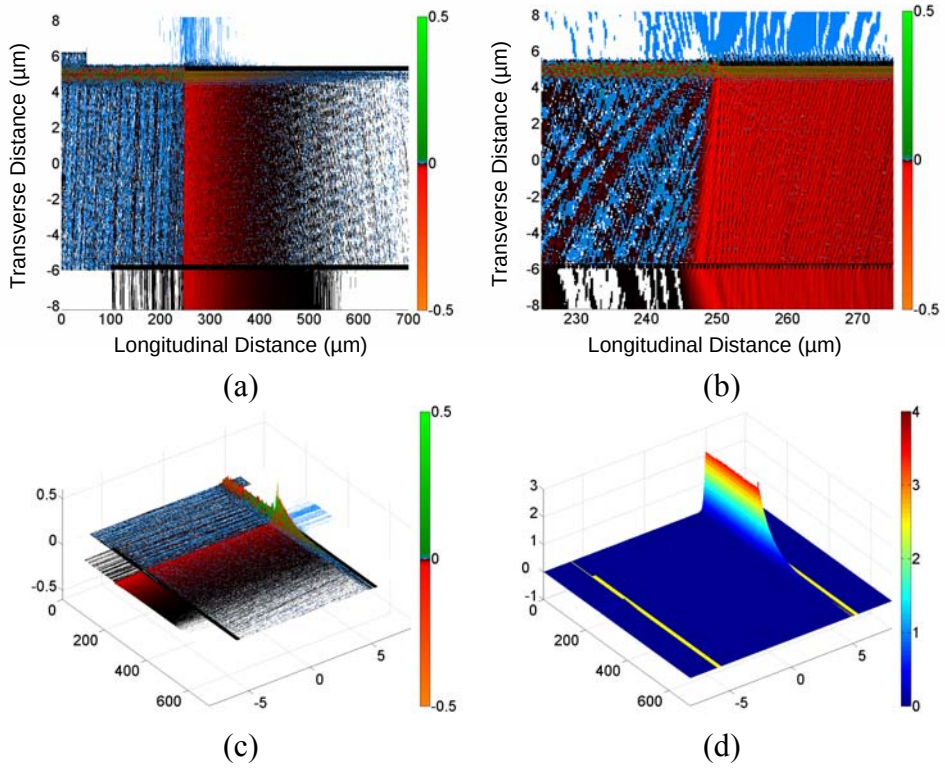

Figure 8-13 Power flow in a dual grating coupler with a superstrate grating having a 220 nm period, 250 nm depth, and 50% fill factor, and a substrate grating having a 586.67 nm period, a 260 nm depth, and a 30% fill factor, which show the splitting of diffracted energy between the substrate region (96%) and superstrate region (~2%). (a) Transverse power flow over the entire computational window. (b) Transverse power flow near the initial superstrate grating interface. (c)-(d) 3D view of transverse and normal power flow showing the power magnitude.

Figure 8-14(a) shows the near-field transverse Poynting vector component at 2 µm from the substrate grating surface and Figure 8-14(b) shows the angular spectrum of this Transverse Poynting vector component calculated using a discrete Fourier transform performed on our non-uniformly spaced longitudinal sampling window. As can be seen in this angular spectrum the vast majority of the light coupled from the device is located in a very narrow angular range around a diffraction angle of 34º.

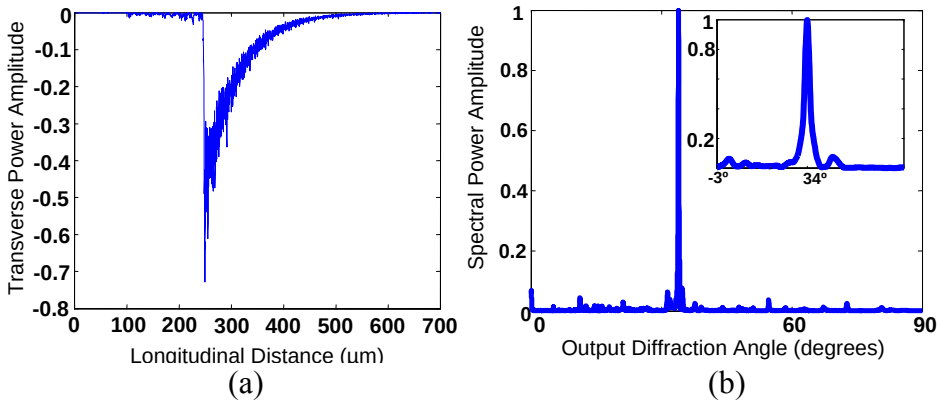

Figure 8-14 (a) Transverse power flow in air at 2 μm from the surface of the substrate grating. (b) Angular spectrum of the transverse power in air, and an inset showing the shape of the angular spectrum at ± 3º of its maximum value.

Figure 8-15(a) shows this transverse Poynting vector component propagated through 100 μm of air by performing an inverse discrete Fourier transform. Figure 8-15(b) shows this same transverse Poynting vector component spatially filtered at ±3º around the peak 34º angular spectrum component, which clearly shows how energy can be concentrated in a particularly narrow angular range and whose spectral profile can be maintained over a long propagation distance.

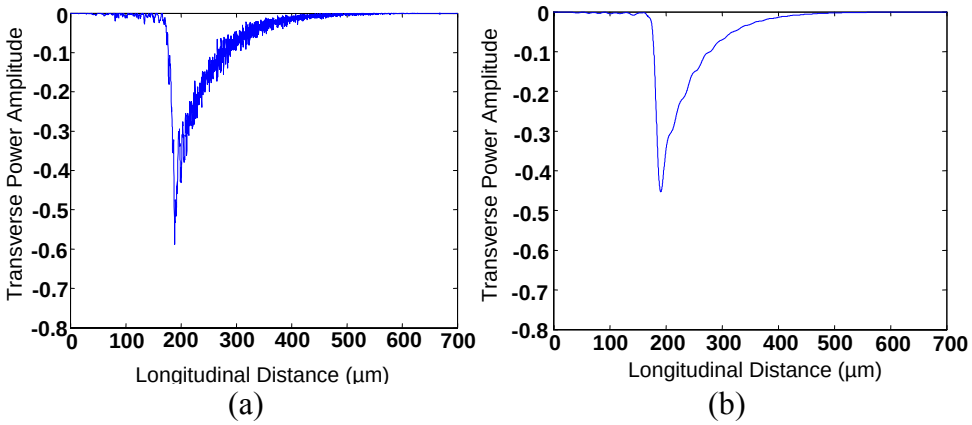

Figure 8-15 (a) Transverse power flow in air at 100 μm from the surface of the substrate grating, calculated by propagating the angular spectrum using an Inverse Discrete Fourier Transform. (b) Transverse power flow in air at 100 μm from the surface of the substrate grating spatially filtered at ± 3º of the maximum angular spectrum component.

8.2.6 Spectral Response of the Dual Grating Coupler

The spectral response of the dual grating coupler was modeled using the final geometry and varying the wavelength over a 100 nm range (01 nm sampling) as shown in Figure 8-16.

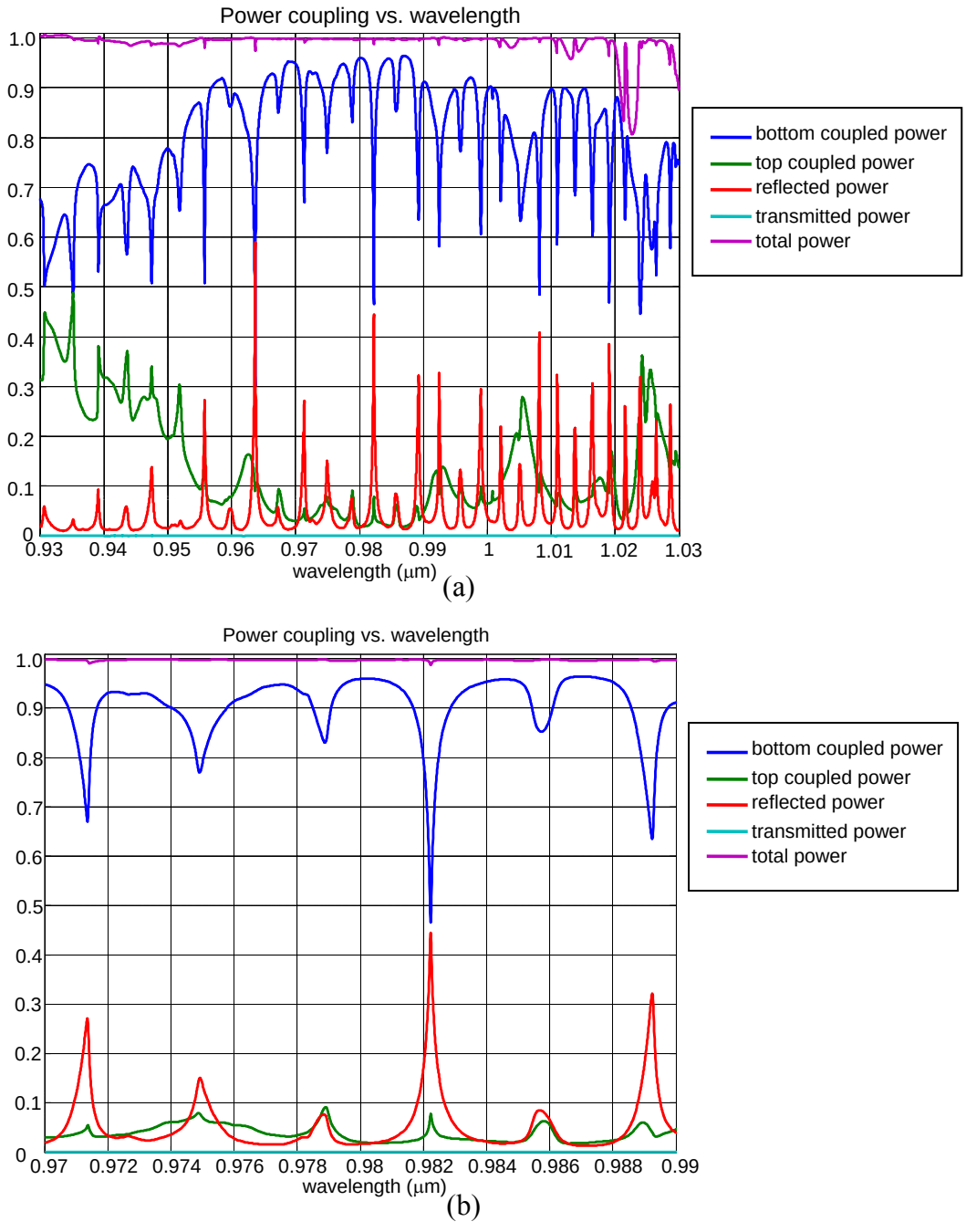

Figure 8-16 (a) Broadband spectral response of the dual grating output coupler. (b) Narrowband response around the design wavelength of 980 nm.

In a similar manner to the testing of the effect of variable substrate thickness in section 8.2.5, a number of resonances can be observed in the power output from the bottom of the structure as well as in the total reflected power. By examining the individual reflection coefficients for each of the high order modes in the input waveguide, once again the phenomena of coupling to supermodes of the input waveguide. And while this supermode coupling occurs at a more frequent interval for a variable wavelength with a fixed thickness, than for a variable thickness with a fixed wavelength, the effect is the same. By ignoring the individual resonances, the presence of a 25 to 30 nm band over which the output coupling is over 90% shows the effectiveness of the dual grating structure for acting as a broadband output coupler.

8.3 Dual Grating Coupler Conclusions

By rigorously modeling, both separately and together, the waveguide and two gratings contained in a dual grating device, a novel all-dielectric unidirectional output grating coupler was designed. The all-dielectric dual grating coupler is robust in that it does not depend on any type of resonance or any type of phase matching between the two gratings and is also tolerant to potential variations in numerous grating parameters. The device eliminates the need for any additional material deposition post-etching and fits neatly within the recently developed framework of dual sided wafer processing.

CHAPTER 9 CONCLUSIONS AND FUTURE PERSPECTIVES

This research study aimed to investigate the integration of disparate optical components, namely waveguides and gratings, in individual device structures that provide enhanced functionality due to integration. To accomplish this task, a combination of numerical methods for rigorously solving Maxwell's equations on wavelength and subwavelength scales and analytical methods for interpreting data and understanding the underlying physical processes were used in driving the design process. Despite the numerical and computationally intensive means of building the necessary tools and performing the various device studies, the end goal of the process always remains an increased understanding of the relevant device physics; the capabilities and the limitations of tightly integrated bulk waveguides and periodic structures.

The numerical tools utilized in performing the physical device studies included both the transcendental equations governing the properties of eigenmodes in multilayer slab waveguides and one-dimensional periodic lamellar gratings, as well as the Rigorous Coupled Wave Analysis (RCWA)/Fourier harmonic modal method for 1D, 2D, and 3D periodic optical structures. The later modal method (RCWA) was combined with two separate, numerically stable, mode-matching/energy-propagation techniques, the enhanced transmittance matrix (T-Matrix) technique and the scattering matrix (S-Matrix) technique, in order to create a rigorous, efficient, and flexible computational tool for modeling a variety of discrete or continuous, symmetric or asymmetric, periodic or aperiodic, wavelength scale integrated optical devices. In this work's main body, as well as the attached appendices, a thorough description of the various components of these mathematical techniques has been provided along with a description of how these components were built into a single computational modeling tool capable of efficiently handling a wide variety of cases.

These numerical tools were applied in the modeling of a multilayer, multimode, waveguide grating, guided mode resonance (GMR) filter. Initially, the real-valued dispersion properties of the multilayer, multimode GMR filter was modeled by coupling an effective medium representation of a lamellar grating etched into the top layer of a multilayer structure with the transcendental modal equation representation of the multilayer slab waveguide. By holding the parameters of the grating layer constant, it was shown that the resonant responses of multiple spectral resonances can be controlled from a coarse to a fine separation by only controlling the thicknesses of a two-material multilayer slab waveguide. Then by utilizing the RCWA/S-Matrix representation of the multilayer, multimode GMR filter, the complex-valued modal dispersion bands were used for studying the angular acceptance bandwidth of multiple spectral resonances. By simultaneously engineering multiple dispersion band edges, through the variation of multiple material layers, a multilayer, multimode GMR filter was designed that had broadened angular acceptance for multiple wavelengths and whose angular resonances were centered at the same angle of incidence. The use of a multi-wavelength guided mode resonant reflection filter with broadened angular acceptance at a single incident angle could be especially useful at oblique incidence since the reflected beams would be spatially separated from the input beams but would not require additional optics for re-collimating the two beams upon reflection. This collimation of would allow for interference effects for the two wavelengths to be easily observed in a sensing environment, to maintain multiwavelength mode locking as a mirror in a multiwavelength laser cavity, or to act as a compact multiple wavelength add/drop filter in a communications environment.

The properties of reflection and transmission responses in guided mode resonance filters were then studied in the presence of a linear loss or a linear gain in the multilayer structure's

main guiding layer. By varying the linear loss for set structural parameters, an enhanced resonant absorption was shown to occur at the design wavelength for a non-zero value for the layer's complex refractive index, but a large loss value was shown to eliminate the resonance altogether with most of the previous resonantly reflected energy being transmitted. Adding a lossy material to a guided mode resonant filter would potentially be useful as a current producing spectral sensor. By varying the gain coefficient of the guiding layer's complex refractive index, significantly increased amplitudes for both the resonant reflection and resonant transmission were shown to occur at the design wavelength, with a significantly narrowed bandwidth in both cases. The broadband reflection and transmission baselines were increased with increasing gain values as well. Adding gain to a guided mode resonant filter could potentially be useful as an integrated mirror/resonator/amplifier for either a vertical cavity laser or as a means for altering an incident free space optical beam in an optical pumping regime.

The idea of incorporating a low-index horizontal and transverse periodicity in a vertical slab waveguide was studied for the possibility of its use as an integrated resonant reflection filter for an input guided mode. In applying two-dimensional modeling, with an effective index approximation utilized for the vertical direction, the possibility of a low-index periodic inclusion looked promising. By incorporating both a diffractive grating that produced symmetric $\pm 1^{st}$ order diffraction in the high index region, as well as subwavelength anti-reflective gratings producing only 0^{th} order diffraction, two-dimensional models produce a narrowband resonant reflection response with a nearly 100% contrast between in band and out of band reflection. But the results obtained for the application of three-dimensional RCWA modeling suggest that a low-index periodic inclusion in a high index waveguide produces only a lossy resonator cavity where energy is diffracted vertically out of the input waveguide mode. A final answer to the question

of whether low-index transverse periodic inclusions could produce a narrowband guided mode resonant reflection filter was not definitively solved and remains an open problem.

A combination of multilayer waveguide modal modeling, analytical application of the grating equation, infinite transverse grating RCWA modeling, and transversely finite RCWA modeling for integrated optics was utilized in the study and design of an all-dielectric unidirectional grating output coupler. By analyzing both gratings individually and together as a single device, a robust output coupler was designed that depends neither on phase matching of the gratings nor any resonances in the structure, and the device was shown to be very tolerant to potential fabrication errors in numerous grating parameters.

For the specific devices studied in this dissertation, areas for further study could still be made in each case. For the multilayered, multimode GMR filters, finding a rigorous means of modeling these structures having a finite-spatial size would help to determine the effect that a finite size has on each individual mode and the overall device operation. Also, the idea of a multilayered, multimode GMR filter can be extended to two-dimensional gratings, which would help in the design of a polarization independent, multi-wavelength GMR filter with broadened angular acceptance at a single obliquely incident angle. For the study of the effects of gain or loss on a GMR filter, the integration of more complex and accurate material models for the gain or loss would show how a resonant mode interacts with a real material. For the embedded waveguide resonant grating filter, the use of more powerful computational hardware, or possibly more tightly written code for present hardware, will allow for the rigorous and accurate modeling of three-dimensional without the memory limitation problems and long computation times that plagued the current study. If a design for an embedded waveguide grating resonant filter for an input guided mode can be designed, then that would provide a compact means of spatially and

spectrally filtering a guided mode and would also be more easily fabricated than transversely periodic higher index inclusions. For the dual grating output coupler, more powerful computational systems will allow for the solution of eigenmode problems for larger waveguides that more closely match the size of real devices. More powerful models will also allow for slight random variations that appear in real materials while maintaining overall periodicity, and possibly allow for more complex spatial relationships between the two gratings (such as a tilting of the bottom grating) and the rigorous modeling of a full three dimensional waveguide dual grating output coupler.

Moving forward the methods utilized in this study can evolve in a number of manners. First, through the use of more powerful computational hardware and smarter serial and parallel algorithms, the device sizes and complexity of the optical structures that can be numerically studied and designed will increase. This will allow for more components of differing discrete and continuous geometries to be studied in an integrated fashion, and will allow for design of entire integrated optics systems in a rigorous manner. Second, the linear optical models utilized here will be enhanced to include the ability to solve for various non-linear optical phenomena [156, 157] as well as being coupled to various electrical [158], thermal, mechanical, and material models that will provide true multi-physics modeling capabilities on multiple spatial scales. All of which will provide the ability to gain a more comprehensive view of how these devices operate and allow for rapid virtual prototyping of these integrated optical structures.

APPENDIX A. ELECTROMAGNETIC PRELIMINARIES

Any description of the interaction between electromagnetic fields and any material medium should always begin with the beautifully defined Maxwell's Equations of electromagnetism. A similar derivation to that contained in this section can be found in any good textbook on electrodynamics [38, 54, 159, 160].

A.1 Deriving the Linear Time-Harmonic Maxwell's Equations

The differential form of Maxwell's Equations can be stated as follows:

$$\nabla \times \vec{E} + \frac{\partial \vec{B}}{\partial t} = 0 \qquad \text{(Faraday's induction law)} \qquad \text{(A.1.1)}$$

$$\nabla \times \vec{H} - \frac{\partial \vec{D}}{\partial t} = \vec{J} \qquad \text{(generalized Ampère's law)} \qquad \text{(A.1.2)}$$

$$\nabla \cdot \vec{B} = 0 \qquad \text{(Gauss' magnetic field law)} \qquad \text{(A.1.3)}$$

$$\nabla \cdot \vec{D} = \rho \qquad \text{(Gauss' electric field law)} \qquad \text{(A.1.4)}$$

where $\frac{\partial}{\partial t}$ is the partial derivative operator with respect to time, $\nabla = \left(\partial/\partial x, \partial/\partial y, \partial/\partial z\right)$ is the spatial partial derivative operator, $\vec{E}$, $\vec{H}$, $\vec{B}$, $\vec{D}$, and ρ are the electric field strength (volts/meter), magnetic field strength (amperes/meter), magnetic flux density (webers/meter^2), electric displacement (coulombs/meter^2), and electric charge density (coulombs/meter^3).

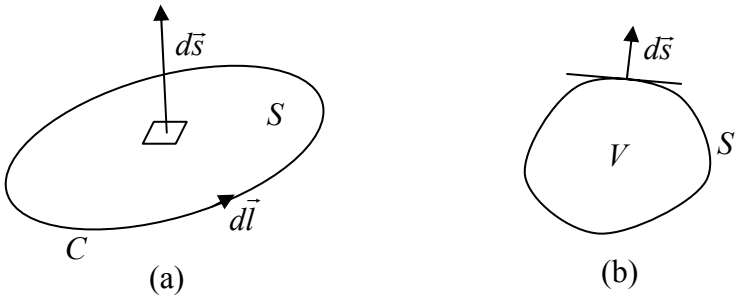

Figure A-1 (a) A sketch showing the relationship between a vector area element on a surface and the direction of traversal on a contour of that surface. (b) A sketch showing a volume bounded by a closed surface and the orientation of a vector area directed outward from that surface.

Upon integration of equation (A.1.1) over a surface, *S*, that is bounded by a contour, *C*, as shown in Figure A-1 and making use of Stokes' theorem and the divergence theorem from vector analysis, Maxwell's Equations may be placed in their integral form. Stokes' theorem states that for any piecewise smooth orientable surface, *S*, bounded by a closed, piecewise smooth curve, *C*, having positive orientation, performing a contour integral of the component of a continuous vector field having a continuous first partial derivative and is tangential to that contour is equivalent to performing a surface integral of the component of the curl of that vector field normal to the surface.

$$\oint_C \vec{F}(\vec{r},t)\cdot\hat{T}(\vec{r})dl = \iint_S \left(\nabla\times\vec{F}(\vec{r},t)\right)\cdot\hat{n}(\vec{r})dS \qquad \text{(Stokes' Theorem)} \qquad \text{(A.1.5)}$$

In Equation (A.1.5), $\vec{F}(\vec{r},t)$ is a vector field defined for a spatial position vector $\vec{r}$ and time *t*, $\hat{T}(\vec{r})$ is the unit tangent vector along contour *C*, and $\hat{n}(\vec{r})$ is the unit normal vector across surface *S*.

The divergence theorem states that for any solid of volume *V* having an outwardly oriented surface *S*, performing a surface integration over *S* of a vector field that has continuous first partial derivatives in an open set containing *V* is equivalent to performing a volume integration over *V* of the divergence of that vector field.

$$\oiint_S \vec{F}(\vec{r},t)\cdot\hat{n}(\vec{r})dS = \iiint_V \left(\nabla\cdot\vec{F}(\vec{r},t)\right)dV \qquad \text{(Divergence Theorem)} \qquad \text{(A.1.6)}$$

Applying Stokes' Theorem to Equations (A.1.1) and (A.1.2) and applying the divergence theorem to Equations (A.1.3) and (A.1.4) leads to Maxwell's Equations in their integral form.

$$\oint_C \vec{E}(\vec{r},t)\cdot d\vec{l} = -\frac{d}{dt}\oiint_S \vec{B}(\vec{r},t)\cdot d\vec{s} \qquad \text{(A.1.7)}$$

$$\oint_C \vec{H}(\vec{r},t)\cdot d\vec{l} = \frac{d}{dt}\oiint_S \vec{D}(\vec{r},t)\cdot d\vec{s} + \oiint_S \vec{J}(\vec{r},t)\cdot d\vec{s} \qquad \text{(A.1.8)}$$

$$\oiint_S \vec{B}(\vec{r},t)\cdot d\vec{s} = 0 \tag{A.1.9}$$

$$\oiint_S \vec{D}(\vec{r},t)\cdot d\vec{s} = \int_V \rho dV \tag{A.1.10}$$

$$\oiint_S \vec{J}(\vec{r},t)\cdot d\vec{s} = -\frac{d}{dt}\int_V \rho dV \tag{A.1.11}$$

For passive dielectric waveguides and gratings, source and current free regions are generally considered such that $\rho = 0$ and $\vec{J} = 0$. Given that the fields to be considered in this study are generally of a time-harmonic nature, a generic vector field, $\vec{F}(\vec{r},t)$ can be expressed as

$$\vec{F}(\vec{r},t) = \vec{F}(\vec{r})\exp(-j\omega t) \tag{A.1.12}$$

The electric displacement and the magnetic flux density are the result of the interaction between the material medium and the electric and magnetic fields respectively. $\vec{B}$ and $\vec{D}$ are related to $\vec{H}$ and $\vec{E}$ through the following constitutive relationships:

$$\vec{B} = \mu_0\vec{H} + \vec{M} \tag{A.1.13}$$

$$\vec{D} = \varepsilon_0\vec{E} + \vec{P} \tag{A.1.14}$$

where ε_0 is the permittivity of free space, μ_0 is the permeability of free space, and $\vec{M}$ and $\vec{P}$ are the magnetic and electric polarizations induced in the medium by the fields. For linear media, the magnetic and electric polarizations can be expressed in terms of $\vec{H}$, $\vec{E}$, and the magnetic and electric susceptibility tensors, χ_m and χ_e as follows:

$$\vec{M} = \mu_0[\chi_m]\vec{H} \tag{A.1.15}$$

$$\vec{P} = \varepsilon_0[\chi_e]\vec{E} \tag{A.1.16}$$

By inserting equations (A.1.7) and (A.1.8) into (A.1.9) and (A.1.10) respectively, the constitutive relationships can be expressed in terms of the magnetic permeability and electric permittivity tensors within the media as follows:

$$\vec{B} = \mu_0\left(1 + [\chi_m]\right)\vec{H} = \mu_0[\mu]\vec{H} \quad \text{(A.1.17)}$$

$$\vec{D} = \varepsilon_0\left(1 + [\chi_e]\right)\vec{E} = \varepsilon_0[\varepsilon]\vec{E}\,. \quad \text{(A.1.18)}$$

Consequently, the time-harmonic, source and current free version of Maxwell's equations can be expressed as

$$\nabla \times \vec{E} = j\omega\mu_0[\mu]\vec{H} \quad \text{(A.1.19)}$$

$$\nabla \times \vec{H} = -j\omega\varepsilon_0[\varepsilon]\vec{E} \quad \text{(A.1.20)}$$

$$\nabla \cdot \vec{B} = 0 \quad \text{(A.1.21)}$$

$$\nabla \cdot \vec{D} = 0 \quad \text{(A.1.22)}$$

A.2 Boundary Conditions Between Two Media

The versions of Maxwell's equations presented in section 2.1.1 are valid for any continuous medium, but at the surface between two dissimilar media, the permittivity, permeability, and conductivity of each medium may change abruptly from one medium to the other. In order to maintain a solution to the equations from one media to the next, boundary conditions must be imposed on the field vectors at the interface. To derive these boundary conditions, we consider a curved surface, *S*, separating medium 1, having constitutive parameters ε_1, μ_1 and medium 2, having constitutive parameters ε_2, μ_2, whose surface normal, $\hat{n}$, is positive in medium 1, as shown in Figure A-2.

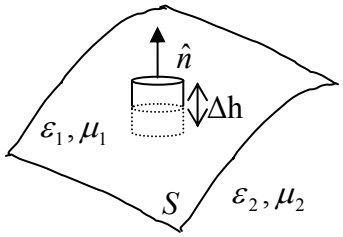

Figure A-2 An interface surface, *S*, located between two separate electromagnetic media with a surface normal, $\hat{n}$, and a pillbox used in determining the boundary conditions for the electric displacement and magnetic flux density.

A small circular cylindrical pillbox of height Δh is bisected by surface *S*. To determine the boundary condition on the magnetic flux density vector, a surface integral of $\vec{B}$ is performed over the surface of the pillbox. For a cylinder having a small cross-sectional area, Δs, $\vec{B}_1$ and $\vec{B}_2$ may be considered to be constant over each respective circular end. As the height approaches zero, Δh → 0, the location of the circular ends of the cylinder approach surface *S* and the magnitudes of $\vec{B}_1$ and $\vec{B}_2$ over the cylinder's curved surface on either side of *S* become negligible. Using Equation (A.1.9), the following condition on the normal component of the magnetic flux density at an interface can be expressed as

$$\left(\vec{B}_2 - \vec{B}_1\right) \cdot \hat{n} = 0 \tag{A.2.1}$$

Equation (A.2.1) shows that the normal component of the magnetic flux density is continuous across a surface boundary. By performing a similar surface integration involving the electric displacements, $\vec{D}_1$ and $\vec{D}_2$, the use of Equation (A.1.10) produces the following expression describing the boundary condition on the normal component of the electric displacement.

$$\left(\vec{D}_2 - \vec{D}_1\right) \cdot \hat{n} = \lim_{\Delta h \to 0} \rho \ \Delta h = \rho_s \tag{A.2.2}$$

Equation (A.2.2) shows that there is a discontinuity in the electric displacement at an interface between two media that is equal to the amount of electric charge located on that surface. In a source free environment, no surface charge is present; consequently the normal component of the electric displacement is continuous at the boundary between two media.

To find the boundary conditions for tangential field components, a rectangular loop of area, ΔA, having a length, Δl, and a height Δh is bisected by surface S as shown in Figure A-3.

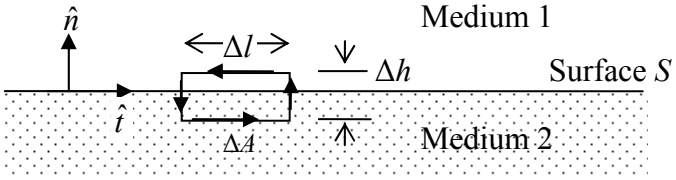

Figure A-3 A sketch of an interface between two media and a rectangular loop used for determining the boundary conditions of tangential field components.

As the height of the rectangular loop approaches zeros, $\Delta h \rightarrow 0$, the surface integrals on the right hand side of Equations (A.1.7) approaches a value of zero. Upon taking the difference between expressions for $\vec{E}_1$ and $\vec{E}_2$ involving the left hand side of Equation (A.1.7), the boundary conditions on the tangential electric field component can be expressed in the following manner:

$$\left(\vec{E}_2 - \vec{E}_1\right) \cdot \hat{t} = 0 \tag{A.2.3}$$

Expressions for tangential boundary conditions may also be derived by taking the vector cross product of the unit normal vector, $\hat{n}$, with the right hand sides of Equations (A.1.7) and (A.1.8) as the loop height, $\Delta h \rightarrow 0$.

$$\hat{n} \times \left(\vec{E}_2 - \vec{E}_1\right) = 0 \tag{A.2.4}$$

$$\hat{n} \times \left(\vec{H}_2 - \vec{H}_1\right) = \lim_{\Delta h \rightarrow 0} \vec{J}\ \Delta h = \vec{J}_{surface} \tag{A.2.5}$$

Equation (A.2.5) shows that the tangential magnetic field is discontinuous by an amount equal to the surface current density at the interface of the two media. In the case where no current is present, the tangential magnetic field is continuous at the boundary.

A.3 Conservation of Energy and the Poynting Theorem

By taking the dot product of Equation (A.1.1) with $\vec{H}$ and the dot product of Equation (A.1.2) with $-\vec{E}$, as well as making use of the following vector identity:

$$\nabla \cdot \left(\vec{A} \times \vec{B}\right) = \vec{B} \cdot \left(\nabla \times \vec{A}\right) - \vec{A} \cdot \left(\nabla \times \vec{B}\right) \tag{A.3.1}$$

the following expression relating $\vec{E}$, $\vec{H}$, $\vec{B}$, and $\vec{D}$ can be obtained:

$$\vec{E}(\vec{r},t) \cdot \frac{\partial \vec{D}(\vec{r},t)}{\partial t} + \vec{H}(\vec{r},t) \cdot \frac{\partial \vec{B}(\vec{r},t)}{\partial t} = -\nabla \cdot \left(\vec{E}(\vec{r},t) \times \vec{H}(\vec{r},t)\right) - \vec{E}(\vec{r},t) \cdot \vec{J}(\vec{r},t) \tag{A.3.2}$$

If the right hand side of Equation (A.3.2) can be assumed to be a time varying quantity of a scalar function $W(\vec{r},t)$, then Equation (A.3.2) may be expressed as

$$\vec{E}(\vec{r},t) \cdot \frac{\partial \vec{D}(\vec{r},t)}{\partial t} + \vec{H}(\vec{r},t) \cdot \frac{\partial \vec{B}(\vec{r},t)}{\partial t} = \frac{\partial W(\vec{r},t)}{\partial t} \tag{A.3.3}$$

which may also be written as

$$\frac{\partial W(\vec{r},t)}{\partial t} = -\nabla \cdot \mathrm{P}(\vec{r},t) - Q(\vec{r},t) \tag{A.3.4}$$

where

$$\begin{aligned} \mathrm{P}(\vec{r},t) &= \vec{E}(\vec{r},t) \times \vec{H}(\vec{r},t) \\ \mathrm{P}(\vec{r},t) &= \frac{1}{2}\mathrm{Re}\left(\vec{E}(\vec{r},t) \times \vec{H}(\vec{r},t)^{*}\right) + \frac{1}{2}\mathrm{Re}\left[\left(\vec{E}(\vec{r},t) \times \vec{H}(\vec{r},t)\right)e^{(-j2\omega t)}\right] \end{aligned} \tag{A.3.5}$$

is the instantaneous Poynting vector and complex Poynting vector with units of watts/m^2 and $Q(\vec{r},t)$ represents the energy dissipated in a medium per unit volume per second. The Poynting

vector is a measure of the amount of power in a unit area whose surface normal is perpendicular to both the electric and magnetic fields. Equation (A.3.4) represents a form of conservation of energy and is known as the differential form of Poynting's Theorem.

A.4 Lorentz Reciprocity Theorem

The concept of reciprocity in electromagnetism refers to the idea that for time harmonic fields, the system response to a source is unchanged if the position of the source and the receiver are interchanged [161]. In the context of dielectric waveguides and gratings, the concept of reciprocity is useful for establishing orthogonality of the system's eigenmodes. Here we follow the derivations as given by Kong [38] and Bienstman [54]. Establishing the concept of reciprocity involves the consideration of the electric and magnetic fields established by two sources. In terms of Maxwell's equations in a single linear isotropic media, the relationships between the first source $\vec{J}_1$ and its corresponding fields $\vec{E}_1$ and $\vec{H}_1$, and the second source $\vec{J}_2$ and its corresponding fields $\vec{E}_2$ and $\vec{H}_2$ can be expressed as follows:

$$\nabla \times \vec{E}_1 = -j\omega\mu\vec{H}_1 \tag{A.4.1}$$
$$\nabla \times \vec{H}_1 = j\omega\varepsilon\vec{E}_1 + \vec{J}_1 \tag{A.4.2}$$
$$\nabla \times \vec{E}_2 = -j\omega\mu\vec{H}_2 \tag{A.4.3}$$
$$\nabla \times \vec{H}_2 = j\omega\varepsilon\vec{E}_2 + \vec{J}_2 \tag{A.4.4}$$

Expressions involving the curl of the electric or magnetic fields due to one source are then multiplied by the magnetic or electric fields corresponding to the other source as follows:

$$\vec{H}_2 \cdot \left(\nabla \times \vec{E}_1\right) = -j\omega\mu\vec{H}_2\vec{H}_1 \tag{A.4.5}$$
$$\vec{E}_2 \cdot \left(\nabla \times \vec{H}_1\right) = j\omega\varepsilon\vec{E}_2\vec{E}_1 + \vec{E}_2\vec{J}_1 \tag{A.4.6}$$
$$\vec{H}_1 \cdot \left(\nabla \times \vec{E}_2\right) = -j\omega\mu\vec{H}_1\vec{H}_2 \tag{A.4.7}$$
$$\vec{E}_1 \cdot \left(\nabla \times \vec{H}_2\right) = j\omega\varepsilon\vec{E}_1\vec{E}_2 + \vec{E}_1\vec{J}_2 \tag{A.4.8}$$

Then by combining these equations as, (A.4.5) – (A.4.7) + (A.4.6) – (A.4.8), and making use of the vector identity in (A.3.1), we obtain the following expression:

$$\nabla \cdot \left(\vec{E}_1 \times \vec{H}_2 - \vec{E}_2 \times \vec{H}_1 \right) = \vec{J}_1 \cdot \vec{E}_2 - \vec{J}_2 \cdot \vec{E}_1 \tag{A.4.9}$$

Lorentz's reciprocity theorem is then obtained by integrating both sides over a volume V with a surface S containing both of the sources and then making use of the divergence theorem (A.1.6) on the left hand side of the expression to obtain:

$$\oiint_S \left(\vec{E}_1 \times \vec{H}_2 - \vec{E}_2 \times \vec{H}_1 \right) \cdot d\vec{S} = \iiint_V \left(\vec{J}_1 \cdot \vec{E}_2 - \vec{J}_2 \cdot \vec{E}_1 \right) \cdot dV \tag{A.4.10}$$

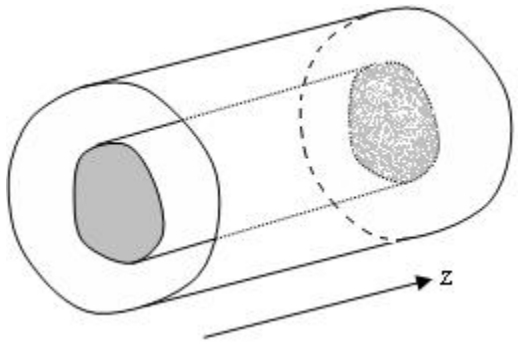

Figure A-4 A z-invariant cylinder with two end faces and three total surfaces used in establishing Lorentz's reciprocity theorem.

For cylindrical and planar z-invariant wave guiding media, we again follow the derivation of Bienstman [54], and define the volume to be a cylinder whose axis is in the *z*-direction. The surface of the cylinder is then composed of three surfaces: the curved surface of the cylinder and the two flat ends of the cylinder. This allows the surface integral on the right hand side of (A.1.40) to be divided into three separate surface integrals, one for each surface. The integral for the curved surface involves the use of boundary conditions that are often of the Dirichlet type (the field equals zero) for open structures whose fields decay at infinity, or of the Dirichlet or Neumann type (where the field or its derivative is zero) for structures having perfect

electric or magnetic conducting walls. For perfectly conducting spatially periodic media, a derivation of the Lorentz reciprocity theorem can be found in Petit et al [37]. Defining the expression:

$$\vec{F} = \vec{E}_1 \times \vec{H}_2 - \vec{E}_2 \times \vec{H}_1 \tag{A.4.11}$$

an integral involving the two ends of the cylinder may be expressed as follows:

$$\begin{aligned} \iint_{S_1} \vec{F} \cdot d\vec{S}_1 + \iint_{S_2} \vec{F} \cdot d\vec{S}_2 &= -\iint_{S_1} F_z dS + \iint_{S_2} F_z dS \\ \iint_{S_1} \vec{F} \cdot d\vec{S}_1 + \iint_{S_2} \vec{F} \cdot d\vec{S}_2 &= \iint_{S_1} \left(F_{z+\Delta z} - F_z\right) dS \end{aligned} \tag{A.4.12}$$

The fields on the right hand side of (A.4.11) contained within volume V are independent of z as Δz approaches zero. Consequently, the volume integral of (A.4.11) can be expressed as a surface integral multiplied by Δz:

$$\iiint_V \left(\vec{J}_1 \cdot \vec{E}_2 - \vec{J}_2 \cdot \vec{E}_1\right) \cdot dV = \Delta z \oiint_S \left(\vec{J}_1 \cdot \vec{E}_2 - \vec{J}_2 \cdot \vec{E}_1\right) \cdot d\vec{S} \tag{A.4.13}$$

The Lorentz reciprocity theorem for longitudinally invariant media can then be obtained by equating the left hand sides of (A.4.12) and (A.4.13), dividing by Δz and then taking the limit as Δz approaches zero:

$$\iint_S \frac{\partial}{\partial z} \left(\vec{E}_1 \times \vec{H}_2 - \vec{E}_2 \times \vec{H}_1\right) \cdot \hat{u}_z dS = \iint_S \left(\vec{J}_1 \cdot \vec{E}_2 - \vec{J}_2 \cdot \vec{E}_1\right) \cdot d\vec{S} \tag{A.4.14}$$

This theorem will be useful in the next section for establishing the orthogonality of electromagnetic eigenmodes.

APPENDIX B. SPATIAL HARMONIC GRIDS IN 1D, 2D AND 3D SYSTEMS

In numerical spectral methods, continuous and discrete quantities are approximated through the use of series expansions of orthogonal basis functions by retaining a finite number of terms [162]. Each term in the resulting series has an initially unknown coefficient whose value is determined by both the value of the function over the computational window and the boundary conditions of that window. Regardless of the dimensionality of the problem, the nature of matrix computation requires that the relationship between the two quantities on each side of the equation be expressed as a matrix relation between two one-dimensional arrays. For one-dimensional problems, an initial series expansion is itself one-dimensional, and by relating every term in the first one-dimensional array to every term in the second one-dimensional array, the resulting expression fits naturally into the requirements for matrix computation.

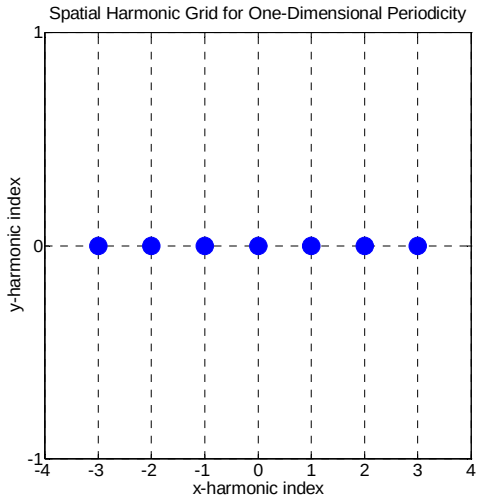

(a)

x-harmonic index	y-harmonic index
0	0
1	0
-1	0
2	0
-2	0
3	0
-3	0

(b)

Figure B-1 (a) A one-dimensional spatial harmonic grid used in modeling a one-dimensional periodicity. (b) The associated initial 0^{th}-order harmonic indexing for the one dimensional grid.

Figure B-1 shows an example of a discrete harmonic grid that can be used in a one-dimensional series expansion, as well as an initial 0^{th} harmonic ordering of the series terms that becomes very convenient for information handling purposes.

In two-dimensional and three-dimensional spectral method models [24], the series expansions themselves are second rank and third rank tensors respectively. In order to create series relations that may be conveniently modeled using digital computation methods, these second rank and third rank tensors must be transformed into effective one-dimensional arrays. Relating every element in two of these effective one-dimensional arrays creates the necessary coupling matrix for solving the modal problem of interest. Figure B.2 shows a square two-dimensional and a cubic three-dimensional grid, as well as tables showing the corresponding harmonic ordering based on the spectral distance of grid points from the origin.

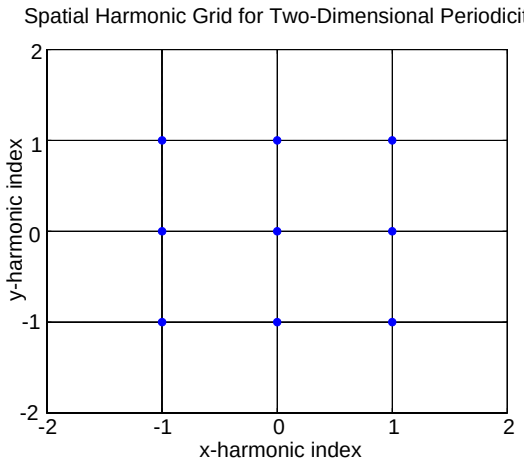

(a)

x-index	y-index
0	0
1	0
-1	0
0	1
0	-1
1	1
-1	1
1	-1
-1	-1

(b)

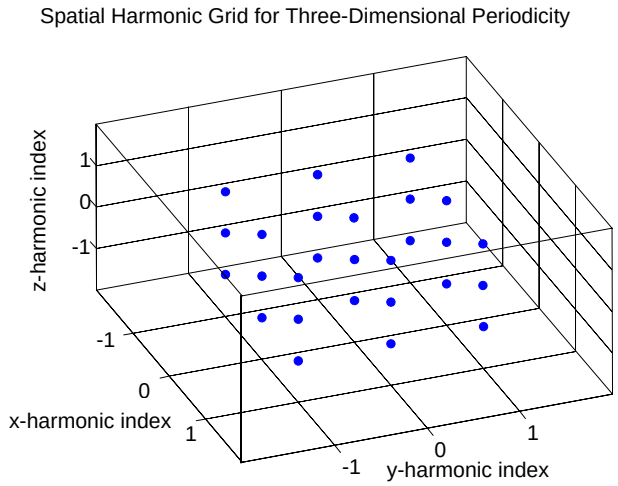

(c)

x-index	y-index	z-index
0	0	0
1	0	0
-1	0	0
0	1	0
0	-1	0
0	0	1
0	0	-1
1	1	0
-1	1	0
1	-1	0
-1	-1	0
1	0	1
-1	0	1
1	0	-1
-1	0	-1
0	1	1
0	-1	1
0	1	-1
0	-1	-1
1	1	1
-1	1	1
1	-1	1
1	1	-1
-1	-1	1
-1	1	-1
1	-1	-1

(d)

Figure B-2 (a) A square grid of Fourier harmonics for a two-dimensionally periodic system. (b) The associated initial 0^{th}-order harmonic indexing based on both distance from the origin and pairing of orders for symmetry operations. (c) A cubic grid of Fourier harmonics for a three-dimensionally periodic system. (d) The associated initial 0^{th}-order harmonic indexing based on both distance from the origin and pairing of orders for symmetry operations.

The spatial harmonic expansions in two or three dimensions allows for a wide range of flexibility in how those series can be truncated. Equation B.1 provides one example of truncating a two-dimensional grid of harmonics within the bounds of conic sections in a two-dimensional plane.

$$\left(\frac{x_{\text{harmonic index}}}{\left(\frac{N_x - 1}{2} \right)^2} \right)^{bow} + \left(\frac{y_{\text{harmonic index}}}{\left(\frac{N_y - 1}{2} \right)^2} \right)^{bow} \leq 1 \qquad \text{(B.1)}$$

By performing these non-rectangular grid truncations, the spatial harmonics can be retained that are most likely to produce rapid modal convergence and most likely to contribute to energy propagation in mode matching problems. Figure B.3 shows the truncation of a 101x101 square grid of harmonics when the conic section power factor is 0.25, 0.5, 0.75, and 1.0 respectively.

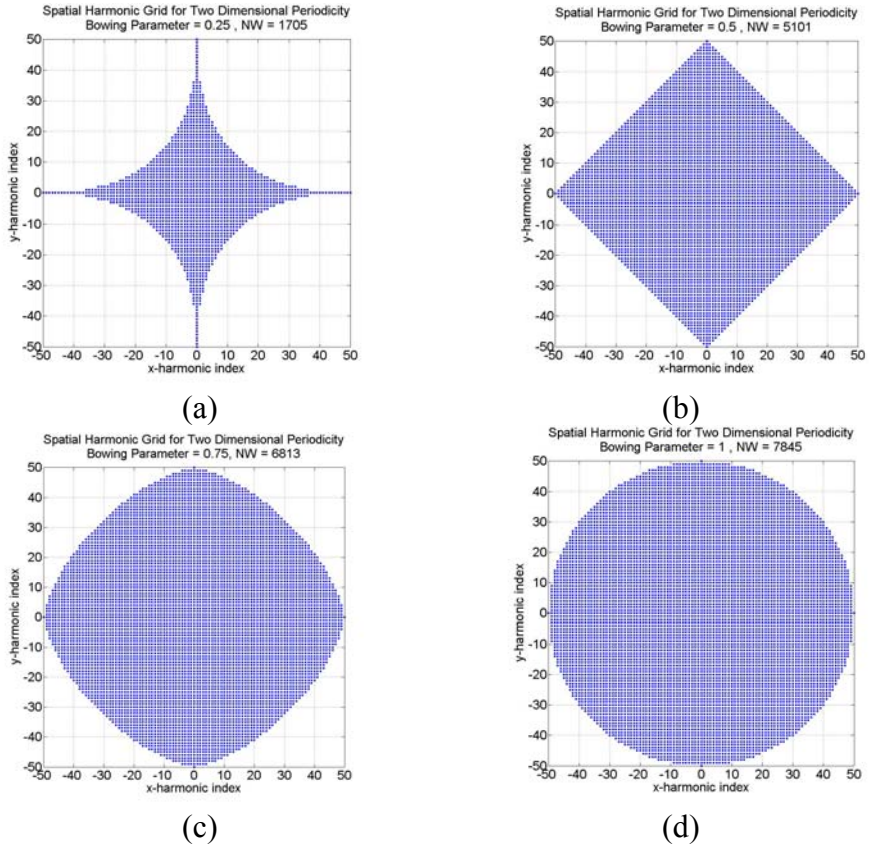

Figure B-3 Truncated spatial harmonic grids for two periodic dimensions with truncation *bow* parameters equal to (a) 0.25 (b) 0.5 (c) 0.75 (d) 1.0.

APPENDIX C. DETERMINING THE FOURIER COUPLING COEFFICIENTS IN 1D, 2D, AND 3D

In solving the modal problem for periodic optical structures using Fourier series expansions, the most critical aspects of the method for determining numerically accurate and physically consistent solutions are the means of representing the coupling coefficients between spatial harmonics of the electric and magnetic fields [24-28, 31, 39, 163, 164]. To determine these coupling coefficients requires use of Fourier series expansions of the spatial distribution of materials (permittivity and permeability), as well as the creation of a coupling matrix used for performing a discrete convolution between the field spatial harmonic expansions and the material spatial harmonic expansions.

In its original form [12], the RCWA made use of a single method, the "Laurent Rule", for performing the analytical Fourier transforms, series expansions, and discrete convolutions necessary to obtain a system's coupling coefficients regardless of a problem's input polarization or material properties. In certain situations, most notably metallic gratings in TM polarization, the RCWA was shown to have poor numerical convergence as a function of the number of spatial harmonics retained in the model. Based on an empirical numerical study performed by Lalanne and Morris [26], and later put on more firm mathematical footing by Li [163], the poor numerical convergence for metallic gratings in TM polarization was attributed to the use of an improper method of performing discrete convolutions between two Fourier series representing functions that share collocated jump discontinuities but whose product is to be a continuous function. Li established a set of three rules describing various means of handling the multiplication of series expansions when one or both of the series expansions possess collocated jump discontinuities, and showed that when a proper method, the so called "inverse-rule," is utilized in proper circumstances for performing these Fourier series expansions and discrete convolutions, the convergence problem associated with metallic gratings in TM polarization can

be eliminated. The method of applying the "inverse-rule" has come to be known as the Fast Fourier Factorization (FFF) method, and has now been applied to not only Fourier series methods, but also other orthogonal function expansion methods as well [165, 166]. To find a full mathematical justification of the "inverse-rule" and Fast Fourier Factorization the reader is directed to the works by Li [27-31, 61, 163], and Popov et. al [167-169]. This appendix aims to show how to implement both the original expansions method in 1D, 2D, and 3D periodic systems, as well as a version of the Fast Fourier Factorization method in 1D and 2D periodic systems. While they have been implemented, it should be noted that Fast Fourier Factorization methods in 2D and 3D systems do not possess the property of mathematical uniqueness.

C.1 One-dimensional coupling coefficients

For a one dimensional binary grating, such as the one shown in Figure C.1, the function representing the permittivity distribution in the grating layer is a piecewise continuous periodic function with jump discontinuities at the grating ridge/groove interfaces. Two components of the electric and magnetic fields (E_z, E_y, H_z, H_y) are tangential to the grating ridge/groove interfaces, and one component of each field (E_x, H_x) is normal to these interfaces.

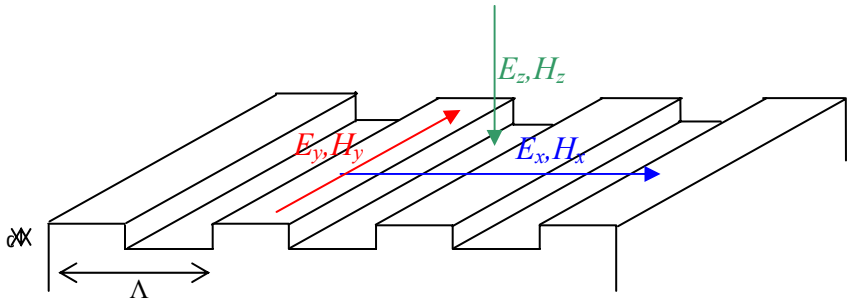

Figure C-1 A sketch showing the high and low index permittivity/permeability distributions for a one-dimensionally periodic structure and the electric and magnetic field components in relation to that periodicity.

The tangential components of these fields (E_z, E_y, H_z, H_y) are continuous across the grating ridge/groove interfaces. Consequently, the product of the continuous function for the field and a discontinuous function for the material allows for the use of the standard "Laurent-rule" for performing the necessary discrete convolution. The normal components of the fields (E_x, H_x) are discontinuous across the boundary, but the product of these normal fields with the material property functions (ε_x,μ_x) lead to continuous quantities for the electric displacement (D_x) and magnetic flux density (B_x). Consequently, the "inverse-rule" of Fast Fourier Factorization is applicable in these cases.

C.1.1 Constructing 1D Coupling Coefficients for the Laurent Rule

The Fourier series expansion for the permittivity components in directions perpendicular to the grating vector can be expressed generically as follows:

$$\varepsilon_y(x) = \varepsilon_z(x) = \sum_{-p}^{+p} A_p e^{+j\frac{2\pi}{\Lambda}px} \tag{C.1.1}$$

For a grating composed of M separate permittivity regions the coefficients of this series can be expressed as follows:

$$A_p = \frac{1}{\Lambda}\sum_{m=1}^{M}\varepsilon_m \int_{x_{left,m}}^{x_{right,m}} e^{-j\frac{2\pi}{\Lambda}px}\,dx \tag{C.1.2}$$

$$A_p = \delta_{(p,0)}\varepsilon_L + \sum_{m=1}^{M}(\varepsilon_m - \varepsilon_L)\exp\left(-j\frac{2\pi}{\Lambda}p\left(\frac{x_{right,m}+x_{left,m}}{2}\right)\right)\mathrm{sinc}(pf)f \tag{C.1.3}$$

$$A_p = \delta_{(p,0)}\varepsilon_L + \sum_{m=1}^{M}(\varepsilon_m - \varepsilon_L)A^x_{p,m} \tag{C.1.4}$$

where $A_{p,m}^{x} = \exp\left(-j\frac{2\pi}{\Lambda}p\left(\frac{x_{right,m}+x_{left,m}}{2}\right)\right)\mathrm{sinc}(pf)f$, $f = \left(\frac{x_{right,m}-x_{left,m}}{\Lambda}\right)$, ε_L is the background permittivity, ε_m is the permittivity of the m^{th} region, and $\mathrm{sinc}(x) = \frac{\sin(\pi x)}{\pi x}$.

The coupling coefficient matrix used in the discrete convolution mutually couples all harmonics used in the spatial harmonic expansions of the electric and magnetic fields. This coupling coefficient matrix takes on the following form:

$$[C^{y,z}] = \begin{bmatrix} A_{(0\to 0)} & A_{(0\to 1)} & A_{(0\to -1)} & \cdots & A_{(0\to p-1)} & A_{(0\to -p+1)} & A_{(0\to p)} & A_{(0\to -p)} \\ A_{(1\to 0)} & A_{(1\to 1)} & A_{(1\to -1)} & \cdots & A_{(1\to p-1)} & A_{(1\to -p+1)} & A_{(1\to p)} & A_{(1\to -p)} \\ A_{-(1\to 0)} & A_{(-1\to 1)} & A_{(-1\to -1)} & \cdots & A_{(-1\to p-1)} & A_{(-1\to -p+1)} & A_{(-1\to p)} & A_{-(1\to -p)} \\ \vdots & \vdots & \vdots & \ddots & \vdots & \vdots & \vdots & \vdots \\ A_{(p-1\to 0)} & A_{(p-1\to 1)} & A_{(p-1\to -1)} & \cdots & A_{(p-1\to p-1)} & A_{(p-1\to -p+1)} & A_{(p-1\to p)} & A_{(p-1\to -p)} \\ A_{(-p+1\to 0)} & A_{(-p+1\to 1)} & A_{(-p+1\to -1)} & \cdots & A_{(-p+1\to p-1)} & A_{(-p+1\to -p+1)} & A_{(-p+1\to p)} & A_{(-p+1\to -p)} \\ A_{(p\to 0)} & A_{(p\to 1)} & A_{(p\to -1)} & \cdots & A_{(p\to p-1)} & A_{(p\to -p+1)} & A_{(p\to p)} & A_{(p\to -p)} \\ A_{(-p\to 0)} & A_{(-p\to 1)} & A_{(-p\to -1)} & \cdots & A_{(-p\to p-1)} & A_{(-p\to -p+1)} & A_{(-p\to p)} & A_{(-p\to -p)} \end{bmatrix} \quad \text{(C.1.5)}$$

$$[C^{y,z}] = \begin{bmatrix} A_0 & A_{-1} & A_{+1} & \cdots & A_{-p+1} & A_{p-1} & A_{-p} & A_{+p} \\ A_{+1} & A_0 & A_{+2} & \cdots & A_{-p+2} & A_{+p} & A_{-p+1} & A_{p+1} \\ A_{-1} & A_{-2} & A_0 & \cdots & A_{-p} & A_{p-2} & A_{-p-1} & A_{p-1} \\ \vdots & \vdots & \vdots & \ddots & \vdots & \vdots & \vdots & \vdots \\ A_{p-1} & A_{p-2} & A_p & \cdots & A_0 & A_{2p-2} & A_{-1} & A_{2p-1} \\ A_{-p+1} & A_{-p} & A_{-p+2} & \cdots & A_{-2p+2} & A_0 & A_{-2p+1} & A_{+1} \\ A_p & A_{p-1} & A_{p+1} & \cdots & A_{2p+1} & A_{2p-1} & A_0 & A_{2p} \\ A_{-p} & A_{-p-1} & A_{-p-1} & \cdots & A_{-2p+1} & A_{-1} & A_{-2p} & A_0 \end{bmatrix} \quad \text{(C.1.6)}$$

where the subscripts denote the difference between two spatial harmonics, $C_{p_1,p_2}^{y,z} = A_{p_1-p_2}$. The matrix in Equation (C.1.5) is a Toeplitz matrix that has been permuted into a form convenient for the diffraction and wave propagation problems utilized in the RCWA. In determining the

elements of this coupling coefficient matrix, only the terms in the Fourier series expansion of the permittivity from -2p to +2p need to be initially stored in memory, and the coupling coefficient matrix can be filled from these values. Application of this matrix for the coupling coefficients between two separate Fourier series expansions is an implementation of the "Laurent-rule."

C.1.2 Constructing 1D Coupling Coefficients for the Inverse Rule

The Fourier series expansion for the permittivity components in directions parallel to the grating vector is determined by means of an impermittivity expansion:

$$\frac{1}{\varepsilon_x(x)} = \sum_{-p}^{+p} B_p e^{+j\frac{2\pi}{\Lambda}px} \tag{C.1.7}$$

For a grating composed of M separate permittivity regions the coefficients of this series can be expressed as follows:

$$B_p = \frac{1}{\Lambda}\sum_{m=1}^{M}\frac{1}{\varepsilon_m}\int_{x_{left,m}}^{x_{right,m}} e^{-j\frac{2\pi}{\Lambda}px}dx \tag{C.1.8}$$

$$B_p = \delta_{(p,0)}\frac{1}{\varepsilon_L} + \sum_{m=1}^{M}\left(\frac{1}{\varepsilon_m}-\frac{1}{\varepsilon_L}\right)\exp\left(-j\frac{2\pi}{\Lambda}p\left(\frac{x_{right,m}+x_{left,m}}{2}\right)\right)\mathrm{sinc}(pf)f \tag{C.1.9}$$

$$B_p = \delta_{(p,0)}\frac{1}{\varepsilon_L} + \sum_{m=1}^{M}\left(\frac{1}{\varepsilon_m}-\frac{1}{\varepsilon_L}\right)B^x_{p,m} \tag{C.1.10}$$

where $B_p^x = \exp\left(-j\frac{2\pi}{\Lambda}p\left(\frac{x_{right,m}+x_{left,m}}{2}\right)\right)\mathrm{sinc}(pf)f$, $f = \left(\frac{x_{right,m}-x_{left,m}}{\Lambda}\right)$, ε_L is the background permittivity, ε_m is the permittivity of the m^{th} region, and $\mathrm{sinc}(x) = \frac{\sin(\pi x)}{\pi x}$.

As with the tangential component coupling coefficient matrices, the normal component coupling coefficient matrix used in the discrete convolution mutually couples all spatial harmonics used in the series expansions of the electric and magnetic fields, but in this case the impermittivity was

modeled as a Fourier series expansion. Using the impermittitvity series expansion to model the permittivity coupling coefficient matrix involves the following matrix inverse:

$$\left[C^x\right]=\begin{bmatrix} B_{(0\to 0)} & B_{(0\to 1)} & B_{(0\to -1)} & \cdots & B_{(0\to p-1)} & B_{(0\to -p+1)} & B_{(0\to p)} & B_{(0\to -p)} \\ B_{(1\to 0)} & B_{(1\to 1)} & B_{(1\to -1)} & \cdots & B_{(1\to p-1)} & B_{(1\to -p+1)} & B_{(1\to p)} & B_{(1\to -p)} \\ B_{(-1\to 0)} & B_{(-1\to 1)} & B_{(-1\to -1)} & \cdots & B_{(-1\to p-1)} & B_{(-1\to -p+1)} & B_{(-1\to p)} & B_{(-1\to -p)} \\ \vdots & \vdots & \vdots & \ddots & \vdots & \vdots & \vdots & \vdots \\ B_{(p-1\to 0)} & B_{(p-1\to 1)} & B_{(p-1\to -1)} & \cdots & B_{(p-1\to p-1)} & B_{(p-1\to -p+1)} & B_{(p-1\to p)} & B_{(p-1\to -p)} \\ B_{(-p+1\to 0)} & B_{(-p+1\to 1)} & B_{(-p+1\to -1)} & \cdots & B_{(-p+1\to p-1)} & B_{(-p+1\to -p+1)} & B_{(-p+1\to p)} & B_{(-p+1\to -p)} \\ B_{(p\to 0)} & B_{(p\to 1)} & B_{(p\to -1)} & \cdots & B_{(p\to p-1)} & B_{(p\to -p+1)} & B_{(p\to p)} & B_{(p\to -p)} \\ B_{(-p\to 0)} & B_{(-p\to 1)} & B_{(-p\to -1)} & \cdots & B_{(-p\to p-1)} & B_{(-p\to -p+1)} & B_{(-p\to p)} & B_{(-p\to -p)} \end{bmatrix}^{-1} \tag{C.1.9}$$

$$\left[C^x\right]=\begin{bmatrix} B_0 & B_{-1} & B_{+1} & \cdots & B_{-p+1} & B_{p-1} & B_{-p} & B_p \\ B_{+1} & B_0 & B_{+2} & \cdots & B_{-p+2} & B_p & B_{-p+1} & B_{p+1} \\ B_{-1} & B_{-2} & B_0 & \cdots & B_{-p} & B_{p-2} & B_{-p-1} & B_{p-1} \\ \vdots & \vdots & \vdots & \ddots & \vdots & \vdots & \vdots & \vdots \\ B_{p-1} & B_{p-2} & B_p & \cdots & B_0 & B_{2p-2} & B_{-1} & B_{2p-1} \\ B_{-p+1} & B_{-p} & B_{-p+2} & \cdots & B_{-2p+2} & B_0 & B_{-2p+1} & B_1 \\ B_p & B_{p-1} & B_{p+1} & \cdots & B_{2p+1} & B_{2p-1} & B_0 & B_{2p} \\ B_{-p} & B_{-p-1} & B_{-p-1} & \cdots & B_{-2p+1} & B_{-1} & B_{-2p} & B_0 \end{bmatrix}^{-1} \tag{C.1.10}$$

$$\left[C^x\right]=\begin{bmatrix} C^x_{0,0} & C^x_{0,1} & C^x_{0,-1} & \cdots & C^x_{0,p-1} & C^x_{0,-p+1} & C^x_{0,p} & C^x_{0,-p} \\ C^x_{1,0} & C^x_{1,1} & C^x_{1,-1} & \cdots & C^x_{1,p-1} & C^x_{1,-p+1} & C^x_{1,p} & C^x_{1,-p} \\ C^x_{-1,0} & C^x_{-1,1} & C^x_{-1,-1} & \cdots & C^x_{-1,p-1} & C^x_{-1,-p+1} & C^x_{-1,p} & C^x_{-1,-p} \\ \vdots & \vdots & \vdots & \ddots & \vdots & \vdots & \vdots & \vdots \\ C^x_{p-1,0} & C^x_{p-1,1} & C^x_{p-1,-1} & \cdots & C^x_{p-1,p-1} & C^x_{p-1,-p+1} & C^x_{p-1,p} & C^x_{p-1,-p} \\ C^x_{-p+1,0} & C^x_{-p+1,1} & C^x_{-p+1,-1} & \cdots & C^x_{-p+1,p-1} & C^x_{-p+1,-p+1} & C^x_{-p+1,p} & C^x_{-p+1,-p} \\ C^x_{p,0} & C^x_{p,1} & C^x_{p,-1} & \cdots & C^x_{p,p-1} & C^x_{p,-p+1} & C^x_{p,p} & C^x_{p,-p} \\ C^x_{-p,0} & C^x_{-p,1} & C^x_{-p,-1} & \cdots & C^x_{-p,p-1} & C^x_{-p,-p+1} & C^x_{-p,p} & C^x_{-p,p} \end{bmatrix} \tag{C.1.11}$$

In this case, the use of a matrix inversion means that all elements in the resulting coupling coefficient matrix depend upon all terms used in the spatial harmonic series expansion of the impermittivity function. Consequently, the terms in the impermittivity series expansion from -2p to +2p must be initially stored in memory and used to fill the matrix whose inverse determines the coupling coefficients. Use of the matrix in Equation (C.1.11) as the coupling coefficients between two Fourier series expansions is an implementation of the "inverse-rule."

C.2 Two-Dimensional Coupling Coefficients

In attempting to determine the coupling coefficients associated with structures that are periodic in two transverse spatial dimensions, there is an ambiguous definition of what constitutes the global normal and tangential components of a the field within a unit cell. For the field in a direction normal to both of the grating vectors, the definition is not ambiguous and the electric and magnetic field components are continuous across the grating groove/ridge interfaces. Consequently, the multiplication of the continuous field functions with the discontinuous material functions allows for safe use of the Laurent rule for the discrete convolution. For the field components in the plane of the two grating vectors, the fields can be normal to the grating's ridge/groove interfaces in some regions within the unit cell, tangential to those interfaces in other regions, and devoid of either classification in other separate regions within the unit cells. The fact that the material distributions can take on both elliptical and polygonal transverse shapes adds to the ambiguity in trying to assign a global label to a field's transverse or normal properties over the entire unit cell. Consequently, application of the inverse rule is not a straightforward approach as it was in one-dimensional periodic systems, and does not actually possess the properties of mathematical uniqueness. In the first two sub-sections, coupling coefficient

expansions for two dimensionally periodic structures possessing square and elliptical geometries will be described. In the third subsection, a method of determining the transverse component coupling coefficient matrices for rectangular features that makes partial use of the inverse rule will be described.

C.2.1 Constructing 2D Coupling Coefficients for Rectangular Features Using the Laurent Rule

While the nature of a transverse two-dimensional periodic structure is in no way limited to having its directions of periodicity along the axes of a regular Cartesian coordinate system, for simplicity this derivation will only consider orthogonal grating vectors. For a thorough explanation of performing Fourier series expansions on two-dimensional skew-periodic lattices, the reader is referred to the excellent text by Papoulis [170]. A simple schematic diagram in Figure C.2 shows the relationships between the normal field component direction and unit cell ridge/groove interfaces for doubly periodic structures with rectangular features.

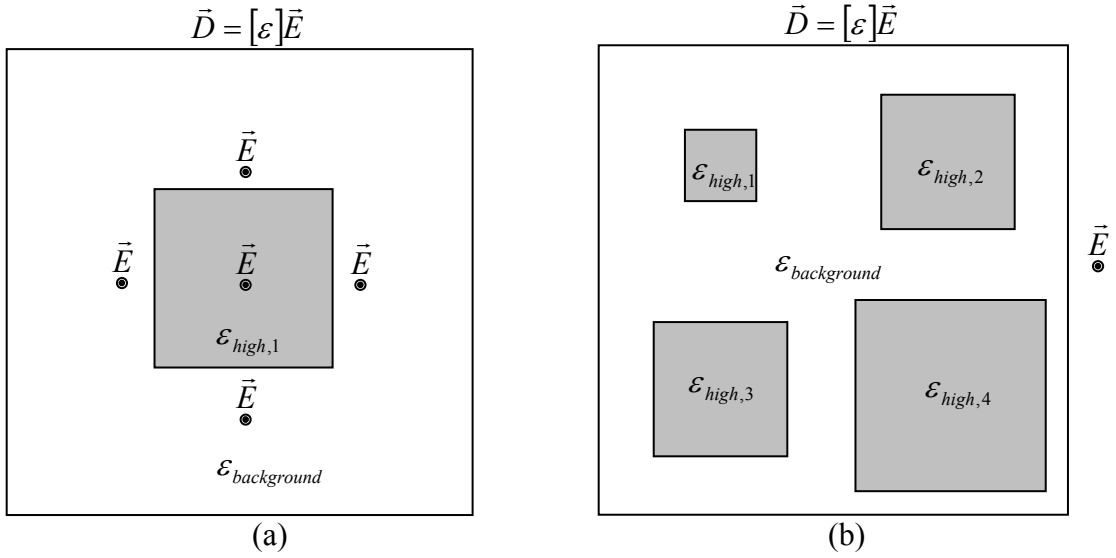

Figure C-2 (a) A sketch showing the permittivity distribution within a unit cell for a simple, binary, two-dimensional grating, as well as the electric field perpendicular to the plane of periodicities. (b) A similar sketch for a unit cell with multiple high index features.

A simple Fourier series expansion of a two-dimensional periodic structure with orthogonal periodic directions can be expressed as follows:

$$\varepsilon(x) = \sum_{-p}^{+p} \sum_{-q}^{+q} A_{p,q} e^{+j2\pi\left(\frac{px}{\Lambda_x} + \frac{qy}{\Lambda_y}\right)} \tag{C.2.1}$$

where Λ_x and Λ_y are the periodicities in the *x* and *y* directions respectively. Determination of the series expansion coefficients for a unit cell with M distinct permittivity regions can be expressed in the following manner:

$$A_{p,q} = \sum_{m=1}^{M} \varepsilon_m \frac{1}{\Lambda_x} \int_{x_{left,m}}^{x_{right,m}} e^{-j\frac{2\pi}{\Lambda_x}px} dx \frac{1}{\Lambda_y} \int_{y_{bottom,m}}^{y_{top,m}} e^{-j\frac{2\pi}{\Lambda_y}py} dy \tag{C.2.2}$$

$$A_{p,q} = \delta_{(p,0)(q,0)}\varepsilon_L + \sum_{m=1}^{M}(\varepsilon_m - \varepsilon_L)\exp\left(-j\frac{2\pi}{\Lambda_x}p\left(\frac{x_{right,m} + x_{left,m}}{2}\right)\right)\mathrm{sinc}(pf_x)f_x \exp\left(-j\frac{2\pi}{\Lambda_y}q\left(\frac{y_{top,m} + y_{bottom,m}}{2}\right)\right)\mathrm{sinc}(qf_y)f_y \tag{C.2.3}$$

$$A_{p,q} = \varepsilon_L \delta_{(p,0),(q,0)} + \sum_{m=1}^{M}(\varepsilon_m - \varepsilon_L) A^x_{p,m} A^y_{q,m} \tag{C.2.4}$$

where A^x and A^y are one-dimensional arrays defined as follows:

$$A^x_{p,m} = \exp\left(-j\frac{2\pi}{\Lambda_x}p\left(\frac{x_{right,m} + x_{left,m}}{2}\right)\right)\mathrm{sinc}(pf_x)f_x,$$

$$A^y_{q,m} = \exp\left(-j\frac{2\pi}{\Lambda_y}q\left(\frac{y_{top,m} + x_{bottom,m}}{2}\right)\right)\mathrm{sinc}(qf_y)f_y,$$

and

$$f_x = \left(\frac{x_{right,m} - x_{left,m}}{\Lambda_x}\right),\ x_{center} = \left(\frac{x_{right,m} + x_{left,m}}{2}\right),$$

$$f_y = \left(\frac{y_{top,m} - y_{bottom,m}}{\Lambda_y}\right),\ y_{center} = \left(\frac{y_{top,m} + y_{bottom,m}}{2}\right),$$

ε_L is the background permittivity, ε_m is the permittivity of the m^{th} region, and $\mathrm{sinc}(x) = \frac{\sin(\pi x)}{\pi x}$.

The coupling coefficients matrix can then be directly filled using the following relationships:

$$C^{x,y,z}_{(p_2 \to p_1),(q_2 \to q_1)} = \sum_{m=1}^{M} (\varepsilon_m - \varepsilon_L) A^{x}_{(p_2 - p_1),m} A^{y}_{(q_2 - q_1),m} \tag{C.2.5}$$

$$C^{x,y,z}_{(p_2 \to p_1 = p_2),(q_2 \to q_1 = q_2)} = \varepsilon_L + \sum_{m=1}^{M} (\varepsilon_m - \varepsilon_L) A^{x}_{0,m} A^{y}_{0,m} \tag{C.2.6}$$

In the classic method of performing the coupling coefficient expansion, the same method of creating the coupling matrix is used for every component of the permittivity/permeability tensor.

C.2.2 Constructing 2D Coupling Coefficients for Elliptical Features Using the Laurent Rule

An analytical construction of the coupling coefficients for elliptically shaped features on an orthogonal or skew-periodic lattice requires the use of the Laurent expansion, as there is no unique method for classifying the normal and tangential components of the transverse fields over an entire unit cell, and the method presented in the next subsection only applies to parallelogram shaped features. Once again, a simple Fourier series expansion of a two-dimensional periodic structure with orthogonal periodic directions can be expressed as follows:

$$\varepsilon(x) = \sum_{-p}^{+p} \sum_{-q}^{+q} A_{p,q} e^{+j2\pi\left(\frac{px}{\Lambda_x} + \frac{qy}{\Lambda_y}\right)} \tag{C.2.7}$$

where Λ_x and Λ_y are the periodicities in the *x* and *y* directions respectively.

Determination of the series expansion coefficients for a unit cell with M distinct permittivity elliptical regions can be expressed in the following manner:

$$A_{p,q} = \frac{1}{area\_of\_unit\_cell} \sum_{m=1}^{M} \varepsilon_m \int_{-\infty}^{\infty} e^{-j\frac{2\pi}{\Lambda_x} px} \int_{-y_2(x),m}^{y_1(x),m} e^{-j\frac{2\pi}{\Lambda_y} py} dy dx \tag{C.2.8}$$

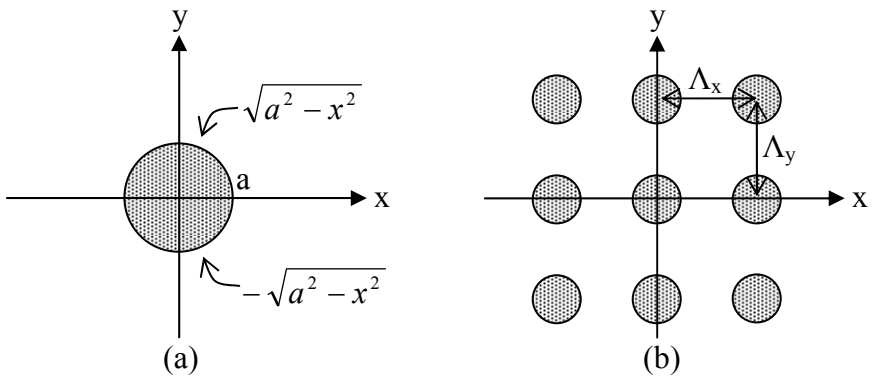

Figure C-3 (a) Single unit cell of a two-dimensionally periodic system with a circular feature of radius *a*. (b) A sketch of a two-dimensionally periodic system with circular features showing the lattice spacing in the x and y directions.

For a circle of radius *a* centered at the origin, as shown in Figure B.3, the bounds on the *y* integral can be expressed as follows:

$$y_1(x) = y_2(x) = y(x) = \begin{cases} \sqrt{a^2 - x^2} & |x| < a \\ 0 & |x| > a \end{cases} \tag{C.2.9}$$

By making the substitution, $x = a\sin\theta$, can be expressed as a Hankel transform, whose solution is as follows:

$$A_{p,q} = \sum_{m=1}^{M} \varepsilon_m \frac{\pi a_m^2}{area\_of\_unit\_cell} \text{sombrero}\left(2a_m\sqrt{\left(\frac{p}{\Lambda_x}\right)^2 + \left(\frac{q}{\Lambda_y}\right)^2}\right) \exp\left(-j\left(\frac{2\pi}{\Lambda_x}px_{center} + \frac{2\pi}{\Lambda_y}qy_{center}\right)\right) \tag{C.2.10}$$

where the sombrero function is defined as $\text{sombrero}(x) = 2\frac{J_1(\pi x)}{\pi x}$ and $J_1(x)$ is the first order Bessel function of the first kind. For an elliptical feature with one axis of length *a* along the x-direction and another axis of length *b* along the y-direction, the elements of the coupling coefficient matrix can be expressed as follows:

$$A_{p,q} = \sum_{m=1}^{M} \varepsilon_m \frac{\pi a_m b_m}{area\_of\_unit\_cell} \text{sombrero}\left(2\sqrt{\left(\frac{a_m p}{\Lambda_x}\right)^2 + \left(\frac{b_m q}{\Lambda_y}\right)^2}\right) \exp\left(-j\left(\frac{2\pi}{\Lambda_x}px_{center} + \frac{2\pi}{\Lambda_y}qy_{center}\right)\right) \tag{C.2.11}$$

C.2.3 Constructing 2D Coupling Coefficients for Rectangular Features Using the Inverse Rule

In attempting to make use of the inverse rule for a two dimensionally periodic structure with rectangular features, the methods utilized for determining the coupling coefficients are different for the transverse and longitudinal components. For the longitudinal components that interact with the longitudinal fields (E_z and H_z), the method presented in subsection C.2.1 is utilized. For the transverse components that interact with the transverse fields, a separate approach is taken. In this approach, the grating unit cell is divided into N_x strips that are parallel to the direction of the x-direction field component as shown in Figure B.4.

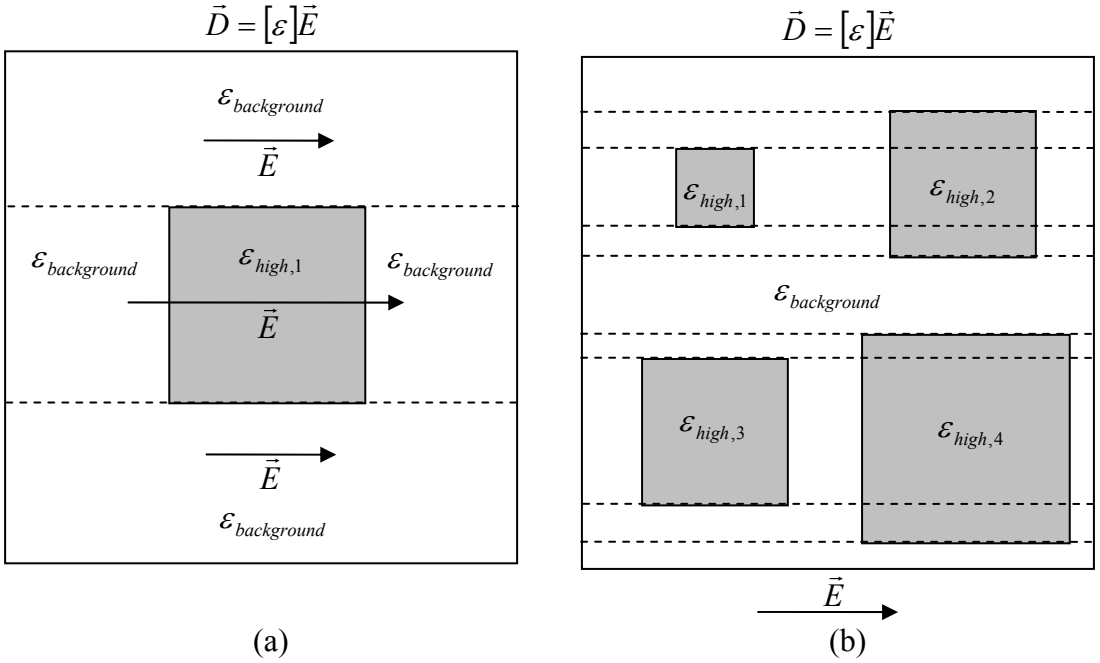

Figure C-4 (a) Permittivity distribution for a two-dimensional simple binary unit cell with one rectangular feature, and the strips used for determining the coupling coefficient expansion for an electric field shown in the x-direction. (b) A similar drawing for a unit cell with multiple features.

Within each strip, the strip is then divided into M_y sections in the orthogonal direction based on the number of material interfaces present. An impermittivity expansion is then performed within each strip as follows:

$$\frac{1}{\varepsilon_m(y)} = \sum_{-q_1}^{+q_1} B_q^{y,n_x,m_y} e^{+j\frac{2\pi}{\Lambda_y}qy} \tag{C.2.12}$$

$$B_q^{y,n_x} = \frac{1}{\Lambda_y} \sum_{m_y=1}^{M_y} \frac{1}{\varepsilon_m} \int_{y_{bottom,n_x,m_y}}^{y_{top,n_x,m_y}} e^{-j\frac{2\pi}{\Lambda_y}py}\, dy \tag{C.2.13}$$

$$B_q^{y,n_x} = \delta_{(p,0)} \frac{1}{\varepsilon_L} + \sum_{m_y=1}^{M_y} \left(\frac{1}{\varepsilon_{n_x,m_y}} - \frac{1}{\varepsilon_L} \right) \exp\left(-j\frac{2\pi}{\Lambda_y} q \left(\frac{y_{top,m_y} + y_{bottom,m_y}}{2} \right) \right) \operatorname{sinc}\left(q f_{y,n_x,m_y} \right) f_{y,n_x,m_y} \tag{C.2.14}$$

Obtaining the permittivity coupling coefficients associated with the discontinuous material distribution that couples with a discontinuous field but produces a continuous electric displacement involves an inversion of the impermittivity coupling coefficient matrix in this direction.

$$\left[C^{y,n_x}\right] = \begin{bmatrix} B_{(0\to 0)}^{y,n_x} & B_{(0\to 1)}^{y,n_x} & B_{(0\to -1)}^{y,n_x} & \cdots & B_{(0\to q-1)}^{y,n_x} & B_{(0\to -q+1)}^{y,n_x} & B_{(0\to q)}^{y,n_x} & B_{(0\to q)}^{y,n_x} \\ B_{(1\to 0)}^{y,n_x} & B_{(1\to 1)}^{y,n_x} & B_{(1\to -1)}^{y,n_x} & \cdots & B_{(1\to q-1)}^{y,n_x} & B_{(1\to -q+1)}^{y,n_x} & B_{(1\to q)}^{y,n_x} & B_{(1\to -q)}^{y,n_x} \\ B_{(-1\to 0)}^{y,n_x} & B_{(-1\to 1)}^{y,n_x} & B_{(-1\to -1)}^{y,n_x} & \cdots & B_{(-1\to q-1)}^{y,n_x} & B_{(-1\to -q+1)}^{y,n_x} & B_{(-1\to q)}^{y,n_x} & B_{(-1\to -q)}^{y,n_x} \\ \vdots & \vdots & \vdots & \ddots & \vdots & \vdots & \vdots & \vdots \\ B_{(q-1\to 0)}^{y,n_x} & B_{(q-1\to 1)}^{y,n_x} & B_{(q-1\to -1)}^{y,n_x} & \cdots & B_{(q-1\to q-1)}^{y,n_x} & B_{(q-1\to -q+1)}^{y,n_x} & B_{(q-1\to q)}^{y,n_x} & B_{(q-1\to -q)}^{y,n_x} \\ B_{(-q+1\to 0)}^{y,n_x} & B_{(-q+1\to 1)}^{y,n_x} & B_{(-q+1\to -1)}^{y,n_x} & \cdots & B_{(-q+1\to q-1)}^{y,n_x} & B_{(-q+1\to -q+1)}^{y,n_x} & B_{(-q+1\to q)}^{y,n_x} & B_{(-q+1\to -q)}^{y,n_x} \\ B_{(q\to 0)}^{y,n_x} & B_{(q\to 1)}^{y,n_x} & B_{(q\to -1)}^{y,n_x} & \cdots & B_{(q\to q-1)}^{y,n_x} & B_{(q\to -q+1)}^{y,n_x} & B_{(q\to q)}^{y,n_x} & B_{(q\to -q)}^{y,n_x} \\ B_{(-q\to 0)}^{y,n_x} & B_{(-q\to 1)}^{y,n_x} & B_{(-q\to -1)}^{y,n_x} & \cdots & B_{(-q\to q-1)}^{y,n_x} & B_{(-q\to -q+1)}^{y,n_x} & B_{(-q\to q)}^{y,n_x} & B_{(-q\to -q)}^{y,n_x} \end{bmatrix}^{-1} \tag{C.2.15}$$

$$\left[C^{y,n_x}\right]=\begin{bmatrix} B_0^{y,n_x} & B_{-1}^{y,n_x} & B_1^{y,n_x} & \cdots & B_{-q+1}^{y,n_x} & B_{q-1}^{y,n_x} & B_{-q}^{y,n_x} & B_{-q}^{y,n_x} \\ B_1^{y,n_x} & B_0^{y,n_x} & B_2^{y,n_x} & \cdots & B_{-q+2}^{y,n_x} & B_q^{y,n_x} & B_{-q+1}^{y,n_x} & B_{q+1}^{y,n_x} \\ B_{-1}^{y,n_x} & B_{-2}^{y,n_x} & B_0^{y,n_x} & \cdots & B_{-q}^{y,n_x} & B_{q-2}^{y,n_x} & B_{-q-1}^{y,n_x} & B_{q-1}^{y,n_x} \\ \vdots & \vdots & \vdots & \ddots & \vdots & \vdots & \vdots & \vdots \\ B_{q-1}^{y,n_x} & B_{q-2}^{y,n_x} & B_q^{y,n_x} & \cdots & B_0^{y,n_x} & B_{2q-2}^{y,n_x} & B_{-1}^{y,n_x} & B_{2q-1}^{y,n_x} \\ B_{-q+1}^{y,n_x} & B_{-q}^{y,n_x} & B_{-q+2}^{y,n_x} & \cdots & B_{-2q+2}^{y,n_x} & B_0^{y,n_x} & B_{-2q+1}^{y,n_x} & B_1^{y,n_x} \\ B_q^{y,n_x} & B_{q-1}^{y,n_x} & B_{q+1}^{y,n_x} & \cdots & B_1^{y,n_x} & B_{2q-1}^{y,n_x} & B_0^{y,n_x} & B_{2q}^{y,n_x} \\ B_{-q}^{y,n_x} & B_{-q-1}^{y,n_x} & B_{-q+1}^{y,n_x} & \cdots & B_{-2q+1}^{y,n_x} & B_{-1}^{y,n_x} & B_{-2q}^{y,n_x} & B_0^{y,n_x} \end{bmatrix}^{-1} \tag{C.2.16}$$

$$\left[C^{y,n_x}\right]=\begin{bmatrix} C_{0,0}^{y,n_x} & C_{0,1}^{y,n_x} & C_{0,-1}^{y,n_x} & \cdots & C_{0,q-1}^{y,n_x} & C_{0,-q+1}^{y,n_x} & C_{0,q}^{y,n_x} & C_{0,-q}^{y,n_x} \\ C_{1,0}^{y,n_x} & C_{1,1}^{y,n_x} & C_{1,-1}^{y,n_x} & \cdots & C_{1,q-1}^{y,n_x} & C_{1,-q+1}^{y,n_x} & C_{1,q}^{y,n_x} & C_{1,-q}^{y,n_x} \\ C_{-1,0}^{y,n_x} & C_{-1,1}^{y,n_x} & C_{-1,-1}^{y,n_x} & \cdots & C_{-1,q-1}^{y,n_x} & C_{-1,-q+1}^{y,n_x} & C_{-1,q}^{y,n_x} & C_{-1,-q}^{y,n_x} \\ \vdots & \vdots & \vdots & \ddots & \vdots & \vdots & \vdots & \vdots \\ C_{q-1,0}^{y,n_x} & C_{q-1,1}^{y,n_x} & C_{q-1,-1}^{y,n_x} & \cdots & C_{q-1,q-1}^{y,n_x} & C_{q-1,-q+1}^{y,n_x} & C_{q-1,q}^{y,n_x} & C_{q-1,-q}^{y,n_x} \\ C_{-q+1,0}^{y,n_x} & C_{-q+1,1}^{y,n_x} & C_{-q+1,-1}^{y,n_x} & \cdots & C_{-q+1,q-1}^{y,n_x} & C_{-q+1,-q+1}^{y,n_x} & C_{-q+1,q}^{y,n_x} & C_{-q+1,-q}^{y,n_x} \\ C_{q,0}^{y,n_x} & C_{q,1}^{y,n_x} & C_{q,-1}^{y,n_x} & \cdots & C_{q,q-1}^{y,n_x} & C_{q,-q+1}^{y,n_x} & C_{q,q}^{y,n_x} & C_{q,-q}^{y,n_x} \\ C_{-q,0}^{y,n_x} & C_{-q,1}^{y,n_x} & C_{-q,-1}^{y,n_x} & \cdots & C_{-q,q-1}^{y,n_x} & C_{-q,-q+1}^{y,n_x} & C_{-q,q}^{y,n_x} & C_{-q,q}^{y,n_x} \end{bmatrix} \tag{C.2.17}$$

The result of Equation (C.2.17) is the permittivity coupling coefficient matrix for each of the N_x strips in the unit cell. To obtain the global permittivity coupling coefficient matrix, the individual strip coupling coefficients for the y-harmonics are utilized in a Fourier series expansion in the x-direction over all N_x strips.

$$C^{y}_{(p_2\to p_1),(q_2\to q_1)} = \sum_{n_x=1}^{N_x} C^{y,n_x}_{(q_2\to q_1)} \frac{1}{\Lambda_x} \int_{x_{left,n_x}}^{x_{right,n_x}} e^{-j\frac{2\pi}{\Lambda_x}(p_2-p_1)x}\, dx \tag{C.2.18}$$

$$C^{y}_{(p_2\to p_1),(q_2\to q_1)} = \sum_{n_x=1}^{N_x} C^{y,n_x}_{(q_2\to q_1)} A^{x,n_x}_{(p_2\to p_1)} \tag{C.2.19}$$

where A^{x,n_x} is a one-dimensional array whose values are defined as follows:

$$A^{x,n_x}_{(p_2 \to p_1)} = \exp\left(- j \frac{2\pi}{\Lambda_x} (p_2 - p_1) \left(\frac{x_{right,n_x} + x_{left,n_x}}{2} \right) \right) \text{sinc}\left((p_2 - p_1) f_x \right) f_x \qquad \text{(C.2.20)}$$

Each element of the global coupling coefficient matrix created in Equation (C.2.19) involves a multiplication between the proper element of the C^{y,n_x} matrix and the A^{x,n_x} array, as well as a summation of these resulting products over all N_x strips in the unit cell.

The process of determining the coupling coefficient matrix associated with the permittivity/permeability tensor element in the orthogonal direction follows similar logic where the unit cell is cut into strips as shown in Figure C.5.

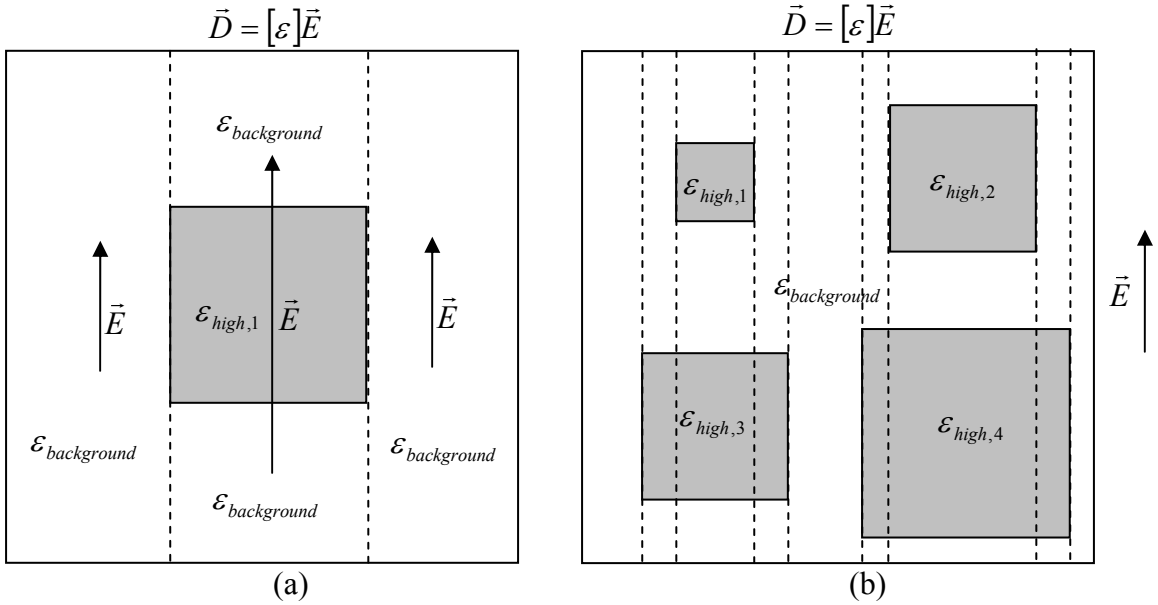

Figure C-5 (a) Permittivity distribution for a two-dimensional simple binary unit cell with one rectangular feature, and the strips used for determining the coupling coefficient expansion for an electric field shown in the y-direction. (b) A similar drawing for a unit cell with multiple features.

C.3 Three-Dimensional Coupling Coefficients

C.3.1 Constructing 3D Coupling Coefficients for Rectangular Features Using the Laurent Rule

For constructing the coupling coefficients necessary for modeling three dimensionally periodic systems using RCWA modal expansions, the Laurent rule expansions are the most straightforward means of accomplishing this task, but as with the previous invocations of the Laurent rule, the resulting series expansions do suffer from Gibbs' phenomena at all material interfaces and corner points. A simple schematic diagram in Figure C.6 shows the permittivity layout for simplest rectangular binary unit cell as well as a more complicated unit cell. Much like for a two-dimensional periodicity, a three-dimensional periodicity creates ambiguity in terms of where a particular field component is normal or tangential to a particular electromagnetic feature over the entire unit cell. The Laurent rule ignores this ambiguity and treats the Fourier expansion the same in every direction.

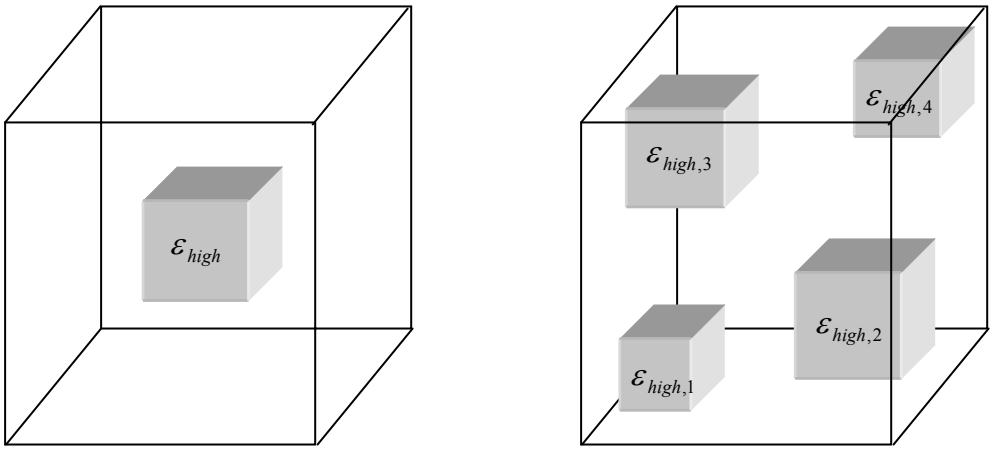

Figure C-6 A sketch of two possible 3D unit cells with rectangular features: (a) a simple single feature cell (b) a generic multifeature cell.

A simple Fourier series expansion of a two-dimensional periodic structure with orthogonal periodic directions can be expressed as follows:

$$\varepsilon(x,y,z)=\sum_{-p}^{+p}\sum_{-q}^{+q}\sum_{-r}^{+r}A_{p,q,r}e^{+j2\pi\left(\frac{px}{\Lambda_x}+\frac{qy}{\Lambda_y}+\frac{rz}{\Lambda_z}\right)} \tag{C.2.21}$$

where Λ_x, Λ_y, Λ_z are the periodicities in the x, y, and z directions respectively. Determination of the series expansion coefficients for a unit cell with M distinct permittivity regions can be expressed in the following manner:

$$A_{p,q,r}=\sum_{m=1}^{M}\varepsilon_m\frac{1}{\Lambda_x}\int_{x_{left,m}}^{x_{right,m}}e^{-j\frac{2\pi}{\Lambda_x}px}dx\frac{1}{\Lambda_y}\int_{y_{bottom,m}}^{y_{top,m}}e^{-j\frac{2\pi}{\Lambda_y}qy}dy\frac{1}{\Lambda_z}\int_{z_{bottom,m}}^{z_{top,m}}e^{-j\frac{2\pi}{\Lambda_z}rz}dz \tag{C.2.22}$$

$$\begin{aligned}A_{p,q,r}=\delta_{(p,0)(q,0)(r,0)}\varepsilon_L+\sum_{m=1}^{M}(\varepsilon_m-\varepsilon_L)&\exp\left(-j\frac{2\pi}{\Lambda_x}p\left(\frac{x_{right,m}+x_{left,m}}{2}\right)\right)\mathrm{sinc}(pf_x)f_x\\&\exp\left(-j\frac{2\pi}{\Lambda_y}q\left(\frac{y_{top,m}+y_{bottom,m}}{2}\right)\right)\mathrm{sinc}(qf_y)f_y\\&\exp\left(-j\frac{2\pi}{\Lambda_y}r\left(\frac{z_{front,m}+z_{back,m}}{2}\right)\right)\mathrm{sinc}(rf_z)f_z\end{aligned} \tag{C.2.23}$$

$$A_{p,q,r}=\varepsilon_L\delta_{(p,0),(q,0),(r,0)}+\sum_{m=1}^{M}(\varepsilon_m-\varepsilon_L)A_{p,m}^{x}A_{q,m}^{y}A_{r,m}^{z} \tag{C.2.24}$$

where A^x and A^y are one-dimensional arrays defined as follows:

$$A_{p,m}^{x}=\exp\left(-j\frac{2\pi}{\Lambda_x}p\left(\frac{x_{right,m}+x_{left,m}}{2}\right)\right)\mathrm{sinc}(pf_x)f_x,$$

$$A_{q,m}^{y}=\exp\left(-j\frac{2\pi}{\Lambda_y}q\left(\frac{y_{top,m}+y_{bottom,m}}{2}\right)\right)\mathrm{sinc}(pf_y)f_y,$$

$$A_{r,m}^{z}=\exp\left(-j\frac{2\pi}{\Lambda_x}r\left(\frac{z_{front,m}+z_{back,m}}{2}\right)\right)\mathrm{sinc}(pf_z)f_z,$$

and

$$f_x=\left(\frac{x_{right,m}-x_{left,m}}{\Lambda_x}\right),\ x_{center}=\left(\frac{x_{right,m}+x_{left,m}}{2}\right),$$

$$f_y = \left(\frac{y_{top,m} - y_{bottom,m}}{\Lambda_y} \right),\ y_{center} = \left(\frac{y_{top,m} + y_{bottom,m}}{2} \right),$$

$$f_z = \left(\frac{z_{front,m} - z_{back,m}}{\Lambda_z} \right),\ z_{center} = \left(\frac{z_{front,m} + z_{back,m}}{2} \right),$$

ε_L is the background permittivity, ε_m is the permittivity of the m^{th} region, and $\mathrm{sinc}(x) = \frac{\sin(\pi x)}{\pi x}$.

The coupling coefficients matrix can then be directly filled using the following relationships:

$$C^{x,y,z}_{(p_2 \to p_1),(q_2 \to q_1),(r_2 \to r_1)} = \sum_{m=1}^{M} (\varepsilon_m - \varepsilon_L) A^x_{(p_2 - p_1),m} A^y_{(q_2 - q_1),m} A^z_{(r_2 - r_1),m} \quad \text{(C.2.25)}$$

$$C^{x,y,z}_{(p_2 \to p_1 = p_2),(q_2 \to q_1 = q_2),(r_2 \to r_1 = r_2)} = \varepsilon_L + \sum_{m=1}^{M} (\varepsilon_m - \varepsilon_L) A^x_{0,m} A^y_{0,m} A^z_{0,m} \quad \text{(C.2.26)}$$

In the classic method of performing the coupling coefficient expansion, the Laurent rule for creating the coupling matrix is utilized for every component of the permittivity/permeability tensor. Various means of performing the inverse rule have been introduced for systems with more than one dimension of periodicity [27, 31, 169], but mathematical proofs of improved numerical convergence accuracy as well as mathematical uniqueness have not yet been provided.

APPENDIX D. MAKING USE OF TRANSVERSE SYMMETRY: GROUP THEORY IN GRATING THEORY

In any type of numerical spectral method, the accuracy of the solution that one can obtain in any given model depends upon not only the choice of basis set utilized but also on the number of basis functions retained in the computation. In most cases, the more basis functions that are retained in a given computation, the more accurate the obtained result will be. The limitation on the number of basis functions that can be retained in any given computation is a physical limitation, generally depending on the amount of computer memory (random access memory, virtual memory, and/or hard disk space) available for storing data generated by a model's computations. Apart from the physical limitations associated with system memory, increasing the number of basis functions used in a given computation also increases the total number of floating point operations needed to complete a computational run and leads to increased computation times. In certain cases, specifically when a model possesses proper symmetries, both the issue of memory requirements and computational time can be reduced by taking advantage of these symmetries.

In the case of using frequency-domain spectral methods to model waveguide and diffraction grating problems, a model must possess two separate types of symmetry concurrently, structural symmetry and input wave symmetry, in order to take advantage of either. This appendix will provide a description of the conditions necessary for taking advantage of symmetry in one-dimensional and two-dimensional modal problems, as well as for the determination of field distributions. The application of group theoretic concepts to RCWA was first formally applied by the Li group [27, 33-35, 171], but while that work expresses symmetric matrix reductions by operating on the material coupling matrices, in this appendix symmetry will be applied to the equations for the electric and magnetic fields directly.

D.1 σ_x-Symmetry in One-Dimensional Systems

In a layered, one-dimensional distribution of materials, a system that is transversely symmetric about the center of a computational window, which also has symmetric boundary conditions, can be computationally reduced in size if it is accompanied by a symmetric or an anti-symmetric energy input. As the transverse axis associated with this one-dimensional variation is normally associated with the *x*-axis, the group theoretic name for this type of symmetry is σ_x-symmetry. The application of σ_x-symmetry to a one-dimensional system can take on one of two different forms depending on the polarization of the input wave. For a system that is polarized in the *y*-direction, the following relationships hold between various field harmonic elements:

$$E_{y,m} = E_{y,-m} \tag{D.1.1}$$

$$H_{x,m} = H_{x,-m} \tag{D.1.2}$$

The original system of coupled wave equations relating E_y and H_x takes on the following matrix relationship:

$$\frac{\partial}{\partial z'}\begin{bmatrix} E_{y,0} \\ E_{y,1} \\ E_{y,-1} \\ E_{y,2} \\ E_{y,-2} \\ \vdots \end{bmatrix} = \begin{bmatrix} A_{0\to 0} & A_{0\to 1} & A_{0\to -1} & A_{0\to 2} & A_{0\to -2} & \cdots \\ A_{1\to 0} & A_{1\to 1} & A_{1\to -1} & A_{1\to 2} & A_{1\to -2} & \cdots \\ A_{-1\to 0} & A_{-1\to 1} & A_{-1\to -1} & A_{-1\to 2} & A_{-1\to -2} & \cdots \\ A_{2\to 0} & A_{2\to 1} & A_{2\to -1} & A_{2\to 2} & A_{2\to -2} & \cdots \\ A_{-2\to 0} & A_{-2\to 1} & A_{-2\to -1} & A_{-2\to 2} & A_{-2\to -2} & \cdots \\ \vdots & \vdots & \vdots & \vdots & \vdots & \ddots \end{bmatrix}\begin{bmatrix} H_{x,0} \\ H_{x,1} \\ H_{x,-1} \\ H_{x,2} \\ H_{x,-2} \\ \vdots \end{bmatrix} \tag{D.1.3}$$

Applying Equations (D.1.1) and (D.1.2) to (D.1.3) yields the following matrix relationships:

$$\frac{\partial}{\partial z'}\begin{bmatrix} E_{y,0} \\ E_{y,1} \\ E_{y,1} \\ E_{y,2} \\ E_{y,2} \\ \vdots \end{bmatrix} = \begin{bmatrix} A_{0\to 0} & A_{0\to 1} & A_{0\to 1} & A_{0\to 2} & A_{0\to 2} & \cdots \\ A_{1\to 0} & A_{1\to 1} & A_{1\to 1} & A_{1\to 2} & A_{1\to 2} & \cdots \\ A_{1\to 0} & A_{1\to 1} & A_{1\to 1} & A_{1\to 2} & A_{1\to 2} & \cdots \\ A_{2\to 0} & A_{2\to 1} & A_{2\to 1} & A_{2\to 2} & A_{2\to 2} & \cdots \\ A_{2\to 0} & A_{2\to 1} & A_{2\to 1} & A_{2\to 2} & A_{2\to 2} & \cdots \\ \vdots & \vdots & \vdots & \vdots & \vdots & \ddots \end{bmatrix}\begin{bmatrix} H_{x,0} \\ H_{x,1} \\ H_{x,1} \\ H_{x,2} \\ H_{x,2} \\ \vdots \end{bmatrix} \tag{D.1.4}$$

This system of equations can be reduced in size without any loss of generality as follows:

$$\frac{\partial}{\partial z'}\begin{bmatrix} E_{y,0} \\ E_{y,1} \\ E_{y,2} \\ \vdots \end{bmatrix} = \begin{bmatrix} A_{0\to 0} & 2A_{0\to 1} & 2A_{0\to 2} & \cdots \\ A_{1\to 0} & 2A_{1\to 1} & 2A_{1\to 2} & \cdots \\ A_{2\to 0} & 2A_{2\to 1} & 2A_{2\to 2} & \cdots \\ \vdots & \vdots & \vdots & \ddots \end{bmatrix}\begin{bmatrix} H_{x,0} \\ H_{x,1} \\ H_{x,2} \\ \vdots \end{bmatrix} \tag{D.1.5}$$

When the input wave is polarized in the *x*-direction, a similar relationship holds between the field components H_y and E_x.

D.2 σ_x- and σ_y-Symmetry in Two-Dimensional Systems

In a two-dimensionally periodic medium, there is a possibility for the occurrence of two types of one-dimensional transverse symmetries. When the material property distribution has mirror symmetry about the *x*-axis of the computational window, the system is said to possess σ_x - symmetry, and similarly when mirror symmetry is present about the *y*-axis, the system is said to possess σ_y - symmetry.

When the system possesses σ_x - symmetry, and the input field is polarized in the *y*-direction, the resulting electric and magnetic field harmonics have the following relationships:

$$E_{x,m,n} = -E_{x,m,-n} \tag{D.2.1}$$
$$E_{y,m,n} = E_{y,m,-n} \tag{D.2.2}$$
$$H_{x,m,n} = H_{x,m,-n} \tag{D.2.3}$$
$$H_{y,m,n} = -H_{y,m,-n} \tag{D.2.4}$$

The matrix relationship between the derivative of the electric field components and the magnetic field components can be expressed as follows:

$$\frac{\partial}{\partial z'}\begin{bmatrix} E_{y,0,0} \\ E_{y,1,0} \\ E_{y,-1,0} \\ E_{y,0,1} \\ E_{y,0,-1} \\ E_{y,1,1} \\ E_{y,-1,1} \\ E_{y,1,-1} \\ E_{y,-1,-1} \\ \vdots \\ \hline E_{x,0,0} \\ E_{x,1,0} \\ E_{x,-1,0} \\ E_{x,0,1} \\ E_{x,0,-1} \\ E_{x,1,1} \\ E_{x,-1,1} \\ E_{x,1,-1} \\ E_{x,-1,-1} \\ \vdots \end{bmatrix} = \begin{bmatrix} A^{y\to y}_{0\to 0,0\to 0} & A^{y\to y}_{0\to 1,0\to 0} & A^{y\to y}_{0\to -1,0\to 0} & A^{y\to y}_{0\to 0,0\to 1} & A^{y\to y}_{0\to 0,0\to -1} & A^{y\to y}_{0\to 1,0\to 1} & A^{y\to y}_{0\to -1,0\to 1} & A^{y\to y}_{0\to 1,0\to -1} & A^{y\to y}_{0\to -1,0\to -1} & \cdots \\ A^{y\to y}_{1\to 0,0\to 0} & A^{y\to y}_{1\to 1,0\to 0} & A^{y\to y}_{1\to -1,0\to 0} & A^{y\to y}_{1\to 0,0\to 1} & A^{y\to y}_{1\to 0,0\to -1} & A^{y\to y}_{1\to 1,0\to 1} & A^{y\to y}_{1\to -1,0\to 1} & A^{y\to y}_{1\to 1,0\to -1} & A^{y\to y}_{1\to -1,0\to -1} & \cdots \\ A^{y\to y}_{-1\to 0,0\to 0} & A^{y\to y}_{-1\to 1,0\to 0} & A^{y\to y}_{-1\to -1,0\to 0} & A^{y\to y}_{-1\to 0,0\to 1} & A^{y\to y}_{-1\to 0,0\to -1} & A^{y\to y}_{-1\to 1,0\to 1} & A^{y\to y}_{-1\to -1,0\to 1} & A^{y\to y}_{-1\to 1,0\to -1} & A^{y\to y}_{-1\to -1,0\to -1} & \cdots \\ A^{y\to y}_{0\to 0,1\to 0} & A^{y\to y}_{0\to 1,1\to 0} & A^{y\to y}_{0\to -1,1\to 0} & A^{y\to y}_{0\to 0,1\to 1} & A^{y\to y}_{0\to 0,1\to -1} & A^{y\to y}_{0\to 1,1\to 1} & A^{y\to y}_{0\to -1,1\to 1} & A^{y\to y}_{0\to 1,1\to -1} & A^{y\to y}_{0\to -1,1\to -1} & \cdots \\ A^{y\to y}_{0\to 0,-1\to 0} & A^{y\to y}_{0\to 1,-1\to 0} & A^{y\to y}_{0\to -1,-1\to 0} & A^{y\to y}_{0\to 0,-1\to 1} & A^{y\to y}_{0\to 0,-1\to -1} & A^{y\to y}_{0\to 1,-1\to 1} & A^{y\to y}_{0\to -1,-1\to 1} & A^{y\to y}_{0\to 1,-1\to -1} & A^{y\to y}_{0\to -1,-1\to -1} & \cdots \\ A^{y\to y}_{1\to 0,1\to 0} & A^{y\to y}_{1\to 1,1\to 0} & A^{y\to y}_{1\to -1,1\to 0} & A^{y\to y}_{1\to 0,1\to 1} & A^{y\to y}_{1\to 0,1\to -1} & A^{y\to y}_{1\to 1,1\to 1} & A^{y\to y}_{1\to -1,1\to 1} & A^{y\to y}_{1\to 1,1\to -1} & A^{y\to y}_{1\to -1,1\to -1} & \cdots \\ A^{y\to y}_{-1\to 0,1\to 0} & A^{y\to y}_{-1\to 1,1\to 0} & A^{y\to y}_{-1\to -1,1\to 0} & A^{y\to y}_{-1\to 0,1\to 1} & A^{y\to y}_{-1\to 0,1\to -1} & A^{y\to y}_{-1\to 1,1\to 1} & A^{y\to y}_{-1\to -1,1\to 1} & A^{y\to y}_{-1\to 1,1\to -1} & A^{y\to y}_{-1\to -1,1\to -1} & \cdots \\ A^{y\to y}_{1\to 0,-1\to 0} & A^{y\to y}_{1\to 1,-1\to 0} & A^{y\to y}_{1\to -1,-1\to 0} & A^{y\to y}_{1\to 0,-1\to 1} & A^{y\to y}_{1\to 0,-1\to -1} & A^{y\to y}_{1\to 1,-1\to 1} & A^{y\to y}_{1\to -1,-1\to 1} & A^{y\to y}_{1\to 1,-1\to -1} & A^{y\to y}_{1\to -1,-1\to -1} & \cdots \\ A^{y\to y}_{-1\to 0,-1\to 0} & A^{y\to y}_{-1\to 1,-1\to 0} & A^{y\to y}_{-1\to -1,-1\to 0} & A^{y\to y}_{-1\to 0,-1\to 1} & A^{y\to y}_{-1\to 0,-1\to -1} & A^{y\to y}_{-1\to 1,-1\to 1} & A^{y\to y}_{-1\to -1,-1\to 1} & A^{y\to y}_{-1\to 1,-1\to -1} & A^{y\to y}_{-1\to -1,-1\to -1} & \cdots \\ \vdots & \vdots & \vdots & \vdots & \vdots & \vdots & \vdots & \vdots & \vdots & \ddots \\ \hline A^{x\to y}_{0\to 0,0\to 0} & A^{x\to y}_{0\to 1,0\to 0} & A^{x\to y}_{0\to -1,0\to 0} & A^{x\to y}_{0\to 0,0\to 1} & A^{x\to y}_{0\to 0,0\to -1} & A^{x\to y}_{0\to 1,0\to 1} & A^{x\to y}_{0\to -1,0\to 1} & A^{x\to y}_{0\to 1,0\to -1} & A^{x\to y}_{0\to -1,0\to -1} & \cdots \\ A^{x\to y}_{1\to 0,0\to 0} & A^{x\to y}_{1\to 1,0\to 0} & A^{x\to y}_{1\to -1,0\to 0} & A^{x\to y}_{1\to 0,0\to 1} & A^{x\to y}_{1\to 0,0\to -1} & A^{x\to y}_{1\to 1,0\to 1} & A^{x\to y}_{1\to -1,0\to 1} & A^{x\to y}_{1\to 1,0\to -1} & A^{x\to y}_{1\to -1,0\to -1} & \cdots \\ A^{x\to y}_{-1\to 0,0\to 0} & A^{x\to y}_{-1\to 1,0\to 0} & A^{x\to y}_{-1\to -1,0\to 0} & A^{x\to y}_{-1\to 0,0\to 1} & A^{x\to y}_{-1\to 0,0\to -1} & A^{x\to y}_{-1\to 1,0\to 1} & A^{x\to y}_{-1\to -1,0\to 1} & A^{x\to y}_{-1\to 1,0\to -1} & A^{x\to y}_{-1\to -1,0\to -1} & \cdots \\ A^{x\to y}_{0\to 0,1\to 0} & A^{x\to y}_{0\to 1,1\to 0} & A^{x\to y}_{0\to -1,1\to 0} & A^{x\to y}_{0\to 0,1\to 1} & A^{x\to y}_{0\to 0,1\to -1} & A^{x\to y}_{0\to 1,1\to 1} & A^{x\to y}_{0\to -1,1\to 1} & A^{x\to y}_{0\to 1,1\to -1} & A^{x\to y}_{0\to -1,1\to -1} & \cdots \\ A^{x\to y}_{0\to 0,-1\to 0} & A^{x\to y}_{0\to 1,-1\to 0} & A^{x\to y}_{0\to -1,-1\to 0} & A^{x\to y}_{0\to 0,-1\to 1} & A^{x\to y}_{0\to 0,-1\to -1} & A^{x\to y}_{0\to 1,-1\to 1} & A^{x\to y}_{0\to -1,-1\to 1} & A^{x\to y}_{0\to 1,-1\to -1} & A^{x\to y}_{0\to -1,-1\to -1} & \cdots \\ A^{x\to y}_{1\to 0,1\to 0} & A^{x\to y}_{1\to 1,1\to 0} & A^{x\to y}_{1\to -1,1\to 0} & A^{x\to y}_{1\to 0,1\to 1} & A^{x\to y}_{1\to 0,1\to -1} & A^{x\to y}_{1\to 1,1\to 1} & A^{x\to y}_{1\to -1,1\to 1} & A^{x\to y}_{1\to 1,1\to -1} & A^{x\to y}_{1\to -1,1\to -1} & \cdots \\ A^{x\to y}_{-1\to 0,1\to 0} & A^{x\to y}_{-1\to 1,1\to 0} & A^{x\to y}_{-1\to -1,1\to 0} & A^{x\to y}_{-1\to 0,1\to 1} & A^{x\to y}_{-1\to 0,1\to -1} & A^{x\to y}_{-1\to 1,1\to 1} & A^{x\to y}_{-1\to -1,1\to 1} & A^{x\to y}_{-1\to 1,1\to -1} & A^{x\to y}_{-1\to -1,1\to -1} & \cdots \\ A^{x\to y}_{1\to 0,-1\to 0} & A^{x\to y}_{1\to 1,-1\to 0} & A^{x\to y}_{1\to -1,-1\to 0} & A^{x\to y}_{1\to 0,-1\to 1} & A^{x\to y}_{1\to 0,-1\to -1} & A^{x\to y}_{1\to 1,-1\to 1} & A^{x\to y}_{1\to -1,-1\to 1} & A^{x\to y}_{1\to 1,-1\to -1} & A^{x\to y}_{1\to -1,-1\to -1} & \cdots \\ A^{x\to y}_{-1\to 0,-1\to 0} & A^{x\to y}_{-1\to 1,-1\to 0} & A^{x\to y}_{-1\to -1,-1\to 0} & A^{x\to y}_{-1\to 0,-1\to 1} & A^{x\to y}_{-1\to 0,-1\to -1} & A^{x\to y}_{-1\to 1,-1\to 1} & A^{x\to y}_{-1\to -1,-1\to 1} & A^{x\to y}_{-1\to 1,-1\to -1} & A^{x\to y}_{-1\to -1,-1\to -1} & \cdots \\ \vdots & \vdots & \vdots & \vdots & \vdots & \vdots & \vdots & \vdots & \vdots & \ddots \end{bmatrix}$$

$$\cdots \begin{bmatrix} A^{y\to x}_{0\to 0,0\to 0} & A^{y\to x}_{0\to 1,0\to 0} & A^{y\to x}_{0\to -1,0\to 0} & A^{y\to x}_{0\to 0,0\to 1} & A^{y\to x}_{0\to 0,0\to -1} & A^{y\to x}_{0\to 1,0\to 1} & A^{y\to x}_{0\to -1,0\to 1} & A^{y\to x}_{0\to 1,0\to -1} & A^{y\to x}_{0\to -1,0\to -1} & \cdots \\ A^{y\to x}_{1\to 0,0\to 0} & A^{y\to x}_{1\to 1,0\to 0} & A^{y\to x}_{1\to -1,0\to 0} & A^{y\to x}_{1\to 0,0\to 1} & A^{y\to x}_{1\to 0,0\to -1} & A^{y\to x}_{1\to 1,0\to 1} & A^{y\to x}_{1\to -1,0\to 1} & A^{y\to x}_{1\to 1,0\to -1} & A^{y\to x}_{1\to -1,0\to -1} & \cdots \\ A^{y\to x}_{-1\to 0,0\to 0} & A^{y\to x}_{-1\to 1,0\to 0} & A^{y\to x}_{-1\to -1,0\to 0} & A^{y\to x}_{-1\to 0,0\to 1} & A^{y\to x}_{-1\to 0,0\to -1} & A^{y\to x}_{-1\to 1,0\to 1} & A^{y\to x}_{-1\to -1,0\to 1} & A^{y\to x}_{-1\to 1,0\to -1} & A^{y\to x}_{-1\to -1,0\to -1} & \cdots \\ A^{y\to x}_{0\to 0,1\to 0} & A^{y\to x}_{0\to 1,1\to 0} & A^{y\to x}_{0\to -1,1\to 0} & A^{y\to x}_{0\to 0,1\to 1} & A^{y\to x}_{0\to 0,1\to -1} & A^{y\to x}_{0\to 1,1\to 1} & A^{y\to x}_{0\to -1,1\to 1} & A^{y\to x}_{0\to 1,1\to -1} & A^{y\to x}_{0\to -1,1\to -1} & \cdots \\ A^{y\to x}_{0\to 0,-1\to 0} & A^{y\to x}_{0\to 1,-1\to 0} & A^{y\to x}_{0\to -1,-1\to 0} & A^{y\to x}_{0\to 0,-1\to 1} & A^{y\to x}_{0\to 0,-1\to -1} & A^{y\to x}_{0\to 1,-1\to 1} & A^{y\to x}_{0\to -1,-1\to 1} & A^{y\to x}_{0\to 1,-1\to -1} & A^{y\to x}_{0\to -1,-1\to -1} & \cdots \\ A^{y\to x}_{1\to 0,1\to 0} & A^{y\to x}_{1\to 1,1\to 0} & A^{y\to x}_{1\to -1,1\to 0} & A^{y\to x}_{1\to 0,1\to 1} & A^{y\to x}_{1\to 0,1\to -1} & A^{y\to x}_{1\to 1,1\to 1} & A^{y\to x}_{1\to -1,1\to 1} & A^{y\to x}_{1\to 1,1\to -1} & A^{y\to x}_{1\to -1,1\to -1} & \cdots \\ A^{y\to x}_{-1\to 0,1\to 0} & A^{y\to x}_{-1\to 1,1\to 0} & A^{y\to x}_{-1\to -1,1\to 0} & A^{y\to x}_{-1\to 0,1\to 1} & A^{y\to x}_{-1\to 0,1\to -1} & A^{y\to x}_{-1\to 1,1\to 1} & A^{y\to x}_{-1\to -1,1\to 1} & A^{y\to x}_{-1\to 1,1\to -1} & A^{y\to x}_{-1\to -1,1\to -1} & \cdots \\ A^{y\to x}_{1\to 0,-1\to 0} & A^{y\to x}_{1\to 1,-1\to 0} & A^{y\to x}_{1\to -1,-1\to 0} & A^{y\to x}_{1\to 0,-1\to 1} & A^{y\to x}_{1\to 0,-1\to -1} & A^{y\to x}_{1\to 1,-1\to 1} & A^{y\to x}_{1\to -1,-1\to 1} & A^{y\to x}_{1\to 1,-1\to -1} & A^{y\to x}_{1\to -1,-1\to -1} & \cdots \\ A^{y\to x}_{-1\to 0,-1\to 0} & A^{y\to x}_{-1\to 1,-1\to 0} & A^{y\to x}_{-1\to -1,-1\to 0} & A^{y\to x}_{-1\to 0,-1\to 1} & A^{y\to x}_{-1\to 0,-1\to -1} & A^{y\to x}_{-1\to 1,-1\to 1} & A^{y\to x}_{-1\to -1,-1\to 1} & A^{y\to x}_{-1\to 1,-1\to -1} & A^{y\to x}_{-1\to -1,-1\to -1} & \cdots \\ \vdots & \vdots & \vdots & \vdots & \vdots & \vdots & \vdots & \vdots & \vdots & \ddots \\ \hline A^{x\to x}_{0\to 0,0\to 0} & A^{x\to x}_{0\to 1,0\to 0} & A^{x\to x}_{0\to -1,0\to 0} & A^{x\to x}_{0\to 0,0\to 1} & A^{x\to x}_{0\to 0,0\to -1} & A^{x\to x}_{0\to 1,0\to 1} & A^{x\to x}_{0\to -1,0\to 1} & A^{x\to x}_{0\to 1,0\to -1} & A^{x\to x}_{0\to -1,0\to -1} & \cdots \\ A^{x\to x}_{1\to 0,0\to 0} & A^{x\to x}_{1\to 1,0\to 0} & A^{x\to x}_{1\to -1,0\to 0} & A^{x\to x}_{1\to 0,0\to 1} & A^{x\to x}_{1\to 0,0\to -1} & A^{x\to x}_{1\to 1,0\to 1} & A^{x\to x}_{1\to -1,0\to 1} & A^{x\to x}_{1\to 1,0\to -1} & A^{x\to x}_{1\to -1,0\to -1} & \cdots \\ A^{x\to x}_{-1\to 0,0\to 0} & A^{x\to x}_{-1\to 1,0\to 0} & A^{x\to x}_{-1\to -1,0\to 0} & A^{x\to x}_{-1\to 0,0\to 1} & A^{x\to x}_{-1\to 0,0\to -1} & A^{x\to x}_{-1\to 1,0\to 1} & A^{x\to x}_{-1\to -1,0\to 1} & A^{x\to x}_{-1\to 1,0\to -1} & A^{x\to x}_{-1\to -1,0\to -1} & \cdots \\ A^{x\to x}_{0\to 0,1\to 0} & A^{x\to x}_{0\to 1,1\to 0} & A^{x\to x}_{0\to -1,1\to 0} & A^{x\to x}_{0\to 0,1\to 1} & A^{x\to x}_{0\to 0,1\to -1} & A^{x\to x}_{0\to 1,1\to 1} & A^{x\to x}_{0\to -1,1\to 1} & A^{x\to x}_{0\to 1,1\to -1} & A^{x\to x}_{0\to -1,1\to -1} & \cdots \\ A^{x\to x}_{0\to 0,-1\to 0} & A^{x\to x}_{0\to 1,-1\to 0} & A^{x\to x}_{0\to -1,-1\to 0} & A^{x\to x}_{0\to 0,-1\to 1} & A^{x\to x}_{0\to 0,-1\to -1} & A^{x\to x}_{0\to 1,-1\to 1} & A^{x\to x}_{0\to -1,-1\to 1} & A^{x\to x}_{0\to 1,-1\to -1} & A^{x\to x}_{0\to -1,-1\to -1} & \cdots \\ A^{x\to x}_{1\to 0,1\to 0} & A^{x\to x}_{1\to 1,1\to 0} & A^{x\to x}_{1\to -1,1\to 0} & A^{x\to x}_{1\to 0,1\to 1} & A^{x\to x}_{1\to 0,1\to -1} & A^{x\to x}_{1\to 1,1\to 1} & A^{x\to x}_{1\to -1,1\to 1} & A^{x\to x}_{1\to 1,1\to -1} & A^{x\to x}_{1\to -1,1\to -1} & \cdots \\ A^{x\to x}_{-1\to 0,1\to 0} & A^{x\to x}_{-1\to 1,1\to 0} & A^{x\to x}_{-1\to -1,1\to 0} & A^{x\to x}_{-1\to 0,1\to 1} & A^{x\to x}_{-1\to 0,1\to -1} & A^{x\to x}_{-1\to 1,1\to 1} & A^{x\to x}_{-1\to -1,1\to 1} & A^{x\to x}_{-1\to 1,1\to -1} & A^{x\to x}_{-1\to -1,1\to -1} & \cdots \\ A^{x\to x}_{1\to 0,-1\to 0} & A^{x\to x}_{1\to 1,-1\to 0} & A^{x\to x}_{1\to -1,-1\to 0} & A^{x\to x}_{1\to 0,-1\to 1} & A^{x\to x}_{1\to 0,-1\to -1} & A^{x\to x}_{1\to 1,-1\to 1} & A^{x\to x}_{1\to -1,-1\to 1} & A^{x\to x}_{1\to 1,-1\to -1} & A^{x\to x}_{1\to -1,-1\to -1} & \cdots \\ A^{x\to x}_{-1\to 0,-1\to 0} & A^{x\to x}_{-1\to 1,-1\to 0} & A^{x\to x}_{-1\to -1,-1\to 0} & A^{x\to x}_{-1\to 0,-1\to 1} & A^{x\to x}_{-1\to 0,-1\to -1} & A^{x\to x}_{-1\to 1,-1\to 1} & A^{x\to x}_{-1\to -1,-1\to 1} & A^{x\to x}_{-1\to 1,-1\to -1} & A^{x\to x}_{-1\to -1,-1\to -1} & \cdots \\ \vdots & \vdots & \vdots & \vdots & \vdots & \vdots & \vdots & \vdots & \vdots & \ddots \end{bmatrix} \begin{bmatrix} H_{y,0,0} \\ H_{y,1,0} \\ H_{y,-1,0} \\ H_{y,0,1} \\ H_{y,0,-1} \\ H_{y,1,1} \\ H_{y,-1,1} \\ H_{y,1,-1} \\ H_{y,-1,-1} \\ \vdots \\ \hline H_{x,0,0} \\ H_{x,1,0} \\ H_{x,-1,0} \\ H_{x,0,1} \\ H_{x,0,-1} \\ H_{x,1,1} \\ H_{x,-1,1} \\ H_{x,1,-1} \\ H_{x,-1,-1} \\ \vdots \end{bmatrix} \tag{D.2.5}$$

Similarly, the matrix relationship between the derivative of the magnetic field components and the electric field components can be expressed as follows:

$$\frac{\partial}{\partial z'}\begin{bmatrix} H_{y,0,0} \\ H_{y,1,0} \\ H_{y,-1,0} \\ H_{y,0,1} \\ H_{y,0,-1} \\ H_{y,1,1} \\ H_{y,-1,1} \\ H_{y,1,-1} \\ H_{y,-1,-1} \\ \vdots \\ \hline H_{x,0,0} \\ H_{x,1,0} \\ H_{x,-1,0} \\ H_{x,0,1} \\ H_{x,0,-1} \\ H_{x,1,1} \\ H_{x,-1,1} \\ H_{x,1,-1} \\ H_{x,-1,-1} \\ \vdots \end{bmatrix} = \begin{bmatrix} B^{y\to y}_{0\to 0,0\to 0} & B^{y\to y}_{0\to 1,0\to 0} & B^{y\to y}_{0\to -1,0\to 0} & B^{y\to y}_{0\to 0,0\to 1} & B^{y\to y}_{0\to 0,0\to -1} & B^{y\to y}_{0\to 1,0\to 1} & B^{y\to y}_{0\to -1,0\to 1} & B^{y\to y}_{0\to 1,0\to -1} & B^{y\to y}_{0\to -1,0\to -1} & \cdots \\ B^{y\to y}_{1\to 0,0\to 0} & B^{y\to y}_{1\to 1,0\to 0} & B^{y\to y}_{1\to -1,0\to 0} & B^{y\to y}_{1\to 0,0\to 1} & B^{y\to y}_{1\to 0,0\to -1} & B^{y\to y}_{1\to 1,0\to 1} & B^{y\to y}_{1\to -1,0\to 1} & B^{y\to y}_{1\to 1,0\to -1} & B^{y\to y}_{1\to -1,0\to -1} & \cdots \\ B^{y\to y}_{-1\to 0,0\to 0} & B^{y\to y}_{-1\to 1,0\to 0} & B^{y\to y}_{-1\to -1,0\to 0} & B^{y\to y}_{-1\to 0,0\to 1} & B^{y\to y}_{-1\to 0,0\to -1} & B^{y\to y}_{-1\to 1,0\to 1} & B^{y\to y}_{-1\to -1,0\to 1} & B^{y\to y}_{-1\to 1,0\to -1} & B^{y\to y}_{-1\to -1,0\to -1} & \cdots \\ B^{y\to y}_{0\to 0,1\to 0} & B^{y\to y}_{0\to 1,1\to 0} & B^{y\to y}_{0\to -1,1\to 0} & B^{y\to y}_{0\to 0,1\to 1} & B^{y\to y}_{0\to 0,1\to -1} & B^{y\to y}_{0\to 1,1\to 1} & B^{y\to y}_{0\to -1,1\to 1} & B^{y\to y}_{0\to 1,1\to -1} & B^{y\to y}_{0\to -1,1\to -1} & \cdots \\ B^{y\to y}_{0\to 0,-1\to 0} & B^{y\to y}_{0\to 1,-1\to 0} & B^{y\to y}_{0\to -1,-1\to 0} & B^{y\to y}_{0\to 0,-1\to 1} & B^{y\to y}_{0\to 0,-1\to -1} & B^{y\to y}_{0\to 1,-1\to 1} & B^{y\to y}_{0\to -1,-1\to 1} & B^{y\to y}_{0\to 1,-1\to -1} & B^{y\to y}_{0\to -1,-1\to -1} & \cdots \\ B^{y\to y}_{1\to 0,1\to 0} & B^{y\to y}_{1\to 1,1\to 0} & B^{y\to y}_{1\to -1,1\to 0} & B^{y\to y}_{1\to 0,1\to 1} & B^{y\to y}_{1\to 0,1\to -1} & B^{y\to y}_{1\to 1,1\to 1} & B^{y\to y}_{1\to -1,1\to 1} & B^{y\to y}_{1\to 1,1\to -1} & B^{y\to y}_{1\to -1,1\to -1} & \cdots \\ B^{y\to y}_{-1\to 0,1\to 0} & B^{y\to y}_{-1\to 1,1\to 0} & B^{y\to y}_{-1\to -1,1\to 0} & B^{y\to y}_{-1\to 0,1\to 1} & B^{y\to y}_{-1\to 0,1\to -1} & B^{y\to y}_{-1\to 1,1\to 1} & B^{y\to y}_{-1\to -1,1\to 1} & B^{y\to y}_{-1\to 1,1\to -1} & B^{y\to y}_{-1\to -1,1\to -1} & \cdots \\ B^{y\to y}_{1\to 0,-1\to 0} & B^{y\to y}_{1\to 1,-1\to 0} & B^{y\to y}_{1\to -1,-1\to 0} & B^{y\to y}_{1\to 0,-1\to 1} & B^{y\to y}_{1\to 0,-1\to -1} & B^{y\to y}_{1\to 1,-1\to 1} & B^{y\to y}_{1\to -1,-1\to 1} & B^{y\to y}_{1\to 1,-1\to -1} & B^{y\to y}_{1\to -1,-1\to -1} & \cdots \\ B^{y\to y}_{-1\to 0,-1\to 0} & B^{y\to y}_{-1\to 1,-1\to 0} & B^{y\to y}_{-1\to -1,-1\to 0} & B^{y\to y}_{-1\to 0,-1\to 1} & B^{y\to y}_{-1\to 0,-1\to -1} & B^{y\to y}_{-1\to 1,-1\to 1} & B^{y\to y}_{-1\to -1,-1\to 1} & B^{y\to y}_{-1\to 1,-1\to -1} & B^{y\to y}_{-1\to -1,-1\to -1} & \cdots \\ \vdots & \vdots & \vdots & \vdots & \vdots & \vdots & \vdots & \vdots & \vdots & \ddots \\ \hline B^{x\to y}_{0\to 0,0\to 0} & B^{x\to y}_{0\to 1,0\to 0} & B^{x\to y}_{0\to -1,0\to 0} & B^{x\to y}_{0\to 0,0\to 1} & B^{x\to y}_{0\to 0,0\to -1} & B^{x\to y}_{0\to 1,0\to 1} & B^{x\to y}_{0\to -1,0\to 1} & B^{x\to y}_{0\to 1,0\to -1} & B^{x\to y}_{0\to -1,0\to -1} & \cdots \\ B^{x\to y}_{1\to 0,0\to 0} & B^{x\to y}_{1\to 1,0\to 0} & B^{x\to y}_{1\to -1,0\to 0} & B^{x\to y}_{1\to 0,0\to 1} & B^{x\to y}_{1\to 0,0\to -1} & B^{x\to y}_{1\to 1,0\to 1} & B^{x\to y}_{1\to -1,0\to 1} & B^{x\to y}_{1\to 1,0\to -1} & B^{x\to y}_{1\to -1,0\to -1} & \cdots \\ B^{x\to y}_{-1\to 0,0\to 0} & B^{x\to y}_{-1\to 1,0\to 0} & B^{x\to y}_{-1\to -1,0\to 0} & B^{x\to y}_{-1\to 0,0\to 1} & B^{x\to y}_{-1\to 0,0\to -1} & B^{x\to y}_{-1\to 1,0\to 1} & B^{x\to y}_{-1\to -1,0\to 1} & B^{x\to y}_{-1\to 1,0\to -1} & B^{x\to y}_{-1\to -1,0\to -1} & \cdots \\ B^{x\to y}_{0\to 0,1\to 0} & B^{x\to y}_{0\to 1,1\to 0} & B^{x\to y}_{0\to -1,1\to 0} & B^{x\to y}_{0\to 0,1\to 1} & B^{x\to y}_{0\to 0,1\to -1} & B^{x\to y}_{0\to 1,1\to 1} & B^{x\to y}_{0\to -1,1\to 1} & B^{x\to y}_{0\to 1,1\to -1} & B^{x\to y}_{0\to -1,1\to -1} & \cdots \\ B^{x\to y}_{0\to 0,-1\to 0} & B^{x\to y}_{0\to 1,-1\to 0} & B^{x\to y}_{0\to -1,-1\to 0} & B^{x\to y}_{0\to 0,-1\to 1} & B^{x\to y}_{0\to 0,-1\to -1} & B^{x\to y}_{0\to 1,-1\to 1} & B^{x\to y}_{0\to -1,-1\to 1} & B^{x\to y}_{0\to 1,-1\to -1} & B^{x\to y}_{0\to -1,-1\to -1} & \cdots \\ B^{x\to y}_{1\to 0,1\to 0} & B^{x\to y}_{1\to 1,1\to 0} & B^{x\to y}_{1\to -1,1\to 0} & B^{x\to y}_{1\to 0,1\to 1} & B^{x\to y}_{1\to 0,1\to -1} & B^{x\to y}_{1\to 1,1\to 1} & B^{x\to y}_{1\to -1,1\to 1} & B^{x\to y}_{1\to 1,1\to -1} & B^{x\to y}_{1\to -1,1\to -1} & \cdots \\ B^{x\to y}_{-1\to 0,1\to 0} & B^{x\to y}_{-1\to 1,1\to 0} & B^{x\to y}_{-1\to -1,1\to 0} & B^{x\to y}_{-1\to 0,1\to 1} & B^{x\to y}_{-1\to 0,1\to -1} & B^{x\to y}_{-1\to 1,1\to 1} & B^{x\to y}_{-1\to -1,1\to 1} & B^{x\to y}_{-1\to 1,1\to -1} & B^{x\to y}_{-1\to -1,1\to -1} & \cdots \\ B^{x\to y}_{1\to 0,-1\to 0} & B^{x\to y}_{1\to 1,-1\to 0} & B^{x\to y}_{1\to -1,-1\to 0} & B^{x\to y}_{1\to 0,-1\to 1} & B^{x\to y}_{1\to 0,-1\to -1} & B^{x\to y}_{1\to 1,-1\to 1} & B^{x\to y}_{1\to -1,-1\to 1} & B^{x\to y}_{1\to 1,-1\to -1} & B^{x\to y}_{1\to -1,-1\to -1} & \cdots \\ B^{x\to y}_{-1\to 0,-1\to 0} & B^{x\to y}_{-1\to 1,-1\to 0} & B^{x\to y}_{-1\to -1,-1\to 0} & B^{x\to y}_{-1\to 0,-1\to 1} & B^{x\to y}_{-1\to 0,-1\to -1} & B^{x\to y}_{-1\to 1,-1\to 1} & B^{x\to y}_{-1\to -1,-1\to 1} & B^{x\to y}_{-1\to 1,-1\to -1} & B^{x\to y}_{-1\to -1,-1\to -1} & \cdots \\ \vdots & \vdots & \vdots & \vdots & \vdots & \vdots & \vdots & \vdots & \vdots & \ddots \end{bmatrix}$$

$$\cdots \begin{bmatrix} B^{y\to x}_{0\to 0,0\to 0} & B^{y\to x}_{0\to 1,0\to 0} & B^{y\to x}_{0\to -1,0\to 0} & B^{y\to x}_{0\to 0,0\to 1} & B^{y\to x}_{0\to 0,0\to -1} & B^{y\to x}_{0\to 1,0\to 1} & B^{y\to x}_{0\to -1,0\to 1} & B^{y\to x}_{0\to 1,0\to -1} & B^{y\to x}_{0\to -1,0\to -1} & \cdots \\ B^{y\to x}_{1\to 0,0\to 0} & B^{y\to x}_{1\to 1,0\to 0} & B^{y\to x}_{1\to -1,0\to 0} & B^{y\to x}_{1\to 0,0\to 1} & B^{y\to x}_{1\to 0,0\to -1} & B^{y\to x}_{1\to 1,0\to 1} & B^{y\to x}_{1\to -1,0\to 1} & B^{y\to x}_{1\to 1,0\to -1} & B^{y\to x}_{1\to -1,0\to -1} & \cdots \\ B^{y\to x}_{-1\to 0,0\to 0} & B^{y\to x}_{-1\to 1,0\to 0} & B^{y\to x}_{-1\to -1,0\to 0} & B^{y\to x}_{-1\to 0,0\to 1} & B^{y\to x}_{-1\to 0,0\to -1} & B^{y\to x}_{-1\to 1,0\to 1} & B^{y\to x}_{-1\to -1,0\to 1} & B^{y\to x}_{-1\to 1,0\to -1} & B^{y\to x}_{-1\to -1,0\to -1} & \cdots \\ B^{y\to x}_{0\to 0,1\to 0} & B^{y\to x}_{0\to 1,1\to 0} & B^{y\to x}_{0\to -1,1\to 0} & B^{y\to x}_{0\to 0,1\to 1} & B^{y\to x}_{0\to 0,1\to -1} & B^{y\to x}_{0\to 1,1\to 1} & B^{y\to x}_{0\to -1,1\to 1} & B^{y\to x}_{0\to 1,1\to -1} & B^{y\to x}_{0\to -1,1\to -1} & \cdots \\ B^{y\to x}_{0\to 0,-1\to 0} & B^{y\to x}_{0\to 1,-1\to 0} & B^{y\to x}_{0\to -1,-1\to 0} & B^{y\to x}_{0\to 0,-1\to 1} & B^{y\to x}_{0\to 0,-1\to -1} & B^{y\to x}_{0\to 1,-1\to 1} & B^{y\to x}_{0\to -1,-1\to 1} & B^{y\to x}_{0\to 1,-1\to -1} & B^{y\to x}_{0\to -1,-1\to -1} & \cdots \\ B^{y\to x}_{1\to 0,1\to 0} & B^{y\to x}_{1\to 1,1\to 0} & B^{y\to x}_{1\to -1,1\to 0} & B^{y\to x}_{1\to 0,1\to 1} & B^{y\to x}_{1\to 0,1\to -1} & B^{y\to x}_{1\to 1,1\to 1} & B^{y\to x}_{1\to -1,1\to 1} & B^{y\to x}_{1\to 1,1\to -1} & B^{y\to x}_{1\to -1,1\to -1} & \cdots \\ B^{y\to x}_{-1\to 0,1\to 0} & B^{y\to x}_{-1\to 1,1\to 0} & B^{y\to x}_{-1\to -1,1\to 0} & B^{y\to x}_{-1\to 0,1\to 1} & B^{y\to x}_{-1\to 0,1\to -1} & B^{y\to x}_{-1\to 1,1\to 1} & B^{y\to x}_{-1\to -1,1\to 1} & B^{y\to x}_{-1\to 1,1\to -1} & B^{y\to x}_{-1\to -1,1\to -1} & \cdots \\ B^{y\to x}_{1\to 0,-1\to 0} & B^{y\to x}_{1\to 1,-1\to 0} & B^{y\to x}_{1\to -1,-1\to 0} & B^{y\to x}_{1\to 0,-1\to 1} & B^{y\to x}_{1\to 0,-1\to -1} & B^{y\to x}_{1\to 1,-1\to 1} & B^{y\to x}_{1\to -1,-1\to 1} & B^{y\to x}_{1\to 1,-1\to -1} & B^{y\to x}_{1\to -1,-1\to -1} & \cdots \\ B^{y\to x}_{-1\to 0,-1\to 0} & B^{y\to x}_{-1\to 1,-1\to 0} & B^{y\to x}_{-1\to -1,-1\to 0} & B^{y\to x}_{-1\to 0,-1\to 1} & B^{y\to x}_{-1\to 0,-1\to -1} & B^{y\to x}_{-1\to 1,-1\to 1} & B^{y\to x}_{-1\to -1,-1\to 1} & B^{y\to x}_{-1\to 1,-1\to -1} & B^{y\to x}_{-1\to -1,-1\to -1} & \cdots \\ \vdots & \vdots & \vdots & \vdots & \vdots & \vdots & \vdots & \vdots & \vdots & \ddots \\ \hline B^{x\to x}_{0\to 0,0\to 0} & B^{x\to x}_{0\to 1,0\to 0} & B^{x\to x}_{0\to -1,0\to 0} & B^{x\to x}_{0\to 0,0\to 1} & B^{x\to x}_{0\to 0,0\to -1} & B^{x\to x}_{0\to 1,0\to 1} & B^{x\to x}_{0\to -1,0\to 1} & B^{x\to x}_{0\to 1,0\to -1} & B^{x\to x}_{0\to -1,0\to -1} & \cdots \\ B^{x\to x}_{1\to 0,0\to 0} & B^{x\to x}_{1\to 1,0\to 0} & B^{x\to x}_{1\to -1,0\to 0} & B^{x\to x}_{1\to 0,0\to 1} & B^{x\to x}_{1\to 0,0\to -1} & B^{x\to x}_{1\to 1,0\to 1} & B^{x\to x}_{1\to -1,0\to 1} & B^{x\to x}_{1\to 1,0\to -1} & B^{x\to x}_{1\to -1,0\to -1} & \cdots \\ B^{x\to x}_{-1\to 0,0\to 0} & B^{x\to x}_{-1\to 1,0\to 0} & B^{x\to x}_{-1\to -1,0\to 0} & B^{x\to x}_{-1\to 0,0\to 1} & B^{x\to x}_{-1\to 0,0\to -1} & B^{x\to x}_{-1\to 1,0\to 1} & B^{x\to x}_{-1\to -1,0\to 1} & B^{x\to x}_{-1\to 1,0\to -1} & B^{x\to x}_{-1\to -1,0\to -1} & \cdots \\ B^{x\to x}_{0\to 0,1\to 0} & B^{x\to x}_{0\to 1,1\to 0} & B^{x\to x}_{0\to -1,1\to 0} & B^{x\to x}_{0\to 0,1\to 1} & B^{x\to x}_{0\to 0,1\to -1} & B^{x\to x}_{0\to 1,1\to 1} & B^{x\to x}_{0\to -1,1\to 1} & B^{x\to x}_{0\to 1,1\to -1} & B^{x\to x}_{0\to -1,1\to -1} & \cdots \\ B^{x\to x}_{0\to 0,-1\to 0} & B^{x\to x}_{0\to 1,-1\to 0} & B^{x\to x}_{0\to -1,-1\to 0} & B^{x\to x}_{0\to 0,-1\to 1} & B^{x\to x}_{0\to 0,-1\to -1} & B^{x\to x}_{0\to 1,-1\to 1} & B^{x\to x}_{0\to -1,-1\to 1} & B^{x\to x}_{0\to 1,-1\to -1} & B^{x\to x}_{0\to -1,-1\to -1} & \cdots \\ B^{x\to x}_{1\to 0,1\to 0} & B^{x\to x}_{1\to 1,1\to 0} & B^{x\to x}_{1\to -1,1\to 0} & B^{x\to x}_{1\to 0,1\to 1} & B^{x\to x}_{1\to 0,1\to -1} & B^{x\to x}_{1\to 1,1\to 1} & B^{x\to x}_{1\to -1,1\to 1} & B^{x\to x}_{1\to 1,1\to -1} & B^{x\to x}_{1\to -1,1\to -1} & \cdots \\ B^{x\to x}_{-1\to 0,1\to 0} & B^{x\to x}_{-1\to 1,1\to 0} & B^{x\to x}_{-1\to -1,1\to 0} & B^{x\to x}_{-1\to 0,1\to 1} & B^{x\to x}_{-1\to 0,1\to -1} & B^{x\to x}_{-1\to 1,1\to 1} & B^{x\to x}_{-1\to -1,1\to 1} & B^{x\to x}_{-1\to 1,1\to -1} & B^{x\to x}_{-1\to -1,1\to -1} & \cdots \\ B^{x\to x}_{1\to 0,-1\to 0} & B^{x\to x}_{1\to 1,-1\to 0} & B^{x\to x}_{1\to -1,-1\to 0} & B^{x\to x}_{1\to 0,-1\to 1} & B^{x\to x}_{1\to 0,-1\to -1} & B^{x\to x}_{1\to 1,-1\to 1} & B^{x\to x}_{1\to -1,-1\to 1} & B^{x\to x}_{1\to 1,-1\to -1} & B^{x\to x}_{1\to -1,-1\to -1} & \cdots \\ B^{x\to x}_{-1\to 0,-1\to 0} & B^{x\to x}_{-1\to 1,-1\to 0} & B^{x\to x}_{-1\to -1,-1\to 0} & B^{x\to x}_{-1\to 0,-1\to 1} & B^{x\to x}_{-1\to 0,-1\to -1} & B^{x\to x}_{-1\to 1,-1\to 1} & B^{x\to x}_{-1\to -1,-1\to 1} & B^{x\to x}_{-1\to 1,-1\to -1} & B^{x\to x}_{-1\to -1,-1\to -1} & \cdots \\ \vdots & \vdots & \vdots & \vdots & \vdots & \vdots & \vdots & \vdots & \vdots & \ddots \end{bmatrix} \begin{bmatrix} E_{y,0,0} \\ E_{y,1,0} \\ E_{y,-1,0} \\ E_{y,0,1} \\ E_{y,0,-1} \\ E_{y,1,1} \\ E_{y,-1,1} \\ E_{y,1,-1} \\ E_{y,-1,-1} \\ \vdots \\ \hline E_{x,0,0} \\ E_{x,1,0} \\ E_{x,-1,0} \\ E_{x,0,1} \\ E_{x,0,-1} \\ E_{x,1,1} \\ E_{x,-1,1} \\ E_{x,1,-1} \\ E_{x,-1,-1} \\ \vdots \end{bmatrix} \tag{D.2.6}$$

For the elements listed in Equations (D.2.5) and (D.2.6), the symmetry relationships in Equations (D.2.1) – (D.2.4) can be expressed in matrix form as follows:

$$\begin{bmatrix} E_{y,0,0} \\ E_{y,1,0} \\ E_{y,-1,0} \\ E_{y,0,1} \\ E_{y,0,-1} \\ E_{y,1,1} \\ E_{y,-1,1} \\ E_{y,1,-1} \\ E_{y,-1,-1} \\ \vdots \end{bmatrix} = \begin{bmatrix} 1 & 0 & 0 & 0 & 0 & 0 & 0 & 0 & 0 & \cdots \\ 0 & 1 & 0 & 0 & 0 & 0 & 0 & 0 & 0 & \cdots \\ 0 & 0 & 1 & 0 & 0 & 0 & 0 & 0 & 0 & \cdots \\ 0 & 0 & 0 & 1 & 0 & 0 & 0 & 0 & 0 & \cdots \\ 0 & 0 & 0 & 0 & 1 & 0 & 0 & 0 & 0 & \cdots \\ 0 & 0 & 0 & 0 & 0 & 1 & 0 & 0 & 0 & \cdots \\ 0 & 0 & 0 & 0 & 0 & 0 & 1 & 0 & 0 & \cdots \\ 0 & 0 & 0 & 0 & 0 & 0 & 0 & 1 & 0 & \cdots \\ 0 & 0 & 0 & 0 & 0 & 0 & 0 & 0 & 1 & \cdots \\ \vdots & \vdots & \vdots & \vdots & \vdots & \vdots & \vdots & \vdots & \vdots & \ddots \end{bmatrix} \begin{bmatrix} E_{y,0,0} \\ E_{y,1,0} \\ E_{y,1,0} \\ E_{y,0,1} \\ E_{y,0,-1} \\ E_{y,1,1} \\ E_{y,1,1} \\ E_{y,1,-1} \\ E_{y,1,-1} \\ \vdots \end{bmatrix} \tag{D.2.7}$$

$$\begin{bmatrix} E_{x,0,0} \\ E_{x,1,0} \\ E_{x,-1,0} \\ E_{x,0,1} \\ E_{x,0,-1} \\ E_{x,1,1} \\ E_{x,-1,1} \\ E_{x,1,-1} \\ E_{x,-1,-1} \\ \vdots \end{bmatrix} = \begin{bmatrix} 1 & 0 & 0 & 0 & 0 & 0 & 0 & 0 & 0 & \cdots \\ 0 & 1 & 0 & 0 & 0 & 0 & 0 & 0 & 0 & \cdots \\ 0 & 0 & -1 & 0 & 0 & 0 & 0 & 0 & 0 & \cdots \\ 0 & 0 & 0 & 1 & 0 & 0 & 0 & 0 & 0 & \cdots \\ 0 & 0 & 0 & 0 & 1 & 0 & 0 & 0 & 0 & \cdots \\ 0 & 0 & 0 & 0 & 0 & 1 & 0 & 0 & 0 & \cdots \\ 0 & 0 & 0 & 0 & 0 & 0 & -1 & 0 & 0 & \cdots \\ 0 & 0 & 0 & 0 & 0 & 0 & 0 & 1 & 0 & \cdots \\ 0 & 0 & 0 & 0 & 0 & 0 & 0 & 0 & -1 & \cdots \\ \vdots & \vdots & \vdots & \vdots & \vdots & \vdots & \vdots & \vdots & \vdots & \ddots \end{bmatrix} \begin{bmatrix} E_{x,0,0} \\ E_{x,1,0} \\ E_{x,1,0} \\ E_{x,0,1} \\ E_{x,0,-1} \\ E_{x,1,1} \\ E_{x,1,1} \\ E_{x,1,-1} \\ E_{x,1,-1} \\ \vdots \end{bmatrix} \tag{D.2.8}$$

$$\begin{bmatrix} H_{y,0,0} \\ H_{y,1,0} \\ H_{y,-1,0} \\ H_{y,0,1} \\ H_{y,0,-1} \\ H_{y,1,1} \\ H_{y,-1,1} \\ H_{y,1,-1} \\ H_{y,-1,-1} \\ \vdots \end{bmatrix} = \begin{bmatrix} 1 & 0 & 0 & 0 & 0 & 0 & 0 & 0 & 0 & \cdots \\ 0 & 1 & 0 & 0 & 0 & 0 & 0 & 0 & 0 & \cdots \\ 0 & 0 & -1 & 0 & 0 & 0 & 0 & 0 & 0 & \cdots \\ 0 & 0 & 0 & 1 & 0 & 0 & 0 & 0 & 0 & \cdots \\ 0 & 0 & 0 & 0 & 1 & 0 & 0 & 0 & 0 & \cdots \\ 0 & 0 & 0 & 0 & 0 & 1 & 0 & 0 & 0 & \cdots \\ 0 & 0 & 0 & 0 & 0 & 0 & -1 & 0 & 0 & \cdots \\ 0 & 0 & 0 & 0 & 0 & 0 & 0 & 1 & 0 & \cdots \\ 0 & 0 & 0 & 0 & 0 & 0 & 0 & 0 & -1 & \cdots \\ \vdots & \vdots & \vdots & \vdots & \vdots & \vdots & \vdots & \vdots & \vdots & \ddots \end{bmatrix} \begin{bmatrix} H_{y,0,0} \\ H_{y,1,0} \\ H_{y,1,0} \\ H_{y,0,1} \\ H_{y,0,-1} \\ H_{y,1,1} \\ H_{y,1,1} \\ H_{y,1,-1} \\ H_{y,1,-1} \\ \vdots \end{bmatrix} \tag{D.2.9}$$

$$\begin{bmatrix} H_{x,0,0} \\ H_{x,1,0} \\ H_{x,-1,0} \\ H_{x,0,1} \\ H_{x,0,-1} \\ H_{x,1,1} \\ H_{x,-1,1} \\ H_{x,1,-1} \\ H_{x,-1,-1} \\ \vdots \end{bmatrix} = \begin{bmatrix} 1 & 0 & 0 & 0 & 0 & 0 & 0 & 0 & 0 & \cdots \\ 0 & 1 & 0 & 0 & 0 & 0 & 0 & 0 & 0 & \cdots \\ 0 & 0 & 1 & 0 & 0 & 0 & 0 & 0 & 0 & \cdots \\ 0 & 0 & 0 & 1 & 0 & 0 & 0 & 0 & 0 & \cdots \\ 0 & 0 & 0 & 0 & 1 & 0 & 0 & 0 & 0 & \cdots \\ 0 & 0 & 0 & 0 & 0 & 1 & 0 & 0 & 0 & \cdots \\ 0 & 0 & 0 & 0 & 0 & 0 & 1 & 0 & 0 & \cdots \\ 0 & 0 & 0 & 0 & 0 & 0 & 0 & 1 & 0 & \cdots \\ 0 & 0 & 0 & 0 & 0 & 0 & 0 & 0 & 1 & \cdots \\ \vdots & \vdots & \vdots & \vdots & \vdots & \vdots & \vdots & \vdots & \vdots & \ddots \end{bmatrix} \begin{bmatrix} H_{x,0,0} \\ H_{x,1,0} \\ H_{x,1,0} \\ H_{x,0,1} \\ H_{x,0,-1} \\ H_{x,1,1} \\ H_{x,1,1} \\ H_{x,1,-1} \\ H_{x,1,-1} \\ \vdots \end{bmatrix} \tag{D.2.10}$$

Applying Equations (D.2.7) – (D.2.10) to Equations (D.2.5) and (D.2.6) produces the following matrix relationships:

$$\frac{\partial}{\partial z'}\begin{bmatrix} E_{y,0,0} \\ E_{y,1,0} \\ E_{y,1,0} \\ E_{y,0,1} \\ E_{y,0,-1} \\ E_{y,1,1} \\ E_{y,1,1} \\ E_{y,1,-1} \\ E_{y,1,-1} \\ \vdots \\ \hline E_{x,0,0} \\ E_{x,1,0} \\ E_{x,1,0} \\ E_{x,0,1} \\ E_{x,0,-1} \\ E_{x,1,1} \\ E_{x,1,1} \\ E_{x,1,-1} \\ E_{x,1,-1} \\ \vdots \end{bmatrix} = \left[\begin{array}{ccccccccc} A^{y\to y}_{0\to 0,0\to 0} & A^{y\to y}_{0\to 1,0\to 0} & -A^{y\to y}_{0\to 1,0\to 0} & A^{y\to y}_{0\to 0,0\to 1} & A^{y\to y}_{0\to 0,0\to -1} & A^{y\to y}_{0\to 1,0\to 1} & -A^{y\to y}_{0\to 1,0\to 1} & A^{y\to y}_{0\to 1,0\to -1} & -A^{y\to y}_{0\to 1,0\to -1} & \cdots \\ A^{y\to y}_{1\to 0,0\to 0} & A^{y\to y}_{1\to 1,0\to 0} & -A^{y\to y}_{1\to 1,0\to 0} & A^{y\to y}_{1\to 0,0\to 1} & A^{y\to y}_{1\to 0,0\to -1} & A^{y\to y}_{1\to 1,0\to 1} & -A^{y\to y}_{1\to 1,0\to 1} & A^{y\to y}_{1\to 1,0\to -1} & -A^{y\to y}_{1\to 1,0\to -1} & \cdots \\ A^{y\to y}_{1\to 0,0\to 0} & A^{y\to y}_{1\to 1,0\to 0} & -A^{y\to y}_{1\to 1,0\to 0} & A^{y\to y}_{1\to 0,0\to 1} & A^{y\to y}_{1\to 0,0\to -1} & A^{y\to y}_{1\to 1,0\to 1} & -A^{y\to y}_{1\to 1,0\to 1} & A^{y\to y}_{1\to 1,0\to -1} & -A^{y\to y}_{1\to 1,0\to -1} & \cdots \\ A^{y\to y}_{0\to 0,1\to 0} & A^{y\to y}_{0\to 1,1\to 0} & -A^{y\to y}_{0\to 1,1\to 0} & A^{y\to y}_{0\to 0,1\to 1} & A^{y\to y}_{0\to 0,1\to -1} & A^{y\to y}_{0\to 1,1\to 1} & -A^{y\to y}_{0\to 1,1\to 1} & A^{y\to y}_{0\to 1,1\to -1} & -A^{y\to y}_{0\to 1,1\to -1} & \cdots \\ A^{y\to y}_{0\to 0,-1\to 0} & A^{y\to y}_{0\to 1,-1\to 0} & -A^{y\to y}_{0\to 1,-1\to 0} & A^{y\to y}_{0\to 0,-1\to 1} & A^{y\to y}_{0\to 0,-1\to -1} & A^{y\to y}_{0\to 1,-1\to 1} & -A^{y\to y}_{0\to 1,-1\to 1} & A^{y\to y}_{0\to 1,-1\to -1} & -A^{y\to y}_{0\to 1,-1\to -1} & \cdots \\ A^{y\to y}_{1\to 0,1\to 0} & A^{y\to y}_{1\to 1,1\to 0} & -A^{y\to y}_{1\to 1,1\to 0} & A^{y\to y}_{1\to 0,1\to 1} & A^{y\to y}_{1\to 0,1\to -1} & A^{y\to y}_{1\to 1,1\to 1} & -A^{y\to y}_{1\to 1,1\to 1} & A^{y\to y}_{1\to 1,1\to -1} & -A^{y\to y}_{1\to 1,1\to -1} & \cdots \\ A^{y\to y}_{1\to 0,1\to 0} & A^{y\to y}_{1\to 1,1\to 0} & -A^{y\to y}_{1\to 1,1\to 0} & A^{y\to y}_{1\to 0,1\to 1} & A^{y\to y}_{1\to 0,1\to -1} & A^{y\to y}_{1\to 1,1\to 1} & -A^{y\to y}_{1\to 1,1\to 1} & A^{y\to y}_{1\to 1,1\to -1} & -A^{y\to y}_{1\to 1,1\to -1} & \cdots \\ A^{y\to y}_{1\to 0,-1\to 0} & A^{y\to y}_{1\to 1,-1\to 0} & -A^{y\to y}_{1\to 1,-1\to 0} & A^{y\to y}_{1\to 0,-1\to 1} & A^{y\to y}_{1\to 0,-1\to -1} & A^{y\to y}_{1\to 1,-1\to 1} & -A^{y\to y}_{1\to 1,-1\to 1} & A^{y\to y}_{1\to 1,-1\to -1} & -A^{y\to y}_{1\to 1,-1\to -1} & \cdots \\ A^{y\to y}_{1\to 0,-1\to 0} & A^{y\to y}_{1\to 1,-1\to 0} & -A^{y\to y}_{1\to 1,-1\to 0} & A^{y\to y}_{1\to 0,-1\to 1} & A^{y\to y}_{1\to 0,-1\to -1} & A^{y\to y}_{1\to 1,-1\to 1} & -A^{y\to y}_{1\to 1,-1\to 1} & A^{y\to y}_{1\to 1,-1\to -1} & -A^{y\to y}_{1\to 1,-1\to -1} & \cdots \\ \vdots & \vdots & \vdots & \vdots & \vdots & \vdots & \vdots & \vdots & \vdots & \ddots \\ \hline A^{x\to y}_{0\to 0,0\to 0} & A^{x\to y}_{0\to 1,0\to 0} & -A^{x\to y}_{0\to 1,0\to 0} & A^{x\to y}_{0\to 0,0\to 1} & A^{x\to y}_{0\to 0,0\to -1} & A^{x\to y}_{0\to 1,0\to 1} & -A^{x\to y}_{0\to 1,0\to 1} & A^{x\to y}_{0\to 1,0\to -1} & -A^{x\to y}_{0\to 1,0\to -1} & \cdots \\ A^{x\to y}_{1\to 0,0\to 0} & A^{x\to y}_{1\to 1,0\to 0} & -A^{x\to y}_{1\to 1,0\to 0} & A^{x\to y}_{1\to 0,0\to 1} & A^{x\to y}_{1\to 0,0\to -1} & A^{x\to y}_{1\to 1,0\to 1} & -A^{x\to y}_{1\to 1,0\to 1} & A^{x\to y}_{1\to 1,0\to -1} & -A^{x\to y}_{1\to 1,0\to -1} & \cdots \\ -A^{x\to y}_{1\to 0,0\to 0} & -A^{x\to y}_{1\to 1,0\to 0} & A^{x\to y}_{-1\to 1,0\to 0} & -A^{x\to y}_{1\to 0,0\to 1} & -A^{x\to y}_{1\to 0,0\to -1} & -A^{x\to y}_{1\to 1,0\to 1} & A^{x\to y}_{1\to 1,0\to 1} & -A^{x\to y}_{1\to 1,0\to -1} & A^{x\to y}_{1\to 1,0\to -1} & \cdots \\ A^{x\to y}_{0\to 0,1\to 0} & A^{x\to y}_{0\to 1,1\to 0} & -A^{x\to y}_{0\to 1,1\to 0} & A^{x\to y}_{0\to 0,1\to 1} & A^{x\to y}_{0\to 0,1\to -1} & A^{x\to y}_{0\to 1,1\to 1} & -A^{x\to y}_{0\to 1,1\to 1} & A^{x\to y}_{0\to 1,1\to -1} & -A^{x\to y}_{0\to 1,1\to -1} & \cdots \\ A^{x\to y}_{0\to 0,-1\to 0} & A^{x\to y}_{0\to 1,-1\to 0} & -A^{x\to y}_{0\to 1,-1\to 0} & A^{x\to y}_{0\to 0,-1\to 1} & A^{x\to y}_{0\to 0,-1\to -1} & A^{x\to y}_{0\to 1,-1\to 1} & -A^{x\to y}_{0\to 1,-1\to 1} & A^{x\to y}_{0\to 1,-1\to -1} & -A^{x\to y}_{0\to 1,-1\to -1} & \cdots \\ A^{x\to y}_{1\to 0,1\to 0} & A^{x\to y}_{1\to 1,1\to 0} & -A^{x\to y}_{1\to 1,1\to 0} & A^{x\to y}_{1\to 0,1\to 1} & A^{x\to y}_{1\to 0,1\to -1} & A^{x\to y}_{1\to 1,1\to 1} & -A^{x\to y}_{1\to 1,1\to 1} & A^{x\to y}_{1\to 1,1\to -1} & -A^{x\to y}_{1\to 1,1\to -1} & \cdots \\ -A^{x\to y}_{1\to 0,1\to 0} & -A^{x\to y}_{1\to 1,1\to 0} & A^{x\to y}_{-1\to 1,1\to 0} & -A^{x\to y}_{1\to 0,1\to 1} & -A^{x\to y}_{1\to 0,1\to -1} & -A^{x\to y}_{1\to 1,1\to 1} & A^{x\to y}_{1\to 1,1\to 1} & -A^{x\to y}_{1\to 1,1\to -1} & A^{x\to y}_{1\to 1,1\to -1} & \cdots \\ A^{x\to y}_{1\to 0,-1\to 0} & A^{x\to y}_{1\to 1,-1\to 0} & -A^{x\to y}_{1\to 1,-1\to 0} & A^{x\to y}_{1\to 0,-1\to 1} & A^{x\to y}_{1\to 0,-1\to -1} & A^{x\to y}_{1\to 1,-1\to 1} & -A^{x\to y}_{1\to 1,-1\to 1} & A^{x\to y}_{1\to 1,-1\to -1} & -A^{x\to y}_{1\to 1,-1\to -1} & \cdots \\ -A^{x\to y}_{1\to 0,-1\to 0} & -A^{x\to y}_{1\to 1,-1\to 0} & A^{x\to y}_{-1\to 1,-1\to 0} & -A^{x\to y}_{1\to 0,-1\to 1} & -A^{x\to y}_{1\to 0,-1\to -1} & -A^{x\to y}_{1\to 1,-1\to 1} & A^{x\to y}_{1\to 1,-1\to 1} & -A^{x\to y}_{1\to 1,-1\to -1} & A^{x\to y}_{1\to 1,-1\to -1} & \cdots \\ \vdots & \vdots & \vdots & \vdots & \vdots & \vdots & \vdots & \vdots & \vdots & \ddots \end{array}\right]$$

$$\cdots \left[\begin{array}{ccccccccc} A^{y\to x}_{0\to 0,0\to 0} & A^{y\to x}_{0\to 1,0\to 0} & A^{y\to x}_{0\to 1,0\to 0} & A^{y\to x}_{0\to 0,0\to 1} & A^{y\to x}_{0\to 0,0\to -1} & A^{y\to x}_{0\to 1,0\to 1} & A^{y\to x}_{0\to -1,0\to 1} & A^{y\to x}_{0\to 1,0\to -1} & A^{y\to x}_{0\to 1,0\to -1} & \cdots \\ A^{y\to x}_{1\to 0,0\to 0} & A^{y\to x}_{1\to 1,0\to 0} & A^{y\to x}_{1\to -1,0\to 0} & A^{y\to x}_{1\to 0,0\to 1} & A^{y\to x}_{1\to 0,0\to -1} & A^{y\to x}_{1\to 1,0\to 1} & A^{y\to x}_{1\to -1,0\to 1} & A^{y\to x}_{1\to 1,0\to -1} & A^{y\to x}_{1\to 1,0\to -1} & \cdots \\ A^{y\to x}_{1\to 0,0\to 0} & A^{y\to x}_{1\to 1,0\to 0} & A^{y\to x}_{1\to -1,0\to 0} & A^{y\to x}_{1\to 0,0\to 1} & A^{y\to x}_{1\to 0,0\to -1} & A^{y\to x}_{1\to 1,0\to 1} & A^{y\to x}_{1\to -1,0\to 1} & A^{y\to x}_{1\to 1,0\to -1} & A^{y\to x}_{1\to 1,0\to -1} & \cdots \\ A^{y\to x}_{0\to 0,1\to 0} & A^{y\to x}_{0\to 1,1\to 0} & A^{y\to x}_{0\to -1,1\to 0} & A^{y\to x}_{0\to 0,1\to 1} & A^{y\to x}_{0\to 0,1\to -1} & A^{y\to x}_{0\to 1,1\to 1} & A^{y\to x}_{0\to -1,1\to 1} & A^{y\to x}_{0\to 1,1\to -1} & A^{y\to x}_{0\to 1,1\to -1} & \cdots \\ A^{y\to x}_{0\to 0,-1\to 0} & A^{y\to x}_{0\to 1,-1\to 0} & A^{y\to x}_{0\to -1,-1\to 0} & A^{y\to x}_{0\to 0,-1\to 1} & A^{y\to x}_{0\to 0,-1\to -1} & A^{y\to x}_{0\to 1,-1\to 1} & A^{y\to x}_{0\to -1,-1\to 1} & A^{y\to x}_{0\to 1,-1\to -1} & A^{y\to x}_{0\to 1,-1\to -1} & \cdots \\ A^{y\to x}_{1\to 0,1\to 0} & A^{y\to x}_{1\to 1,1\to 0} & A^{y\to x}_{1\to -1,1\to 0} & A^{y\to x}_{1\to 0,1\to 1} & A^{y\to x}_{1\to 0,1\to -1} & A^{y\to x}_{1\to 1,1\to 1} & A^{y\to x}_{1\to -1,1\to 1} & A^{y\to x}_{1\to 1,1\to -1} & A^{y\to x}_{1\to 1,1\to -1} & \cdots \\ A^{y\to x}_{1\to 0,1\to 0} & A^{y\to x}_{1\to 1,1\to 0} & A^{y\to x}_{1\to -1,1\to 0} & A^{y\to x}_{1\to 0,1\to 1} & A^{y\to x}_{1\to 0,1\to -1} & A^{y\to x}_{1\to 1,1\to 1} & A^{y\to x}_{1\to -1,1\to 1} & A^{y\to x}_{1\to 1,1\to -1} & A^{y\to x}_{1\to 1,1\to -1} & \cdots \\ A^{y\to x}_{1\to 0,-1\to 0} & A^{y\to x}_{1\to 1,-1\to 0} & A^{y\to x}_{1\to -1,-1\to 0} & A^{y\to x}_{1\to 0,-1\to 1} & A^{y\to x}_{1\to 0,-1\to -1} & A^{y\to x}_{1\to 1,-1\to 1} & A^{y\to x}_{1\to -1,-1\to 1} & A^{y\to x}_{1\to 1,-1\to -1} & A^{y\to x}_{1\to 1,-1\to -1} & \cdots \\ A^{y\to x}_{1\to 0,-1\to 0} & A^{y\to x}_{1\to 1,-1\to 0} & A^{y\to x}_{1\to -1,-1\to 0} & A^{y\to x}_{1\to 0,-1\to 1} & A^{y\to x}_{1\to 0,-1\to -1} & A^{y\to x}_{1\to 1,-1\to 1} & A^{y\to x}_{1\to -1,-1\to 1} & A^{y\to x}_{1\to 1,-1\to -1} & A^{y\to x}_{1\to 1,-1\to -1} & \cdots \\ \vdots & \vdots & \vdots & \vdots & \vdots & \vdots & \vdots & \vdots & \vdots & \ddots \\ \hline A^{x\to x}_{0\to 0,0\to 0} & A^{x\to x}_{0\to 1,0\to 0} & A^{x\to x}_{0\to 1,0\to 0} & A^{x\to x}_{0\to 0,0\to 1} & A^{x\to x}_{0\to 0,0\to -1} & A^{x\to x}_{0\to 1,0\to 1} & A^{x\to x}_{0\to 1,0\to 1} & A^{x\to x}_{0\to 1,0\to -1} & A^{x\to x}_{0\to 1,0\to -1} & \cdots \\ A^{x\to x}_{1\to 0,0\to 0} & A^{x\to x}_{1\to 1,0\to 0} & A^{x\to x}_{1\to 1,0\to 0} & A^{x\to x}_{1\to 0,0\to 1} & A^{x\to x}_{1\to 0,0\to -1} & A^{x\to x}_{1\to 1,0\to 1} & A^{x\to x}_{1\to 1,0\to 1} & A^{x\to x}_{1\to 1,0\to -1} & A^{x\to x}_{1\to 1,0\to -1} & \cdots \\ -A^{x\to x}_{1\to 0,0\to 0} & -A^{x\to x}_{1\to 1,0\to 0} & -A^{x\to x}_{1\to 1,0\to 0} & -A^{x\to x}_{1\to 0,0\to 1} & -A^{x\to x}_{1\to 0,0\to -1} & -A^{x\to x}_{1\to 1,0\to 1} & -A^{x\to x}_{1\to 1,0\to 1} & -A^{x\to x}_{1\to 1,0\to -1} & -A^{x\to x}_{1\to 1,0\to -1} & \cdots \\ A^{x\to x}_{0\to 0,1\to 0} & A^{x\to x}_{0\to 1,1\to 0} & A^{x\to x}_{0\to 1,1\to 0} & A^{x\to x}_{0\to 0,1\to 1} & A^{x\to x}_{0\to 0,1\to -1} & A^{x\to x}_{0\to 1,1\to 1} & A^{x\to x}_{0\to 1,1\to 1} & A^{x\to x}_{0\to 1,1\to -1} & A^{x\to x}_{0\to 1,1\to -1} & \cdots \\ A^{x\to x}_{0\to 0,-1\to 0} & A^{x\to x}_{0\to 1,-1\to 0} & A^{x\to x}_{0\to 1,-1\to 0} & A^{x\to x}_{0\to 0,-1\to 1} & A^{x\to x}_{0\to 0,-1\to -1} & A^{x\to x}_{0\to 1,-1\to 1} & A^{x\to x}_{0\to 1,-1\to 1} & A^{x\to x}_{0\to 1,-1\to -1} & A^{x\to x}_{0\to 1,-1\to -1} & \cdots \\ A^{x\to x}_{1\to 0,1\to 0} & A^{x\to x}_{1\to 1,1\to 0} & A^{x\to x}_{1\to 1,1\to 0} & A^{x\to x}_{1\to 0,1\to 1} & A^{x\to x}_{1\to 0,1\to -1} & A^{x\to x}_{1\to 1,1\to 1} & A^{x\to x}_{1\to 1,1\to 1} & A^{x\to x}_{1\to 1,1\to -1} & A^{x\to x}_{1\to 1,1\to -1} & \cdots \\ -A^{x\to x}_{1\to 0,1\to 0} & -A^{x\to x}_{1\to 1,1\to 0} & -A^{x\to x}_{1\to 1,1\to 0} & -A^{x\to x}_{1\to 0,1\to 1} & -A^{x\to x}_{1\to 0,1\to -1} & -A^{x\to x}_{1\to 1,1\to 1} & -A^{x\to x}_{1\to 1,1\to 1} & -A^{x\to x}_{1\to 1,1\to -1} & -A^{x\to x}_{1\to 1,1\to -1} & \cdots \\ A^{x\to x}_{1\to 0,-1\to 0} & A^{x\to x}_{1\to 1,-1\to 0} & A^{x\to x}_{1\to 1,-1\to 0} & A^{x\to x}_{1\to 0,-1\to 1} & A^{x\to x}_{1\to 0,-1\to -1} & A^{x\to x}_{1\to 1,-1\to 1} & A^{x\to x}_{1\to 1,-1\to 1} & A^{x\to x}_{1\to 1,-1\to -1} & A^{x\to x}_{1\to 1,-1\to -1} & \cdots \\ -A^{x\to x}_{1\to 0,-1\to 0} & -A^{x\to x}_{1\to 1,-1\to 0} & -A^{x\to x}_{1\to 1,-1\to 0} & -A^{x\to x}_{1\to 0,-1\to 1} & -A^{x\to x}_{1\to 0,-1\to -1} & -A^{x\to x}_{1\to 1,-1\to 1} & -A^{x\to x}_{1\to 1,-1\to 1} & -A^{x\to x}_{1\to 1,-1\to -1} & -A^{x\to x}_{1\to 1,-1\to -1} & \cdots \\ \vdots & \vdots & \vdots & \vdots & \vdots & \vdots & \vdots & \vdots & \vdots & \ddots \end{array}\right] \begin{bmatrix} H_{y,0,0} \\ H_{y,1,0} \\ H_{y,1,0} \\ H_{y,0,1} \\ H_{y,0,-1} \\ H_{y,1,1} \\ H_{y,1,1} \\ H_{y,1,-1} \\ H_{y,1,-1} \\ \vdots \\ \hline H_{x,0,0} \\ H_{x,1,0} \\ H_{x,1,0} \\ H_{x,0,1} \\ H_{x,0,-1} \\ H_{x,1,1} \\ H_{x,1,1} \\ H_{x,1,-1} \\ H_{x,1,-1} \\ \vdots \end{bmatrix} \tag{D.2.11}$$

$$\frac{\partial}{\partial z'}\begin{bmatrix} H_{y,0,0} \\ H_{y,1,0} \\ H_{y,1,0} \\ H_{y,0,1} \\ H_{y,0,-1} \\ H_{y,1,1} \\ H_{y,1,1} \\ H_{y,1,-1} \\ H_{y,1,-1} \\ \vdots \\ \hline H_{x,0,0} \\ H_{x,1,0} \\ H_{x,1,0} \\ H_{x,0,1} \\ H_{x,0,-1} \\ H_{x,1,1} \\ H_{x,1,1} \\ H_{x,1,-1} \\ H_{x,1,-1} \\ \vdots \end{bmatrix} = \begin{bmatrix} B^{y\to y}_{0\to 0,0\to 0} & B^{y\to y}_{0\to 1,0\to 0} & B^{y\to y}_{0\to 1,0\to 0} & B^{y\to y}_{0\to 0,0\to 1} & B^{y\to y}_{0\to 0,0\to -1} & B^{y\to y}_{0\to 1,0\to 1} & B^{y\to y}_{0\to 1,0\to 1} & B^{y\to y}_{0\to 1,0\to -1} & B^{y\to y}_{0\to 1,0\to -1} & \cdots \\ B^{y\to y}_{1\to 0,0\to 0} & B^{y\to y}_{1\to 1,0\to 0} & B^{y\to y}_{1\to 1,0\to 0} & B^{y\to y}_{1\to 0,0\to 1} & B^{y\to y}_{1\to 0,0\to -1} & B^{y\to y}_{1\to 1,0\to 1} & B^{y\to y}_{1\to 1,0\to 1} & B^{y\to y}_{1\to 1,0\to -1} & B^{y\to y}_{1\to 1,0\to -1} & \cdots \\ -B^{y\to y}_{1\to 0,0\to 0} & -B^{y\to y}_{1\to 1,0\to 0} & -B^{y\to y}_{1\to 1,0\to 0} & -B^{y\to y}_{1\to 0,0\to 1} & -B^{y\to y}_{1\to 0,0\to -1} & -B^{y\to y}_{1\to 1,0\to 1} & -B^{y\to y}_{1\to 1,0\to 1} & -B^{y\to y}_{1\to 1,0\to -1} & -B^{y\to y}_{1\to 1,0\to -1} & \cdots \\ B^{y\to y}_{0\to 0,1\to 0} & B^{y\to y}_{0\to 1,1\to 0} & B^{y\to y}_{0\to 1,1\to 0} & B^{y\to y}_{0\to 0,1\to 1} & B^{y\to y}_{0\to 0,1\to -1} & B^{y\to y}_{0\to 1,1\to 1} & B^{y\to y}_{0\to 1,1\to 1} & B^{y\to y}_{0\to 1,1\to -1} & B^{y\to y}_{0\to 1,1\to -1} & \cdots \\ B^{y\to y}_{0\to 0,-1\to 0} & B^{y\to y}_{0\to 1,-1\to 0} & B^{y\to y}_{0\to 1,-1\to 0} & B^{y\to y}_{0\to 0,-1\to 1} & B^{y\to y}_{0\to 0,-1\to -1} & B^{y\to y}_{0\to 1,-1\to 1} & B^{y\to y}_{0\to 1,-1\to 1} & B^{y\to y}_{0\to 1,-1\to -1} & B^{y\to y}_{0\to 1,-1\to -1} & \cdots \\ B^{y\to y}_{1\to 0,1\to 0} & B^{y\to y}_{1\to 1,1\to 0} & B^{y\to y}_{1\to 1,1\to 0} & B^{y\to y}_{1\to 0,1\to 1} & B^{y\to y}_{1\to 0,1\to -1} & B^{y\to y}_{1\to 1,1\to 1} & B^{y\to y}_{1\to 1,1\to 1} & B^{y\to y}_{1\to 1,1\to -1} & B^{y\to y}_{1\to 1,1\to -1} & \cdots \\ -B^{y\to y}_{1\to 0,1\to 0} & -B^{y\to y}_{1\to 1,1\to 0} & -B^{y\to y}_{1\to 1,1\to 0} & -B^{y\to y}_{1\to 0,1\to 1} & -B^{y\to y}_{1\to 0,1\to -1} & -B^{y\to y}_{1\to 1,1\to 1} & -B^{y\to y}_{1\to 1,1\to 1} & -B^{y\to y}_{1\to 1,1\to -1} & -B^{y\to y}_{1\to 1,1\to -1} & \cdots \\ B^{y\to y}_{1\to 0,-1\to 0} & B^{y\to y}_{1\to 1,-1\to 0} & B^{y\to y}_{1\to 1,-1\to 0} & B^{y\to y}_{1\to 0,-1\to 1} & B^{y\to y}_{1\to 0,-1\to -1} & B^{y\to y}_{1\to 1,-1\to 1} & B^{y\to y}_{1\to 1,-1\to 1} & B^{y\to y}_{1\to 1,-1\to -1} & B^{y\to y}_{1\to 1,-1\to -1} & \cdots \\ -B^{y\to y}_{1\to 0,-1\to 0} & -B^{y\to y}_{1\to 1,-1\to 0} & -B^{y\to y}_{1\to 1,-1\to 0} & -B^{y\to y}_{1\to 0,-1\to 1} & -B^{y\to y}_{1\to 0,-1\to -1} & -B^{y\to y}_{1\to 1,-1\to 1} & -B^{y\to y}_{1\to 1,-1\to 1} & -B^{y\to y}_{1\to 1,-1\to -1} & -B^{y\to y}_{1\to 1,-1\to -1} & \cdots \\ \vdots & \vdots & \vdots & \vdots & \vdots & \vdots & \vdots & \vdots & \vdots & \ddots \\ \hline B^{x\to y}_{0\to 0,0\to 0} & B^{x\to y}_{0\to 1,0\to 0} & B^{x\to y}_{0\to 1,0\to 0} & B^{x\to y}_{0\to 0,0\to 1} & B^{x\to y}_{0\to 0,0\to -1} & B^{x\to y}_{0\to 1,0\to 1} & B^{x\to y}_{0\to 1,0\to 1} & B^{x\to y}_{0\to 1,0\to -1} & B^{x\to y}_{0\to 1,0\to -1} & \cdots \\ B^{x\to y}_{1\to 0,0\to 0} & B^{x\to y}_{1\to 1,0\to 0} & B^{x\to y}_{1\to 1,0\to 0} & B^{x\to y}_{1\to 0,0\to 1} & B^{x\to y}_{1\to 0,0\to -1} & B^{x\to y}_{1\to 1,0\to 1} & B^{x\to y}_{1\to 1,0\to 1} & B^{x\to y}_{1\to 1,0\to -1} & B^{x\to y}_{1\to 1,0\to -1} & \cdots \\ B^{x\to y}_{1\to 0,0\to 0} & B^{x\to y}_{1\to 1,0\to 0} & B^{x\to y}_{1\to 1,0\to 0} & B^{x\to y}_{1\to 0,0\to 1} & B^{x\to y}_{1\to 0,0\to -1} & B^{x\to y}_{1\to 1,0\to 1} & B^{x\to y}_{1\to 1,0\to 1} & B^{x\to y}_{1\to 1,0\to -1} & B^{x\to y}_{1\to 1,0\to -1} & \cdots \\ B^{x\to y}_{0\to 0,1\to 0} & B^{x\to y}_{0\to 1,1\to 0} & B^{x\to y}_{0\to 1,1\to 0} & B^{x\to y}_{0\to 0,1\to 1} & B^{x\to y}_{0\to 0,1\to -1} & B^{x\to y}_{0\to 1,1\to 1} & B^{x\to y}_{0\to 1,1\to 1} & B^{x\to y}_{0\to 1,1\to -1} & B^{x\to y}_{0\to 1,1\to -1} & \cdots \\ B^{x\to y}_{0\to 0,-1\to 0} & B^{x\to y}_{0\to 1,-1\to 0} & B^{x\to y}_{0\to 1,-1\to 0} & B^{x\to y}_{0\to 0,-1\to 1} & B^{x\to y}_{0\to 0,-1\to -1} & B^{x\to y}_{0\to 1,-1\to 1} & B^{x\to y}_{0\to 1,-1\to 1} & B^{x\to y}_{0\to 1,-1\to -1} & B^{x\to y}_{0\to 1,-1\to -1} & \cdots \\ B^{x\to y}_{1\to 0,1\to 0} & B^{x\to y}_{1\to 1,1\to 0} & B^{x\to y}_{1\to 1,1\to 0} & B^{x\to y}_{1\to 0,1\to 1} & B^{x\to y}_{1\to 0,1\to -1} & B^{x\to y}_{1\to 1,1\to 1} & B^{x\to y}_{1\to 1,1\to 1} & B^{x\to y}_{1\to 1,1\to -1} & B^{x\to y}_{1\to 1,1\to -1} & \cdots \\ B^{x\to y}_{1\to 0,1\to 0} & B^{x\to y}_{1\to 1,1\to 0} & B^{x\to y}_{1\to 1,1\to 0} & B^{x\to y}_{1\to 0,1\to 1} & B^{x\to y}_{1\to 0,1\to -1} & B^{x\to y}_{1\to 1,1\to 1} & B^{x\to y}_{1\to 1,1\to 1} & B^{x\to y}_{1\to 1,1\to -1} & B^{x\to y}_{1\to 1,1\to -1} & \cdots \\ B^{x\to y}_{1\to 0,-1\to 0} & B^{x\to y}_{1\to 1,-1\to 0} & B^{x\to y}_{1\to 1,-1\to 0} & B^{x\to y}_{1\to 0,-1\to 1} & B^{x\to y}_{1\to 0,-1\to -1} & B^{x\to y}_{1\to 1,-1\to 1} & B^{x\to y}_{1\to 1,-1\to 1} & B^{x\to y}_{1\to 1,-1\to -1} & B^{x\to y}_{1\to 1,-1\to -1} & \cdots \\ B^{x\to y}_{1\to 0,-1\to 0} & B^{x\to y}_{1\to 1,-1\to 0} & B^{x\to y}_{1\to 1,-1\to 0} & B^{x\to y}_{1\to 0,-1\to 1} & B^{x\to y}_{1\to 0,-1\to -1} & B^{x\to y}_{1\to 1,-1\to 1} & B^{x\to y}_{1\to 1,-1\to 1} & B^{x\to y}_{1\to 1,-1\to -1} & B^{x\to y}_{1\to 1,-1\to -1} & \cdots \\ \vdots & \vdots & \vdots & \vdots & \vdots & \vdots & \vdots & \vdots & \vdots & \ddots \end{bmatrix}$$

$$\cdots \begin{bmatrix} B^{y\to x}_{0\to 0,0\to 0} & B^{y\to x}_{0\to 1,0\to 0} & -B^{y\to x}_{0\to -1,0\to 0} & B^{y\to x}_{0\to 0,0\to 1} & B^{y\to x}_{0\to 0,0\to -1} & B^{y\to x}_{0\to 1,0\to 1} & -B^{y\to x}_{0\to -1,0\to 1} & B^{y\to x}_{0\to 1,0\to -1} & -B^{y\to x}_{0\to 1,0\to -1} & \cdots \\ B^{y\to x}_{1\to 0,0\to 0} & B^{y\to x}_{1\to 1,0\to 0} & -B^{y\to x}_{1\to -1,0\to 0} & B^{y\to x}_{1\to 0,0\to 1} & B^{y\to x}_{1\to 0,0\to -1} & B^{y\to x}_{1\to 1,0\to 1} & -B^{y\to x}_{1\to -1,0\to 1} & B^{y\to x}_{1\to 1,0\to -1} & -B^{y\to x}_{1\to 1,0\to -1} & \cdots \\ -B^{y\to x}_{1\to 0,0\to 0} & -B^{y\to x}_{1\to 1,0\to 0} & B^{y\to x}_{1\to -1,0\to 0} & -B^{y\to x}_{1\to 0,0\to 1} & -B^{y\to x}_{-1\to 0,0\to -1} & -B^{y\to x}_{1\to 1,0\to 1} & B^{y\to x}_{1\to -1,0\to 1} & -B^{y\to x}_{1\to 1,0\to -1} & B^{y\to x}_{1\to -1,0\to -1} & \cdots \\ B^{y\to x}_{0\to 0,1\to 0} & B^{y\to x}_{0\to 1,1\to 0} & -B^{y\to x}_{0\to -1,1\to 0} & B^{y\to x}_{0\to 0,1\to 1} & B^{y\to x}_{0\to 0,1\to -1} & B^{y\to x}_{0\to 1,1\to 1} & -B^{y\to x}_{0\to -1,1\to 1} & B^{y\to x}_{0\to 1,1\to -1} & -B^{y\to x}_{0\to 1,1\to -1} & \cdots \\ B^{y\to x}_{0\to 0,-1\to 0} & B^{y\to x}_{0\to 1,-1\to 0} & -B^{y\to x}_{0\to -1,-1\to 0} & B^{y\to x}_{0\to 0,-1\to 1} & B^{y\to x}_{0\to 0,-1\to -1} & B^{y\to x}_{0\to 1,-1\to 1} & -B^{y\to x}_{0\to -1,-1\to 1} & B^{y\to x}_{0\to 1,-1\to -1} & -B^{y\to x}_{0\to 1,-1\to -1} & \cdots \\ B^{y\to x}_{1\to 0,1\to 0} & B^{y\to x}_{1\to 1,1\to 0} & -B^{y\to x}_{1\to -1,1\to 0} & B^{y\to x}_{1\to 0,1\to 1} & B^{y\to x}_{1\to 0,1\to -1} & B^{y\to x}_{1\to 1,1\to 1} & -B^{y\to x}_{1\to -1,1\to 1} & B^{y\to x}_{1\to 1,1\to -1} & -B^{y\to x}_{1\to 1,1\to -1} & \cdots \\ -B^{y\to x}_{1\to 0,1\to 0} & -B^{y\to x}_{1\to 1,1\to 0} & B^{y\to x}_{1\to -1,1\to 0} & -B^{y\to x}_{1\to 0,1\to 1} & -B^{y\to x}_{1\to 0,1\to -1} & -B^{y\to x}_{1\to 1,1\to 1} & B^{y\to x}_{1\to -1,1\to 1} & -B^{y\to x}_{1\to 1,1\to -1} & B^{y\to x}_{1\to -1,1\to -1} & \cdots \\ B^{y\to x}_{1\to 0,-1\to 0} & B^{y\to x}_{1\to 1,-1\to 0} & -B^{y\to x}_{1\to -1,-1\to 0} & B^{y\to x}_{1\to 0,-1\to 1} & B^{y\to x}_{1\to 0,-1\to -1} & B^{y\to x}_{1\to 1,-1\to 1} & -B^{y\to x}_{1\to -1,-1\to 1} & B^{y\to x}_{1\to 1,-1\to -1} & -B^{y\to x}_{1\to 1,-1\to -1} & \cdots \\ -B^{y\to x}_{1\to 0,-1\to 0} & -B^{y\to x}_{1\to 1,-1\to 0} & B^{y\to x}_{1\to -1,-1\to 0} & -B^{y\to x}_{1\to 0,-1\to 1} & -B^{y\to x}_{1\to 0,-1\to -1} & -B^{y\to x}_{1\to 1,-1\to 1} & B^{y\to x}_{1\to -1,-1\to 1} & -B^{y\to x}_{1\to 1,-1\to -1} & B^{y\to x}_{1\to -1,-1\to -1} & \cdots \\ \vdots & \vdots & \vdots & \vdots & \vdots & \vdots & \vdots & \vdots & \vdots & \ddots \\ \hline B^{x\to x}_{0\to 0,0\to 0} & B^{x\to x}_{0\to 1,0\to 0} & -B^{x\to x}_{0\to 1,0\to 0} & B^{x\to x}_{0\to 0,0\to 1} & B^{x\to x}_{0\to 0,0\to -1} & B^{x\to x}_{0\to 1,0\to 1} & -B^{x\to x}_{0\to 1,0\to 1} & B^{x\to x}_{0\to 1,0\to -1} & -B^{x\to x}_{0\to 1,0\to -1} & \cdots \\ B^{x\to x}_{1\to 0,0\to 0} & B^{x\to x}_{1\to 1,0\to 0} & -B^{x\to x}_{1\to 1,0\to 0} & B^{x\to x}_{1\to 0,0\to 1} & B^{x\to x}_{1\to 0,0\to -1} & B^{x\to x}_{1\to 1,0\to 1} & -B^{x\to x}_{1\to 1,0\to 1} & B^{x\to x}_{1\to 1,0\to -1} & -B^{x\to x}_{1\to 1,0\to -1} & \cdots \\ B^{x\to x}_{1\to 0,0\to 0} & B^{x\to x}_{1\to 1,0\to 0} & -B^{x\to x}_{1\to 1,0\to 0} & B^{x\to x}_{1\to 0,0\to 1} & B^{x\to x}_{1\to 0,0\to -1} & B^{x\to x}_{1\to 1,0\to 1} & -B^{x\to x}_{1\to 1,0\to 1} & B^{x\to x}_{1\to 1,0\to -1} & -B^{x\to x}_{1\to 1,0\to -1} & \cdots \\ B^{x\to x}_{0\to 0,1\to 0} & B^{x\to x}_{0\to 1,1\to 0} & -B^{x\to x}_{0\to 1,1\to 0} & B^{x\to x}_{0\to 0,1\to 1} & B^{x\to x}_{0\to 0,1\to -1} & B^{x\to x}_{0\to 1,1\to 1} & -B^{x\to x}_{0\to 1,1\to 1} & B^{x\to x}_{0\to 1,1\to -1} & -B^{x\to x}_{0\to 1,1\to -1} & \cdots \\ B^{x\to x}_{0\to 0,-1\to 0} & B^{x\to x}_{0\to 1,-1\to 0} & -B^{x\to x}_{0\to 1,-1\to 0} & B^{x\to x}_{0\to 0,-1\to 1} & B^{x\to x}_{0\to 0,-1\to -1} & B^{x\to x}_{0\to 1,-1\to 1} & -B^{x\to x}_{0\to 1,-1\to 1} & B^{x\to x}_{0\to 1,-1\to -1} & -B^{x\to x}_{0\to 1,-1\to -1} & \cdots \\ B^{x\to x}_{1\to 0,1\to 0} & B^{x\to x}_{1\to 1,1\to 0} & -B^{x\to x}_{1\to 1,1\to 0} & B^{x\to x}_{1\to 0,1\to 1} & B^{x\to x}_{1\to 0,1\to -1} & B^{x\to x}_{1\to 1,1\to 1} & -B^{x\to x}_{1\to 1,1\to 1} & B^{x\to x}_{1\to 1,1\to -1} & -B^{x\to x}_{1\to 1,1\to -1} & \cdots \\ B^{x\to x}_{1\to 0,1\to 0} & B^{x\to x}_{1\to 1,1\to 0} & -B^{x\to x}_{1\to 1,1\to 0} & B^{x\to x}_{1\to 0,1\to 1} & B^{x\to x}_{1\to 0,1\to -1} & B^{x\to x}_{1\to 1,1\to 1} & -B^{x\to x}_{1\to 1,1\to 1} & B^{x\to x}_{1\to 1,1\to -1} & -B^{x\to x}_{1\to 1,1\to -1} & \cdots \\ B^{x\to x}_{1\to 0,-1\to 0} & B^{x\to x}_{1\to 1,-1\to 0} & -B^{x\to x}_{1\to 1,-1\to 0} & B^{x\to x}_{1\to 0,-1\to 1} & B^{x\to x}_{1\to 0,-1\to -1} & B^{x\to x}_{1\to 1,-1\to 1} & -B^{x\to x}_{1\to 1,-1\to 1} & B^{x\to x}_{1\to 1,-1\to -1} & -B^{x\to x}_{1\to 1,-1\to -1} & \cdots \\ B^{x\to x}_{1\to 0,-1\to 0} & B^{x\to x}_{1\to 1,-1\to 0} & -B^{x\to x}_{1\to 1,-1\to 0} & B^{x\to x}_{1\to 0,-1\to 1} & B^{x\to x}_{1\to 0,-1\to -1} & B^{x\to x}_{1\to 1,-1\to 1} & -B^{x\to x}_{1\to 1,-1\to 1} & B^{x\to x}_{1\to 1,-1\to -1} & -B^{x\to x}_{1\to 1,-1\to -1} & \cdots \\ \vdots & \vdots & \vdots & \vdots & \vdots & \vdots & \vdots & \vdots & \vdots & \ddots \end{bmatrix} \begin{bmatrix} E_{y,0,0} \\ E_{y,1,0} \\ E_{y,1,0} \\ E_{y,0,1} \\ E_{y,0,-1} \\ E_{y,1,1} \\ E_{y,1,1} \\ E_{y,1,-1} \\ E_{y,1,-1} \\ \vdots \\ \hline E_{x,0,0} \\ E_{x,1,0} \\ E_{x,1,0} \\ E_{x,0,1} \\ E_{x,0,-1} \\ E_{x,1,1} \\ E_{x,1,1} \\ E_{x,1,-1} \\ E_{x,1,-1} \\ \vdots \end{bmatrix} \tag{D.2.12}$$

By taking the derivative of Equation (D.2.11) with respect to z' and inserting Equation (D.2.12), the resulting matrix eigenvalue equation can be written as follows:

$$\frac{\partial^2}{\partial z'^2}\begin{bmatrix} E_{y,0,0} \\ E_{y,1,0} \\ E_{y,1,0} \\ E_{y,0,1} \\ E_{y,0,-1} \\ E_{y,1,1} \\ E_{y,1,1} \\ E_{y,1,-1} \\ E_{y,1,-1} \\ \vdots \\ \hline E_{x,0,0} \\ E_{x,1,0} \\ E_{x,1,0} \\ E_{x,0,1} \\ E_{x,0,-1} \\ E_{x,1,1} \\ E_{x,1,1} \\ E_{x,1,-1} \\ E_{x,1,-1} \\ \vdots \end{bmatrix} = \left[\begin{array}{ccccccccc|c} C^{y\to y}_{0\to 0,0\to 0} & C^{y\to y}_{0\to 1,0\to 0} & C^{y\to y}_{0\to 1,0\to 0} & C^{y\to y}_{0\to 0,0\to 1} & C^{y\to y}_{0\to 0,0\to -1} & C^{y\to y}_{0\to 1,0\to 1} & C^{y\to y}_{0\to 1,0\to 1} & C^{y\to y}_{0\to 1,0\to -1} & C^{y\to y}_{0\to 1,0\to -1} & \cdots \\ C^{y\to y}_{1\to 0,0\to 0} & C^{y\to y}_{1\to 1,0\to 0} & C^{y\to y}_{1\to 1,0\to 0} & C^{y\to y}_{1\to 0,0\to 1} & C^{y\to y}_{1\to 0,0\to -1} & C^{y\to y}_{1\to 1,0\to 1} & C^{y\to y}_{1\to 1,0\to 1} & C^{y\to y}_{1\to 1,0\to -1} & C^{y\to y}_{1\to 1,0\to -1} & \cdots \\ C^{y\to y}_{1\to 0,0\to 0} & C^{y\to y}_{1\to 1,0\to 0} & C^{y\to y}_{1\to 1,0\to 0} & C^{y\to y}_{1\to 0,0\to 1} & C^{y\to y}_{1\to 0,0\to -1} & C^{y\to y}_{1\to 1,0\to 1} & C^{y\to y}_{1\to 1,0\to 1} & C^{y\to y}_{1\to 1,0\to -1} & C^{y\to y}_{1\to 1,0\to -1} & \cdots \\ C^{y\to y}_{0\to 0,1\to 0} & C^{y\to y}_{0\to 1,1\to 0} & C^{y\to y}_{0\to 1,1\to 0} & C^{y\to y}_{0\to 0,1\to 1} & C^{y\to y}_{0\to 0,1\to -1} & C^{y\to y}_{0\to 1,1\to 1} & C^{y\to y}_{0\to 1,1\to 1} & C^{y\to y}_{0\to 1,1\to -1} & C^{y\to y}_{0\to 1,1\to -1} & \cdots \\ C^{y\to y}_{0\to 0,-1\to 0} & C^{y\to y}_{0\to 1,-1\to 0} & C^{y\to y}_{0\to 1,-1\to 0} & C^{y\to y}_{0\to 0,-1\to 1} & C^{y\to y}_{0\to 0,-1\to -1} & C^{y\to y}_{0\to 1,-1\to 1} & C^{y\to y}_{0\to 1,-1\to 1} & C^{y\to y}_{0\to 1,-1\to -1} & C^{y\to y}_{0\to 1,-1\to -1} & \cdots \\ C^{y\to y}_{1\to 0,1\to 0} & C^{y\to y}_{1\to 1,1\to 0} & C^{y\to y}_{1\to 1,1\to 0} & C^{y\to y}_{1\to 0,1\to 1} & C^{y\to y}_{1\to 0,1\to -1} & C^{y\to y}_{1\to 1,1\to 1} & C^{y\to y}_{1\to 1,1\to 1} & C^{y\to y}_{1\to 1,1\to -1} & C^{y\to y}_{1\to 1,1\to -1} & \cdots \\ C^{y\to y}_{1\to 0,1\to 0} & C^{y\to y}_{1\to 1,1\to 0} & C^{y\to y}_{1\to 1,1\to 0} & C^{y\to y}_{1\to 0,1\to 1} & C^{y\to y}_{1\to 0,1\to -1} & C^{y\to y}_{1\to 1,1\to 1} & C^{y\to y}_{1\to 1,1\to 1} & C^{y\to y}_{1\to 1,1\to -1} & C^{y\to y}_{1\to 1,1\to -1} & \cdots \\ C^{y\to y}_{1\to 0,-1\to 0} & C^{y\to y}_{1\to 1,-1\to 0} & C^{y\to y}_{1\to 1,-1\to 0} & C^{y\to y}_{1\to 0,-1\to 1} & C^{y\to y}_{1\to 0,-1\to -1} & C^{y\to y}_{1\to 1,-1\to 1} & C^{y\to y}_{1\to 1,-1\to 1} & C^{y\to y}_{1\to 1,-1\to -1} & C^{y\to y}_{1\to 1,-1\to -1} & \cdots \\ C^{y\to y}_{1\to 0,-1\to 0} & C^{y\to y}_{1\to 1,-1\to 0} & C^{y\to y}_{1\to 1,-1\to 0} & C^{y\to y}_{1\to 0,-1\to 1} & C^{y\to y}_{1\to 0,-1\to -1} & C^{y\to y}_{1\to 1,-1\to 1} & C^{y\to y}_{1\to 1,-1\to 1} & C^{y\to y}_{1\to 1,-1\to -1} & C^{y\to y}_{1\to 1,-1\to -1} & \cdots \\ \vdots & \vdots & \vdots & \vdots & \vdots & \vdots & \vdots & \vdots & \vdots & \ddots \\ \hline C^{x\to y}_{0\to 0,0\to 0} & C^{x\to y}_{0\to 1,0\to 0} & C^{x\to y}_{0\to 1,0\to 0} & C^{x\to y}_{0\to 0,0\to 1} & C^{x\to y}_{0\to 0,0\to -1} & C^{x\to y}_{0\to 1,0\to 1} & C^{x\to y}_{0\to 1,0\to 1} & C^{x\to y}_{0\to 1,0\to -1} & C^{x\to y}_{0\to 1,0\to -1} & \cdots \\ C^{x\to y}_{1\to 0,0\to 0} & C^{x\to y}_{1\to 1,0\to 0} & C^{x\to y}_{1\to 1,0\to 0} & C^{x\to y}_{1\to 0,0\to 1} & C^{x\to y}_{1\to 0,0\to -1} & C^{x\to y}_{1\to 1,0\to 1} & C^{x\to y}_{1\to 1,0\to 1} & C^{x\to y}_{1\to 1,0\to -1} & C^{x\to y}_{1\to 1,0\to -1} & \cdots \\ -C^{x\to y}_{1\to 0,0\to 0} & -C^{x\to y}_{1\to 1,0\to 0} & -C^{x\to y}_{1\to 1,0\to 0} & -C^{x\to y}_{1\to 0,0\to 1} & -C^{x\to y}_{1\to 0,0\to -1} & -C^{x\to y}_{1\to 1,0\to 1} & -C^{x\to y}_{1\to 1,0\to 1} & -C^{x\to y}_{1\to 1,0\to -1} & -C^{x\to y}_{1\to 1,0\to -1} & \cdots \\ C^{x\to y}_{0\to 0,1\to 0} & C^{x\to y}_{0\to 1,1\to 0} & C^{x\to y}_{0\to 1,1\to 0} & C^{x\to y}_{0\to 0,1\to 1} & C^{x\to y}_{0\to 0,1\to -1} & C^{x\to y}_{0\to 1,1\to 1} & C^{x\to y}_{0\to 1,1\to 1} & C^{x\to y}_{0\to 1,1\to -1} & C^{x\to y}_{0\to 1,1\to -1} & \cdots \\ C^{x\to y}_{0\to 0,-1\to 0} & C^{x\to y}_{0\to 1,-1\to 0} & C^{x\to y}_{0\to 1,-1\to 0} & C^{x\to y}_{0\to 0,-1\to 1} & C^{x\to y}_{0\to 0,-1\to -1} & C^{x\to y}_{0\to 1,-1\to 1} & C^{x\to y}_{0\to 1,-1\to 1} & C^{x\to y}_{0\to 1,-1\to -1} & C^{x\to y}_{0\to 1,-1\to -1} & \cdots \\ C^{x\to y}_{1\to 0,1\to 0} & C^{x\to y}_{1\to 1,1\to 0} & C^{x\to y}_{1\to 1,1\to 0} & C^{x\to y}_{1\to 0,1\to 1} & C^{x\to y}_{1\to 0,1\to -1} & C^{x\to y}_{1\to 1,1\to 1} & C^{x\to y}_{1\to 1,1\to 1} & C^{x\to y}_{1\to 1,1\to -1} & C^{x\to y}_{1\to 1,1\to -1} & \cdots \\ -C^{x\to y}_{1\to 0,1\to 0} & -C^{x\to y}_{1\to 1,1\to 0} & -C^{x\to y}_{1\to 1,1\to 0} & -C^{x\to y}_{1\to 0,1\to 1} & -C^{x\to y}_{1\to 0,1\to -1} & -C^{x\to y}_{1\to 1,1\to 1} & -C^{x\to y}_{1\to 1,1\to 1} & -C^{x\to y}_{1\to 1,1\to -1} & -C^{x\to y}_{1\to 1,1\to -1} & \cdots \\ C^{x\to y}_{1\to 0,-1\to 0} & C^{x\to y}_{1\to 1,-1\to 0} & C^{x\to y}_{1\to 1,-1\to 0} & C^{x\to y}_{1\to 0,-1\to 1} & C^{x\to y}_{1\to 0,-1\to -1} & C^{x\to y}_{1\to 1,-1\to 1} & C^{x\to y}_{1\to 1,-1\to 1} & C^{x\to y}_{1\to 1,-1\to -1} & C^{x\to y}_{1\to 1,-1\to -1} & \cdots \\ -C^{x\to y}_{1\to 0,-1\to 0} & -C^{x\to y}_{1\to 1,-1\to 0} & -C^{x\to y}_{1\to 1,-1\to 0} & -C^{x\to y}_{1\to 0,-1\to 1} & -C^{x\to y}_{1\to 0,-1\to -1} & -C^{x\to y}_{1\to 1,-1\to 1} & -C^{x\to y}_{1\to 1,-1\to 1} & -C^{x\to y}_{1\to 1,-1\to -1} & -C^{x\to y}_{1\to 1,-1\to -1} & \cdots \\ \vdots & \vdots & \vdots & \vdots & \vdots & \vdots & \vdots & \vdots & \vdots & \ddots \end{array}\right]$$

$$\cdots \left[\begin{array}{ccccccccc|c} C^{y\to x}_{0\to 0,0\to 0} & C^{y\to x}_{0\to 1,0\to 0} & -C^{y\to x}_{0\to -1,0\to 0} & C^{y\to x}_{0\to 0,0\to 1} & C^{y\to x}_{0\to 0,0\to -1} & C^{y\to x}_{0\to 1,0\to 1} & -C^{y\to x}_{0\to -1,0\to 1} & C^{y\to x}_{0\to 1,0\to -1} & -C^{y\to x}_{0\to 1,0\to -1} & \cdots \\ C^{y\to x}_{1\to 0,0\to 0} & C^{y\to x}_{1\to 1,0\to 0} & -C^{y\to x}_{1\to -1,0\to 0} & C^{y\to x}_{1\to 0,0\to 1} & C^{y\to x}_{1\to 0,0\to -1} & C^{y\to x}_{1\to 1,0\to 1} & -C^{y\to x}_{1\to -1,0\to 1} & C^{y\to x}_{1\to 1,0\to -1} & -C^{y\to x}_{1\to 1,0\to -1} & \cdots \\ C^{y\to x}_{1\to 0,0\to 0} & C^{y\to x}_{1\to 1,0\to 0} & -C^{y\to x}_{1\to -1,0\to 0} & C^{y\to x}_{1\to 0,0\to 1} & C^{y\to x}_{-1\to 0,0\to -1} & C^{y\to x}_{1\to 1,0\to 1} & -C^{y\to x}_{1\to -1,0\to 1} & C^{y\to x}_{1\to 1,0\to -1} & -C^{y\to x}_{1\to 1,0\to -1} & \cdots \\ C^{y\to x}_{0\to 0,1\to 0} & C^{y\to x}_{0\to 1,1\to 0} & -C^{y\to x}_{0\to -1,1\to 0} & C^{y\to x}_{0\to 0,1\to 1} & C^{y\to x}_{0\to 0,1\to -1} & C^{y\to x}_{0\to 1,1\to 1} & -C^{y\to x}_{0\to -1,1\to 1} & C^{y\to x}_{0\to 1,1\to -1} & -C^{y\to x}_{0\to 1,1\to -1} & \cdots \\ C^{y\to x}_{0\to 0,-1\to 0} & C^{y\to x}_{0\to 1,-1\to 0} & -C^{y\to x}_{0\to -1,-1\to 0} & C^{y\to x}_{0\to 0,-1\to 1} & C^{y\to x}_{0\to 0,-1\to -1} & C^{y\to x}_{0\to 1,-1\to 1} & -C^{y\to x}_{0\to -1,-1\to 1} & C^{y\to x}_{0\to 1,-1\to -1} & -C^{y\to x}_{0\to 1,-1\to -1} & \cdots \\ C^{y\to x}_{1\to 0,1\to 0} & C^{y\to x}_{1\to 1,1\to 0} & -C^{y\to x}_{1\to -1,1\to 0} & C^{y\to x}_{1\to 0,1\to 1} & C^{y\to x}_{1\to 0,1\to -1} & C^{y\to x}_{1\to 1,1\to 1} & -C^{y\to x}_{1\to -1,1\to 1} & C^{y\to x}_{1\to 1,1\to -1} & -C^{y\to x}_{1\to 1,1\to -1} & \cdots \\ C^{y\to x}_{1\to 0,1\to 0} & C^{y\to x}_{1\to 1,1\to 0} & -C^{y\to x}_{1\to -1,1\to 0} & C^{y\to x}_{1\to 0,1\to 1} & C^{y\to x}_{1\to 0,1\to -1} & C^{y\to x}_{1\to 1,1\to 1} & -C^{y\to x}_{1\to -1,1\to 1} & C^{y\to x}_{1\to 1,1\to -1} & -C^{y\to x}_{1\to 1,1\to -1} & \cdots \\ C^{y\to x}_{1\to 0,-1\to 0} & C^{y\to x}_{1\to 1,-1\to 0} & -C^{y\to x}_{1\to -1,-1\to 0} & C^{y\to x}_{1\to 0,-1\to 1} & C^{y\to x}_{1\to 0,-1\to -1} & C^{y\to x}_{1\to 1,-1\to 1} & -C^{y\to x}_{1\to -1,-1\to 1} & C^{y\to x}_{1\to 1,-1\to -1} & -C^{y\to x}_{1\to 1,-1\to -1} & \cdots \\ C^{y\to x}_{1\to 0,-1\to 0} & C^{y\to x}_{1\to 1,-1\to 0} & -C^{y\to x}_{1\to -1,-1\to 0} & C^{y\to x}_{1\to 0,-1\to 1} & C^{y\to x}_{1\to 0,-1\to -1} & C^{y\to x}_{1\to 1,-1\to 1} & -C^{y\to x}_{1\to -1,-1\to 1} & C^{y\to x}_{1\to 1,-1\to -1} & -C^{y\to x}_{1\to 1,-1\to -1} & \cdots \\ \vdots & \vdots & \vdots & \vdots & \vdots & \vdots & \vdots & \vdots & \vdots & \ddots \\ \hline C^{x\to x}_{0\to 0,0\to 0} & C^{x\to x}_{0\to 1,0\to 0} & -C^{x\to x}_{0\to 1,0\to 0} & C^{x\to x}_{0\to 0,0\to 1} & C^{x\to x}_{0\to 0,0\to -1} & C^{x\to x}_{0\to 1,0\to 1} & -C^{x\to x}_{0\to 1,0\to 1} & C^{x\to x}_{0\to 1,0\to -1} & -C^{x\to x}_{0\to 1,0\to -1} & \cdots \\ C^{x\to x}_{1\to 0,0\to 0} & C^{x\to x}_{1\to 1,0\to 0} & -C^{x\to x}_{1\to 1,0\to 0} & C^{x\to x}_{1\to 0,0\to 1} & C^{x\to x}_{1\to 0,0\to -1} & C^{x\to x}_{1\to 1,0\to 1} & -C^{x\to x}_{1\to 1,0\to 1} & C^{x\to x}_{1\to 1,0\to -1} & -C^{x\to x}_{1\to 1,0\to -1} & \cdots \\ -C^{x\to x}_{1\to 0,0\to 0} & -C^{x\to x}_{1\to 1,0\to 0} & C^{x\to x}_{1\to 1,0\to 0} & -C^{x\to x}_{1\to 0,0\to 1} & -C^{x\to x}_{1\to 0,0\to -1} & -C^{x\to x}_{1\to 1,0\to 1} & C^{x\to x}_{1\to 1,0\to 1} & -C^{x\to x}_{1\to 1,0\to -1} & C^{x\to x}_{1\to 1,0\to -1} & \cdots \\ C^{x\to x}_{0\to 0,1\to 0} & C^{x\to x}_{0\to 1,1\to 0} & -C^{x\to x}_{0\to 1,1\to 0} & C^{x\to x}_{0\to 0,1\to 1} & C^{x\to x}_{0\to 0,1\to -1} & C^{x\to x}_{0\to 1,1\to 1} & -C^{x\to x}_{0\to 1,1\to 1} & C^{x\to x}_{0\to 1,1\to -1} & -C^{x\to x}_{0\to 1,1\to -1} & \cdots \\ C^{x\to x}_{0\to 0,-1\to 0} & C^{x\to x}_{0\to 1,-1\to 0} & -C^{x\to x}_{0\to 1,-1\to 0} & C^{x\to x}_{0\to 0,-1\to 1} & C^{x\to x}_{0\to 0,-1\to -1} & C^{x\to x}_{0\to 1,-1\to 1} & -C^{x\to x}_{0\to 1,-1\to 1} & C^{x\to x}_{0\to 1,-1\to -1} & -C^{x\to x}_{0\to 1,-1\to -1} & \cdots \\ C^{x\to x}_{1\to 0,1\to 0} & C^{x\to x}_{1\to 1,1\to 0} & -C^{x\to x}_{1\to 1,1\to 0} & C^{x\to x}_{1\to 0,1\to 1} & C^{x\to x}_{1\to 0,1\to -1} & C^{x\to x}_{1\to 1,1\to 1} & -C^{x\to x}_{1\to 1,1\to 1} & C^{x\to x}_{1\to 1,1\to -1} & -C^{x\to x}_{1\to 1,1\to -1} & \cdots \\ -C^{x\to x}_{1\to 0,1\to 0} & -C^{x\to x}_{1\to 1,1\to 0} & C^{x\to x}_{1\to 1,1\to 0} & -C^{x\to x}_{1\to 0,1\to 1} & -C^{x\to x}_{1\to 0,1\to -1} & -C^{x\to x}_{1\to 1,1\to 1} & C^{x\to x}_{1\to 1,1\to 1} & -C^{x\to x}_{1\to 1,1\to -1} & C^{x\to x}_{1\to 1,1\to -1} & \cdots \\ C^{x\to x}_{1\to 0,-1\to 0} & C^{x\to x}_{1\to 1,-1\to 0} & -C^{x\to x}_{1\to 1,-1\to 0} & C^{x\to x}_{1\to 0,-1\to 1} & C^{x\to x}_{1\to 0,-1\to -1} & C^{x\to x}_{1\to 1,-1\to 1} & -C^{x\to x}_{1\to 1,-1\to 1} & C^{x\to x}_{1\to 1,-1\to -1} & -C^{x\to x}_{1\to 1,-1\to -1} & \cdots \\ -C^{x\to x}_{1\to 0,-1\to 0} & -C^{x\to x}_{1\to 1,-1\to 0} & C^{x\to x}_{1\to 1,-1\to 0} & -C^{x\to x}_{1\to 0,-1\to 1} & -C^{x\to x}_{1\to 0,-1\to -1} & -C^{x\to x}_{1\to 1,-1\to 1} & C^{x\to x}_{1\to 1,-1\to 1} & -C^{x\to x}_{1\to 1,-1\to -1} & C^{x\to x}_{1\to 1,-1\to -1} & \cdots \\ \vdots & \vdots & \vdots & \vdots & \vdots & \vdots & \vdots & \vdots & \vdots & \ddots \end{array}\right] \begin{bmatrix} E_{y,0,0} \\ E_{y,1,0} \\ E_{y,1,0} \\ E_{y,0,1} \\ E_{y,0,-1} \\ E_{y,1,1} \\ E_{y,1,1} \\ E_{y,1,-1} \\ E_{y,1,-1} \\ \vdots \\ \hline E_{x,0,0} \\ E_{x,1,0} \\ E_{x,1,0} \\ E_{x,0,1} \\ E_{x,0,-1} \\ E_{x,1,1} \\ E_{x,1,1} \\ E_{x,1,-1} \\ E_{x,1,-1} \\ \vdots \end{bmatrix} \tag{D.2.13}$$

This system of equations can be reduced in size without any loss of generality as follows:

$$\frac{\partial^2}{\partial z'^2}\begin{bmatrix} E_{y,0,0} \\ E_{y,1,0} \\ E_{y,0,1} \\ E_{y,0,-1} \\ E_{y,1,1} \\ E_{y,1,-1} \\ \vdots \\ \hline E_{x,0,0} \\ E_{x,1,0} \\ E_{x,0,1} \\ E_{x,0,-1} \\ E_{x,1,1} \\ E_{x,1,-1} \\ \vdots \end{bmatrix} = \left[\begin{array}{cccccc|c} C^{y\to y}_{0\to 0,0\to 0} & 2C^{y\to y}_{0\to 1,0\to 0} & C^{y\to y}_{0\to 0,0\to 1} & C^{y\to y}_{0\to 0,0\to -1} & 2C^{y\to y}_{0\to 1,0\to 1} & 2C^{y\to y}_{0\to 1,0\to -1} & \cdots \\ C^{y\to y}_{1\to 0,0\to 0} & 2C^{y\to y}_{1\to 1,0\to 0} & C^{y\to y}_{1\to 0,0\to 1} & C^{y\to y}_{1\to 0,0\to -1} & 2C^{y\to y}_{1\to 1,0\to 1} & 2C^{y\to y}_{1\to 1,0\to -1} & \cdots \\ C^{y\to y}_{0\to 0,1\to 0} & 2C^{y\to y}_{0\to 1,1\to 0} & C^{y\to y}_{0\to 0,1\to 1} & C^{y\to y}_{0\to 0,1\to -1} & 2C^{y\to y}_{0\to 1,1\to 1} & 2C^{y\to y}_{0\to 1,1\to -1} & \cdots \\ C^{y\to y}_{0\to 0,-1\to 0} & 2C^{y\to y}_{0\to 1,-1\to 0} & C^{y\to y}_{0\to 0,-1\to 1} & C^{y\to y}_{0\to 0,-1\to -1} & 2C^{y\to y}_{0\to 1,-1\to 1} & 2C^{y\to y}_{0\to 1,-1\to -1} & \cdots \\ C^{y\to y}_{1\to 0,1\to 0} & 2C^{y\to y}_{1\to 1,1\to 0} & C^{y\to y}_{1\to 0,1\to 1} & C^{y\to y}_{1\to 0,1\to -1} & 2C^{y\to y}_{1\to 1,1\to 1} & 2C^{y\to y}_{1\to 1,1\to -1} & \cdots \\ C^{y\to y}_{1\to 0,-1\to 0} & 2C^{y\to y}_{1\to 1,-1\to 0} & C^{y\to y}_{1\to 0,-1\to 1} & C^{y\to y}_{1\to 0,-1\to -1} & 2C^{y\to y}_{1\to 1,-1\to 1} & 2C^{y\to y}_{1\to 1,-1\to -1} & \cdots \\ \vdots & \vdots & \vdots & \vdots & \vdots & \vdots & \ddots \\ \hline C^{x\to y}_{0\to 0,0\to 0} & 2C^{x\to y}_{0\to 1,0\to 0} & C^{x\to y}_{0\to 0,0\to 1} & C^{x\to y}_{0\to 0,0\to -1} & 2C^{x\to y}_{0\to 1,0\to 1} & 2C^{x\to y}_{0\to 1,0\to -1} & \cdots \\ 0 & 0 & 0 & 0 & 0 & 0 & \cdots \\ C^{x\to y}_{0\to 0,1\to 0} & 2C^{x\to y}_{0\to 1,1\to 0} & C^{x\to y}_{0\to 0,1\to 1} & C^{x\to y}_{0\to 0,1\to -1} & 2C^{x\to y}_{0\to 1,1\to 1} & 2C^{x\to y}_{0\to 1,1\to -1} & \cdots \\ C^{x\to y}_{0\to 0,-1\to 0} & 2C^{x\to y}_{0\to 1,-1\to 0} & C^{x\to y}_{0\to 0,-1\to 1} & C^{x\to y}_{0\to 0,-1\to -1} & 2C^{x\to y}_{0\to 1,-1\to 1} & 2C^{x\to y}_{0\to 1,-1\to -1} & \cdots \\ 0 & 0 & 0 & 0 & 0 & 0 & \cdots \\ 0 & 0 & 0 & 0 & 0 & 0 & \cdots \\ \vdots & \vdots & \vdots & \vdots & \vdots & \vdots & \ddots \end{array}\right.$$

$$\cdots \left[\begin{array}{cccccc|c} C^{y\to x}_{0\to 0,0\to 0} & 0 & C^{y\to x}_{0\to 0,0\to 1} & C^{y\to x}_{0\to 0,0\to -1} & 0 & 0 & \cdots \\ 2C^{y\to x}_{1\to 0,0\to 0} & 0 & 2C^{y\to x}_{1\to 0,0\to 1} & 2C^{y\to x}_{1\to 0,0\to -1} & 0 & 0 & \cdots \\ C^{y\to x}_{0\to 0,1\to 0} & 0 & C^{y\to x}_{0\to 0,1\to 1} & C^{y\to x}_{0\to 0,1\to -1} & 0 & 0 & \cdots \\ C^{y\to x}_{0\to 0,-1\to 0} & 0 & C^{y\to x}_{0\to 0,-1\to 1} & C^{y\to x}_{0\to 0,-1\to -1} & 0 & 0 & \cdots \\ 2C^{y\to x}_{1\to 0,1\to 0} & 0 & 2C^{y\to x}_{1\to 0,1\to 1} & 2C^{y\to x}_{1\to 0,1\to -1} & 0 & 0 & \cdots \\ 2C^{y\to x}_{1\to 0,-1\to 0} & 0 & 2C^{y\to x}_{1\to 0,-1\to 1} & 2C^{y\to x}_{1\to 0,-1\to -1} & 0 & 0 & \cdots \\ \vdots & \vdots & \vdots & \vdots & \vdots & \vdots & \ddots \\ \hline C^{x\to x}_{0\to 0,0\to 0} & 0 & C^{x\to x}_{0\to 0,0\to 1} & C^{x\to x}_{0\to 0,0\to -1} & 0 & 0 & \cdots \\ 0 & 0 & 0 & 0 & 0 & 0 & \cdots \\ C^{x\to x}_{0\to 0,1\to 0} & 0 & C^{x\to x}_{0\to 0,1\to 1} & C^{x\to x}_{0\to 0,1\to -1} & 0 & 0 & \cdots \\ C^{x\to x}_{0\to 0,-1\to 0} & 0 & C^{x\to x}_{0\to 0,-1\to 1} & C^{x\to x}_{0\to 0,-1\to -1} & 0 & 0 & \cdots \\ 0 & 0 & 0 & 0 & 0 & 0 & \cdots \\ 0 & 0 & 0 & 0 & 0 & 0 & \cdots \\ \vdots & \vdots & \vdots & \vdots & \vdots & \vdots & \ddots \end{array}\right] \begin{bmatrix} E_{y,0,0} \\ E_{y,1,0} \\ E_{y,0,1} \\ E_{y,0,-1} \\ E_{y,1,1} \\ E_{y,1,-1} \\ \vdots \\ \hline E_{x,0,0} \\ E_{x,1,0} \\ E_{x,0,1} \\ E_{x,0,-1} \\ E_{x,1,1} \\ E_{x,1,-1} \\ \vdots \end{bmatrix} \tag{D.2.14}$$

A further reduction of the matrix is then possible by eliminating the rows and columns containing all zero values, leading to a final reduced matrix eigenvalue equation.

$$\frac{\partial^2}{\partial z'^2}\begin{bmatrix} E_{y,0,0} \\ E_{y,1,0} \\ E_{y,0,1} \\ E_{y,0,-1} \\ E_{y,1,1} \\ E_{y,1,-1} \\ \vdots \\ \hline E_{x,0,0} \\ E_{x,0,1} \\ E_{x,0,-1} \\ \vdots \end{bmatrix} = \begin{bmatrix} C^{y\to y}_{0\to 0,0\to 0} & 2C^{y\to y}_{0\to 1,0\to 0} & C^{y\to y}_{0\to 0,0\to 1} & C^{y\to y}_{0\to 0,0\to -1} & 2C^{y\to y}_{0\to 1,0\to 1} & 2C^{y\to y}_{0\to 1,0\to -1} & \cdots \\ C^{y\to y}_{1\to 0,0\to 0} & 2C^{y\to y}_{1\to 1,0\to 0} & C^{y\to y}_{1\to 0,0\to 1} & C^{y\to y}_{1\to 0,0\to -1} & 2C^{y\to y}_{1\to 1,0\to 1} & 2C^{y\to y}_{1\to 1,0\to -1} & \cdots \\ C^{y\to y}_{0\to 0,1\to 0} & 2C^{y\to y}_{0\to 1,1\to 0} & C^{y\to y}_{0\to 0,1\to 1} & C^{y\to y}_{0\to 0,1\to -1} & 2C^{y\to y}_{0\to 1,1\to 1} & 2C^{y\to y}_{0\to 1,1\to -1} & \cdots \\ C^{y\to y}_{0\to 0,-1\to 0} & 2C^{y\to y}_{0\to 1,-1\to 0} & C^{y\to y}_{0\to 0,-1\to 1} & C^{y\to y}_{0\to 0,-1\to -1} & 2C^{y\to y}_{0\to 1,-1\to 1} & 2C^{y\to y}_{0\to 1,-1\to -1} & \cdots \\ C^{y\to y}_{1\to 0,1\to 0} & 2C^{y\to y}_{1\to 1,1\to 0} & C^{y\to y}_{1\to 0,1\to 1} & C^{y\to y}_{1\to 0,1\to -1} & 2C^{y\to y}_{1\to 1,1\to 1} & 2C^{y\to y}_{1\to 1,1\to -1} & \cdots \\ C^{y\to y}_{1\to 0,-1\to 0} & 2C^{y\to y}_{1\to 1,-1\to 0} & C^{y\to y}_{1\to 0,-1\to 1} & C^{y\to y}_{1\to 0,-1\to -1} & 2C^{y\to y}_{1\to 1,-1\to 1} & 2C^{y\to y}_{1\to 1,-1\to -1} & \cdots \\ \vdots & \vdots & \vdots & \vdots & \vdots & \vdots & \ddots \\ \hline C^{x\to y}_{0\to 0,0\to 0} & 2C^{x\to y}_{0\to 1,0\to 0} & C^{x\to y}_{0\to 0,0\to 1} & C^{x\to y}_{0\to 0,0\to -1} & 2C^{x\to y}_{0\to 1,0\to 1} & 2C^{x\to y}_{0\to 1,0\to -1} & \cdots \\ C^{x\to y}_{0\to 0,1\to 0} & 2C^{x\to y}_{0\to 1,1\to 0} & C^{x\to y}_{0\to 0,1\to 1} & C^{x\to y}_{0\to 0,1\to -1} & 2C^{x\to y}_{0\to 1,1\to 1} & 2C^{x\to y}_{0\to 1,1\to -1} & \cdots \\ C^{x\to y}_{0\to 0,-1\to 0} & 2C^{x\to y}_{0\to 1,-1\to 0} & C^{x\to y}_{0\to 0,-1\to 1} & C^{x\to y}_{0\to 0,-1\to -1} & 2C^{x\to y}_{0\to 1,-1\to 1} & 2C^{x\to y}_{0\to 1,-1\to -1} & \cdots \\ \vdots & \vdots & \vdots & \vdots & \vdots & \vdots & \ddots \end{bmatrix}$$

$$\begin{bmatrix} C^{y\to x}_{0\to 0,0\to 0} & C^{y\to x}_{0\to 0,0\to 1} & C^{y\to x}_{0\to 0,0\to -1} & \cdots \\ 2C^{y\to x}_{1\to 0,0\to 0} & 2C^{y\to x}_{1\to 0,0\to 1} & 2C^{y\to x}_{1\to 0,0\to -1} & \cdots \\ C^{y\to x}_{0\to 0,1\to 0} & C^{y\to x}_{0\to 0,1\to 1} & C^{y\to x}_{0\to 0,1\to -1} & \cdots \\ C^{y\to x}_{0\to 0,-1\to 0} & C^{y\to x}_{0\to 0,-1\to 1} & C^{y\to x}_{0\to 0,-1\to -1} & \cdots \\ 2C^{y\to x}_{1\to 0,1\to 0} & 2C^{y\to x}_{1\to 0,1\to 1} & 2C^{y\to x}_{1\to 0,1\to -1} & \cdots \\ 2C^{y\to x}_{1\to 0,-1\to 0} & 2C^{y\to x}_{1\to 0,-1\to 1} & 2C^{y\to x}_{1\to 0,-1\to -1} & \cdots \\ \vdots & \vdots & \vdots & \ddots \\ \hline C^{x\to x}_{0\to 0,0\to 0} & C^{x\to x}_{0\to 0,0\to 1} & C^{x\to x}_{0\to 0,0\to -1} & \cdots \\ C^{x\to x}_{0\to 0,1\to 0} & C^{x\to x}_{0\to 0,1\to 1} & C^{x\to x}_{0\to 0,1\to -1} & \cdots \\ C^{x\to x}_{0\to 0,-1\to 0} & C^{x\to x}_{0\to 0,-1\to 1} & C^{x\to x}_{0\to 0,-1\to -1} & \cdots \\ \vdots & \vdots & \vdots & \ddots \end{bmatrix} \begin{bmatrix} E_{y,0,0} \\ E_{y,1,0} \\ E_{y,0,1} \\ E_{y,0,-1} \\ E_{y,1,1} \\ E_{y,1,-1} \\ \vdots \\ \hline E_{x,0,0} \\ E_{x,0,1} \\ E_{x,0,-1} \\ \vdots \end{bmatrix} \tag{D.2.15}$$

For a system possessing σ_x - symmetry, with an input field polarized in the *x*-direction, the relationships between the electric and magnetic field harmonic elements are the following:

$$E_{x,m,n} = E_{x,m,-n} \tag{D.2.16}$$

$$E_{y,m,n} = -E_{y,m,-n} \tag{D.2.17}$$

$$H_{x,m,n} = -H_{x,m,-n} \tag{D.2.18}$$

$$H_{y,m,n} = H_{y,m,-n} \tag{D.2.19}$$

Determining the reduced eigenvalue equation matrix in this case follows similar logic to the derivation in Equations (D.2.6) – (D.2.15). Similarly, for a system possessing σ_y - symmetry, the relationships between the electric and magnetic field harmonic elements for an input field polarized in the *y*-direction are as follows:

$$E_{x,m,n} = E_{x,m,-n} \tag{D.2.20}$$

$$E_{y,m,n} = -E_{y,m,-n} \tag{D.2.21}$$

$$H_{x,m,n} = -H_{x,m,-n} \tag{D.2.22}$$
$$H_{y,m,n} = H_{y,m,-n} \tag{D.2.23}$$

and for an input field polarized in the *x*-direction, the relationships are the following:

$$E_{x,m,n} = -E_{x,m,-n} \tag{D.2.24}$$
$$E_{y,m,n} = E_{y,m,-n} \tag{D.2.25}$$
$$H_{x,m,n} = H_{x,m,-n} \tag{D.2.26}$$
$$H_{y,m,n} = -H_{y,m,-n} \tag{D.2.27}$$

The process of reducing the coupled wave equation matrix and solving the eigenmode problem then proceeds in a similar manner.

D.3 C_{2v} Symmetry in Two-Dimensional Systems

For a system possessing material symmetry along the x- and y-axes, the presence of a field that is polarized along either the x- or y-axis as well creates the possibility of an even further reduction in the size of the coupled wave equation eigenmode problem. The group theoretic name for this point group is C_{2v} symmetry. The relationships between the field harmonics in a C_{2v} symmetric setting with fields polarized along the y-direction are the following:

$$E_{x,m,n} = -E_{x,m,-n} = -E_{x,-m,n} = E_{x,-m,-n} \tag{D.3.1}$$
$$E_{y,m,n} = E_{y,m,-n} = E_{y,-m,n} = E_{y,-m,-n} \tag{D.3.2}$$
$$H_{x,m,n} = H_{x,m,-n} = H_{x,-m,n} = H_{x,-m,-n} \tag{D.3.3}$$
$$H_{y,m,n} = -H_{y,m,-n} = -H_{y,-m,n} = H_{y,-m,-n} \tag{D.3.4}$$

The matrix relationship between the derivative of the electric field components and the magnetic field components can be expressed as follows:

$$\frac{\partial}{\partial z'}\begin{bmatrix} E_{y,0,0} \\ E_{y,1,0} \\ E_{y,-1,0} \\ E_{y,0,1} \\ E_{y,0,-1} \\ E_{y,1,1} \\ E_{y,-1,1} \\ E_{y,1,-1} \\ E_{y,-1,-1} \\ \vdots \\ \hline E_{x,0,0} \\ E_{x,1,0} \\ E_{x,-1,0} \\ E_{x,0,1} \\ E_{x,0,-1} \\ E_{x,1,1} \\ E_{x,-1,1} \\ E_{x,1,-1} \\ E_{x,-1,-1} \\ \vdots \end{bmatrix} = \begin{bmatrix} A^{y\to y}_{0\to 0,0\to 0} & A^{y\to y}_{0\to 1,0\to 0} & A^{y\to y}_{0\to -1,0\to 0} & A^{y\to y}_{0\to 0,0\to 1} & A^{y\to y}_{0\to 0,0\to -1} & A^{y\to y}_{0\to 1,0\to 1} & A^{y\to y}_{0\to -1,0\to 1} & A^{y\to y}_{0\to 1,0\to -1} & A^{y\to y}_{0\to -1,0\to -1} & \cdots \\ A^{y\to y}_{1\to 0,0\to 0} & A^{y\to y}_{1\to 1,0\to 0} & A^{y\to y}_{1\to -1,0\to 0} & A^{y\to y}_{1\to 0,0\to 1} & A^{y\to y}_{1\to 0,0\to -1} & A^{y\to y}_{1\to 1,0\to 1} & A^{y\to y}_{1\to -1,0\to 1} & A^{y\to y}_{1\to 1,0\to -1} & A^{y\to y}_{1\to -1,0\to -1} & \cdots \\ A^{y\to y}_{-1\to 0,0\to 0} & A^{y\to y}_{-1\to 1,0\to 0} & A^{y\to y}_{-1\to -1,0\to 0} & A^{y\to y}_{-1\to 0,0\to 1} & A^{y\to y}_{-1\to 0,0\to -1} & A^{y\to y}_{-1\to 1,0\to 1} & A^{y\to y}_{-1\to -1,0\to 1} & A^{y\to y}_{-1\to 1,0\to -1} & A^{y\to y}_{-1\to -1,0\to -1} & \cdots \\ A^{y\to y}_{0\to 0,1\to 0} & A^{y\to y}_{0\to 1,1\to 0} & A^{y\to y}_{0\to -1,1\to 0} & A^{y\to y}_{0\to 0,1\to 1} & A^{y\to y}_{0\to 0,1\to -1} & A^{y\to y}_{0\to 1,1\to 1} & A^{y\to y}_{0\to -1,1\to 1} & A^{y\to y}_{0\to 1,1\to -1} & A^{y\to y}_{0\to -1,1\to -1} & \cdots \\ A^{y\to y}_{0\to 0,-1\to 0} & A^{y\to y}_{0\to 1,-1\to 0} & A^{y\to y}_{0\to -1,-1\to 0} & A^{y\to y}_{0\to 0,-1\to 1} & A^{y\to y}_{0\to 0,-1\to -1} & A^{y\to y}_{0\to 1,-1\to 1} & A^{y\to y}_{0\to -1,-1\to 1} & A^{y\to y}_{0\to 1,-1\to -1} & A^{y\to y}_{0\to -1,-1\to -1} & \cdots \\ A^{y\to y}_{1\to 0,1\to 0} & A^{y\to y}_{1\to 1,1\to 0} & A^{y\to y}_{1\to -1,1\to 0} & A^{y\to y}_{1\to 0,1\to 1} & A^{y\to y}_{1\to 0,1\to -1} & A^{y\to y}_{1\to 1,1\to 1} & A^{y\to y}_{1\to -1,1\to 1} & A^{y\to y}_{1\to 1,1\to -1} & A^{y\to y}_{1\to -1,1\to -1} & \cdots \\ A^{y\to y}_{-1\to 0,1\to 0} & A^{y\to y}_{-1\to 1,1\to 0} & A^{y\to y}_{-1\to -1,1\to 0} & A^{y\to y}_{-1\to 0,1\to 1} & A^{y\to y}_{-1\to 0,1\to -1} & A^{y\to y}_{-1\to 1,1\to 1} & A^{y\to y}_{-1\to -1,1\to 1} & A^{y\to y}_{-1\to 1,1\to -1} & A^{y\to y}_{-1\to -1,1\to -1} & \cdots \\ A^{y\to y}_{1\to 0,-1\to 0} & A^{y\to y}_{1\to 1,-1\to 0} & A^{y\to y}_{1\to -1,-1\to 0} & A^{y\to y}_{1\to 0,-1\to 1} & A^{y\to y}_{1\to 0,-1\to -1} & A^{y\to y}_{1\to 1,-1\to 1} & A^{y\to y}_{1\to -1,-1\to 1} & A^{y\to y}_{1\to 1,-1\to -1} & A^{y\to y}_{1\to -1,-1\to -1} & \cdots \\ A^{y\to y}_{-1\to 0,-1\to 0} & A^{y\to y}_{-1\to 1,-1\to 0} & A^{y\to y}_{-1\to -1,-1\to 0} & A^{y\to y}_{-1\to 0,-1\to 1} & A^{y\to y}_{-1\to 0,-1\to -1} & A^{y\to y}_{-1\to 1,-1\to 1} & A^{y\to y}_{-1\to -1,-1\to 1} & A^{y\to y}_{-1\to 1,-1\to -1} & A^{y\to y}_{-1\to -1,-1\to -1} & \cdots \\ \vdots & \vdots & \vdots & \vdots & \vdots & \vdots & \vdots & \vdots & \vdots & \ddots \\ \hline A^{x\to y}_{0\to 0,0\to 0} & A^{x\to y}_{0\to 1,0\to 0} & A^{x\to y}_{0\to -1,0\to 0} & A^{x\to y}_{0\to 0,0\to 1} & A^{x\to y}_{0\to 0,0\to -1} & A^{x\to y}_{0\to 1,0\to 1} & A^{x\to y}_{0\to -1,0\to 1} & A^{x\to y}_{0\to 1,0\to -1} & A^{x\to y}_{0\to -1,0\to -1} & \cdots \\ A^{x\to y}_{1\to 0,0\to 0} & A^{x\to y}_{1\to 1,0\to 0} & A^{x\to y}_{1\to -1,0\to 0} & A^{x\to y}_{1\to 0,0\to 1} & A^{x\to y}_{1\to 0,0\to -1} & A^{x\to y}_{1\to 1,0\to 1} & A^{x\to y}_{1\to -1,0\to 1} & A^{x\to y}_{1\to 1,0\to -1} & A^{x\to y}_{1\to -1,0\to -1} & \cdots \\ A^{x\to y}_{-1\to 0,0\to 0} & A^{x\to y}_{-1\to 1,0\to 0} & A^{x\to y}_{-1\to -1,0\to 0} & A^{x\to y}_{-1\to 0,0\to 1} & A^{x\to y}_{-1\to 0,0\to -1} & A^{x\to y}_{-1\to 1,0\to 1} & A^{x\to y}_{-1\to -1,0\to 1} & A^{x\to y}_{-1\to 1,0\to -1} & A^{x\to y}_{-1\to -1,0\to -1} & \cdots \\ A^{x\to y}_{0\to 0,1\to 0} & A^{x\to y}_{0\to 1,1\to 0} & A^{x\to y}_{0\to -1,1\to 0} & A^{x\to y}_{0\to 0,1\to 1} & A^{x\to y}_{0\to 0,1\to -1} & A^{x\to y}_{0\to 1,1\to 1} & A^{x\to y}_{0\to -1,1\to 1} & A^{x\to y}_{0\to 1,1\to -1} & A^{x\to y}_{0\to -1,1\to -1} & \cdots \\ A^{x\to y}_{0\to 0,-1\to 0} & A^{x\to y}_{0\to 1,-1\to 0} & A^{x\to y}_{0\to -1,-1\to 0} & A^{x\to y}_{0\to 0,-1\to 1} & A^{x\to y}_{0\to 0,-1\to -1} & A^{x\to y}_{0\to 1,-1\to 1} & A^{x\to y}_{0\to -1,-1\to 1} & A^{x\to y}_{0\to 1,-1\to -1} & A^{x\to y}_{0\to -1,-1\to -1} & \cdots \\ A^{x\to y}_{1\to 0,1\to 0} & A^{x\to y}_{1\to 1,1\to 0} & A^{x\to y}_{1\to -1,1\to 0} & A^{x\to y}_{1\to 0,1\to 1} & A^{x\to y}_{1\to 0,1\to -1} & A^{x\to y}_{1\to 1,1\to 1} & A^{x\to y}_{1\to -1,1\to 1} & A^{x\to y}_{1\to 1,1\to -1} & A^{x\to y}_{1\to -1,1\to -1} & \cdots \\ A^{x\to y}_{-1\to 0,1\to 0} & A^{x\to y}_{-1\to 1,1\to 0} & A^{x\to y}_{-1\to -1,1\to 0} & A^{x\to y}_{-1\to 0,1\to 1} & A^{x\to y}_{-1\to 0,1\to -1} & A^{x\to y}_{-1\to 1,1\to 1} & A^{x\to y}_{-1\to -1,1\to 1} & A^{x\to y}_{-1\to 1,1\to -1} & A^{x\to y}_{-1\to -1,1\to -1} & \cdots \\ A^{x\to y}_{1\to 0,-1\to 0} & A^{x\to y}_{1\to 1,-1\to 0} & A^{x\to y}_{1\to -1,-1\to 0} & A^{x\to y}_{1\to 0,-1\to 1} & A^{x\to y}_{1\to 0,-1\to -1} & A^{x\to y}_{1\to 1,-1\to 1} & A^{x\to y}_{1\to -1,-1\to 1} & A^{x\to y}_{1\to 1,-1\to -1} & A^{x\to y}_{1\to -1,-1\to -1} & \cdots \\ A^{x\to y}_{-1\to 0,-1\to 0} & A^{x\to y}_{-1\to 1,-1\to 0} & A^{x\to y}_{-1\to -1,-1\to 0} & A^{x\to y}_{-1\to 0,-1\to 1} & A^{x\to y}_{-1\to 0,-1\to -1} & A^{x\to y}_{-1\to 1,-1\to 1} & A^{x\to y}_{-1\to -1,-1\to 1} & A^{x\to y}_{-1\to 1,-1\to -1} & A^{x\to y}_{-1\to -1,-1\to -1} & \cdots \\ \vdots & \vdots & \vdots & \vdots & \vdots & \vdots & \vdots & \vdots & \vdots & \ddots \end{bmatrix}$$

$$\cdots \begin{bmatrix} A^{y\to x}_{0\to 0,0\to 0} & A^{y\to x}_{0\to 1,0\to 0} & A^{y\to x}_{0\to -1,0\to 0} & A^{y\to x}_{0\to 0,0\to 1} & A^{y\to x}_{0\to 0,0\to -1} & A^{y\to x}_{0\to 1,0\to 1} & A^{y\to x}_{0\to -1,0\to 1} & A^{y\to x}_{0\to 1,0\to -1} & A^{y\to x}_{0\to -1,0\to -1} & \cdots \\ A^{y\to x}_{1\to 0,0\to 0} & A^{y\to x}_{1\to 1,0\to 0} & A^{y\to x}_{1\to -1,0\to 0} & A^{y\to x}_{1\to 0,0\to 1} & A^{y\to x}_{1\to 0,0\to -1} & A^{y\to x}_{1\to 1,0\to 1} & A^{y\to x}_{1\to -1,0\to 1} & A^{y\to x}_{1\to 1,0\to -1} & A^{y\to x}_{1\to -1,0\to -1} & \cdots \\ A^{y\to x}_{-1\to 0,0\to 0} & A^{y\to x}_{-1\to 1,0\to 0} & A^{y\to x}_{-1\to -1,0\to 0} & A^{y\to x}_{-1\to 0,0\to 1} & A^{y\to x}_{-1\to 0,0\to -1} & A^{y\to x}_{-1\to 1,0\to 1} & A^{y\to x}_{-1\to -1,0\to 1} & A^{y\to x}_{-1\to 1,0\to -1} & A^{y\to x}_{-1\to -1,0\to -1} & \cdots \\ A^{y\to x}_{0\to 0,1\to 0} & A^{y\to x}_{0\to 1,1\to 0} & A^{y\to x}_{0\to -1,1\to 0} & A^{y\to x}_{0\to 0,1\to 1} & A^{y\to x}_{0\to 0,1\to -1} & A^{y\to x}_{0\to 1,1\to 1} & A^{y\to x}_{0\to -1,1\to 1} & A^{y\to x}_{0\to 1,1\to -1} & A^{y\to x}_{0\to -1,1\to -1} & \cdots \\ A^{y\to x}_{0\to 0,-1\to 0} & A^{y\to x}_{0\to 1,-1\to 0} & A^{y\to x}_{0\to -1,-1\to 0} & A^{y\to x}_{0\to 0,-1\to 1} & A^{y\to x}_{0\to 0,-1\to -1} & A^{y\to x}_{0\to 1,-1\to 1} & A^{y\to x}_{0\to -1,-1\to 1} & A^{y\to x}_{0\to 1,-1\to -1} & A^{y\to x}_{0\to -1,-1\to -1} & \cdots \\ A^{y\to x}_{1\to 0,1\to 0} & A^{y\to x}_{1\to 1,1\to 0} & A^{y\to x}_{1\to -1,1\to 0} & A^{y\to x}_{1\to 0,1\to 1} & A^{y\to x}_{1\to 0,1\to -1} & A^{y\to x}_{1\to 1,1\to 1} & A^{y\to x}_{1\to -1,1\to 1} & A^{y\to x}_{1\to 1,1\to -1} & A^{y\to x}_{1\to -1,1\to -1} & \cdots \\ A^{y\to x}_{-1\to 0,1\to 0} & A^{y\to x}_{-1\to 1,1\to 0} & A^{y\to x}_{-1\to -1,1\to 0} & A^{y\to x}_{-1\to 0,1\to 1} & A^{y\to x}_{-1\to 0,1\to -1} & A^{y\to x}_{-1\to 1,1\to 1} & A^{y\to x}_{-1\to -1,1\to 1} & A^{y\to x}_{-1\to 1,1\to -1} & A^{y\to x}_{-1\to -1,1\to -1} & \cdots \\ A^{y\to x}_{1\to 0,-1\to 0} & A^{y\to x}_{1\to 1,-1\to 0} & A^{y\to x}_{1\to -1,-1\to 0} & A^{y\to x}_{1\to 0,-1\to 1} & A^{y\to x}_{1\to 0,-1\to -1} & A^{y\to x}_{1\to 1,-1\to 1} & A^{y\to x}_{1\to -1,-1\to 1} & A^{y\to x}_{1\to 1,-1\to -1} & A^{y\to x}_{1\to -1,-1\to -1} & \cdots \\ A^{y\to x}_{-1\to 0,-1\to 0} & A^{y\to x}_{-1\to 1,-1\to 0} & A^{y\to x}_{-1\to -1,-1\to 0} & A^{y\to x}_{-1\to 0,-1\to 1} & A^{y\to x}_{-1\to 0,-1\to -1} & A^{y\to x}_{-1\to 1,-1\to 1} & A^{y\to x}_{-1\to -1,-1\to 1} & A^{y\to x}_{-1\to 1,-1\to -1} & A^{y\to x}_{-1\to -1,-1\to -1} & \cdots \\ \vdots & \vdots & \vdots & \vdots & \vdots & \vdots & \vdots & \vdots & \vdots & \ddots \\ \hline A^{x\to x}_{0\to 0,0\to 0} & A^{x\to x}_{0\to 1,0\to 0} & A^{x\to x}_{0\to -1,0\to 0} & A^{x\to x}_{0\to 0,0\to 1} & A^{x\to x}_{0\to 0,0\to -1} & A^{x\to x}_{0\to 1,0\to 1} & A^{x\to x}_{0\to -1,0\to 1} & A^{x\to x}_{0\to 1,0\to -1} & A^{x\to x}_{0\to -1,0\to -1} & \cdots \\ A^{x\to x}_{1\to 0,0\to 0} & A^{x\to x}_{1\to 1,0\to 0} & A^{x\to x}_{1\to -1,0\to 0} & A^{x\to x}_{1\to 0,0\to 1} & A^{x\to x}_{1\to 0,0\to -1} & A^{x\to x}_{1\to 1,0\to 1} & A^{x\to x}_{1\to -1,0\to 1} & A^{x\to x}_{1\to 1,0\to -1} & A^{x\to x}_{1\to -1,0\to -1} & \cdots \\ A^{x\to x}_{-1\to 0,0\to 0} & A^{x\to x}_{-1\to 1,0\to 0} & A^{x\to x}_{-1\to -1,0\to 0} & A^{x\to x}_{-1\to 0,0\to 1} & A^{x\to x}_{-1\to 0,0\to -1} & A^{x\to x}_{-1\to 1,0\to 1} & A^{x\to x}_{-1\to -1,0\to 1} & A^{x\to x}_{-1\to 1,0\to -1} & A^{x\to x}_{-1\to -1,0\to -1} & \cdots \\ A^{x\to x}_{0\to 0,1\to 0} & A^{x\to x}_{0\to 1,1\to 0} & A^{x\to x}_{0\to -1,1\to 0} & A^{x\to x}_{0\to 0,1\to 1} & A^{x\to x}_{0\to 0,1\to -1} & A^{x\to x}_{0\to 1,1\to 1} & A^{x\to x}_{0\to -1,1\to 1} & A^{x\to x}_{0\to 1,1\to -1} & A^{x\to x}_{0\to -1,1\to -1} & \cdots \\ A^{x\to x}_{0\to 0,-1\to 0} & A^{x\to x}_{0\to 1,-1\to 0} & A^{x\to x}_{0\to -1,-1\to 0} & A^{x\to x}_{0\to 0,-1\to 1} & A^{x\to x}_{0\to 0,-1\to -1} & A^{x\to x}_{0\to 1,-1\to 1} & A^{x\to x}_{0\to -1,-1\to 1} & A^{x\to x}_{0\to 1,-1\to -1} & A^{x\to x}_{0\to -1,-1\to -1} & \cdots \\ A^{x\to x}_{1\to 0,1\to 0} & A^{x\to x}_{1\to 1,1\to 0} & A^{x\to x}_{1\to -1,1\to 0} & A^{x\to x}_{1\to 0,1\to 1} & A^{x\to x}_{1\to 0,1\to -1} & A^{x\to x}_{1\to 1,1\to 1} & A^{x\to x}_{1\to -1,1\to 1} & A^{x\to x}_{1\to 1,1\to -1} & A^{x\to x}_{1\to -1,1\to -1} & \cdots \\ A^{x\to x}_{-1\to 0,1\to 0} & A^{x\to x}_{-1\to 1,1\to 0} & A^{x\to x}_{-1\to -1,1\to 0} & A^{x\to x}_{-1\to 0,1\to 1} & A^{x\to x}_{-1\to 0,1\to -1} & A^{x\to x}_{-1\to 1,1\to 1} & A^{x\to x}_{-1\to -1,1\to 1} & A^{x\to x}_{-1\to 1,1\to -1} & A^{x\to x}_{-1\to -1,1\to -1} & \cdots \\ A^{x\to x}_{1\to 0,-1\to 0} & A^{x\to x}_{1\to 1,-1\to 0} & A^{x\to x}_{1\to -1,-1\to 0} & A^{x\to x}_{1\to 0,-1\to 1} & A^{x\to x}_{1\to 0,-1\to -1} & A^{x\to x}_{1\to 1,-1\to 1} & A^{x\to x}_{1\to -1,-1\to 1} & A^{x\to x}_{1\to 1,-1\to -1} & A^{x\to x}_{1\to -1,-1\to -1} & \cdots \\ A^{x\to x}_{-1\to 0,-1\to 0} & A^{x\to x}_{-1\to 1,-1\to 0} & A^{x\to x}_{-1\to -1,-1\to 0} & A^{x\to x}_{-1\to 0,-1\to 1} & A^{x\to x}_{-1\to 0,-1\to -1} & A^{x\to x}_{-1\to 1,-1\to 1} & A^{x\to x}_{-1\to -1,-1\to 1} & A^{x\to x}_{-1\to 1,-1\to -1} & A^{x\to x}_{-1\to -1,-1\to -1} & \cdots \\ \vdots & \vdots & \vdots & \vdots & \vdots & \vdots & \vdots & \vdots & \vdots & \ddots \end{bmatrix} \begin{bmatrix} H_{y,0,0} \\ H_{y,1,0} \\ H_{y,-1,0} \\ H_{y,0,1} \\ H_{y,0,-1} \\ H_{y,1,1} \\ H_{y,-1,1} \\ H_{y,1,-1} \\ H_{y,-1,-1} \\ \vdots \\ \hline H_{x,0,0} \\ H_{x,1,0} \\ H_{x,-1,0} \\ H_{x,0,1} \\ H_{x,0,-1} \\ H_{x,1,1} \\ H_{x,-1,1} \\ H_{x,1,-1} \\ H_{x,-1,-1} \\ \vdots \end{bmatrix} \tag{D.3.5}$$

Similarly, the matrix relationship between the derivative of the magnetic field components and the electric field components can be expressed as follows:

$$\frac{\partial}{\partial z'}\begin{bmatrix} H_{y,0,0} \\ H_{y,1,0} \\ H_{y,-1,0} \\ H_{y,0,1} \\ H_{y,0,-1} \\ H_{y,1,1} \\ H_{y,-1,1} \\ H_{y,1,-1} \\ H_{y,-1,-1} \\ \vdots \\ \hline H_{x,0,0} \\ H_{x,1,0} \\ H_{x,-1,0} \\ H_{x,0,1} \\ H_{x,0,-1} \\ H_{x,1,1} \\ H_{x,-1,1} \\ H_{x,1,-1} \\ H_{x,-1,-1} \\ \vdots \end{bmatrix} = \begin{bmatrix} B^{y\to y}_{0\to 0,0\to 0} & B^{y\to y}_{0\to 1,0\to 0} & B^{y\to y}_{0\to -1,0\to 0} & B^{y\to y}_{0\to 0,0\to 1} & B^{y\to y}_{0\to 0,0\to -1} & B^{y\to y}_{0\to 1,0\to 1} & B^{y\to y}_{0\to -1,0\to 1} & B^{y\to y}_{0\to 1,0\to -1} & B^{y\to y}_{0\to -1,0\to -1} & \cdots \\ B^{y\to y}_{1\to 0,0\to 0} & B^{y\to y}_{1\to 1,0\to 0} & B^{y\to y}_{1\to -1,0\to 0} & B^{y\to y}_{1\to 0,0\to 1} & B^{y\to y}_{1\to 0,0\to -1} & B^{y\to y}_{1\to 1,0\to 1} & B^{y\to y}_{1\to -1,0\to 1} & B^{y\to y}_{1\to 1,0\to -1} & B^{y\to y}_{1\to -1,0\to -1} & \cdots \\ B^{y\to y}_{-1\to 0,0\to 0} & B^{y\to y}_{-1\to 1,0\to 0} & B^{y\to y}_{-1\to -1,0\to 0} & B^{y\to y}_{-1\to 0,0\to 1} & B^{y\to y}_{-1\to 0,0\to -1} & B^{y\to y}_{-1\to 1,0\to 1} & B^{y\to y}_{-1\to -1,0\to 1} & B^{y\to y}_{-1\to 1,0\to -1} & B^{y\to y}_{-1\to -1,0\to -1} & \cdots \\ B^{y\to y}_{0\to 0,1\to 0} & B^{y\to y}_{0\to 1,1\to 0} & B^{y\to y}_{0\to -1,1\to 0} & B^{y\to y}_{0\to 0,1\to 1} & B^{y\to y}_{0\to 0,1\to -1} & B^{y\to y}_{0\to 1,1\to 1} & B^{y\to y}_{0\to -1,1\to 1} & B^{y\to y}_{0\to 1,1\to -1} & B^{y\to y}_{0\to -1,1\to -1} & \cdots \\ B^{y\to y}_{0\to 0,-1\to 0} & B^{y\to y}_{0\to 1,-1\to 0} & B^{y\to y}_{0\to -1,-1\to 0} & B^{y\to y}_{0\to 0,-1\to 1} & B^{y\to y}_{0\to 0,-1\to -1} & B^{y\to y}_{0\to 1,-1\to 1} & B^{y\to y}_{0\to -1,-1\to 1} & B^{y\to y}_{0\to 1,-1\to -1} & B^{y\to y}_{0\to -1,-1\to -1} & \cdots \\ B^{y\to y}_{1\to 0,1\to 0} & B^{y\to y}_{1\to 1,1\to 0} & B^{y\to y}_{1\to -1,1\to 0} & B^{y\to y}_{1\to 0,1\to 1} & B^{y\to y}_{1\to 0,1\to -1} & B^{y\to y}_{1\to 1,1\to 1} & B^{y\to y}_{1\to -1,1\to 1} & B^{y\to y}_{1\to 1,1\to -1} & B^{y\to y}_{1\to -1,1\to -1} & \cdots \\ B^{y\to y}_{-1\to 0,1\to 0} & B^{y\to y}_{-1\to 1,1\to 0} & B^{y\to y}_{-1\to -1,1\to 0} & B^{y\to y}_{-1\to 0,1\to 1} & B^{y\to y}_{-1\to 0,1\to -1} & B^{y\to y}_{-1\to 1,1\to 1} & B^{y\to y}_{-1\to -1,1\to 1} & B^{y\to y}_{-1\to 1,1\to -1} & B^{y\to y}_{-1\to -1,1\to -1} & \cdots \\ B^{y\to y}_{1\to 0,-1\to 0} & B^{y\to y}_{1\to 1,-1\to 0} & B^{y\to y}_{1\to -1,-1\to 0} & B^{y\to y}_{1\to 0,-1\to 1} & B^{y\to y}_{1\to 0,-1\to -1} & B^{y\to y}_{1\to 1,-1\to 1} & B^{y\to y}_{1\to -1,-1\to 1} & B^{y\to y}_{1\to 1,-1\to -1} & B^{y\to y}_{1\to -1,-1\to -1} & \cdots \\ B^{y\to y}_{-1\to 0,-1\to 0} & B^{y\to y}_{-1\to 1,-1\to 0} & B^{y\to y}_{-1\to -1,-1\to 0} & B^{y\to y}_{-1\to 0,-1\to 1} & B^{y\to y}_{-1\to 0,-1\to -1} & B^{y\to y}_{-1\to 1,-1\to 1} & B^{y\to y}_{-1\to -1,-1\to 1} & B^{y\to y}_{-1\to 1,-1\to -1} & B^{y\to y}_{-1\to -1,-1\to -1} & \cdots \\ \vdots & \vdots & \vdots & \vdots & \vdots & \vdots & \vdots & \vdots & \vdots & \ddots \\ \hline B^{x\to y}_{0\to 0,0\to 0} & B^{x\to y}_{0\to 1,0\to 0} & B^{x\to y}_{0\to -1,0\to 0} & B^{x\to y}_{0\to 0,0\to 1} & B^{x\to y}_{0\to 0,0\to -1} & B^{x\to y}_{0\to 1,0\to 1} & B^{x\to y}_{0\to -1,0\to 1} & B^{x\to y}_{0\to 1,0\to -1} & B^{x\to y}_{0\to -1,0\to -1} & \cdots \\ B^{x\to y}_{1\to 0,0\to 0} & B^{x\to y}_{1\to 1,0\to 0} & B^{x\to y}_{1\to -1,0\to 0} & B^{x\to y}_{1\to 0,0\to 1} & B^{x\to y}_{1\to 0,0\to -1} & B^{x\to y}_{1\to 1,0\to 1} & B^{x\to y}_{1\to -1,0\to 1} & B^{x\to y}_{1\to 1,0\to -1} & B^{x\to y}_{1\to -1,0\to -1} & \cdots \\ B^{x\to y}_{-1\to 0,0\to 0} & B^{x\to y}_{-1\to 1,0\to 0} & B^{x\to y}_{-1\to -1,0\to 0} & B^{x\to y}_{-1\to 0,0\to 1} & B^{x\to y}_{-1\to 0,0\to -1} & B^{x\to y}_{-1\to 1,0\to 1} & B^{x\to y}_{-1\to -1,0\to 1} & B^{x\to y}_{-1\to 1,0\to -1} & B^{x\to y}_{-1\to -1,0\to -1} & \cdots \\ B^{x\to y}_{0\to 0,1\to 0} & B^{x\to y}_{0\to 1,1\to 0} & B^{x\to y}_{0\to -1,1\to 0} & B^{x\to y}_{0\to 0,1\to 1} & B^{x\to y}_{0\to 0,1\to -1} & B^{x\to y}_{0\to 1,1\to 1} & B^{x\to y}_{0\to -1,1\to 1} & B^{x\to y}_{0\to 1,1\to -1} & B^{x\to y}_{0\to -1,1\to -1} & \cdots \\ B^{x\to y}_{0\to 0,-1\to 0} & B^{x\to y}_{0\to 1,-1\to 0} & B^{x\to y}_{0\to -1,-1\to 0} & B^{x\to y}_{0\to 0,-1\to 1} & B^{x\to y}_{0\to 0,-1\to -1} & B^{x\to y}_{0\to 1,-1\to 1} & B^{x\to y}_{0\to -1,-1\to 1} & B^{x\to y}_{0\to 1,-1\to -1} & B^{x\to y}_{0\to -1,-1\to -1} & \cdots \\ B^{x\to y}_{1\to 0,1\to 0} & B^{x\to y}_{1\to 1,1\to 0} & B^{x\to y}_{1\to -1,1\to 0} & B^{x\to y}_{1\to 0,1\to 1} & B^{x\to y}_{1\to 0,1\to -1} & B^{x\to y}_{1\to 1,1\to 1} & B^{x\to y}_{1\to -1,1\to 1} & B^{x\to y}_{1\to 1,1\to -1} & B^{x\to y}_{1\to -1,1\to -1} & \cdots \\ B^{x\to y}_{-1\to 0,1\to 0} & B^{x\to y}_{-1\to 1,1\to 0} & B^{x\to y}_{-1\to -1,1\to 0} & B^{x\to y}_{-1\to 0,1\to 1} & B^{x\to y}_{-1\to 0,1\to -1} & B^{x\to y}_{-1\to 1,1\to 1} & B^{x\to y}_{-1\to -1,1\to 1} & B^{x\to y}_{-1\to 1,1\to -1} & B^{x\to y}_{-1\to -1,1\to -1} & \cdots \\ B^{x\to y}_{1\to 0,-1\to 0} & B^{x\to y}_{1\to 1,-1\to 0} & B^{x\to y}_{1\to -1,-1\to 0} & B^{x\to y}_{1\to 0,-1\to 1} & B^{x\to y}_{1\to 0,-1\to -1} & B^{x\to y}_{1\to 1,-1\to 1} & B^{x\to y}_{1\to -1,-1\to 1} & B^{x\to y}_{1\to 1,-1\to -1} & B^{x\to y}_{1\to -1,-1\to -1} & \cdots \\ B^{x\to y}_{-1\to 0,-1\to 0} & B^{x\to y}_{-1\to 1,-1\to 0} & B^{x\to y}_{-1\to -1,-1\to 0} & B^{x\to y}_{-1\to 0,-1\to 1} & B^{x\to y}_{-1\to 0,-1\to -1} & B^{x\to y}_{-1\to 1,-1\to 1} & B^{x\to y}_{-1\to -1,-1\to 1} & B^{x\to y}_{-1\to 1,-1\to -1} & B^{x\to y}_{-1\to -1,-1\to -1} & \cdots \\ \vdots & \vdots & \vdots & \vdots & \vdots & \vdots & \vdots & \vdots & \vdots & \ddots \end{bmatrix}$$

$$\cdots \begin{bmatrix} B^{y\to x}_{0\to 0,0\to 0} & B^{y\to x}_{0\to 1,0\to 0} & B^{y\to x}_{0\to -1,0\to 0} & B^{y\to x}_{0\to 0,0\to 1} & B^{y\to x}_{0\to 0,0\to -1} & B^{y\to x}_{0\to 1,0\to 1} & B^{y\to x}_{0\to -1,0\to 1} & B^{y\to x}_{0\to 1,0\to -1} & B^{y\to x}_{0\to -1,0\to -1} & \cdots \\ B^{y\to x}_{1\to 0,0\to 0} & B^{y\to x}_{1\to 1,0\to 0} & B^{y\to x}_{1\to -1,0\to 0} & B^{y\to x}_{1\to 0,0\to 1} & B^{y\to x}_{1\to 0,0\to -1} & B^{y\to x}_{1\to 1,0\to 1} & B^{y\to x}_{1\to -1,0\to 1} & B^{y\to x}_{1\to 1,0\to -1} & B^{y\to x}_{1\to -1,0\to -1} & \cdots \\ B^{y\to x}_{-1\to 0,0\to 0} & B^{y\to x}_{-1\to 1,0\to 0} & B^{y\to x}_{-1\to -1,0\to 0} & B^{y\to x}_{-1\to 0,0\to 1} & B^{y\to x}_{-1\to 0,0\to -1} & B^{y\to x}_{-1\to 1,0\to 1} & B^{y\to x}_{-1\to -1,0\to 1} & B^{y\to x}_{-1\to 1,0\to -1} & B^{y\to x}_{-1\to -1,0\to -1} & \cdots \\ B^{y\to x}_{0\to 0,1\to 0} & B^{y\to x}_{0\to 1,1\to 0} & B^{y\to x}_{0\to -1,1\to 0} & B^{y\to x}_{0\to 0,1\to 1} & B^{y\to x}_{0\to 0,1\to -1} & B^{y\to x}_{0\to 1,1\to 1} & B^{y\to x}_{0\to -1,1\to 1} & B^{y\to x}_{0\to 1,1\to -1} & B^{y\to x}_{0\to -1,1\to -1} & \cdots \\ B^{y\to x}_{0\to 0,-1\to 0} & B^{y\to x}_{0\to 1,-1\to 0} & B^{y\to x}_{0\to -1,-1\to 0} & B^{y\to x}_{0\to 0,-1\to 1} & B^{y\to x}_{0\to 0,-1\to -1} & B^{y\to x}_{0\to 1,-1\to 1} & B^{y\to x}_{0\to -1,-1\to 1} & B^{y\to x}_{0\to 1,-1\to -1} & B^{y\to x}_{0\to -1,-1\to -1} & \cdots \\ B^{y\to x}_{1\to 0,1\to 0} & B^{y\to x}_{1\to 1,1\to 0} & B^{y\to x}_{1\to -1,1\to 0} & B^{y\to x}_{1\to 0,1\to 1} & B^{y\to x}_{1\to 0,1\to -1} & B^{y\to x}_{1\to 1,1\to 1} & B^{y\to x}_{1\to -1,1\to 1} & B^{y\to x}_{1\to 1,1\to -1} & B^{y\to x}_{1\to -1,1\to -1} & \cdots \\ B^{y\to x}_{-1\to 0,1\to 0} & B^{y\to x}_{-1\to 1,1\to 0} & B^{y\to x}_{-1\to -1,1\to 0} & B^{y\to x}_{-1\to 0,1\to 1} & B^{y\to x}_{-1\to 0,1\to -1} & B^{y\to x}_{-1\to 1,1\to 1} & B^{y\to x}_{-1\to -1,1\to 1} & B^{y\to x}_{-1\to 1,1\to -1} & B^{y\to x}_{-1\to -1,1\to -1} & \cdots \\ B^{y\to x}_{1\to 0,-1\to 0} & B^{y\to x}_{1\to 1,-1\to 0} & B^{y\to x}_{1\to -1,-1\to 0} & B^{y\to x}_{1\to 0,-1\to 1} & B^{y\to x}_{1\to 0,-1\to -1} & B^{y\to x}_{1\to 1,-1\to 1} & B^{y\to x}_{1\to -1,-1\to 1} & B^{y\to x}_{1\to 1,-1\to -1} & B^{y\to x}_{1\to -1,-1\to -1} & \cdots \\ B^{y\to x}_{-1\to 0,-1\to 0} & B^{y\to x}_{-1\to 1,-1\to 0} & B^{y\to x}_{-1\to -1,-1\to 0} & B^{y\to x}_{-1\to 0,-1\to 1} & B^{y\to x}_{-1\to 0,-1\to -1} & B^{y\to x}_{-1\to 1,-1\to 1} & B^{y\to x}_{-1\to -1,-1\to 1} & B^{y\to x}_{-1\to 1,-1\to -1} & B^{y\to x}_{-1\to -1,-1\to -1} & \cdots \\ \vdots & \vdots & \vdots & \vdots & \vdots & \vdots & \vdots & \vdots & \vdots & \ddots \\ \hline B^{x\to x}_{0\to 0,0\to 0} & B^{x\to x}_{0\to 1,0\to 0} & B^{x\to x}_{0\to -1,0\to 0} & B^{x\to x}_{0\to 0,0\to 1} & B^{x\to x}_{0\to 0,0\to -1} & B^{x\to x}_{0\to 1,0\to 1} & B^{x\to x}_{0\to -1,0\to 1} & B^{x\to x}_{0\to 1,0\to -1} & B^{x\to x}_{0\to -1,0\to -1} & \cdots \\ B^{x\to x}_{1\to 0,0\to 0} & B^{x\to x}_{1\to 1,0\to 0} & B^{x\to x}_{1\to -1,0\to 0} & B^{x\to x}_{1\to 0,0\to 1} & B^{x\to x}_{1\to 0,0\to -1} & B^{x\to x}_{1\to 1,0\to 1} & B^{x\to x}_{1\to -1,0\to 1} & B^{x\to x}_{1\to 1,0\to -1} & B^{x\to x}_{1\to -1,0\to -1} & \cdots \\ B^{x\to x}_{-1\to 0,0\to 0} & B^{x\to x}_{-1\to 1,0\to 0} & B^{x\to x}_{-1\to -1,0\to 0} & B^{x\to x}_{-1\to 0,0\to 1} & B^{x\to x}_{-1\to 0,0\to -1} & B^{x\to x}_{-1\to 1,0\to 1} & B^{x\to x}_{-1\to -1,0\to 1} & B^{x\to x}_{-1\to 1,0\to -1} & B^{x\to x}_{-1\to -1,0\to -1} & \cdots \\ B^{x\to x}_{0\to 0,1\to 0} & B^{x\to x}_{0\to 1,1\to 0} & B^{x\to x}_{0\to -1,1\to 0} & B^{x\to x}_{0\to 0,1\to 1} & B^{x\to x}_{0\to 0,1\to -1} & B^{x\to x}_{0\to 1,1\to 1} & B^{x\to x}_{0\to -1,1\to 1} & B^{x\to x}_{0\to 1,1\to -1} & B^{x\to x}_{0\to -1,1\to -1} & \cdots \\ B^{x\to x}_{0\to 0,-1\to 0} & B^{x\to x}_{0\to 1,-1\to 0} & B^{x\to x}_{0\to -1,-1\to 0} & B^{x\to x}_{0\to 0,-1\to 1} & B^{x\to x}_{0\to 0,-1\to -1} & B^{x\to x}_{0\to 1,-1\to 1} & B^{x\to x}_{0\to -1,-1\to 1} & B^{x\to x}_{0\to 1,-1\to -1} & B^{x\to x}_{0\to -1,-1\to -1} & \cdots \\ B^{x\to x}_{1\to 0,1\to 0} & B^{x\to x}_{1\to 1,1\to 0} & B^{x\to x}_{1\to -1,1\to 0} & B^{x\to x}_{1\to 0,1\to 1} & B^{x\to x}_{1\to 0,1\to -1} & B^{x\to x}_{1\to 1,1\to 1} & B^{x\to x}_{1\to -1,1\to 1} & B^{x\to x}_{1\to 1,1\to -1} & B^{x\to x}_{1\to -1,1\to -1} & \cdots \\ B^{x\to x}_{-1\to 0,1\to 0} & B^{x\to x}_{-1\to 1,1\to 0} & B^{x\to x}_{-1\to -1,1\to 0} & B^{x\to x}_{-1\to 0,1\to 1} & B^{x\to x}_{-1\to 0,1\to -1} & B^{x\to x}_{-1\to 1,1\to 1} & B^{x\to x}_{-1\to -1,1\to 1} & B^{x\to x}_{-1\to 1,1\to -1} & B^{x\to x}_{-1\to -1,1\to -1} & \cdots \\ B^{x\to x}_{1\to 0,-1\to 0} & B^{x\to x}_{1\to 1,-1\to 0} & B^{x\to x}_{1\to -1,-1\to 0} & B^{x\to x}_{1\to 0,-1\to 1} & B^{x\to x}_{1\to 0,-1\to -1} & B^{x\to x}_{1\to 1,-1\to 1} & B^{x\to x}_{1\to -1,-1\to 1} & B^{x\to x}_{1\to 1,-1\to -1} & B^{x\to x}_{1\to -1,-1\to -1} & \cdots \\ B^{x\to x}_{-1\to 0,-1\to 0} & B^{x\to x}_{-1\to 1,-1\to 0} & B^{x\to x}_{-1\to -1,-1\to 0} & B^{x\to x}_{-1\to 0,-1\to 1} & B^{x\to x}_{-1\to 0,-1\to -1} & B^{x\to x}_{-1\to 1,-1\to 1} & B^{x\to x}_{-1\to -1,-1\to 1} & B^{x\to x}_{-1\to 1,-1\to -1} & B^{x\to x}_{-1\to -1,-1\to -1} & \cdots \\ \vdots & \vdots & \vdots & \vdots & \vdots & \vdots & \vdots & \vdots & \vdots & \ddots \end{bmatrix} \begin{bmatrix} E_{y,0,0} \\ E_{y,1,0} \\ E_{y,-1,0} \\ E_{y,0,1} \\ E_{y,0,-1} \\ E_{y,1,1} \\ E_{y,-1,1} \\ E_{y,1,-1} \\ E_{y,-1,-1} \\ \vdots \\ \hline E_{x,0,0} \\ E_{x,1,0} \\ E_{x,-1,0} \\ E_{x,0,1} \\ E_{x,0,-1} \\ E_{x,1,1} \\ E_{x,-1,1} \\ E_{x,1,-1} \\ E_{x,-1,-1} \\ \vdots \end{bmatrix} \tag{D.3.6}$$

For the elements listed in Equations (D.2.5) and (D.2.6), the symmetry relationships in Equations (D.2.1) – (D.2.4) can be expressed in matrix form as follows:

$$\begin{bmatrix} E_{y,0,0} \\ E_{y,1,0} \\ E_{y,-1,0} \\ E_{y,0,1} \\ E_{y,0,-1} \\ E_{y,1,1} \\ E_{y,-1,1} \\ E_{y,1,-1} \\ E_{y,-1,-1} \\ \vdots \end{bmatrix} = \begin{bmatrix} 1 & 0 & 0 & 0 & 0 & 0 & 0 & 0 & 0 & \cdots \\ 0 & 1 & 0 & 0 & 0 & 0 & 0 & 0 & 0 & \cdots \\ 0 & 0 & 1 & 0 & 0 & 0 & 0 & 0 & 0 & \cdots \\ 0 & 0 & 0 & 1 & 0 & 0 & 0 & 0 & 0 & \cdots \\ 0 & 0 & 0 & 0 & 1 & 0 & 0 & 0 & 0 & \cdots \\ 0 & 0 & 0 & 0 & 0 & 1 & 0 & 0 & 0 & \cdots \\ 0 & 0 & 0 & 0 & 0 & 0 & 1 & 0 & 0 & \cdots \\ 0 & 0 & 0 & 0 & 0 & 0 & 0 & 1 & 0 & \cdots \\ 0 & 0 & 0 & 0 & 0 & 0 & 0 & 0 & 1 & \cdots \\ \vdots & \vdots & \vdots & \vdots & \vdots & \vdots & \vdots & \vdots & \vdots & \ddots \end{bmatrix} \begin{bmatrix} E_{y,0,0} \\ E_{y,1,0} \\ E_{y,1,0} \\ E_{y,0,1} \\ E_{y,0,-1} \\ E_{y,1,1} \\ E_{y,1,1} \\ E_{y,1,-1} \\ E_{y,1,-1} \\ \vdots \end{bmatrix} \tag{D.3.7}$$

$$\begin{bmatrix} E_{x,0,0} \\ E_{x,1,0} \\ E_{x,-1,0} \\ E_{x,0,1} \\ E_{x,0,-1} \\ E_{x,1,1} \\ E_{x,-1,1} \\ E_{x,1,-1} \\ E_{x,-1,-1} \\ \vdots \end{bmatrix} = \begin{bmatrix} 1 & 0 & 0 & 0 & 0 & 0 & 0 & 0 & 0 & \cdots \\ 0 & 1 & 0 & 0 & 0 & 0 & 0 & 0 & 0 & \cdots \\ 0 & 0 & -1 & 0 & 0 & 0 & 0 & 0 & 0 & \cdots \\ 0 & 0 & 0 & 1 & 0 & 0 & 0 & 0 & 0 & \cdots \\ 0 & 0 & 0 & 0 & 1 & 0 & 0 & 0 & 0 & \cdots \\ 0 & 0 & 0 & 0 & 0 & 1 & 0 & 0 & 0 & \cdots \\ 0 & 0 & 0 & 0 & 0 & 0 & -1 & 0 & 0 & \cdots \\ 0 & 0 & 0 & 0 & 0 & 0 & 0 & -1 & 0 & \cdots \\ 0 & 0 & 0 & 0 & 0 & 0 & 0 & 0 & 1 & \cdots \\ \vdots & \vdots & \vdots & \vdots & \vdots & \vdots & \vdots & \vdots & \vdots & \ddots \end{bmatrix} \begin{bmatrix} E_{x,0,0} \\ E_{x,1,0} \\ E_{x,1,0} \\ E_{x,0,1} \\ E_{x,0,-1} \\ E_{x,1,1} \\ E_{x,1,1} \\ E_{x,1,-1} \\ E_{x,1,-1} \\ \vdots \end{bmatrix} \tag{D.3.8}$$

$$\begin{bmatrix} H_{y,0,0} \\ H_{y,1,0} \\ H_{y,-1,0} \\ H_{y,0,1} \\ H_{y,0,-1} \\ H_{y,1,1} \\ H_{y,-1,1} \\ H_{y,1,-1} \\ H_{y,-1,-1} \\ \vdots \end{bmatrix} = \begin{bmatrix} 1 & 0 & 0 & 0 & 0 & 0 & 0 & 0 & 0 & \cdots \\ 0 & 1 & 0 & 0 & 0 & 0 & 0 & 0 & 0 & \cdots \\ 0 & 0 & -1 & 0 & 0 & 0 & 0 & 0 & 0 & \cdots \\ 0 & 0 & 0 & 1 & 0 & 0 & 0 & 0 & 0 & \cdots \\ 0 & 0 & 0 & 0 & 1 & 0 & 0 & 0 & 0 & \cdots \\ 0 & 0 & 0 & 0 & 0 & 1 & 0 & 0 & 0 & \cdots \\ 0 & 0 & 0 & 0 & 0 & 0 & -1 & 0 & 0 & \cdots \\ 0 & 0 & 0 & 0 & 0 & 0 & 0 & -1 & 0 & \cdots \\ 0 & 0 & 0 & 0 & 0 & 0 & 0 & 0 & 1 & \cdots \\ \vdots & \vdots & \vdots & \vdots & \vdots & \vdots & \vdots & \vdots & \vdots & \ddots \end{bmatrix} \begin{bmatrix} H_{y,0,0} \\ H_{y,1,0} \\ H_{y,1,0} \\ H_{y,0,1} \\ H_{y,0,-1} \\ H_{y,1,1} \\ H_{y,1,1} \\ H_{y,1,-1} \\ H_{y,1,-1} \\ \vdots \end{bmatrix} \tag{D.3.9}$$

$$\begin{bmatrix} H_{x,0,0} \\ H_{x,1,0} \\ H_{x,-1,0} \\ H_{x,0,1} \\ H_{x,0,-1} \\ H_{x,1,1} \\ H_{x,-1,1} \\ H_{x,1,-1} \\ H_{x,-1,-1} \\ \vdots \end{bmatrix} = \begin{bmatrix} 1 & 0 & 0 & 0 & 0 & 0 & 0 & 0 & 0 & \cdots \\ 0 & 1 & 0 & 0 & 0 & 0 & 0 & 0 & 0 & \cdots \\ 0 & 0 & 1 & 0 & 0 & 0 & 0 & 0 & 0 & \cdots \\ 0 & 0 & 0 & 1 & 0 & 0 & 0 & 0 & 0 & \cdots \\ 0 & 0 & 0 & 0 & 1 & 0 & 0 & 0 & 0 & \cdots \\ 0 & 0 & 0 & 0 & 0 & 1 & 0 & 0 & 0 & \cdots \\ 0 & 0 & 0 & 0 & 0 & 0 & 1 & 0 & 0 & \cdots \\ 0 & 0 & 0 & 0 & 0 & 0 & 0 & 1 & 0 & \cdots \\ 0 & 0 & 0 & 0 & 0 & 0 & 0 & 0 & 1 & \cdots \\ \vdots & \vdots & \vdots & \vdots & \vdots & \vdots & \vdots & \vdots & \vdots & \ddots \end{bmatrix} \begin{bmatrix} H_{x,0,0} \\ H_{x,1,0} \\ H_{x,1,0} \\ H_{x,0,1} \\ H_{x,0,-1} \\ H_{x,1,1} \\ H_{x,1,1} \\ H_{x,1,-1} \\ H_{x,1,-1} \\ \vdots \end{bmatrix} \tag{D.3.10}$$

Applying Equations (D.3.7) – (D.3.10) to Equations (D.3.5) and (D.3.6) produces the following matrix relationships:

$$\frac{\partial}{\partial z'}\begin{bmatrix} E_{y,0,0} \\ E_{y,1,0} \\ E_{y,1,0} \\ E_{y,0,1} \\ E_{y,0,1} \\ E_{y,1,1} \\ E_{y,1,1} \\ E_{y,1,1} \\ E_{y,1,1} \\ \vdots \\ \hline E_{x,0,0} \\ E_{x,1,0} \\ E_{x,1,0} \\ E_{x,0,1} \\ E_{x,0,1} \\ E_{x,1,1} \\ E_{x,1,1} \\ E_{x,1,1} \\ E_{x,1,1} \\ \vdots \end{bmatrix} = \left[\begin{array}{ccccccccc} A_{0\to0,0\to0}^{y\to y} & A_{0\to1,0\to0}^{y\to y} & -A_{0\to1,0\to0}^{y\to y} & A_{0\to0,0\to1}^{y\to y} & -A_{0\to0,0\to1}^{y\to y} & A_{0\to1,0\to1}^{y\to y} & -A_{0\to1,0\to1}^{y\to y} & -A_{0\to1,0\to1}^{y\to y} & A_{0\to1,0\to1}^{y\to y} & \cdots \\ A_{1\to0,0\to0}^{y\to y} & A_{1\to1,0\to0}^{y\to y} & -A_{1\to1,0\to0}^{y\to y} & A_{1\to0,0\to1}^{y\to y} & -A_{1\to0,0\to1}^{y\to y} & A_{1\to1,0\to1}^{y\to y} & -A_{1\to1,0\to1}^{y\to y} & -A_{1\to1,0\to1}^{y\to y} & A_{1\to1,0\to1}^{y\to y} & \cdots \\ A_{1\to0,0\to0}^{y\to y} & A_{1\to1,0\to0}^{y\to y} & -A_{1\to1,0\to0}^{y\to y} & A_{1\to0,0\to1}^{y\to y} & -A_{1\to0,0\to1}^{y\to y} & A_{1\to1,0\to1}^{y\to y} & -A_{1\to1,0\to1}^{y\to y} & -A_{1\to1,0\to1}^{y\to y} & A_{1\to1,0\to1}^{y\to y} & \cdots \\ A_{0\to0,1\to0}^{y\to y} & A_{0\to1,1\to0}^{y\to y} & -A_{0\to1,1\to0}^{y\to y} & A_{0\to0,1\to1}^{y\to y} & -A_{0\to0,1\to1}^{y\to y} & A_{0\to1,1\to1}^{y\to y} & -A_{0\to1,1\to1}^{y\to y} & -A_{0\to1,1\to1}^{y\to y} & A_{0\to1,1\to1}^{y\to y} & \cdots \\ A_{0\to0,1\to0}^{y\to y} & A_{0\to1,1\to0}^{y\to y} & -A_{0\to1,1\to0}^{y\to y} & A_{0\to0,1\to1}^{y\to y} & -A_{0\to0,1\to1}^{y\to y} & A_{0\to1,1\to1}^{y\to y} & -A_{0\to1,-1\to1}^{y\to y} & -A_{0\to1,-1\to1}^{y\to y} & A_{0\to1,1\to1}^{y\to y} & \cdots \\ A_{1\to0,1\to0}^{y\to y} & A_{1\to1,1\to0}^{y\to y} & -A_{1\to1,1\to0}^{y\to y} & A_{1\to0,1\to1}^{y\to y} & -A_{1\to0,1\to1}^{y\to y} & A_{1\to1,1\to1}^{y\to y} & -A_{1\to1,1\to1}^{y\to y} & -A_{1\to1,1\to1}^{y\to y} & A_{1\to1,1\to1}^{y\to y} & \cdots \\ A_{1\to0,1\to0}^{y\to y} & A_{1\to1,1\to0}^{y\to y} & -A_{1\to1,1\to0}^{y\to y} & A_{1\to0,1\to1}^{y\to y} & -A_{1\to0,1\to1}^{y\to y} & A_{1\to1,1\to1}^{y\to y} & -A_{1\to1,1\to1}^{y\to y} & -A_{1\to1,1\to1}^{y\to y} & A_{1\to1,1\to1}^{y\to y} & \cdots \\ A_{1\to0,1\to0}^{y\to y} & A_{1\to1,1\to0}^{y\to y} & -A_{1\to1,1\to0}^{y\to y} & A_{1\to0,1\to1}^{y\to y} & -A_{1\to0,1\to1}^{y\to y} & A_{1\to1,1\to1}^{y\to y} & -A_{1\to1,1\to1}^{y\to y} & -A_{1\to1,1\to1}^{y\to y} & A_{1\to1,1\to1}^{y\to y} & \cdots \\ \vdots & \vdots & \vdots & \vdots & \vdots & \vdots & \vdots & \vdots & \vdots & \ddots \\ \hline A_{0\to0,0\to0}^{x\to y} & A_{0\to1,0\to0}^{x\to y} & -A_{0\to1,0\to0}^{x\to y} & A_{0\to0,0\to1}^{x\to y} & -A_{0\to0,0\to1}^{x\to y} & A_{0\to1,0\to1}^{x\to y} & -A_{0\to1,0\to1}^{x\to y} & -A_{0\to1,0\to1}^{x\to y} & A_{0\to1,0\to1}^{x\to y} & \cdots \\ A_{1\to0,0\to0}^{x\to y} & A_{1\to1,0\to0}^{x\to y} & -A_{1\to1,0\to0}^{x\to y} & A_{1\to0,0\to1}^{x\to y} & -A_{1\to0,0\to1}^{x\to y} & A_{1\to1,0\to1}^{x\to y} & -A_{1\to1,0\to1}^{x\to y} & -A_{1\to1,0\to1}^{x\to y} & A_{1\to1,0\to1}^{x\to y} & \cdots \\ -A_{1\to0,0\to0}^{x\to y} & -A_{1\to1,0\to0}^{x\to y} & A_{-1\to1,0\to0}^{x\to y} & -A_{1\to0,0\to1}^{x\to y} & A_{1\to0,0\to1}^{x\to y} & -A_{1\to1,0\to1}^{x\to y} & A_{1\to1,0\to1}^{x\to y} & A_{1\to1,0\to1}^{x\to y} & -A_{1\to1,0\to1}^{x\to y} & \cdots \\ A_{0\to0,1\to0}^{x\to y} & A_{0\to1,1\to0}^{x\to y} & -A_{0\to1,1\to0}^{x\to y} & A_{0\to0,1\to1}^{x\to y} & -A_{0\to0,1\to1}^{x\to y} & A_{0\to1,1\to1}^{x\to y} & -A_{0\to1,1\to1}^{x\to y} & -A_{0\to1,1\to1}^{x\to y} & A_{0\to1,1\to1}^{x\to y} & \cdots \\ -A_{0\to0,-1\to0}^{x\to y} & -A_{0\to1,1\to0}^{x\to y} & A_{0\to1,1\to0}^{x\to y} & -A_{0\to0,1\to1}^{x\to y} & A_{0\to0,1\to1}^{x\to y} & -A_{0\to1,1\to1}^{x\to y} & A_{0\to1,1\to1}^{x\to y} & A_{0\to1,-1\to1}^{x\to y} & -A_{0\to1,-1\to1}^{x\to y} & \cdots \\ A_{1\to0,1\to0}^{x\to y} & A_{1\to1,1\to0}^{x\to y} & -A_{1\to1,1\to0}^{x\to y} & A_{1\to0,1\to1}^{x\to y} & -A_{1\to0,1\to1}^{x\to y} & A_{1\to1,1\to1}^{x\to y} & -A_{1\to1,1\to1}^{x\to y} & -A_{1\to1,1\to1}^{x\to y} & A_{1\to1,1\to1}^{x\to y} & \cdots \\ -A_{1\to0,1\to0}^{x\to y} & -A_{1\to1,1\to0}^{x\to y} & A_{1\to1,1\to0}^{x\to y} & -A_{1\to0,1\to1}^{x\to y} & A_{1\to0,1\to1}^{x\to y} & -A_{1\to1,1\to1}^{x\to y} & A_{1\to1,1\to1}^{x\to y} & A_{1\to1,1\to1}^{x\to y} & -A_{1\to1,1\to1}^{x\to y} & \cdots \\ -A_{1\to0,1\to0}^{x\to y} & -A_{1\to1,1\to0}^{x\to y} & A_{1\to1,1\to0}^{x\to y} & -A_{1\to0,1\to1}^{x\to y} & A_{1\to0,1\to1}^{x\to y} & -A_{1\to1,1\to1}^{x\to y} & A_{1\to1,1\to1}^{x\to y} & A_{1\to1,1\to1}^{x\to y} & -A_{1\to1,1\to1}^{x\to y} & \cdots \\ A_{1\to0,1\to0}^{x\to y} & A_{1\to1,1\to0}^{x\to y} & -A_{1\to1,1\to0}^{x\to y} & A_{1\to0,1\to1}^{x\to y} & -A_{1\to0,1\to1}^{x\to y} & A_{1\to1,1\to1}^{x\to y} & -A_{1\to1,1\to1}^{x\to y} & -A_{1\to1,1\to1}^{x\to y} & A_{1\to1,1\to1}^{x\to y} & \cdots \\ \vdots & \vdots & \vdots & \vdots & \vdots & \vdots & \vdots & \vdots & \vdots & \ddots \end{array}\right] \quad \text{(D.3.11)}$$

$$\cdots \left[\begin{array}{ccccccccc} A_{0\to0,0\to0}^{y\to x} & A_{0\to1,0\to0}^{y\to x} & A_{0\to1,0\to0}^{y\to x} & A_{0\to0,0\to1}^{y\to x} & A_{0\to0,0\to1}^{y\to x} & A_{0\to1,0\to1}^{y\to x} & A_{0\to1,0\to1}^{y\to x} & A_{0\to1,0\to1}^{y\to x} & \cdots \\ A_{1\to0,0\to0}^{y\to x} & A_{1\to1,0\to0}^{y\to x} & A_{1\to1,0\to0}^{y\to x} & A_{1\to0,0\to1}^{y\to x} & A_{1\to0,0\to1}^{y\to x} & A_{1\to1,0\to1}^{y\to x} & A_{1\to1,0\to1}^{y\to x} & A_{1\to1,0\to1}^{y\to x} & \cdots \\ A_{1\to0,0\to0}^{y\to x} & A_{1\to1,0\to0}^{y\to x} & A_{1\to1,0\to0}^{y\to x} & A_{1\to0,0\to1}^{y\to x} & A_{1\to0,0\to1}^{y\to x} & A_{1\to1,0\to1}^{y\to x} & A_{1\to1,0\to1}^{y\to x} & A_{1\to1,0\to1}^{y\to x} & \cdots \\ A_{0\to0,1\to0}^{y\to x} & A_{0\to1,1\to0}^{y\to x} & A_{0\to1,1\to0}^{y\to x} & A_{0\to0,1\to1}^{y\to x} & A_{0\to0,1\to1}^{y\to x} & A_{0\to1,1\to1}^{y\to x} & A_{0\to1,1\to1}^{y\to x} & A_{0\to1,1\to1}^{y\to x} & \cdots \\ A_{0\to0,1\to0}^{y\to x} & A_{0\to1,1\to0}^{y\to x} & A_{0\to1,1\to0}^{y\to x} & A_{0\to0,1\to1}^{y\to x} & A_{0\to0,1\to1}^{y\to x} & A_{0\to1,1\to1}^{y\to x} & A_{0\to1,1\to1}^{y\to x} & A_{0\to1,1\to1}^{y\to x} & \cdots \\ A_{1\to0,1\to0}^{y\to x} & A_{1\to1,1\to0}^{y\to x} & A_{1\to1,1\to0}^{y\to x} & A_{1\to0,1\to1}^{y\to x} & A_{1\to0,1\to1}^{y\to x} & A_{1\to1,1\to1}^{y\to x} & A_{1\to1,1\to1}^{y\to x} & A_{1\to1,1\to1}^{y\to x} & \cdots \\ A_{1\to0,1\to0}^{y\to x} & A_{1\to1,1\to0}^{y\to x} & A_{1\to1,1\to0}^{y\to x} & A_{1\to0,1\to1}^{y\to x} & A_{1\to0,1\to1}^{y\to x} & A_{1\to1,1\to1}^{y\to x} & A_{1\to1,1\to1}^{y\to x} & A_{1\to1,1\to1}^{y\to x} & \cdots \\ A_{1\to0,1\to0}^{y\to x} & A_{1\to1,1\to0}^{y\to x} & A_{1\to1,1\to0}^{y\to x} & A_{1\to0,1\to1}^{y\to x} & A_{1\to0,1\to1}^{y\to x} & A_{1\to1,1\to1}^{y\to x} & A_{1\to1,1\to1}^{y\to x} & A_{1\to1,1\to1}^{y\to x} & \cdots \\ \vdots & \vdots & \vdots & \vdots & \vdots & \vdots & \vdots & \vdots & \ddots \\ \hline A_{0\to0,0\to0}^{x\to x} & A_{0\to1,0\to0}^{x\to x} & A_{0\to1,0\to0}^{x\to x} & A_{0\to0,0\to1}^{x\to x} & A_{0\to0,0\to1}^{x\to x} & A_{0\to1,0\to1}^{x\to x} & A_{0\to1,0\to1}^{x\to x} & A_{0\to1,0\to1}^{x\to x} & \cdots \\ A_{1\to0,0\to0}^{x\to x} & A_{1\to1,0\to0}^{x\to x} & A_{1\to1,0\to0}^{x\to x} & A_{1\to0,0\to1}^{x\to x} & A_{1\to0,0\to1}^{x\to x} & A_{1\to1,0\to1}^{x\to x} & A_{1\to1,0\to1}^{x\to x} & A_{1\to1,0\to1}^{x\to x} & \cdots \\ -A_{1\to0,0\to0}^{x\to x} & -A_{1\to1,0\to0}^{x\to x} & -A_{1\to1,0\to0}^{x\to x} & -A_{1\to0,0\to1}^{x\to x} & -A_{1\to0,0\to1}^{x\to x} & -A_{1\to1,0\to1}^{x\to x} & -A_{1\to1,0\to1}^{x\to x} & -A_{1\to1,0\to1}^{x\to x} & \cdots \\ A_{0\to0,1\to0}^{x\to x} & A_{0\to1,1\to0}^{x\to x} & A_{0\to1,1\to0}^{x\to x} & A_{0\to0,1\to1}^{x\to x} & A_{0\to0,1\to1}^{x\to x} & A_{0\to1,1\to1}^{x\to x} & A_{0\to1,1\to1}^{x\to x} & A_{0\to1,1\to1}^{x\to x} & \cdots \\ -A_{0\to0,1\to0}^{x\to x} & -A_{0\to1,1\to0}^{x\to x} & -A_{0\to1,1\to0}^{x\to x} & -A_{0\to0,1\to1}^{x\to x} & -A_{0\to0,1\to1}^{x\to x} & -A_{0\to1,1\to1}^{x\to x} & -A_{0\to1,1\to1}^{x\to x} & -A_{0\to1,1\to1}^{x\to x} & \cdots \\ A_{1\to0,1\to0}^{x\to x} & A_{1\to1,1\to0}^{x\to x} & A_{1\to1,1\to0}^{x\to x} & A_{1\to0,1\to1}^{x\to x} & A_{1\to0,1\to1}^{x\to x} & A_{1\to1,1\to1}^{x\to x} & A_{1\to1,1\to1}^{x\to x} & A_{1\to1,1\to1}^{x\to x} & \cdots \\ -A_{1\to0,1\to0}^{x\to x} & -A_{1\to1,1\to0}^{x\to x} & -A_{1\to1,1\to0}^{x\to x} & -A_{1\to0,1\to1}^{x\to x} & -A_{1\to0,1\to1}^{x\to x} & -A_{1\to1,1\to1}^{x\to x} & -A_{1\to1,1\to1}^{x\to x} & -A_{1\to1,1\to1}^{x\to x} & \cdots \\ -A_{1\to0,1\to0}^{x\to x} & -A_{1\to1,1\to0}^{x\to x} & -A_{1\to1,1\to0}^{x\to x} & -A_{1\to0,1\to1}^{x\to x} & -A_{1\to0,1\to1}^{x\to x} & -A_{1\to1,1\to1}^{x\to x} & -A_{1\to1,1\to1}^{x\to x} & -A_{1\to1,1\to1}^{x\to x} & \cdots \\ A_{1\to0,1\to0}^{x\to x} & A_{1\to1,1\to0}^{x\to x} & A_{1\to1,1\to0}^{x\to x} & A_{1\to0,1\to1}^{x\to x} & A_{1\to0,1\to1}^{x\to x} & A_{1\to1,1\to1}^{x\to x} & A_{1\to1,1\to1}^{x\to x} & A_{1\to1,1\to1}^{x\to x} & \cdots \\ \vdots & \vdots & \vdots & \vdots & \vdots & \vdots & \vdots & \vdots & \ddots \end{array}\right] \begin{bmatrix} H_{y,0,0} \\ H_{y,1,0} \\ H_{y,1,0} \\ H_{y,0,1} \\ H_{y,0,1} \\ H_{y,1,1} \\ H_{y,1,1} \\ H_{y,1,1} \\ H_{y,1,1} \\ \vdots \\ \hline H_{x,0,0} \\ H_{x,1,0} \\ H_{x,1,0} \\ H_{x,0,1} \\ H_{x,0,1} \\ H_{x,1,1} \\ H_{x,1,1} \\ H_{x,1,1} \\ H_{x,1,1} \\ \vdots \end{bmatrix}$$

$$
\frac{\partial}{\partial z'}\begin{bmatrix} H_{y,0,0} \\ H_{y,1,0} \\ H_{y,1,0} \\ H_{y,0,1} \\ H_{y,0,1} \\ H_{y,1,1} \\ H_{y,1,1} \\ H_{y,1,1} \\ H_{y,1,1} \\ \vdots \\ \hline H_{x,0,0} \\ H_{x,1,0} \\ H_{x,1,0} \\ H_{x,0,1} \\ H_{x,0,1} \\ H_{x,1,1} \\ H_{x,1,1} \\ H_{x,1,1} \\ H_{x,1,1} \\ \vdots \end{bmatrix} = \left[\begin{array}{cccccccccc}
B^{y\to y}_{0\to 0,0\to 0} & B^{y\to y}_{0\to 1,0\to 0} & B^{y\to y}_{0\to 1,0\to 0} & B^{y\to y}_{0\to 0,0\to 1} & B^{y\to y}_{0\to 0,0\to 1} & B^{y\to y}_{0\to 1,0\to 1} & B^{y\to y}_{0\to 1,0\to 1} & B^{y\to y}_{0\to 1,0\to 1} & B^{y\to y}_{0\to 1,0\to 1} & \cdots \\
B^{y\to y}_{1\to 0,0\to 0} & B^{y\to y}_{1\to 1,0\to 0} & B^{y\to y}_{1\to 1,0\to 0} & B^{y\to y}_{1\to 0,0\to 1} & B^{y\to y}_{1\to 0,0\to 1} & B^{y\to y}_{1\to 1,0\to 1} & B^{y\to y}_{1\to 1,0\to 1} & B^{y\to y}_{1\to 1,0\to 1} & B^{y\to y}_{1\to 1,0\to 1} & \cdots \\
-B^{y\to y}_{1\to 0,0\to 0} & -B^{y\to y}_{1\to 1,0\to 0} & -B^{y\to y}_{1\to 1,0\to 0} & -B^{y\to y}_{1\to 0,0\to 1} & -B^{y\to y}_{1\to 0,0\to 1} & -B^{y\to y}_{1\to 1,0\to 1} & -B^{y\to y}_{1\to 1,0\to 1} & -B^{y\to y}_{1\to 1,0\to 1} & -B^{y\to y}_{1\to 1,0\to 1} & \cdots \\
B^{y\to y}_{0\to 0,1\to 0} & B^{y\to y}_{0\to 1,1\to 0} & B^{y\to y}_{0\to 1,1\to 0} & B^{y\to y}_{0\to 0,1\to 1} & B^{y\to y}_{0\to 0,1\to 1} & B^{y\to y}_{0\to 1,1\to 1} & B^{y\to y}_{0\to 1,1\to 1} & B^{y\to y}_{0\to 1,1\to 1} & B^{y\to y}_{0\to 1,1\to 1} & \cdots \\
-B^{y\to y}_{0\to 0,1\to 0} & -B^{y\to y}_{0\to 1,1\to 0} & -B^{y\to y}_{0\to 1,1\to 0} & -B^{y\to y}_{0\to 0,1\to 1} & -B^{y\to y}_{0\to 0,1\to 1} & -B^{y\to y}_{0\to 1,1\to 1} & -B^{y\to y}_{0\to 1,1\to 1} & -B^{y\to y}_{0\to 1,1\to 1} & -B^{y\to y}_{0\to 1,1\to 1} & \cdots \\
B^{y\to y}_{1\to 0,1\to 0} & B^{y\to y}_{1\to 1,1\to 0} & B^{y\to y}_{1\to 1,1\to 0} & B^{y\to y}_{1\to 0,1\to 1} & B^{y\to y}_{1\to 0,1\to 1} & B^{y\to y}_{1\to 1,1\to 1} & B^{y\to y}_{1\to 1,1\to 1} & B^{y\to y}_{1\to 1,1\to 1} & B^{y\to y}_{1\to 1,1\to 1} & \cdots \\
-B^{y\to y}_{1\to 0,1\to 0} & -B^{y\to y}_{1\to 1,1\to 0} & -B^{y\to y}_{1\to 1,1\to 0} & -B^{y\to y}_{1\to 0,1\to 1} & -B^{y\to y}_{1\to 0,1\to 1} & -B^{y\to y}_{1\to 1,1\to 1} & -B^{y\to y}_{1\to 1,1\to 1} & -B^{y\to y}_{1\to 1,1\to 1} & -B^{y\to y}_{1\to 1,1\to 1} & \cdots \\
-B^{y\to y}_{1\to 0,1\to 0} & -B^{y\to y}_{1\to 1,1\to 0} & -B^{y\to y}_{1\to 1,1\to 0} & -B^{y\to y}_{1\to 0,1\to 1} & -B^{y\to y}_{1\to 0,1\to 1} & -B^{y\to y}_{1\to 1,1\to 1} & -B^{y\to y}_{1\to 1,1\to 1} & -B^{y\to y}_{1\to 1,1\to 1} & -B^{y\to y}_{1\to 1,1\to 1} & \cdots \\
B^{y\to y}_{1\to 0,1\to 0} & B^{y\to y}_{1\to 1,1\to 0} & B^{y\to y}_{1\to 1,1\to 0} & B^{y\to y}_{1\to 0,1\to 1} & B^{y\to y}_{1\to 0,1\to 1} & B^{y\to y}_{1\to 1,1\to 1} & B^{y\to y}_{1\to 1,1\to 1} & B^{y\to y}_{1\to 1,1\to 1} & B^{y\to y}_{1\to 1,1\to 1} & \cdots \\
\vdots & \vdots & \vdots & \vdots & \vdots & \vdots & \vdots & \vdots & \vdots & \ddots \\
\hline
B^{x\to y}_{0\to 0,0\to 0} & B^{x\to y}_{0\to 1,0\to 0} & B^{x\to y}_{0\to 1,0\to 0} & B^{x\to y}_{0\to 0,0\to 1} & B^{x\to y}_{0\to 0,0\to 1} & B^{x\to y}_{0\to 1,0\to 1} & B^{x\to y}_{0\to 1,0\to 1} & B^{x\to y}_{0\to 1,0\to 1} & B^{x\to y}_{0\to 1,0\to 1} & \cdots \\
B^{x\to y}_{1\to 0,0\to 0} & B^{x\to y}_{1\to 1,0\to 0} & B^{x\to y}_{1\to 1,0\to 0} & B^{x\to y}_{1\to 0,0\to 1} & B^{x\to y}_{1\to 0,0\to 1} & B^{x\to y}_{1\to 1,0\to 1} & B^{x\to y}_{1\to 1,0\to 1} & B^{x\to y}_{1\to 1,0\to 1} & B^{x\to y}_{1\to 1,0\to 1} & \cdots \\
B^{x\to y}_{1\to 0,0\to 0} & B^{x\to y}_{1\to 1,0\to 0} & B^{x\to y}_{1\to 1,0\to 0} & B^{x\to y}_{1\to 0,0\to 1} & B^{x\to y}_{1\to 0,0\to 1} & B^{x\to y}_{1\to 1,0\to 1} & B^{x\to y}_{1\to 1,0\to 1} & B^{x\to y}_{1\to 1,0\to 1} & B^{x\to y}_{1\to 1,0\to 1} & \cdots \\
B^{x\to y}_{0\to 0,1\to 0} & B^{x\to y}_{0\to 1,1\to 0} & B^{x\to y}_{0\to 1,1\to 0} & B^{x\to y}_{0\to 0,1\to 1} & B^{x\to y}_{0\to 0,1\to 1} & B^{x\to y}_{0\to 1,1\to 1} & B^{x\to y}_{0\to 1,1\to 1} & B^{x\to y}_{0\to 1,1\to 1} & B^{x\to y}_{0\to 1,1\to 1} & \cdots \\
B^{x\to y}_{0\to 0,1\to 0} & B^{x\to y}_{0\to 1,1\to 0} & B^{x\to y}_{0\to 1,1\to 0} & B^{x\to y}_{0\to 0,1\to 1} & B^{x\to y}_{0\to 0,1\to 1} & B^{x\to y}_{0\to 1,1\to 1} & B^{x\to y}_{0\to 1,1\to 1} & B^{x\to y}_{0\to 1,1\to 1} & B^{x\to y}_{0\to 1,1\to 1} & \cdots \\
B^{x\to y}_{1\to 0,1\to 0} & B^{x\to y}_{1\to 1,1\to 0} & B^{x\to y}_{1\to 1,1\to 0} & B^{x\to y}_{1\to 0,1\to 1} & B^{x\to y}_{1\to 0,1\to 1} & B^{x\to y}_{1\to 1,1\to 1} & B^{x\to y}_{1\to 1,1\to 1} & B^{x\to y}_{1\to 1,1\to 1} & B^{x\to y}_{1\to 1,1\to 1} & \cdots \\
B^{x\to y}_{1\to 0,1\to 0} & B^{x\to y}_{1\to 1,1\to 0} & B^{x\to y}_{1\to 1,1\to 0} & B^{x\to y}_{1\to 0,1\to 1} & B^{x\to y}_{1\to 0,1\to 1} & B^{x\to y}_{1\to 1,1\to 1} & B^{x\to y}_{1\to 1,1\to 1} & B^{x\to y}_{1\to 1,1\to 1} & B^{x\to y}_{1\to 1,1\to 1} & \cdots \\
B^{x\to y}_{1\to 0,1\to 0} & B^{x\to y}_{1\to 1,1\to 0} & B^{x\to y}_{1\to 1,1\to 0} & B^{x\to y}_{1\to 0,1\to 1} & B^{x\to y}_{1\to 0,1\to 1} & B^{x\to y}_{1\to 1,1\to 1} & B^{x\to y}_{1\to 1,1\to 1} & B^{x\to y}_{1\to 1,1\to 1} & B^{x\to y}_{1\to 1,1\to 1} & \cdots \\
B^{x\to y}_{1\to 0,1\to 0} & B^{x\to y}_{1\to 1,1\to 0} & B^{x\to y}_{1\to 1,1\to 0} & B^{x\to y}_{1\to 0,1\to 1} & B^{x\to y}_{1\to 0,1\to 1} & B^{x\to y}_{1\to 1,1\to 1} & B^{x\to y}_{1\to 1,1\to 1} & B^{x\to y}_{1\to 1,1\to 1} & B^{x\to y}_{1\to 1,1\to 1} & \cdots \\
\vdots & \vdots & \vdots & \vdots & \vdots & \vdots & \vdots & \vdots & \vdots & \ddots
\end{array}\right]
$$

$$
\cdots \left[\begin{array}{cccccccccc}
B^{y\to x}_{0\to 0,0\to 0} & B^{y\to x}_{0\to 1,0\to 0} & -B^{y\to x}_{0\to 1,0\to 0} & B^{y\to x}_{0\to 0,0\to 1} & -B^{y\to x}_{0\to 0,0\to 1} & B^{y\to x}_{0\to 1,0\to 1} & -B^{y\to x}_{0\to 1,0\to 1} & B^{y\to x}_{0\to 1,0\to 1} & -B^{y\to x}_{0\to 1,0\to 1} & \cdots \\
B^{y\to x}_{1\to 0,0\to 0} & B^{y\to x}_{1\to 1,0\to 0} & -B^{y\to x}_{1\to 1,0\to 0} & B^{y\to x}_{1\to 0,0\to 1} & -B^{y\to x}_{1\to 0,0\to 1} & B^{y\to x}_{1\to 1,0\to 1} & -B^{y\to x}_{1\to 1,0\to 1} & B^{y\to x}_{1\to 1,0\to 1} & -B^{y\to x}_{1\to 1,0\to 1} & \cdots \\
-B^{y\to x}_{1\to 0,0\to 0} & -B^{y\to x}_{1\to 1,0\to 0} & B^{y\to x}_{1\to 1,0\to 0} & -B^{y\to x}_{1\to 0,0\to 1} & B^{y\to x}_{1\to 0,0\to 1} & -B^{y\to x}_{1\to 1,0\to 1} & B^{y\to x}_{1\to 1,0\to 1} & -B^{y\to x}_{1\to 1,0\to 1} & B^{y\to x}_{1\to 1,0\to 1} & \cdots \\
B^{y\to x}_{0\to 0,1\to 0} & B^{y\to x}_{0\to 1,1\to 0} & -B^{y\to x}_{0\to 1,1\to 0} & B^{y\to x}_{0\to 0,1\to 1} & -B^{y\to x}_{0\to 0,1\to 1} & B^{y\to x}_{0\to 1,1\to 1} & -B^{y\to x}_{0\to 1,1\to 1} & B^{y\to x}_{0\to 1,1\to 1} & -B^{y\to x}_{0\to 1,1\to 1} & \cdots \\
-B^{y\to x}_{0\to 0,1\to 0} & -B^{y\to x}_{0\to 1,1\to 0} & B^{y\to x}_{0\to 1,1\to 0} & -B^{y\to x}_{0\to 0,1\to 1} & B^{y\to x}_{0\to 0,1\to 1} & -B^{y\to x}_{0\to 1,1\to 1} & B^{y\to x}_{0\to 1,1\to 1} & -B^{y\to x}_{0\to 1,1\to 1} & B^{y\to x}_{0\to 1,1\to 1} & \cdots \\
B^{y\to x}_{1\to 0,1\to 0} & B^{y\to x}_{1\to 1,1\to 0} & -B^{y\to x}_{1\to 1,1\to 0} & B^{y\to x}_{1\to 0,1\to 1} & -B^{y\to x}_{1\to 0,1\to 1} & B^{y\to x}_{1\to 1,1\to 1} & -B^{y\to x}_{1\to 1,1\to 1} & B^{y\to x}_{1\to 1,1\to 1} & -B^{y\to x}_{1\to 1,1\to 1} & \cdots \\
-B^{y\to x}_{1\to 0,1\to 0} & -B^{y\to x}_{1\to 1,1\to 0} & B^{y\to x}_{1\to 1,1\to 0} & -B^{y\to x}_{1\to 0,1\to 1} & B^{y\to x}_{1\to 0,1\to 1} & -B^{y\to x}_{1\to 1,1\to 1} & B^{y\to x}_{1\to 1,1\to 1} & -B^{y\to x}_{1\to 1,1\to 1} & B^{y\to x}_{1\to 1,1\to 1} & \cdots \\
B^{y\to x}_{1\to 0,1\to 0} & B^{y\to x}_{1\to 1,1\to 0} & -B^{y\to x}_{1\to 1,1\to 0} & B^{y\to x}_{1\to 0,1\to 1} & -B^{y\to x}_{1\to 0,1\to 1} & B^{y\to x}_{1\to 1,1\to 1} & -B^{y\to x}_{1\to 1,1\to 1} & B^{y\to x}_{1\to 1,1\to 1} & -B^{y\to x}_{1\to 1,1\to 1} & \cdots \\
-B^{y\to x}_{1\to 0,1\to 0} & -B^{y\to x}_{1\to 1,1\to 0} & B^{y\to x}_{1\to 1,1\to 0} & -B^{y\to x}_{1\to 0,1\to 1} & B^{y\to x}_{1\to 0,1\to 1} & -B^{y\to x}_{1\to 1,1\to 1} & B^{y\to x}_{1\to 1,1\to 1} & -B^{y\to x}_{1\to 1,1\to 1} & B^{y\to x}_{1\to 1,1\to 1} & \cdots \\
\vdots & \vdots & \vdots & \vdots & \vdots & \vdots & \vdots & \vdots & \vdots & \ddots \\
\hline
B^{x\to x}_{0\to 0,0\to 0} & B^{x\to x}_{0\to 1,0\to 0} & -B^{x\to x}_{0\to 1,0\to 0} & B^{x\to x}_{0\to 0,0\to 1} & -B^{x\to x}_{0\to 0,0\to 1} & B^{x\to x}_{0\to 1,0\to 1} & -B^{x\to x}_{0\to 1,0\to 1} & B^{x\to x}_{0\to 1,0\to 1} & -B^{x\to x}_{0\to 1,0\to 1} & \cdots \\
B^{x\to x}_{1\to 0,0\to 0} & B^{x\to x}_{1\to 1,0\to 0} & -B^{x\to x}_{1\to 1,0\to 0} & B^{x\to x}_{1\to 0,0\to 1} & -B^{x\to x}_{1\to 0,0\to 1} & B^{x\to x}_{1\to 1,0\to 1} & -B^{x\to x}_{1\to 1,0\to 1} & B^{x\to x}_{1\to 1,0\to 1} & -B^{x\to x}_{1\to 1,0\to 1} & \cdots \\
B^{x\to x}_{1\to 0,0\to 0} & B^{x\to x}_{1\to 1,0\to 0} & -B^{x\to x}_{1\to 1,0\to 0} & B^{x\to x}_{1\to 0,0\to 1} & -B^{x\to x}_{1\to 0,0\to 1} & B^{x\to x}_{1\to 1,0\to 1} & -B^{x\to x}_{1\to 1,0\to 1} & B^{x\to x}_{1\to 1,0\to 1} & -B^{x\to x}_{1\to 1,0\to 1} & \cdots \\
B^{x\to x}_{0\to 0,1\to 0} & B^{x\to x}_{0\to 1,1\to 0} & -B^{x\to x}_{0\to 1,1\to 0} & B^{x\to x}_{0\to 0,1\to 1} & -B^{x\to x}_{0\to 0,1\to 1} & B^{x\to x}_{0\to 1,1\to 1} & -B^{x\to x}_{0\to 1,1\to 1} & B^{x\to x}_{0\to 1,1\to 1} & -B^{x\to x}_{0\to 1,1\to 1} & \cdots \\
B^{x\to x}_{0\to 0,1\to 0} & B^{x\to x}_{0\to 1,1\to 0} & -B^{x\to x}_{0\to 1,1\to 0} & B^{x\to x}_{0\to 0,1\to 1} & -B^{x\to x}_{0\to 0,1\to 1} & B^{x\to x}_{0\to 1,1\to 1} & -B^{x\to x}_{0\to 1,1\to 1} & B^{x\to x}_{0\to 1,1\to 1} & -B^{x\to x}_{0\to 1,1\to 1} & \cdots \\
B^{x\to x}_{1\to 0,1\to 0} & B^{x\to x}_{1\to 1,1\to 0} & -B^{x\to x}_{1\to 1,1\to 0} & B^{x\to x}_{1\to 0,1\to 1} & -B^{x\to x}_{1\to 0,1\to 1} & B^{x\to x}_{1\to 1,1\to 1} & -B^{x\to x}_{1\to 1,1\to 1} & B^{x\to x}_{1\to 1,1\to 1} & -B^{x\to x}_{1\to 1,1\to 1} & \cdots \\
B^{x\to x}_{1\to 0,1\to 0} & B^{x\to x}_{1\to 1,1\to 0} & -B^{x\to x}_{1\to 1,1\to 0} & B^{x\to x}_{1\to 0,1\to 1} & -B^{x\to x}_{1\to 0,1\to 1} & B^{x\to x}_{1\to 1,1\to 1} & -B^{x\to x}_{1\to 1,1\to 1} & B^{x\to x}_{1\to 1,1\to 1} & -B^{x\to x}_{1\to 1,1\to 1} & \cdots \\
B^{x\to x}_{1\to 0,1\to 0} & B^{x\to x}_{1\to 1,1\to 0} & -B^{x\to x}_{1\to 1,1\to 0} & B^{x\to x}_{1\to 0,1\to 1} & -B^{x\to x}_{1\to 0,1\to 1} & B^{x\to x}_{1\to 1,1\to 1} & -B^{x\to x}_{1\to 1,1\to 1} & B^{x\to x}_{1\to 1,1\to 1} & -B^{x\to x}_{1\to 1,1\to 1} & \cdots \\
\vdots & \vdots & \vdots & \vdots & \vdots & \vdots & \vdots & \vdots & \vdots & \ddots
\end{array}\right]
\begin{bmatrix} E_{y,0,0} \\ E_{y,1,0} \\ E_{y,1,0} \\ E_{y,0,1} \\ E_{y,0,1} \\ E_{y,1,1} \\ E_{y,1,1} \\ E_{y,1,1} \\ E_{y,1,1} \\ \vdots \\ \hline E_{x,0,0} \\ E_{x,1,0} \\ E_{x,1,0} \\ E_{x,0,1} \\ E_{x,0,1} \\ E_{x,1,1} \\ E_{x,1,1} \\ E_{x,1,1} \\ E_{x,1,1} \\ \vdots \end{bmatrix} \tag{D.3.12}
$$

By taking the derivative of Equation (D.3.11) with respect to z' and inserting Equation (D.3.12), the resulting matrix eigenvalue equation can be written as follows:

$$\frac{\partial^2}{\partial z'^2}\begin{bmatrix} E_{y,0,0} \\ E_{y,1,0} \\ E_{y,1,0} \\ E_{y,0,1} \\ E_{y,0,1} \\ E_{y,1,1} \\ E_{y,1,1} \\ E_{y,1,1} \\ E_{y,1,1} \\ \vdots \\ \hline E_{x,0,0} \\ E_{x,1,0} \\ E_{x,1,0} \\ E_{x,0,1} \\ E_{x,0,1} \\ E_{x,1,1} \\ E_{x,1,1} \\ E_{x,1,1} \\ E_{x,1,1} \\ \vdots \end{bmatrix} = \left[\begin{array}{ccccccccccc} C^{y\to y}_{0\to 0,0\to 0} & C^{y\to y}_{0\to 1,0\to 0} & C^{y\to y}_{0\to 1,0\to 0} & C^{y\to y}_{0\to 0,0\to 1} & C^{y\to y}_{0\to 0,0\to 1} & C^{y\to y}_{0\to 1,0\to 1} & C^{y\to y}_{0\to 1,0\to 1} & C^{y\to y}_{0\to 1,0\to 1} & C^{y\to y}_{0\to 1,0\to 1} & \cdots \\ C^{y\to y}_{1\to 0,0\to 0} & C^{y\to y}_{1\to 1,0\to 0} & C^{y\to y}_{1\to 1,0\to 0} & C^{y\to y}_{1\to 0,0\to 1} & C^{y\to y}_{1\to 0,0\to 1} & C^{y\to y}_{1\to 1,0\to 1} & C^{y\to y}_{1\to 1,0\to 1} & C^{y\to y}_{1\to 1,0\to 1} & C^{y\to y}_{1\to 1,0\to 1} & \cdots \\ C^{y\to y}_{1\to 0,0\to 0} & C^{y\to y}_{1\to 1,0\to 0} & C^{y\to y}_{1\to 1,0\to 0} & C^{y\to y}_{1\to 0,0\to 1} & C^{y\to y}_{1\to 0,0\to 1} & C^{y\to y}_{1\to 1,0\to 1} & C^{y\to y}_{1\to 1,0\to 1} & C^{y\to y}_{1\to 1,0\to 1} & C^{y\to y}_{1\to 1,0\to 1} & \cdots \\ C^{y\to y}_{0\to 0,1\to 0} & C^{y\to y}_{0\to 1,1\to 0} & C^{y\to y}_{0\to 1,1\to 0} & C^{y\to y}_{0\to 0,1\to 1} & C^{y\to y}_{0\to 0,1\to 1} & C^{y\to y}_{0\to 1,1\to 1} & C^{y\to y}_{0\to 1,1\to 1} & C^{y\to y}_{0\to 1,1\to 1} & C^{y\to y}_{0\to 1,1\to 1} & \cdots \\ C^{y\to y}_{0\to 0,1\to 0} & C^{y\to y}_{0\to 1,1\to 0} & C^{y\to y}_{0\to 1,1\to 0} & C^{y\to y}_{0\to 0,1\to 1} & C^{y\to y}_{0\to 0,1\to 1} & C^{y\to y}_{0\to 1,1\to 1} & C^{y\to y}_{0\to 1,1\to 1} & C^{y\to y}_{0\to 1,1\to 1} & C^{y\to y}_{0\to 1,1\to 1} & \cdots \\ C^{y\to y}_{1\to 0,1\to 0} & C^{y\to y}_{1\to 1,1\to 0} & C^{y\to y}_{1\to 1,1\to 0} & C^{y\to y}_{1\to 0,1\to 1} & C^{y\to y}_{1\to 0,1\to 1} & C^{y\to y}_{1\to 1,1\to 1} & C^{y\to y}_{1\to 1,1\to 1} & C^{y\to y}_{1\to 1,1\to 1} & C^{y\to y}_{1\to 1,1\to 1} & \cdots \\ C^{y\to y}_{1\to 0,1\to 0} & C^{y\to y}_{1\to 1,1\to 0} & C^{y\to y}_{1\to 1,1\to 0} & C^{y\to y}_{1\to 0,1\to 1} & C^{y\to y}_{1\to 0,1\to 1} & C^{y\to y}_{1\to 1,1\to 1} & C^{y\to y}_{1\to 1,1\to 1} & C^{y\to y}_{1\to 1,1\to 1} & C^{y\to y}_{1\to 1,1\to 1} & \cdots \\ C^{y\to y}_{1\to 0,1\to 0} & C^{y\to y}_{1\to 1,1\to 0} & C^{y\to y}_{1\to 1,1\to 0} & C^{y\to y}_{1\to 0,1\to 1} & C^{y\to y}_{1\to 0,1\to 1} & C^{y\to y}_{1\to 1,1\to 1} & C^{y\to y}_{1\to 1,1\to 1} & C^{y\to y}_{1\to 1,1\to 1} & C^{y\to y}_{1\to 1,1\to 1} & \cdots \\ \vdots & \vdots & \vdots & \vdots & \vdots & \vdots & \vdots & \vdots & \vdots & \ddots \\ \hline C^{x\to y}_{0\to 0,0\to 0} & C^{x\to y}_{0\to 1,0\to 0} & C^{x\to y}_{0\to 1,0\to 0} & C^{x\to y}_{0\to 0,0\to 1} & C^{x\to y}_{0\to 0,0\to 1} & C^{x\to y}_{0\to 1,0\to 1} & C^{x\to y}_{0\to 1,0\to 1} & C^{x\to y}_{0\to 1,0\to 1} & C^{x\to y}_{0\to 1,0\to 1} & \cdots \\ C^{x\to y}_{1\to 0,0\to 0} & C^{x\to y}_{1\to 1,0\to 0} & C^{x\to y}_{1\to 1,0\to 0} & C^{x\to y}_{1\to 0,0\to 1} & C^{x\to y}_{1\to 0,0\to 1} & C^{x\to y}_{1\to 1,0\to 1} & C^{x\to y}_{1\to 1,0\to 1} & C^{x\to y}_{1\to 1,0\to 1} & C^{x\to y}_{1\to 1,0\to 1} & \cdots \\ -C^{x\to y}_{1\to 0,0\to 0} & -C^{x\to y}_{1\to 1,0\to 0} & -C^{x\to y}_{1\to 1,0\to 0} & -C^{x\to y}_{1\to 0,0\to 1} & -C^{x\to y}_{1\to 0,0\to 1} & -C^{x\to y}_{1\to 1,0\to 1} & -C^{x\to y}_{1\to 1,0\to 1} & -C^{x\to y}_{1\to 1,0\to 1} & -C^{x\to y}_{1\to 1,0\to 1} & \cdots \\ C^{x\to y}_{0\to 0,1\to 0} & C^{x\to y}_{0\to 1,1\to 0} & C^{x\to y}_{0\to 1,1\to 0} & C^{x\to y}_{0\to 0,1\to 1} & C^{x\to y}_{0\to 0,1\to 1} & C^{x\to y}_{0\to 1,1\to 1} & C^{x\to y}_{0\to 1,1\to 1} & C^{x\to y}_{0\to 1,1\to 1} & C^{x\to y}_{0\to 1,1\to 1} & \cdots \\ -C^{x\to y}_{0\to 0,1\to 0} & -C^{x\to y}_{0\to 1,1\to 0} & -C^{x\to y}_{0\to 1,1\to 0} & -C^{x\to y}_{0\to 0,1\to 1} & -C^{x\to y}_{0\to 0,1\to 1} & -C^{x\to y}_{0\to 1,1\to 1} & -C^{x\to y}_{0\to 1,1\to 1} & -C^{x\to y}_{0\to 1,1\to 1} & -C^{x\to y}_{0\to 1,1\to 1} & \cdots \\ C^{x\to y}_{1\to 0,1\to 0} & C^{x\to y}_{1\to 1,1\to 0} & C^{x\to y}_{1\to 1,1\to 0} & C^{x\to y}_{1\to 0,1\to 1} & C^{x\to y}_{1\to 0,1\to 1} & C^{x\to y}_{1\to 1,1\to 1} & C^{x\to y}_{1\to 1,1\to 1} & C^{x\to y}_{1\to 1,1\to 1} & C^{x\to y}_{1\to 1,1\to 1} & \cdots \\ -C^{x\to y}_{1\to 0,1\to 0} & -C^{x\to y}_{1\to 1,1\to 0} & -C^{x\to y}_{1\to 1,1\to 0} & -C^{x\to y}_{1\to 0,1\to 1} & -C^{x\to y}_{1\to 0,1\to 1} & -C^{x\to y}_{1\to 1,1\to 1} & -C^{x\to y}_{1\to 1,1\to 1} & -C^{x\to y}_{1\to 1,1\to 1} & -C^{x\to y}_{1\to 1,1\to 1} & \cdots \\ -C^{x\to y}_{0\to 0,1\to 0} & -C^{x\to y}_{0\to 1,1\to 0} & -C^{x\to y}_{0\to 1,1\to 0} & -C^{x\to y}_{0\to 0,1\to 1} & -C^{x\to y}_{0\to 0,1\to 1} & -C^{x\to y}_{0\to 1,1\to 1} & -C^{x\to y}_{0\to 1,1\to 1} & -C^{x\to y}_{0\to 1,1\to 1} & -C^{x\to y}_{0\to 1,1\to 1} & \cdots \\ C^{x\to y}_{1\to 0,1\to 0} & C^{x\to y}_{1\to 1,1\to 0} & C^{x\to y}_{1\to 1,1\to 0} & C^{x\to y}_{1\to 0,1\to 1} & C^{x\to y}_{1\to 0,1\to 1} & C^{x\to y}_{1\to 1,1\to 1} & C^{x\to y}_{1\to 1,1\to 1} & C^{x\to y}_{1\to 1,1\to 1} & C^{x\to y}_{1\to 1,1\to 1} & \cdots \\ \vdots & \vdots & \vdots & \vdots & \vdots & \vdots & \vdots & \vdots & \vdots & \ddots \end{array}\right]$$

$$\cdots \left[\begin{array}{ccccccccccc} C^{y\to x}_{0\to 0,0\to 0} & C^{y\to x}_{0\to 1,0\to 0} & -C^{y\to x}_{0\to 1,0\to 0} & C^{y\to x}_{0\to 0,0\to 1} & -C^{y\to x}_{0\to 0,0\to 1} & C^{y\to x}_{0\to 1,0\to 1} & -C^{y\to x}_{0\to 1,0\to 1} & -C^{y\to x}_{0\to 1,0\to 1} & C^{y\to x}_{0\to 1,0\to 1} & \cdots \\ C^{y\to x}_{1\to 0,0\to 0} & C^{y\to x}_{1\to 1,0\to 0} & -C^{y\to x}_{1\to 1,0\to 0} & C^{y\to x}_{1\to 0,0\to 1} & -C^{y\to x}_{1\to 0,0\to 1} & C^{y\to x}_{1\to 1,0\to 1} & -C^{y\to x}_{1\to 1,0\to 1} & -C^{y\to x}_{1\to 1,0\to 1} & C^{y\to x}_{1\to 1,0\to 1} & \cdots \\ C^{y\to x}_{1\to 0,0\to 0} & C^{y\to x}_{1\to 1,0\to 0} & -C^{y\to x}_{1\to 1,0\to 0} & C^{y\to x}_{1\to 0,0\to 1} & -C^{y\to x}_{1\to 0,0\to 1} & C^{y\to x}_{1\to 1,0\to 1} & -C^{y\to x}_{1\to 1,0\to 1} & -C^{y\to x}_{1\to 1,0\to 1} & C^{y\to x}_{1\to 1,0\to 1} & \cdots \\ C^{y\to x}_{0\to 0,1\to 0} & C^{y\to x}_{0\to 1,1\to 0} & -C^{y\to x}_{0\to 1,1\to 0} & C^{y\to x}_{0\to 0,1\to 1} & -C^{y\to x}_{0\to 0,1\to 1} & C^{y\to x}_{0\to 1,1\to 1} & -C^{y\to x}_{0\to 1,1\to 1} & -C^{y\to x}_{0\to 1,1\to 1} & C^{y\to x}_{0\to 1,1\to 1} & \cdots \\ C^{y\to x}_{0\to 0,1\to 0} & C^{y\to x}_{0\to 1,1\to 0} & -C^{y\to x}_{0\to 1,1\to 0} & C^{y\to x}_{0\to 0,1\to 1} & -C^{y\to x}_{0\to 0,1\to 1} & C^{y\to x}_{0\to 1,1\to 1} & -C^{y\to x}_{0\to 1,1\to 1} & -C^{y\to x}_{0\to 1,1\to 1} & C^{y\to x}_{0\to 1,1\to 1} & \cdots \\ C^{y\to x}_{1\to 0,1\to 0} & C^{y\to x}_{1\to 1,1\to 0} & -C^{y\to x}_{1\to 1,1\to 0} & C^{y\to x}_{1\to 0,1\to 1} & -C^{y\to x}_{1\to 0,1\to 1} & C^{y\to x}_{1\to 1,1\to 1} & -C^{y\to x}_{1\to 1,1\to 1} & -C^{y\to x}_{1\to 1,1\to 1} & C^{y\to x}_{1\to 1,1\to 1} & \cdots \\ C^{y\to x}_{1\to 0,1\to 0} & C^{y\to x}_{1\to 1,1\to 0} & -C^{y\to x}_{1\to 1,1\to 0} & C^{y\to x}_{1\to 0,1\to 1} & -C^{y\to x}_{1\to 0,1\to 1} & C^{y\to x}_{1\to 1,1\to 1} & -C^{y\to x}_{1\to 1,1\to 1} & -C^{y\to x}_{1\to 1,1\to 1} & C^{y\to x}_{1\to 1,1\to 1} & \cdots \\ C^{y\to x}_{1\to 0,1\to 0} & C^{y\to x}_{1\to 1,1\to 0} & -C^{y\to x}_{1\to 1,1\to 0} & C^{y\to x}_{1\to 0,1\to 1} & -C^{y\to x}_{1\to 0,1\to 1} & C^{y\to x}_{1\to 1,1\to 1} & -C^{y\to x}_{1\to 1,1\to 1} & -C^{y\to x}_{1\to 1,1\to 1} & C^{y\to x}_{1\to 1,1\to 1} & \cdots \\ \vdots & \vdots & \vdots & \vdots & \vdots & \vdots & \vdots & \vdots & \vdots & \ddots \\ \hline C^{x\to x}_{0\to 0,0\to 0} & C^{x\to x}_{0\to 1,0\to 0} & -C^{x\to x}_{0\to 1,0\to 0} & C^{x\to x}_{0\to 0,0\to 1} & -C^{x\to x}_{0\to 0,0\to 1} & C^{x\to x}_{0\to 1,0\to 1} & -C^{x\to x}_{0\to 1,0\to 1} & -C^{x\to x}_{0\to 1,0\to 1} & C^{x\to x}_{0\to 1,0\to 1} & \cdots \\ C^{x\to x}_{1\to 0,0\to 0} & C^{x\to x}_{1\to 1,0\to 0} & -C^{x\to x}_{1\to 1,0\to 0} & C^{x\to x}_{1\to 0,0\to 1} & -C^{x\to x}_{1\to 0,0\to 1} & C^{x\to x}_{1\to 1,0\to 1} & -C^{x\to x}_{1\to 1,0\to 1} & -C^{x\to x}_{1\to 1,0\to 1} & C^{x\to x}_{1\to 1,0\to 1} & \cdots \\ -C^{x\to x}_{1\to 0,0\to 0} & -C^{x\to x}_{1\to 1,0\to 0} & C^{x\to x}_{1\to 1,0\to 0} & -C^{x\to x}_{1\to 0,0\to 1} & C^{x\to x}_{1\to 0,0\to 1} & -C^{x\to x}_{1\to 1,0\to 1} & C^{x\to x}_{1\to 1,0\to 1} & C^{x\to x}_{1\to 1,0\to 1} & -C^{x\to x}_{1\to 1,0\to 1} & \cdots \\ C^{x\to x}_{0\to 0,1\to 0} & C^{x\to x}_{0\to 1,1\to 0} & -C^{x\to x}_{0\to 1,1\to 0} & C^{x\to x}_{0\to 0,1\to 1} & -C^{x\to x}_{0\to 0,1\to 1} & C^{x\to x}_{0\to 1,1\to 1} & -C^{x\to x}_{0\to 1,1\to 1} & -C^{x\to x}_{0\to 1,1\to 1} & C^{x\to x}_{0\to 1,1\to 1} & \cdots \\ -C^{x\to x}_{0\to 0,1\to 0} & -C^{x\to x}_{0\to 1,1\to 0} & C^{x\to x}_{0\to 1,1\to 0} & -C^{x\to x}_{0\to 0,1\to 1} & C^{x\to x}_{0\to 0,1\to 1} & -C^{x\to x}_{0\to 1,1\to 1} & C^{x\to x}_{0\to 1,1\to 1} & C^{x\to x}_{0\to 1,1\to 1} & -C^{x\to x}_{0\to 1,1\to 1} & \cdots \\ C^{x\to x}_{1\to 0,1\to 0} & C^{x\to x}_{1\to 1,1\to 0} & -C^{x\to x}_{1\to 1,1\to 0} & C^{x\to x}_{1\to 0,1\to 1} & -C^{x\to x}_{1\to 0,1\to 1} & C^{x\to x}_{1\to 1,1\to 1} & -C^{x\to x}_{1\to 1,1\to 1} & -C^{x\to x}_{1\to 1,1\to 1} & C^{x\to x}_{1\to 1,1\to 1} & \cdots \\ -C^{x\to x}_{1\to 0,1\to 0} & -C^{x\to x}_{1\to 1,1\to 0} & C^{x\to x}_{1\to 1,1\to 0} & -C^{x\to x}_{1\to 0,1\to 1} & C^{x\to x}_{1\to 0,1\to 1} & -C^{x\to x}_{1\to 1,1\to 1} & C^{x\to x}_{1\to 1,1\to 1} & C^{x\to x}_{1\to 1,1\to 1} & -C^{x\to x}_{1\to 1,1\to 1} & \cdots \\ -C^{x\to x}_{1\to 0,1\to 0} & -C^{x\to x}_{1\to 1,1\to 0} & C^{x\to x}_{1\to 1,1\to 0} & -C^{x\to x}_{1\to 0,1\to 1} & C^{x\to x}_{1\to 0,1\to 1} & -C^{x\to x}_{1\to 1,1\to 1} & C^{x\to x}_{1\to 1,1\to 1} & C^{x\to x}_{1\to 1,1\to 1} & -C^{x\to x}_{1\to 1,1\to 1} & \cdots \\ C^{x\to x}_{1\to 0,1\to 0} & C^{x\to x}_{1\to 1,1\to 0} & -C^{x\to x}_{1\to 1,1\to 0} & C^{x\to x}_{1\to 0,1\to 1} & -C^{x\to x}_{1\to 0,1\to 1} & C^{x\to x}_{1\to 1,1\to 1} & -C^{x\to x}_{1\to 1,1\to 1} & -C^{x\to x}_{1\to 1,1\to 1} & C^{x\to x}_{1\to 1,1\to 1} & \cdots \\ \vdots & \vdots & \vdots & \vdots & \vdots & \vdots & \vdots & \vdots & \vdots & \ddots \end{array}\right] \begin{bmatrix} E_{y,0,0} \\ E_{y,1,0} \\ E_{y,1,0} \\ E_{y,0,1} \\ E_{y,0,1} \\ E_{y,1,1} \\ E_{y,1,1} \\ E_{y,1,1} \\ E_{y,1,1} \\ \vdots \\ \hline E_{x,0,0} \\ E_{x,1,0} \\ E_{x,1,0} \\ E_{x,0,1} \\ E_{x,0,1} \\ E_{x,1,1} \\ E_{x,1,1} \\ E_{x,1,1} \\ E_{x,1,1} \\ \vdots \end{bmatrix} \tag{D.3.13}$$

This system of equations can be reduced in size without any loss of generality as follows:

$$\frac{\partial^2}{\partial z'^2}\begin{bmatrix} E_{y,0,0} \\ E_{y,1,0} \\ E_{y,0,1} \\ E_{y,1,1} \\ \vdots \\ \hline E_{x,0,0} \\ E_{x,1,0} \\ E_{x,0,1} \\ E_{x,1,1} \\ \vdots \end{bmatrix} = \left[\begin{array}{cccc:c} C^{y\to y}_{0\to 0,0\to 0} & 2C^{y\to y}_{0\to 1,0\to 0} & 2C^{y\to y}_{0\to 0,0\to 1} & 4C^{y\to y}_{0\to 1,0\to 1} & \cdots \\ C^{y\to y}_{1\to 0,0\to 0} & 2C^{y\to y}_{1\to 1,0\to 0} & 2C^{y\to y}_{1\to 0,0\to 1} & 4C^{y\to y}_{1\to 1,0\to 1} & \cdots \\ C^{y\to y}_{0\to 1,0\to 0} & 2C^{y\to y}_{0\to 1,1\to 0} & 2C^{y\to y}_{0\to 0,1\to 1} & 4C^{y\to y}_{0\to 1,1\to 1} & \cdots \\ C^{y\to y}_{1\to 0,1\to 0} & 2C^{y\to y}_{1\to 1,1\to 0} & 2C^{y\to y}_{1\to 0,1\to 1} & 4C^{y\to y}_{1\to 1,1\to 1} & \cdots \\ \vdots & \vdots & \vdots & \vdots & \ddots \\ \hline C^{x\to y}_{0\to 0,0\to 0} & 2C^{x\to y}_{0\to 1,0\to 0} & 2C^{x\to y}_{0\to 0,0\to 1} & 4C^{x\to y}_{0\to 1,0\to 1} & \cdots \\ 0 & 0 & 0 & 0 & \cdots \\ 0 & 0 & 0 & 0 & \cdots \\ 0 & 0 & 0 & 0 & \cdots \\ \vdots & \vdots & \vdots & \vdots & \ddots \end{array}\right] \left[\begin{array}{c:c} C^{x\to y}_{0\to 0,0\to 0} & \begin{matrix} 0 & 0 & 0 & \cdots \end{matrix} \\ C^{x\to y}_{0\to 0,0\to 0} & \begin{matrix} 0 & 0 & 0 & \cdots \end{matrix} \\ C^{x\to y}_{0\to 0,0\to 0} & \begin{matrix} 0 & 0 & 0 & \cdots \end{matrix} \\ C^{x\to y}_{0\to 0,0\to 0} & \begin{matrix} 0 & 0 & 0 & \cdots \end{matrix} \\ \vdots & \begin{matrix} \vdots & \vdots & \vdots & \ddots \end{matrix} \\ \hline C^{x\to y}_{0\to 0,0\to 0} & \begin{matrix} 0 & 0 & 0 & \cdots \end{matrix} \\ 0 & \begin{matrix} 0 & 0 & 0 & \cdots \end{matrix} \\ 0 & \begin{matrix} 0 & 0 & 0 & \cdots \end{matrix} \\ 0 & \begin{matrix} 0 & 0 & 0 & \cdots \end{matrix} \\ \vdots & \begin{matrix} \vdots & \vdots & \vdots & \ddots \end{matrix} \end{array}\right] \begin{bmatrix} E_{y,0,0} \\ E_{y,1,0} \\ E_{y,0,1} \\ E_{y,1,1} \\ \vdots \\ \hline E_{x,0,0} \\ E_{x,1,0} \\ E_{x,0,1} \\ E_{x,1,1} \\ \vdots \end{bmatrix} \tag{D.3.14}$$

A further reduction of the matrix is then possible by eliminating the rows and columns containing all zero values, leading to a final reduced matrix eigenvalue equation.

$$\frac{\partial^2}{\partial z'^2}\begin{bmatrix} E_{y,0,0} \\ E_{y,1,0} \\ E_{y,0,1} \\ E_{y,1,1} \\ \vdots \\ \hline E_{x,0,0} \\ \vdots \end{bmatrix} = \left[\begin{array}{cccc|c} C^{y\to y}_{0\to 0,0\to 0} & C^{y\to y}_{0\to 1,0\to 0} & C^{y\to y}_{0\to 0,0\to 1} & C^{y\to y}_{0\to 1,0\to 1} & \cdots \\ C^{y\to y}_{1\to 0,0\to 0} & C^{y\to y}_{1\to 1,0\to 0} & C^{y\to y}_{1\to 0,0\to 1} & C^{y\to y}_{1\to 1,0\to 1} & \cdots \\ C^{y\to y}_{0\to 1,1\to 0} & C^{y\to y}_{0\to 1,1\to 0} & C^{y\to y}_{0\to 0,1\to 1} & C^{y\to y}_{0\to 1,1\to 1} & \cdots \\ C^{y\to y}_{1\to 0,1\to 0} & C^{y\to y}_{1\to 1,1\to 0} & C^{y\to y}_{1\to 0,1\to 1} & C^{y\to y}_{1\to 1,1\to 1} & \cdots \\ \vdots & \vdots & \vdots & \vdots & \ddots \\ \hline C^{x\to y}_{0\to 0,0\to 0} & C^{x\to y}_{0\to 1,0\to 0} & C^{x\to y}_{0\to 0,0\to 1} & C^{x\to y}_{0\to 1,0\to 1} & \cdots \\ \vdots & \vdots & \vdots & \vdots & \ddots \end{array}\right] \left[\begin{array}{c|c} C^{y\to x}_{0\to 0,0\to 0} & \cdots \\ C^{y\to x}_{1\to 0,0\to 0} & \cdots \\ C^{y\to x}_{0\to 0,1\to 0} & \cdots \\ C^{y\to x}_{1\to 0,1\to 0} & \cdots \\ \vdots & \ddots \\ \hline C^{x\to x}_{0\to 0,0\to 0} & \cdots \\ \vdots & \ddots \end{array}\right] \begin{bmatrix} E_{y,0,0} \\ E_{y,1,0} \\ E_{y,0,1} \\ E_{y,1,1} \\ \vdots \\ \hline E_{x,0,0} \\ \vdots \end{bmatrix} \tag{D.3.15}$$

For a system possessing x-polarization, with an input field polarized in the *x*-direction, the relationships between the electric and magnetic field harmonic elements are the following:

$$E_{x,m,n} = E_{x,m,-n} = E_{x,-m,n} = E_{x,-m,-n} \tag{D.3.16}$$

$$E_{y,m,n} = -E_{y,m,-n} = -E_{y,-m,n} = E_{y,-m,-n} \tag{D.3.17}$$

$$H_{x,m,n} = -H_{x,m,-n} = -H_{x,-m,n} = H_{x,-m,-n} \tag{D.3.18}$$

$$H_{y,m,n} = H_{y,m,-n} = H_{y,-m,n} = H_{y,-m,-n} \tag{D.3.19}$$

Determining the reduced eigenvalue equation matrix in this case follows similar logic to the derivation in Equations (D.3.6) – (D.3.15).

APPENDIX E. COMMENTS ON SOFTWARE DEVELOPMENT AND DESIGN

When developing the software necessary for the modeling of integrated optical device structures (or any other physical modeling problem for that matter), perfecting the algorithms used for determining layer eigenmodes, wave propagation, and field calculations are only part of the overall computer aided design problem that must be tackled. In order to create a flexible, versatile, and efficient package capable of modeling a variety of different integrated optical structures through a single interface, the entire computational workflow, from defining input parameters to post-processing of output data, needs to be designed in a cohesive manner. While perfecting "the solver" is vitally important, the overall efficiency of the solver is often affected by the quality of the input data being passed to the solver. The entire workflow in an RCWA/S-Matrix computation can take on a number of different forms based on the structure being modeled and the desired output data, but the most common RCWA/S-Matrix workflow can be summarized in the following steps:

1. The geometric and material properties are defined for a device under study.

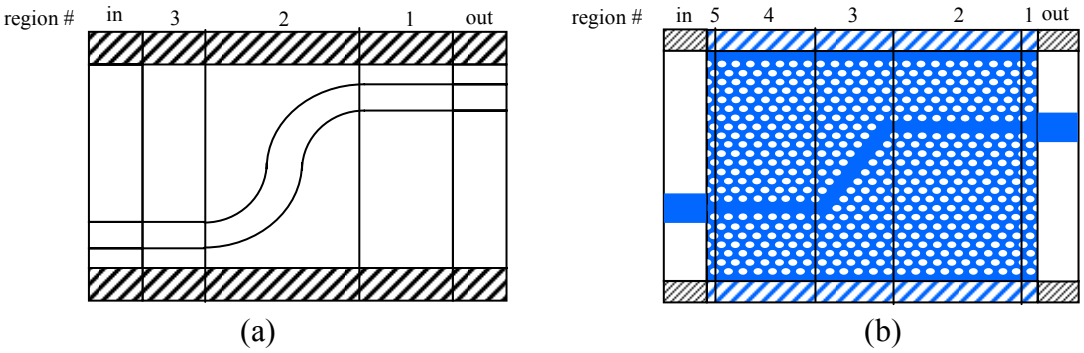

(a) (b)

Figure E-1 (a) Initial "region" layout of the electromagnetic/geometric features in an S-bend waveguide. The geometric features are initially defined as a background permittivity / permeability distribution, rectangular boxes, and annular bends in this case. (b) Initial "region" layout of the electromagnetic/geometric features in a photonic crystal waveguide. The geometric features are initially defined as input/output rectangular boxes, a background permittivity / permeability distribution, a lattice of holes, and individual "defect" sites.

2. The device geometry is then approximated by a stair-cased set of finite thickness, transversely periodic layers whose material properties are longitudinally invariant within each layer, as well as semi-infinite input and output half-space regions.

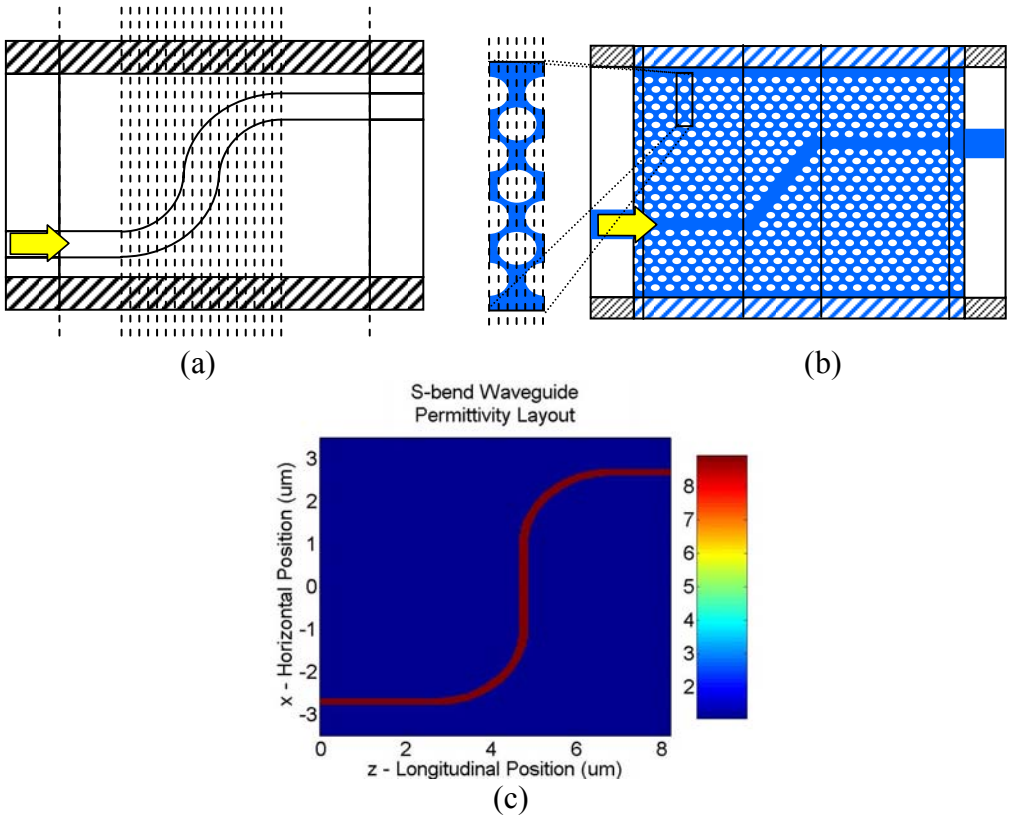

Figure E-2 (a) Longitudinal slicing associated with an S-bend photonic wire waveguide. (b) Longitudinal slicing associated with a bend in a photonic crystal waveguide. (c) Calculated permittivity layout for an S-bend photonic wire waveguide on a transverse and longitudinal spatial grid.

3. Employing properties of a defined input wave (wavelength, angle, and polarization); a global, pseudo-periodic Fourier harmonic basis set is then utilized to represent both the periodic material properties of a transverse unit cell, as well as the tangential phase components of each plane wave basis function.

4. Making appropriate substitutions into Maxwell's equations, these material property and tangential phase expansions are used to create a unique full matrix eigenmode problem for each layer of the system.
5. After determining all desired layer eigenmodes, calculating the field harmonic amplitude distributions in the input and output half-spaces, and optionally throughout the entire multilayered structure, is then accomplished by propagating the defined input energy distribution through the use of a scattering matrix (S-Matrix) mode matching technique that relates the eigenmodes in adjacent layers, as well as Redheffer's star-product operation for concatenating two separate scattering matrices into a larger longitudinal cell scattering matrix.
6. The spatial field harmonic amplitudes throughout the structure can then be used to calculate the modal reflection and transmission coefficients of the system and can be summed on an arbitrary spatial grid in order to visualize the system's distribution of electric fields, magnetic fields, and Poynting vector components.

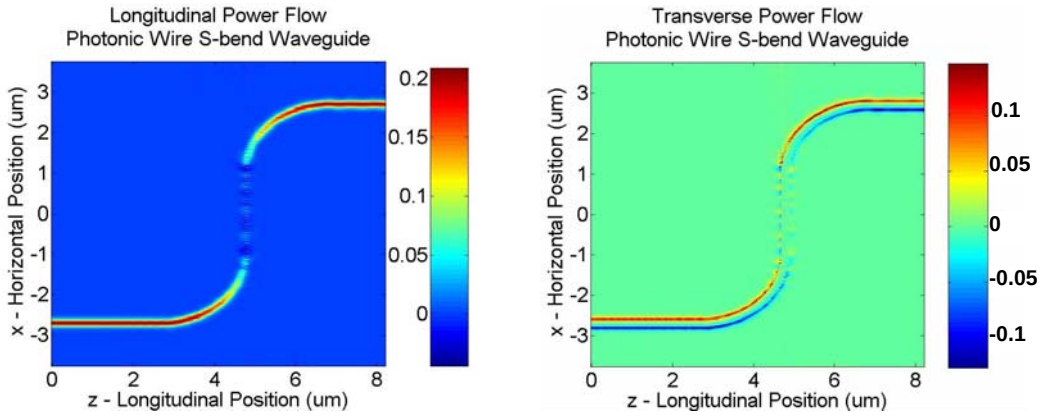

Figure E-3 Calculated Poynting vector magnitudes for power flow through an S-bend waveguide on a transverse and longitudinal spatial grid showing both the (a) longitudinal components (b) transverse components.

7. Post-processing of the output data can then occur for a single set of inputs, the entire process can be repeated numerous times over a single parameter range to obtain a spectral response, or a multi-parameter optimization/evolutionary algorithm study can be performed.

This appendix will discuss how all of these points were addressed in order to write the software used to produce the computational results presented in this dissertation. Much of this section will only be useful when attempting to dissect meanings when viewing the actual code. The code utilized to perform many of the kinds of computations performed in this dissertation will eventually be posted on-line at the MATLAB® Central File Exchange website [172].

E.1 Initial Definition of the Input Wave and Input Geometry

When defining input parameters for an RCWA model, there are three distinct sets of parameters that must be defined initially. The first set of parameters is that set associated with the input plane-wave/mode properties, as well as any variables that are independent of the underlying geometry and materials. Included in this set are the wavelength, incident angle (polar, azimuthal, polarization), and optionally the incident finite beam waist and number of plane waves used to approximate that finite beam, as well as a number of other parameters that determine the nature of the information that is to be determined.

Variable Name	Type	Description
input_order	scalar	In a "Grating" problem, this determines position within the Kronecker delta function for which there is a non-zero value (MATLAB® array ordering is "1-based" like Fortran and not "0-based" like C or Python).
number_of_modes	scalar	In a "Waveguide" problem, this variable determines the number of input modes for which field and power distributions will be calculated.
lambda	scalar	Wavelength in microns.
theta	scalar	Polar angle in degrees
phi	scalar	Azimuthal angle in degrees
polarization_angle	scalar	Polarization angle in degrees
eta	scalar	Grating periodicity tilt angle for non-orthogonal periodicity directions.
Nx	scalar	Number of spatial harmonics utilized along the x-axis in Fourier space.
Ny	scalar	Number of spatial harmonics utilized along the y-axis in Fourier space.
bow	scalar	Bowing parameter used in truncating the total number of harmonics utilized on a 2D grid. Parameter varies from 0 to 1, and keeps all harmonics bounded by the equation: $\left(\frac{x_{\text{harmonic index}}}{\left(\frac{N_x - 1}{2}\right)^2}\right)^{bow} + \left(\frac{y_{\text{harmonic index}}}{\left(\frac{N_y - 1}{2}\right)^2}\right)^{bow} \leq 1$
beam_x_harmonics	scalar	Number of x-direction plane waves used in the spectral decomposition of an input finite beam for a "Grating" problem.
beam_y_harmonics	scalar	Number of y-direction plane waves used in the spectral decomposition of an input finite beam for a "Grating" problem.
beamwaist_xp	scalar	The beam waist in the x-direction of an input finite beam used in a "Grating" problem.

beamwaist_yp	scalar	The beam waist in the y-direction of an input finite beam used in a "Grating" problem.
real_pole_initial	scalar	The value of the real part of the tangential propagation constant utilized in an iterative search for a scattering matrix pole using the iterative technique described in Peng [23].
imag_pole_initial	scalar	The value of the imaginary part of the tangential propagation constant utilized in an iterative search for a scattering matrix pole using the iterative technique described in Peng [23].
pole_determinant_tolerance	scalar	The tolerance value used for stopping the iterative process of determining a scattering matrix pole using the iterative technique described in Peng [23].
grid_truncation	string	A string variable that can be set to "on" or "off" that determines whether a 2D grid of Fourier harmonics will be truncated.
diffraction_type	string	A string variable that sets the problem as either "TE", "TM", "conical", or "twodimensional."
StructureType	string	A string variable that can be set as either "Waveguide" or "Grating". A "Grating" problem by-passes the calculation of all internal field harmonics and only determines the reflection and transmission coefficients in the input and output half-spaces. A "Waveguide" problem allows for the possibility of determining of all desired internal layer fields.
symmetry	string	A string variable that defines the type of symmetry that is present in a particular model ("sigx", "sigy", "c2v", "off").
polarization	string	A string variable that defines the polarization direction of the input wave/mode that is used in symmetry calculations.
perm_expansion	string	A string variable that determines the type of Fourier expansion technique utilized in a 2D grating problem. A value of "regular" uses a standard Fourier expansion in both the x- and y-directions, whereas a value of "inverse" uses a Fast Fourier Factorization technique.
pole_search_type	string	A string variable that defines the type of scattering matrix utilized in the pole search. A value of "transverse"

calculateScatteringMatrices	logical	A logical variable that determines whether any scattering matrices are calculated in either a “Waveguide” or “Grating” problem.
fieldandpowercalculations	logical	A logical variable that determines whether any electric/magnetic field or Poynting vector calculations are performed.
boxedfieldandpowercalculations	logical	A logical variable that determines whether field and power calculations are determined on a full grid or only around a box of the domain.
determineBoxedPower	logical	A logical variable that determines whether the Poynting vector components around a box of the computational domain are summed to determine potential conservation of energy.
calculateFieldHarmonicAmplitudes	logical	A logical variable that determines whether any field harmonic amplitudes are calculated in a “Waveguide” problem.
calculateOnlyInputOutputField Harmonics	logical	A logical variable that determines whether or not the field harmonics in a “Waveguide” problem are only determined in the input and output half-spaces or whether internal field harmonics are calculated as well.
calculatePermMaps	logical	A logical variable that determines whether or not a map of the permittivity, permeability, and absorption/gain are calculated on a spatial grid.
plotInputFiniteBeam	logical	A logical variable that determines whether or not the fields and Poynting vector components of an input finite beam are calculated for a “Grating” problem.
xy_cylinder_present	logical	A logical variable that defines whether or not any cylinder features (with an axis in the longitudinal direction) is present any where in the model. This affects the type of coupling coefficient expansion utilized.
pole_search	logical	A logical variable that determines whether the current structure is used in a scattering matrix pole search.
calculateGeneralizedEigenvalues	logical	A logical variable that determines whether the current structure, or part thereof, is used in a scattering matrix generalized eigenvalue problem of the form in Cao et al. [22]

longitudinalFourierTransform	logical	A logical variable that determines whether the longitudinal field and power components are utilized in an angular spectrum calculation. This angular spectrum can be utilized to propagate a field using a Discrete Fourier Transform.
etched_layers_known	logical	A logical variable used as a switch statement that run code that exploits the binary nature of a material variation in defining eigenproblem and scattering matrix labels. When a geometric/material structure contains the necessary properties, this switch runs a much more efficient code for defining these labels that avoids layer comparison.
material_wavelength_dispersion_ present	logical	A logical variable used as a switch to run code that exploits wavelength dependent material properties.

The second set of parameters includes all relevant geometric distances for the features being modeled as well as their associated electromagnetic material property values (complex permittivity, complex permeability), and the window sizes/grating periodicities which define the transverse boundaries of computational region.

LAMBDA_x	scalar	Period/Window size in x-direction
LAMBDA_y	scalar	Period/Window size in y-direction or second periodic direction if non-orthogonal periodicity directions are present.
eps_background	scalar	Background permittivity for the entire computational domain.
mu_background	scalar	Background permeability for the entire computational domain.
geometric_tolerance	scalar	A scalar value that is used as an acceptable fitting tolerance for all geometric processing and Geometric Bounding Toolbox calculations.
epsn	1D-vector	Permittivity value of the zero-thickness layers (epsn(1)) for "Waveguide" or "Grating" problems, and input halfspace (epsn(2)), and output halfspace (epsn(3)) for "Grating" problems.

mu	1D-vector	Permeability value of the zero-thickness layers (mu(1)) for "Waveguide" or "Grating" problems, and input halfspace (mu(2)), and output halfspace (mu(3)) for "Grating" problems.

Further geometric parameters that define the number of lamellar slices that will be used in representing the target geometric features must also be defined. Included in this set of slicing parameters are parameters that determine the number of slices within a longitudinal unit cell as well as parameters that determine the nature of any longitudinal periodicity that is to be represented in the system.

regions	scalar	A variable defining the number of major longitudinal partitions into which the modeled structure is split.
unit_cells	1D-array of size regions	An array of size regions where each element of the array is the number of elementary longitudinal unit cells (power of 2) contained within a larger conglomerate longitudinal cell called a "region cell" for this region.
reg_cells	1D-array of size regions	An array of size regions where each element of the array is the number of "region cells" (power of 2) contained within a larger conglomerate longitudinal cell called a "section cell" for this region.
w_z	1D cell of size regions	A cell array of size regions where each element of the cell array is an array whose size is the number of slices in an elementary unit cell and where each scalar element is the thickness of an individual slice. This thickness array is ordered from output side as the first element to input side as the output element.
internalslices	1D cell of size regions	A cell array of size regions where each element of the cell array is an array whose size is the number of slices in an elementary unit cell and where each scalar element is the number of locations internal to an individual layer where the field harmonic amplitudes are calculated. The internalslices array within each cell element is ordered from output side as the first element to input side as the output element.
Left	scalar	The negative x location boundary used in laying out the spatial grid for field, power, and perm map calculations.
Right	scalar	The positive x location boundary used in laying out the spatial grid for field, power, and perm map calculations.

x_points	scalar	The number of points used in the x-direction spatial grid for field, power, and perm map calculations.
x	1D-array of size x_points	An array of the x-axis locations for the spatial grid used in calculating field, power, and perm map calculations.
Top	scalar	The positive y location boundary used in laying out the spatial grid for field, power and perm map calculations.
Bottom	scalar	The negative y location boundary used in laying out the spatial grid for field, power and perm map calculations.
y_points	scalar	The number of points used in the y-direction spatial grid for field, power, and perm map calculations.
y	1D-array of size x_points	An array of the y-axis locations for the spatial grid used in calculating field, power, and perm map calculations.

E.2 Performing the Necessary Layer Slicing

In the context of the present work/method, the entire computational domain for a given device structure is split into initial partitions that we call "regions." The naming conventions that were utilized for naming variables in this study evolved over time and may seem a bit confusing to anyone but the author, but hopefully not overly confusing. While the use of object-oriented concepts may have been useful, much of the infrastructure of the code was written before these concepts were considered. Within the code itself, one of the main concepts utilized is a "region," which is an array of data structures representing these major layer partitions that can have a number of possible fields from among the following:

region		
slice	data structure	A data structure itself that contains fields associated with the properties of each individual lamellar layer within an individual "region" unit cell.
slices	scalar	The total number of lamellar layers within an individual "region" elementary unit cell.
symmetric	logical	A logical parameter associated with a given region's longitudinal symmetry or asymmetry properties.

unit_cells	scalar	The number of elementary longitudinal unit cells (power of 2) contained within a larger conglomerate longitudinal cell called a "region cell" for this region.
reg_cells	scalar	The number of "region cells" (power of 2) contained within a larger conglomerate longitudinal cell called a "section cell" for this region.
plotunitcells	logical	A logical parameter used to determine whether field harmonics are calculated at the interfaces on the exterior of every unit cell contained within a region cell, or whether the field harmonics are only calculated on the exterior interfaces of a region cell.
plotslices	logical	A logical parameter used to determine whether field harmonics are calculated at the interfaces of all layers within an elementary unit cell for a region. If "plotunitcells" is false, then this parameter's value has no importance for this region.
symunitscatterlabel	scalar	A label that uniquely identifies the particular elementary longitudinal "unit cell" symmetric scattering matrix associated with this region. If a region consists of only one slice, or if there are no field harmonics to be calculated where a symmetric unit cell scattering matrix associated with this region is needed, then this field remains empty for this region.
symregscatterlabel	scalar	A label that uniquely identifies the particular "region cell" symmetric scattering matrix associated with this region. If a region has only one slice or one "unit cell", or if there are no field harmonics to be calculated where a symmetric region cell scattering matrix associated with this region is needed, then this field remains empty for this region.
symsectionscatterlabel	scalar	A label that uniquely identifies the particular "section cell" symmetric scattering matrix associated with this region. If a region has only one slice, one "unit cell", or one "region cell", or if there are no field harmonics to be calculated where a symmetric section cell scattering matrix associated with this region is needed, then this field remains empty for this region.

asymunitscatterlabel	scalar	A label that uniquely identifies the particular elementary longitudinal "unit cell" asymmetric scattering matrix associated with this region. If a region consists of only one slice, or if there are no field harmonics to be calculated where an asymmetric unit cell scattering matrix associated with this region is needed, then this field remains empty for this region.
asymregscatterlabel	scalar	A label that uniquely identifies the particular "region cell" asymmetric scattering matrix associated with this region. If a region has only one slice or one "unit cell", or if there are no field harmonics to be calculated where an asymmetric region cell scattering matrix associated with this region is needed, then this field remains empty for this region.
asymsectionscatterlabel	scalar	A label that uniquely identifies the particular "section cell" asymmetric scattering matrix associated with this region. If a region has only one slice, one "unit cell", or one "region cell", or if there are no field harmonics to be calculated where an asymmetric section cell scattering matrix associated with this region is needed, then this field remains empty for this region.

As stated above, within an individual "region" data structure, the "slice" field is itself an array of data structures whose fields depend on the type of geometry that is best used to represent the electromagnetic object, as well as the numerical method utilized for performing the coupling coefficient expansions of the material permittivity and permeability. For a computational model having one-dimensional periodicity and light polarized in a TE, TM or conical manner, the "slice" data structure can contain the following fields:

slice		
Sx	scalar	The number of adjacent rectangular boxes into which a lamellar layer is split.
w_x	array of scalars size Sx	The absolute value of the width (in μm) of each rectangular box in a layer, ordered from the $-\Lambda_x/2$ side to the $\Lambda_x/2$ side.
x_centers	array of scalars size Sx	The absolute value of the center (in μm) of each rectangular box in a layer between $(-\Lambda_x/2, \Lambda_x/2)$, ordered from the $-\Lambda_x/2$ side to the $\Lambda_x/2$ side.
f_x	array of scalars size Sx	The relative value of the width/fill factor (between 0 and 1) of each rectangular box in a layer, ordered from the $-\Lambda_x/2$ side to the $\Lambda_x/2$ side. "w_x" divided by the grating period Λ_x.
xs	array of scalars size Sx	The relative shift of the center (between -0.5 to 0.5) of each rectangular box in a layer. "x_centers" divided by the grating period Λ_x.
eps_back	scalar	The background/reference permittivity value for a slice.
mu_back	scalar	The background/reference permeability value for a slice.
d	scalar	The thickness (in μm) of a slice.
eigenlabel	scalar	The label associated with a layer's unique eigenmode problem.
scatterlabel	scalar	The label associate with a layer's unique individual layer scattering matrix.
eps_x	array of scalars size Sx	The x-direction value of the permittivity tensor for each rectangular box in a layer.
eps_y	array of scalars size Sx	The y-direction value of the permittivity tensor for each rectangular box in a layer.
eps_z	array of scalars size Sx	The z-direction value of the permittivity tensor for each rectangular box in a layer.
mu_x	array of scalars size Sx	The x-direction value of the permeability tensor for each rectangular box in a layer.
mu_y	array of scalars size Sx	The y-direction value of the permeability tensor for each rectangular box in a layer.
mu_z	array of scalars size Sx	The z-direction value of the permeability tensor for each rectangular box in a layer.
sig_x	array of scalars size Sx	The x-direction value of the conductivity (absorption/gain parameter) tensor for each rectangular box in a layer.
sig_y	array of scalars size Sx	The y-direction value of the conductivity (absorption/gain parameter) tensor for each rectangular box in a layer.
sig_z	array of scalars size Sx	The z-direction value of the conductivity (absorption/gain parameter) tensor for each rectangular box in a layer.

For a lamellar layer having two orthogonal dimensions of periodicity with electromagnetic features formed entirely from rectangular shapes, the "slice" data structure is formed from the following fields:

slice		
Sx	scalar	The number of rows in the grid of adjacent rectangular boxes into which a lamellar layer is split.
Sy	scalar	The number of columns in the grid of adjacent rectangular boxes into which a lamellar layer is split.
w_x	array of scalars size Sx	The absolute value of the x-width (in μm) of each rectangular box in a layer, ordered from the $-\Lambda_x/2$ side to the $\Lambda_x/2$ side.
w_y	array of scalars size Sy	The absolute value of the y-width (in μm) of each rectangular box in a layer, ordered from the $-\Lambda_y/2$ side to the $\Lambda_y/2$ side.
x_centers	array of scalars size Sx	The absolute value of the x-center (in μm) of each rectangular box in a layer between $(-\Lambda_x/2, \Lambda_x/2)$, ordered from the $-\Lambda_x/2$ side to the $\Lambda_x/2$ side.
y_centers	array of scalars size Sy	The absolute value of the y-center (in μm) of each rectangular box in a layer between $(-\Lambda_y/2, \Lambda_y/2)$, ordered from the $-\Lambda_y/2$ side to the $\Lambda_y/2$ side.
f_x	array of scalars size Sx	The relative value of the x-width/fill factor (between 0 and 1) of each rectangular box in a layer, ordered from the $-\Lambda_x/2$ side to the $\Lambda_x/2$ side. "w_x" divided by the grating period Λ_x.
f_y	array of scalars size Sy	The relative value of the y-width/fill factor (between 0 and 1) of each rectangular box in a layer, ordered from the $-\Lambda_y/2$ side to the $\Lambda_y/2$ side. "w_y" divided by the grating period Λ_y.
xs	array of scalars size Sx	The relative shift of the x-center (between -0.5 to 0.5) of each rectangular box in a layer. "x_centers" divided by the grating period Λ_x.
ys	array of scalars size Sy	The relative shift of the y-center (between -0.5 to 0.5) of each rectangular box in a layer. "y_centers" divided by the grating period Λ_y.
eps_back	scalar	The background/reference permittivity value for a slice.
mu_back	scalar	The background/reference permeability value for a slice.
d	scalar	The thickness (in μm) of a slice.
eigenlabel	scalar	The label associated with a layer's unique eigenmode problem.
scatterlabel	scalar	The label associate with a layer's unique individual layer scattering matrix.
eps_x	array of scalars size (Sy,Sx)	The x-direction value of the permittivity tensor for each rectangular box in a layer.

eps_y	array of scalars size (Sy,Sx)	The y-direction value of the permittivity tensor for each rectangular box in a layer.
eps_z	array of scalars size (Sy,Sx)	The z-direction value of the permittivity tensor for each rectangular box in a layer.
mu_x	array of scalars size (Sy,Sx)	The x-direction value of the permeability tensor for each rectangular box in a layer.
mu_y	array of scalars size (Sy,Sx)	The y-direction value of the permeability tensor for each rectangular box in a layer.
mu_z	array of scalars size (Sy,Sx)	The z-direction value of the permeability tensor for each rectangular box in a layer.
sig_x	array of scalars size (Sy,Sx)	The x-direction value of the conductivity (absorption/gain parameter) tensor for each rectangular box in a layer.
sig_y	array of scalars size (Sy,Sx)	The y-direction value of the conductivity (absorption/gain parameter) tensor for each rectangular box in a layer.
sig_z	array of scalars size (Sy,Sx)	The z-direction value of the conductivity (absorption/gain parameter) tensor for each rectangular box in a layer.

For a lamellar layer having two non-orthogonal dimensions of periodicity or a layer that contains cylindrical features whose axes are in the longitudinal direction, the "slice" data structure is formed from the following fields:

slice		
S	scalar	The number of unique electromagnetic/geometric features in a lamellar layer whose properties are different from the background properties.
feature	Array of data structures of size S	A data structure that contains fields representing the geometric and material properties for each individual electromagnetic/geometric feature in a lamellar layer.
eps_back	scalar	The background/reference permittivity value for a slice.
mu_back	scalar	The background/reference permeability value for a slice.
d	scalar	The thickness (in μm) of a slice.
eigenlabel	scalar	The label associated with a layer's unique eigenmode problem.
scatterlabel	scalar	The label associate with a layer's unique individual layer scattering matrix.

feature		
w_x	array of scalars size S	The absolute value of the x-width (in μm) of each rectangular box in a layer, ordered from the $-\Lambda_x/2$ side to the $\Lambda_x/2$ side.
w_y	array of scalars size S	The absolute value of the y-width (in μm) of each rectangular box in a layer, ordered from the $-\Lambda_y/2$ side to the $\Lambda_y/2$ side.
x_centers	array of scalars size S	The absolute value of the x-center (in μm) of each rectangular box in a layer between $(-\Lambda_x/2, \Lambda_x/2)$, ordered from the $-\Lambda_x/2$ side to the $\Lambda_x/2$ side.
y_centers	array of scalars size S	The absolute value of the y-center (in μm) of each rectangular box in a layer between $(-\Lambda_y/2, \Lambda_y/2)$, ordered from the $-\Lambda_y/2$ side to the $\Lambda_y/2$ side.
f_x	array of scalars size S	The relative value of the x-width/fill factor (between 0 and 1) of each rectangular box in a layer, ordered from the $-\Lambda_x/2$ side to the $\Lambda_x/2$ side. "w_x" divided by the grating period Λ_x.
f_y	array of scalars size S	The relative value of the y-width/fill factor (between 0 and 1) of each rectangular box in a layer, ordered from the $-\Lambda_y/2$ side to the $\Lambda_y/2$ side. "w_y" divided by the grating period Λ_y.
xs	array of scalars size S	The relative shift of the x-center (between -0.5 to 0.5) of each rectangular box in a layer. "x_centers" divided by the grating period Λ_x.
ys	array of scalars size S	The relative shift of the y-center (between -0.5 to 0.5) of each rectangular box in a layer. "y_centers" divided by the grating period Λ_y.
radius	array of scalars of size S	The radius (in μm) of a circular cylindrical feature in the x-y plane
eps_x	array of scalars size S	The x-direction value of the permittivity tensor for each box or cylinder in a layer.
eps_y	array of scalars size S	The y-direction value of the permittivity tensor for each box or cylinder in a layer.
eps_z	array of scalars size S	The z-direction value of the permittivity tensor for each box or cylinder in a layer.
mu_x	array of scalars size S	The x-direction value of the permeability tensor for each box or cylinder in a layer.
mu_y	array of scalars size S	The y-direction value of the permeability tensor for each box or cylinder in a layer.
mu_z	array of scalars size S	The z-direction value of the permeability tensor for each box or cylinder in a layer.
sig_x	array of scalars size S	The x-direction value of the conductivity (absorption/gain parameter) tensor for each box or cylinder in a layer.
sig_y	array of scalars size S	The y-direction value of the conductivity (absorption/gain parameter) tensor for each box or cylinder in a layer.
sig_z	array of scalars size S	The z-direction value of the conductivity (absorption/gain parameter) tensor for each box or cylinder in a layer.

material	array of strings size S	String variable that names the material used in each geometric shape in a region. This string variable is used in calling a function that defines the permittivity, permeability, absorption/gain properties of a box or cylinder.
nonlinear	array of logical variables of size S	A logical variable that defines whether or not a particular electromagnetic/geometric feature possesses non-linearity. Material non-linearity in RCWA computations are modeled by an iterative harmonic balancing technique [156].

Before filling the above data structures, which is explained in the following sections, individual geometric shapes/electromagnetic materials that are independent of the nature of the transverse or longitudinal slicing performed are defined in the following array of "geometricshape" data structures of size regions, where each element of the array can be an array of size "number_of_features," having the following potential fields:

geometricshape		
left	scalar	Left-hand side (negative x-direction) boundary for a rectangular box, radial bend or annular bend feature.
right	scalar	Right-hand side (positive x-direction) boundary for a rectangular box, radial bend or annular bend feature.
front	scalar	Front side (negative z-direction) boundary for a rectangular box, radial bend, annular bend, or xy-cylinder feature.
back	scalar	Back side (positive z-direction) boundary for a rectangular box, radial bend, annular bend, or xy-cylinder feature.
top	scalar	Top side (positive y-direction) boundary for a rectangular box, radial bend, annular bend, or xz-cylinder feature.
bottom	scalar	Bottom side (negative y-direction) boundaries for a rectangular box, radial bend, annular bend, or xz-cylinder feature.
radius	scalar	Radius for a circular xy-cylinder, circular xz-cylinder, and 1^{st}-4^{th} quadrant radial bend or annular bend.
inner_radius	scalar	Inner radius for a circular 1^{st}-4^{th} quadrant annular bend.
outer_radius	scalar	Outer radius for a circular 1^{st}-4^{th} quadrant annular bend.
x_radius	scalar	X-direction major/minor radius for an elliptical cylinder
y_radius	scalar	Y-direction major/minor radius for an elliptical cylinder
z_radius	scalar	Z-direction major/minor radius for an elliptical cylinder

segments	scalar	Number of longitudinal segments used in approximating a continuously varying longitudinal geometry used in constructing geometric shapes for Geometric Bounding Toolbox computations.
x_center	scalar	X-location of the center for a rectangular box, radial bend, annular bend, or cylindrical feature.
y_center	scalar	Y-location of the center for a rectangular box, radial bend, annular bend, or cylindrical feature.
z_center	scalar	Z-location of the center for a rectangular box, radial bend, annular bend, or cylindrical feature.
left_bezier	1D-vector	A real-valued vector of scalar values used in defining the control points of a Bezier curve for a left hand side (negative x-direction) boundary.
right_bezier	1D-vector	A real-valued vector of scalar values used in defining the control points of a Bezier curve for a right hand side (positive x-direction) boundary.
top_bezier	1D-vector	A real-valued vector of scalar values used in defining the control points of a Bezier curve for a top side (positive y-direction) boundary.
bottom_bezier	1D-vector	A real-valued vector of scalar values used in defining the control points of a Bezier curve for a top side (positive y-direction) boundary.
intersectplane	1D-vector	A real-valued vector that defines an inequality for a hyperplane and half-space that will cut a previously defined structure which is defined in the form used for the Geometric Bounding Toolbox.
material	string	A string variable that defines the type of material utilized for a particular electromagnetic/geometric feature.
nonlinear	logical	A logical variable that defines whether or not a particular electromagnetic/geometric feature possesses non-linearity. Material nonlinearity in RCWA computations are modeled by an iterative field convergence/spatial grid technique [156].

E.2.1 Longitudinal Slicing Routines

Upon defining all of the "geometricshape" data structures that are located within a given "region," these geometric shapes must then be processed into a stair-cased set of lamellar layers whose material properties are longitudinally invariant within each layer. The method utilized to perform this processing can be arbitrarily generic and capable of handling any given continuous

or discrete structure, or can be made specific to take advantage of efficiencies that may be gained by exploiting particular structural symmetries or material variations.

For example, in a region containing continuously varying S-bend waveguide geometry, as shown in Figure E.2 (a), longitudinal slicing may consist of splitting the S-bend into a number of layers having equal thicknesses or a more specific algorithm that varies the thickness based on the longitudinal position of the S-bend interfaces at various transverse locations. For the dual grating coupler, the layer slicing performed within a longitudinal unit cell depended on the relative locations of the binary etching interfaces for both a superstrate and substrate grating within a longitudinal supercell period. Similarly, for a photonic crystal waveguide, shown in Figure D.2 (b), the elementary longitudinal unit cell of a region can be sliced into layers based on user defined layer thickness choices, or the layer thicknesses can be calculated based on the relative locations of the holes and a maximum/minimum layer thickness criterion. Depending on the nature of the structure geometry, this longitudinal layer slicing can be either completely decoupled from the required transverse layer slicing, as in the case of modeling butt coupled straight waveguide segments, weakly coupled to the required transverse layer slicing, as is the case for the dual grating structure, or strongly coupled to the required transverse layer slicing, as is the case for any continuously varying geometric shapes.

After performing all necessary longitudinal slicing within a given region, all of the layer thickness values are then compared to one another in an effort to find nearly identical layer thickness values. If two layers are found to have thickness values that are within the defined "geometric_tolerance," then these two layer thickness values are set equal to one another. This step is necessary for two reasons. First, the creation of scattering matrices requires both the properties of a layer's eigenmodes as well as a layer's thickness. If two layers were to have

exactly the same eigenmodes, but had slightly different thickness values (even on the order of machine precision), then they would have different scattering matrices. By setting equal two layer thickness values that are within the value of "geometric_tolerance," the total number of scattering matrices that must be calculated can be minimized. Second, by setting equal all layer thickness values that are within a value of "geometric_tolerance," then any longitudinal symmetry that is present in a given "region" elementary unit cell can be maintained. Doing so allows for the exploitation of symmetry that minimizes memory storage requirements for unit cell, region cell, and section cell scattering matrices. Upon completion of the longitudinal slicing routines, most of the longitudinally dependent variables within a "region" data structure are filled, including "region.unit_cells", "region.reg_cells", "region.slices", and "region.slice.d".

E.2.2 Transverse Slicing Routines

Once all of the longitudinal slicing routines have completed, the next step in pre-processing the geometric/material data is to fill the remainder of the fields of in the "region" data structure, including all of the fields in the "region.slice" data structure. Within any given slice the nature of fields to be filled depends on the type of diffraction/waveguiding problem to be solved (TE, TM, conical, two-dimensional) as discussed at the beginning of this section.

In the case of "twodimensional" diffraction problem where an "inverse" coupling coefficient expansion occurs, "TE," "TM," or "conical" problem, the routines for performing transverse slicing of geometric/material objects into rectangles involves first collecting the location of all transverse material interfaces from every "geometricshape" located within a layer and then testing the material values within any two interfaces against all of the "geometricshapes" in that layer. Here again, the use of the "geometric_tolerance" variable is

important due to the possibility of creating rectangles having transverse widths on the order of machine precision. In the case where a rectangle having a width on the order of machine precision is created, then this rectangle is eliminated from the set of rectangles within the layer. Furthermore, the widths of rectangles are tested for symmetry about the origin of the coordinate system. If the widths of two rectangles are found to be transversely symmetric within the value of "geometric_tolerance," then these two width values are set equal to one another. Similarly, if a central rectangle is suppose to be centered at the origin, but due to numerical round-off errors has been given a center value that is on the order of machine precision, then this center value is set to zero. Doing so maintains symmetry properties in the coupling coefficient expansion matrices to be defined later.

In the case of a "twodimensional" diffraction/waveguiding problem that involves a "regular" coupling coefficient expansion, the fields of the "region.slice" data structures and "region.slice.feature" data structures are filled using a variety of different methods. If a particular "geometricshape" is a cylinder or rectangle that is longitudinally invariant between multiple layers, then these fields are filled by copying values directly from the relevant "geometricshape" data structure into the appropriate field. If a particular "geometricshape" is a longitudinally varying object, then the necessary geometric processing routines are performed, be they Geometric Bounding Toolbox [173] routines or routines written by the present author. If geometric processing is necessary for these longitudinally varying "geometricshape" data structures, then once again the widths of all rectangles created are tested against the "geometric_tolerance" parameter and the location of any centrally located shapes are checked for a non-zero center location that is less than the value of "geometric_tolerance."

E.2.3 Layer comparison/Labeling system

Once all of the initial transversely and longitudinally dependent fields within a "region" data structure are filled, the next step in the geometric/material data pre-processing is to perform a comparison of every layer in the system to determine the total number of eigenmode problems that are to be solved. Every unique eigenmode problem is to be given a different label, which in this setting is called an "eigenlabel." By determining all of the layers that have the same "eigenlabel," the total number of eigenmode problems to be solved can be minimized, which is useful for maximizing the total problem's computational efficiency. The efficiency with which this layer comparison/labeling can be performed depends considerably upon the nature of a device's geometric/material layout, but can be performed in the most generic case by comparing every element of every data structure field, exclusive of the thickness field "d" of the "region(reg).slice(slc)" data structure, to every other element of that same array data structure. When the geometry/material distribution allows for the exploitation of known information compression, as in the case of the dual grating structure whose dual binary etching creates a distinct pattern, the assignment of these "eigenlabels" can be performed in a much more efficient manner. In this case, the "etched_layers_known" logical variable is set to be true and this variable acts as a switch statement to run a more efficient assignment function tailored to a specific device. Finally, a cell array variable is created, "eigenlabel," where each element of the cell is a vector that contains a value of "region.slice.eigenlabel," as well as the label for each associated "region" and "region.slice." The size of this array is equal to the total number of locations within the entire model at which field harmonic amplitudes will be calculated. The size of this array takes into account all values of "plotunitcells," "plotslices," and "internalslices" that are present in each "region."

After assigning all “eigenlabels”, a similar layer comparison routine is performed involving the thickness and “eigenlabel” of every layer in the system to assign each layer a “scatterlabel” value. Upon assigning all “scatterlabel” values, the collection of scatterlabels within every elementary unit cell in each “region” is used to assign unique “symunitscatterlabel” and “asymunitscatterlabel” values depending upon a unit cell’s longitudinal symmetry or asymmetry. These “symunitscatterlabel” and “asymunitscatterlabel” values are then used with each “region’s” number of “unit_cells” to determine unique “symregscatterlabel” and “asymregscatterlabel” values. Similarly, these “symregscatterlabel” and “asymregscatterlabel” values are combined with each “region’s” number of “reg_cells” to determine unique “symsectionscatterlabel” and “asymsectionscatterlabel” values. Upon completing the assignment of all scattering matrix labels, a cell array is created, “scatterlabel,” where each element of the cell contains two fields. The first field is the region and slice label of a layer that is associated with a particular value of “region.slice.scatterlabel” from 1 to “maxscatterlabel,” which is the maximum number of unique individual scattering matrices needed. Upon completing all “scatterlabel” assignments, the geometric pre-processing portion of the code is completed, and the “solver” portion of the code can begin.

E.3 Modal Solver and Scattering Matrix Assignment

In beginning the “solver” portion of the code, the first step is to determine the necessary tangential phase components for each periodic direction present in the system as well as longitudinal direction, layer eigenmodes. For uniform, homogeneous materials, the equations described in sections 2.3.1 and 3.1.1 can be utilized to determine both the tangential and longitudinal phase components. For inhomogeneous periodic layers, the process of determining

layer eigenmodes begins by determining material coupling coefficients, as described in Appendix C, for the spatial harmonic distributions described in Appendix B. These tangential phase expansions and material coupling coefficient expansions are then incorporated into the coupled wave modal expansions described in section 3.1, where any symmetries that are present are exploited as described in Appendix D. After solving for all of the eigenvectors and eigenvalues associated with each "region.eigenlabel" value from 1 to "maxeigenlabel," each of the individual layer scattering matrices are then calculated using the methods described in section 4.3.4, then each of the unit cell, region cell, and section cell scattering matrices to be created are calculated using the Redheffer star product operations defined in section 4.3.2. Finally, the scattering matrices needed to match the input and output halfspace regions to a standard vacuum, zero-thickness, homogeneous region are calculated using the single interface scattering matrix definitions from section 4.3.1.

E.4 Wave Propagation in Layered Media

After defining all single-layer, unit-cell, region-cell, section-cell, and input/output-interface scattering matrices, modeling of energy propagation through the entire system can be performed by choosing the desired input mode(s) and then piecing together scattering matrices to calculate the field harmonic amplitudes throughout the device model. The manner in which cascading of field harmonic amplitudes occurs has a profound effect on the efficiency of an eigenmode-expansion/S-Matrix code. Exploiting the ideas of domain decomposition and binary-based Redheffer star-product multiplication [19, 20] can greatly enhance the computational efficiency of the code, especially when dealing with longitudinally periodic devices or when piecing together sections having longitundal periodicities or symmetries with sections that do not

possess either of these properties. The basics of both the domain decomposition and binary-based multiplication have been explained elsewhere, but in the present implementation, the code is required to handle both of these aspects in a very generic fashion. This implementation requires that any given longitudinal unit cell can be either longitudinally symmetric or asymmetric and can contain an arbitrary number of layers. The idea of domain decomposition is utilized initially to break up a device model into separate "regions," as was shown in Figure E.1 and is shown more generically in Figure E.4 below.

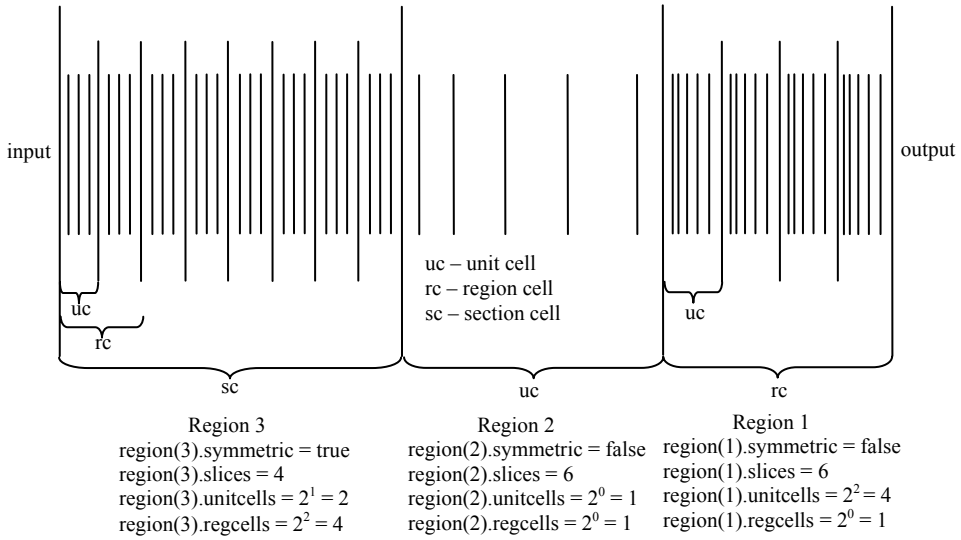

Figure E-4 A sketch showing the various means of domain decomposition utilized in the multilayer wave propagation/scattering matrix methods utilized in this study. The scattering matrix codes utilized in this study exploited multiple levels longitudinal periodicity, where conglomerates of both symmetric and asymmetric cells could be pieced together into a single structure as shown.

The field harmonic amplitudes are then calculated using equations 4.3.13 and 4.3.14 at the longitudinal boundaries of each region. Within each region, the field harmonic amplitudes are then calculated (optionally) at the boundaries of each section cell, taking advantage of binary based star-product multiplication if periodicity is present. Similarly, within each section cell, the

field harmonic amplitudes are calculated (optionally) at the longitudinal boundaries of each region cell, once again taking advantage of binary based star-product multiplication if periodicity is present. Then within each region cell, the same process is performed at the boundary of each unit cell. Once the field harmonics are calculated at the boundary of each longitudinal unit cell, the process can then continue (optionally) to calculate the field harmonic amplitudes at the boundary of each layer within the unit cell. At this point, even in the presence of a longitudinal unit cell, the process of calculating field harmonic amplitudes internal to a unit cell requires the use of left and right hand side scattering matrices that are asymmetric, and therefore do not have the memory storage advantages of scattering matrices for symmetric unit cells. Once the field harmonic amplitudes have been determined at the interfaces of every desired layer in the system, the process can then continue (optionally) to calculate field harmonic amplitudes internal to a periodic layer using the method described by equation 4.3.24. The option of whether or not to calculate field harmonic amplitudes at any of the interfaces described above within any or all regions is controlled by the "calculateFieldHarmonicAmplitudes," "calculateOnlyInputOutputFieldHarmonics," "plotunitcells," "plotslices," and "interalslices" parameters. The choice of how many total longitudinal interfaces are of interest has a very important effect on the overall computational efficiency of the code. In an effort to improve this efficiency, both the ideas of domain decomposition and binary-based star-product multiplication coulf be utilized to leverage the benefits of task parallelism in increasing computational efficiency in a multi-processor computational environment.

E.5 Processing the Field Harmonic Amplitudes/Calculating Fields and Power

Once all of the desired field harmonic amplitudes have been calculated at every layer desired in the device model, these field harmonic amplitude values can be used to determine both the modal reflection and transmission percentages in the input and output half-space regions as well as the field and power distributions throughout the entire multilayered system. Determining the field and power distributions requires the creation of a transverse spatial grid to be utilized for every longitudinal layer of interest. While there is no absolute requirement that this grid is the same for every layer, in the present case a single spatial grid is utilized for every layer. Calculating the electric and magnetic fields at a single longitudinal location requires the use of equations 3.1.1 and 4.3.14, if the location is a homogeneous zero-thickness layer, or equations 3.1.11 and 4.3.25, if the location is a heterogeneous periodic layer. In the presence of transverse symmetries, the exponential terms in equations 3.1.1 and 3.1.11 can be simplified into trigonometric expressions that operate on a reduced number of spatial harmonics, as described in Appendix B, as well as a reduced number of spatial grid points that exploit various mirror symmetric/anti-symmetric properties. Once the discretely sampled electric and magnetic field distributions are calculated, these sampled values can be combined using the Poynting theorem to determine the transverse and longitudinal power flow at every point on the spatial grid. In performing these computations in an interpreted language such as MATLAB®, the concept of "vectorization" of code increases the efficiency of these grid computations tremendously, whereas using loops to fill the grid in a code that is written directly in a compiled language like C, C++, or Fortran would be very efficient given proper nesting of the operations to be performed using each of the various spatial grid loops. As the code used in this study was

written entirely in MATLAB®, proper vectorization of the code, proper nesting of spatial grid loops, and minimization in loop usage were critical for computational efficiency.

E.6 Post-Processing of Calculated Fields and Power

After calculating the modal reflection/transmission values and field/power distributions there are a number of potential data post-processing issues that must be handled. The most obvious issue is visualization of the data. There is an entire sub-field of computer science devoted to computer graphics as well as software packages devoted exclusively to the visualization of numerical data, so a discussion of this field is not the present purpose. In this study, the graphics capabilities of MATLAB® are used for visualizing all of the data. The issues involved in visualizing the fields and power flow, especially for the dual grating coupler device, involved being able to simultaneously view the power flow magnitude and direction over the entire macro-scale of the device (using the "surf" function) while also having the ability to zoom-in on nano-scale variations in the field and power distributions and being able to overlay these values on a contour plot of the device's permittivity layout (using the "contour" function). The graphics capabilities of MATLAB® on the desktop handled these issues quite well, but due to the amount of memory required to calculate the field and power distributions as well as display the required graphics, these steps had to be performed in separate MATLAB® sessions on the one 32-bit processor with 4 GB of RAM that was available.

A second issue that was encountered post-field/power processing was the calculation and summation of power flow in and out of a defined box that was placed within the computational domain. Summation of the power on the input and output interfaces was a straightforward numerical integration that could be performed using Riemann integration on an equally spaced

spatial grid (due to the choice for the transverse spatial grid utilized), but for the two sides of the box along the longitudinal dimension, the grid was a non-uniformly spaced grid. For these two interfaces, a non-uniformly sampled trapezoidal rule numerical integration technique was utilized ("trapz" in MATLAB®). When the power around the box sums to nearly 100%, the computation then possessed conservation of energy to within sampling accuracy. This conservation of energy is a necessary, but not necessarily sufficient, condition for accuracy of the code. The accuracy of a given RCWA model could then be tested by repeating the computation with more spatial harmonic basis functions, and observing convergence in the power calculations or by testing the obtained values against other computational techniques (such as the eigenmode expansion method used in CAMFR [174], an FEM code, or an FDTD code).

A final post-field/power processing issue is the determination of the angular spectrum of the field diffracted from the dual grating coupler device, as discussed in section 8.2.5. Determination of this angular spectrum required the use of a discrete Fourier transform calculation on a non-regularly spaced spatial grid. In this case, the same non-uniformly spaced trapezoidal rule numerical integration technique was utilized for performing both the forward and inverse discrete Fourier transforms.

E.7 Integrating Variable Loops and Optimization Routines

Once the "solver" has been fine-tuned for best performance and all post-processing issues have been decided upon, the next step in structuring the computer aided design tool is to integrate all necessary variable loops into the code. While the most simplistic method of performing calculations over variable wavelengths, angles, polarizations, number of basis functions, geometric variables, and other parameters would be to wrap the entire code in the

loops for each individual variable, this method is also the most inefficient means of achieving the desired outcome. By placing the loops only around those sections of code that are immediately dependent upon a given variable, and extracting all sections of code that are not dependent upon a looped variable, the efficiency of the code can be optimized for spectral calculations over any desired variable. In cases where different sections of code may or may not be dependent upon a loop variable, given other problem parameters, then conditional statements must be added to the code to handle each possible case. An example of this scenario is the inclusion or exclusion of material dispersion properties within a looped wavelength, spectral calculation. If material dispersion is turned off, then the entire geometric processing section of the code can be placed outside of the variable wavelength loop, but if material dispersion is turned on, then the assignment of material properties to a given geometry should be placed within the wavelength loop. In either case, all elements of the "solver" are placed within the wavelength loop, and are repeated for every value of "lambda." The same types of issues can occur with every other variable over which a spectral parameter scan may be performed.

In order to handle collection of spectral data over a number of potentially different variable parameters, while hopefully avoiding the possibility of "code bloat" (i.e. a code whose number of lines grows unnecessarily long) as much as possible, a very convenient solution is to exploit methods of string processing. In MATLAB®, these methods make use of the "eval" and "run" commands to create new code at run-time. The "eval" function accepts string arguments whose contents are in the form of a function. The function contained in this string is then processed as a normal function. By building a string whose contents depend upon the variables over which one is looping, code that is very flexible and reusable in a variety of different situations can be written. The desired output variables could be grouped with iterator strings that

were dependent upon the particular variables over which loops were occurring. A similar argument applies to the use of the "run" command in MATLAB®. The "run" command accepts a string argument that specifies the absolute path to a particular ".m" script file. By making use of the "run" command, separate scripts for processing transversely dependent and longitudinally dependent geometric variables could be written for different devices, while keeping the main computational engine file unchanged. By allowing the user to create code at run-time, MATLAB®, and other scripting languages like Python, allow for the creation of very compact, flexible, and re-useable code. In both cases, the expensive parts of a code, in terms of memory requirements and more so for long run times, can be written in a lower level language, like C/C++ or Fortran, and then called by the scripting language. In such a case, the scripting language acts as the "glue" connecting all of the various parts of the computational workflow.

When all necessary variable loops have been integrated into the code, the task of optimizing either a single output variable value or optimizing the spectral response of a parameter scan can be performed by integrating the entire code with a desired numerical optimization routine. In doing so, similar issues must be considered to those involved in integrating variable loops. For a multi-parameter optimization problem, the optimization routine should be placed only around that section of code upon which the routine's inputs are dependent. By making various segments of code as orthogonal and flexible as possible, this integration can be as efficient and reusable as possible.

LIST OF REFERENCES

1. Maxwell, J.C., *A Treatise on Electricity and Magnetism*. 1873, Oxford: Clarendon.

2. Born, M. and E. Wolf, *Principals of Optics*. 1999, Cambridge: Cambridge University Press.

3. Gaskill, J.D., *Linear Systems, Fourier Transforms, and Optics*. 1978: John Wiley and Sons.

4. Smith, W.J., *Modern Optical Engineering, 3rd edition*. 2000, New York: McGraw-Hill.

5. Macleod, H.A., *Thin Film Optical Filters, 2nd ed.* 1986, New York: Macmillan Publishing Company.

6. Yariv, A. and P. Yeh, *Optical Waves in Crystals*. 1984: John Wiley and Sons.

7. Gaylord, T.K. and M.G. Moharam, *Analysis and applications of optical diffraction by gratings.* Proceedings of the IEEE, 1985. **73**(5): p. 894-937.

8. Debackere, P., et al., *Surface plasmon interferometer in silicon-on-insulator: novel concept for an integrated biosensor.* Optics Express, 2006. **14**(16): p. 7063-7072.

9. Lalanne, P. and E. Silberstein, *Fourier-modal method applied to waveguide computational problems.* Opt. Lett, 2000. **25**(15): p. 1092–1094.

10. Li, L., *Recent advances and present limitations of the electromagnetic theory of diffraction gratings.* Diffractive Optics and Micro-Optics, 2000: p. 2–4.

11. Moharam, M.G. and T.K. Gaylord, *Rigorous coupled-wave analysis of planar-grating diffraction.* J. Opt. Soc. Am, 1981. **71**(7): p. 811-818.

12. Moharam, M.G., et al., *Formulation for stable and efficient implementation of the rigorous coupled-wave analysis of binary gratings.* J. Opt. Soc. Am. A, 1995. **12**(5): p. 1068-1076.

13. Moharam, M.G., et al., *Stable implementation of the rigorous coupled-wave analysis for surface-relief gratings: enhanced transmittance matrix approach.* J. Opt. Soc. Am. A, 1995. **12**(5): p. 1077-1086.

14. Moharam, M.G. and T.K. Gaylord, *Rigorous coupled wave analysis of surface gratings with arbitrary profiles (A).* J. Opt. Soc. Am, 1981. **71**: p. 1573.

15. Moharam, M.G. and T.K. Gaylord, *Diffraction analysis of dielectric surface-relief gratings.* J. Opt. Soc. Am, 1982. **72**(10): p. 1385-1392.

16. Silberstein, E., et al., *Use of grating theories in integrated optics.* J. Opt. Soc. Am. A, 2001. **18**(11): p. 2865-2875.

17. Li, L., *Formulation and comparison of two recursive matrix algorithms for modeling layered diffraction gratings.* J. Opt. Soc. Am. A, 1996. **16**: p. 17.

18. Li, L., *Note on the S-matrix propagation algorithm.* Journal of the Optical Society of America A, 2003. **20**(4): p. 655-660.

19. Moharam, M.G. and A.B. Greenwell, *Efficient rigorous calculations of power flow in grating coupled surface-emitting devices.* Proceedings of SPIE, 2004. **5456**: p. 57.

20. Tervo, J., et al., *Efficient Bragg waveguide-grating analysis by quasi-rigorous approach based on Redheffer's star product.* Opt. Commun., 2001. **198**.

21. Rytov, S.M., *Electromagnetic properties of a finely stratified medium.* Sov. Phys. JETP, 1956. **2**(3): p. 466–475.

22. Cao, Q., P. Lalanne, and J.P. Hugonin, *Stable and efficient Bloch-mode computational method for one-dimensional grating waveguides.* J. Opt. Soc. Am. A, 2002. **19**(2): p. 335-338.

23. Peng, S.T., T. Tamir, and H.L. Bertoni, *Theory of periodic dielectric waveguides.* IEEE Trans. Microwave Theory Tech, 1975. **23**(1): p. 123–133.

24. Boyd, J.P., *Chebyshev and Fourier Spectral Methods*. 2001, Mineola, New York. 118-119.

25. Lalanne, P., *Improved formulation of the coupled-wave method for two-dimensional gratings.* J. Opt. Soc. Am. A, 1997. **14**: p. 1592–1598.

26. Lalanne, P. and G.M. Morris, *Highly improved convergence of the coupled-wave method for TM polarization.* J. Opt. Soc. Am. A, 1996. **13**(4): p. 779–784.

27. Li, L., *New formulation of the Fourier modal method for crossed surface-relief gratings.* J. Opt. Soc. Am. A, 1997. **14**(10): p. 2758-2767.

28. Li, L., *Reformulation of the Fourier modal method for surface-relief gratings made with anisotropic materials.* Journal of Modern Optics, 1998. **45**(7): p. 1313-1334.

29. Li, L., *Mathematical reflections on the Fourier modal method in grating theory.* Frontiers In Applied Mathematics, 2001: p. 111-139.

30. Li, L., *Convergence of electromagnetic field components across discontinuous permittivity profiles: comment.* Journal of the Optical Society of America A, 2002. **19**(7): p. 1443-1444.

31. Li, L., *Fourier modal method for crossed anisotropic gratings with arbitrary permittivity and permeability tensors.* Journal of Optics A: Pure and Applied Optics, 2003. **5**(4): p. 345-355.

32. Ho, K.M., C.T. Chan, and C.M. Soukoulis, *Existence of a photonic gap in periodic dielectric structures.* Physical Review Letters, 1990. **65**(25): p. 3152-3155.

33. Bai, B. and L. Li, *Reduction of computation time for crossed-grating problems: a group-theoretic approach.* Journal of the Optical Society of America A, 2004. **21**(10): p. 1886-1894.

34. Bai, B. and L. Li, *Group-theoretic approach to enhancing the Fourier modal method for crossed gratings with one or two reflection symmetries.* J. Opt. A: Pure Appl. Opt, 2005. **7**: p. 271-278.

35. Bai, B. and L. Li, *Group-theoretic approach to the enhancement of the Fourier modal method for crossed gratings: C2 symmetry case.* Journal of the Optical Society of America A, 2005. **22**(4): p. 654-661.

36. Okamoto, K., *Fundamentals of Optical Waveguides*. 2000: Academic Press.

37. Petit, R., ed. *Electromagnetic Theory of Gratings*. 1980, Springer-Verlag.

38. Kong, J.A., *Theory of Electromagnetic Waves*. 1975: John Wiley and Sons.

39. Moharam, M.G., *personal communication*.

40. Smith, R.E., S.N. Houde-Walter, and G.W. Forbes, *Mode determination for planar waveguide using the four-sheeted dispersion relation.* Quantum Electronics, IEEE Journal of, 1992. **28**(6): p. 1520-1526.

41. Anemogiannis, E., E.N. Glytsis, and T.K. Gaylord, *Efficient solution of eigenvalue equations of optical waveguidingstructures.* Lightwave Technology, Journal of, 1994. **12**(12): p. 2080-2084.

42. Press, W.H., et al., *Bracketing and Bisection*, in *Numerical Recipies in C++* 2002, Cambridge University Press: Cambridge, U.K. p. 354-358.

43. Li, L., *A Modal Analysis of Lamellar Diffraction Gratings in Conical Mountings.* Journal of Modern Optics, 1993. **40**(4): p. 553-573.

44. Li, L., *Multilayer modal method for diffraction gratings of arbitrary profile, depth, and permittivity.* J. Opt. Soc. Am. A, 1993. **10**(12): p. 2581-2591.

45. Neviere, M., *The homogeneous problem*, in *Electromagnetic Theory of Gratings*, R. Petit, Editor. 1980, Springer-Verlag: Berlin.

46. Wood, R.W., *On a Remarkable Case of Uneven Distribution of Light in a Diffraction Grating Spectrum.* Proceedings of the Physical Society of London, 1902. **18**(1): p. 269-275.

47. Rayleigh, L., *Note on the remarkable case of diffraction spectra described by Prof. Wood.* Philos. Mag, 1907. **14**: p. 60–65.

48. Rayleigh, L., *On the Dynamical Theory of Gratings.* Proceedings of the Royal Society of London. Series A, Containing Papers of a Mathematical and Physical Character, 1907. **79**(532): p. 399-416.

49. Evans, L.C., *Partial Differential Equations*. 2000: American Mathematical Society.

50. Strauss, W.A., *Partial Differential Equations: An Introduction*. 1992: John Wiley and Sons.

51. Harari, I., I. Patlashenko, and D. Givoli, *Dirichlet-to-Neumann Maps for Unbounded Wave Guides.* Journal of Computational Physics, 1998. **143**(1): p. 200-223.

52. Huang, Y. and Y. Lu, *Scattering From Periodic Arrays of Cylinders by Dirichlet-to-Neumann Maps.* Journal of lightwave technology, 2006. **24**(9): p. 3448-3453.

53. Schadle, A. and L. Zschiedrich, *Additive Schwarz method for scattering problems using the PML method at interfaces.* ser. Lecture Notes in Computational Science and Engineering, 16th International Conference on Domain Decomposition Methods. Springer, 2005.

54. Bienstman, P., *Rigorous and efficient modeling of wavelength scale photonic components*, in *Dept. of Information Technology*. 2001, University of Gent: Ghent, Belgium.

55. Lee, S.L., Y. Chung, and L. Coldren, *On leaky mode approximations for modal expansion in multilayer open waveguides.* IEEE Journal of Quantum Electronics, 1995. **31**(10): p. 1790-1802.

56. Oliner, A.A., et al., *Guidance and Leakage Properties of a Class of Open Dielectric Waveguides: Part II--New Physical Effects.* Microwave Theory and Techniques, IEEE Transactions on, 1981. **29**(9): p. 855-869.

57. Chen, C.M. and K. Zaki, *Resonant frequencies of dielectric resonators containing guided complex modes.* IEEE Transactions on Microwave Theory and Techniques, 1988. **36**(10): p. 1455-1457.

58. Snyder, A. and J. Love, *Optical Waveguide Theory*. 1983, London: Chapman and Hall.

59. Press, W.H., et al., *Root Finding and Nonlinear Sets of Equations*, in *Numerical Recipes in C++*. 2002, Cambridge University Press.

60. Gaylord, T.K., W.E. Baird, and M.G. Moharam, *Dielectric surface-relief gratings.* Appl. Opt, 1986. **25**(24/15).

61. Li, L. and C.W. Haggans, *Convergence of the coupled-wave method for metallic lamellar diffraction gratings.* Journal of the Optical Society of America. A, Optics and image science, 1993. **10**(6): p. 1184-1189.

62. Moharam, M.G. and T.K. Gaylord, *Three-dimensional vector coupled-wave analysis of planar-grating diffraction.* Optical Society of America, Journal, 1983. **73**: p. 1105-1112.

63. Moharam, M.G. and T.K. Gaylord, *Diffraction of finite beams by dielectric gratings (A).* J. Opt. Soc. Am, 1983.

64. Moharam, M.G. and T.K. Gaylord, *Rigorous coupled-wave analysis of metallic surface-relief gratings.* Optical Society of America, Journal, A: Optics and Image Science, 1986. **3**: p. 1780-1787.

65. Berenger, J.P., *A perfectly matched layer for the absorption of electromagnetic waves.* J. Comput. Phys., 1994. **114**: p. 185-200.

66. Sacks, Z.S., et al., *A perfectly matched anisotropic absorber for use as an absorbing boundary condition.* IEEE Trans. Antennas Propagat., 1995. **43**: p. 1460-1463.

67. Joannopoulos, J.D., R.D. Meade, and J.N. Winn, *Photonic Crystals: Molding the Flow of Light*. 1995, Princeton, New Jersey: Princeton University Press.

68. Joannopoulos, J.D., P.R. Villeneuve, and S. Fan, *Photonic crystals: putting a new twist on light.* Nature, 1997. **386**: p. 143-149.

69. Johnson, S.G. and J.D. Joannopoulos, *Photonic Crystals: The Road from Theory to Practice*. 2002: Kluwer Academic Pub.

70. Kittel, C., *Introduction to solid state physics*. 1971: Wiley New York.

71. Shi, S., C. Chen, and D.W. Prather, *Plane-wave expansion method for calculating band structure of photonic crystal slabs with perfectly matched layers.* Journal of the Optical Society of America A, 2004. **21**(9): p. 1769-1775.

72. Hugonin, J.P., et al., *Fourier modal methods for modeling optical dielectric waveguides.* Optical and Quantum Electronics, 2005. **37**(1): p. 107-119.

73. Hugonin, J.P. and P. Lalanne, *Perfectly matched layers as nonlinear coordinate transforms: a generalized formalization.* Journal of the Optical Society of America A, 2005. **22**(9): p. 1844-1849.

74. Holland, R., *THREDE- A free-field EMP coupling and scattering code(electromagnetic scattering from aircraft).* IEEE Transactions on Nuclear Science, 1977. **24**: p. 2416-2421.

75. Merewether, D.E., *Transient currents induced on a metallic body of revolution by an electromagnetic pulse(Thin metallic body of revolution under electromagnetic pulse, predicting transient induced currents with radiation condition in finite difference solution).* IEEE Transactions on Electromagnetic Compatibility, 1971. **13**: p. 41-44.

76. Holland, R. and J.W. Williams, *Total-field versus scattered-field finite-difference codes: A comparative assessment.* IEEE Trans. Nucl. Sci, 1983. **30**(6): p. 4583–4588.

77. Mur, G., *Absorbing boundary conditions for the finite-difference approximation of the time-domain electromagnetic-field equations.* IEEE Trans. Electromagn. Compat, 1981. **23**(4): p. 377–382.

78. Talfove, A., *Computational Electrodynamics*. 1995, Norwood, MA: Artech House.

79. Chew, W., J. Jin, and E. Michielssen, *Complex Coordinat Stretching as a Generalized Absorbing Boundary Condition.* IEEE Trans. Geosci. Remote Sensing, 1990. **28**: p. 207-214.

80. Chew, W.C., J.M. Jin, and E. Michielssen, *Complex coordinate system as a generalized absorbing boundarycondition.* Antennas and Propagation Society International Symposium, 1997. IEEE., 1997 Digest, 1997. **3**.

81. Yuan, J. and Y.Y. Lu, *Photonic Bandgap Calculations Using Dirichlet-to-Neumann Maps.* J. Comput. Phys, 1997. **136**: p. 585-598.

82. Tan, E.L., *Note on formulation of the enhanced scattering-(transmittance-) matrix approach.* Journal of the Optical Society of America A, 2002. **19**(6): p. 1157-1161.

83. Cotter, N.P.K., T.W. Preist, and J.R. Sambles, *Scattering-matrix approach to multilayer diffraction.* J. Opt. Soc. Am. A, 1995. **12**(5): p. 1097-1103.

84. Tan, E.L., *Enhanced R-matrix algorithms for multilayered diffraction gratings.* Applied Optics, 2006. **45**(20): p. 4803-4809.

85. Gralak, B., S. Enoch, and G. Tayeb, *From scattering or impedance matrices to Bloch modes of photonic crystals.* Journal of the Optical Society of America A, 2002. **19**(8): p. 1547-1554.

86. Li, L., *Bremmer series, R-matrix propagation algorithm, and numerical modeling of diffraction gratings.* J. Opt. Soc. Am. A, 1994. **11**: p. 2829–2836.

87. Tan, E.L., *Hybrid-matrix algorithm for rigorous coupled-wave analysis of multilayered diffraction gratings.* Journal of Modern Optics, 2006. **53**(4): p. 417-428.

88. Frolik, J.L. and A.E. Yagle, *Forward and inverse scattering for discrete layered lossy and absorbing media.* Circuits and Systems II: Analog and Digital Signal Processing, IEEE Transactions on [see also Circuits and Systems II: Express Briefs, IEEE Transactions on], 1997. **44**(9): p. 710-722.

89. Redheffer, R., *Inequalities for a matrix Riccati equation.* J. Math. Mech, 1959. **8**: p. 349-367.

90. Redheffer, R., *The Mycielski-Paszkowski diffusion problem.* J. Math. Mech, 1960. **9**: p. 607-621.

91. Haskell, N.A., *The dispersion of surface waves on multilayered media.* Bull. Seism. Soc. Am, 1953. **43**(1): p. 17-34.

92. Kennett, B.L.N., *Reflections, rays, and reverberations.* Bulletin of the Seismological Society of America, 1974. **64**(6): p. 1685.

93. Kennett, B.L.N., *Seismic Wave Propagation in Stratified Media*. 1983: Cambridge University Press New York.

94. Kennett, B.L.N. and N.J. Kerry, *Seismic waves in a stratified half space.* Geophys. JR Astr. Soc, 1979. **57**(3): p. 557-583.

95. Saastamoinen, P.R., *On propagators and scatterers in wave problems of layered, elastic media--A spectral approach.* Bulletin of the Seismological Society of America, 1980. **70**(4): p. 1125.

96. Stovas, A. and B. Ursin, *Reflection and transmission responses of layered transversely isotropic viscoelastic media.* Geophysical Prospecting, 2003. **51**(5): p. 447-477.

97. Ursin, B., *Review of elastic and electromagnetic wave propagation in horizontally layered media.* Geophysics, 1983. **48**(8): p. 1063-1081.

98. Ursin, B. and K.A. Berteussen, *Comparison of some inverse methods for wave propagation in layered media.* Proceedings of the IEEE, 1986. **74**(3): p. 389-400.

99. Altman, C. and H. Cory, *The generalized thin-film optical method in electromagnetic wave propagation.* Radio Science, 1969. **4**.

100. Griffiths, D.J., *Introduction to quantum mechanics*. 1995, Upper Saddle River, NJ: Prentice Hall.

101. Ding, Y. and R. Magnusson, *Resonant leaky-mode spectral-band engineering and device applications.* Optics Express, 2004. **12**(23): p. 5661-5674.

102. Magnusson, R. and S.S. Wang, *New principle for optical filters.* Applied Physics Letters, 1992. **61**(9): p. 1022-1024.

103. Andrewartha, J.R., J.R. Fox, and I.J. Wilson, *Resonance Anomalies in the Lamellar Grating.* Journal of Modern Optics, 1979. **26**(1): p. 69-89.

104. Andrewartha, J.R., J.R. Fox, and I.J. Wilson, *Further Properties of Lamellar Grating Resonance Anomalies.* Journal of Modern Optics, 1979. **26**(2): p. 197-209.

105. Mashev, L. and E. Popov, *Zero order anomaly of dielectric coated gratings.* Optics Communications, 1985. **55**(6): p. 377-380.

106. Neviere, M., D. Maystre, and P. Vincent, *Application du calcul des modes de propagation a letude theorique des anomalies des reseaux recouverts de dielectrique.* J. Opt. Paris, 1977. **8**: p. 231–242.

107. Popov, E. and B. Bozhkov, *Corrugated waveguides as resonance optical filters-advantages and limitations.* Journal of the Optical Society of America A, 2001. **18**(7): p. 1758-1764.

108. Shin, D.H., et al., *Thin-film multilayer optical filters containing diffractive elements and waveguides.* Proceedings of SPIE, 1997. **3133**: p. 273.

109. Suratteau, J.Y., M. Cadilhac, and R. Petit, *'Sur la détermination numérique des efficacités de certains réseaux diélectriques profonds.* J. Opt.(Paris), 1983. **14**: p. 273-288.

110. Wang, S.S. and R. Magnusson, *Theory and applications of guided-mode resonance filters.* Applied Optics, 1993. **32**(14): p. 2606-2613.

111. Wang, S.S., et al., *Guided-mode resonances in planar dielectric-layer diffraction gratings.* J. Opt. Soc. Am. A, 1990. **7**(8): p. 1470.

112. Magnusson, R. and S.S. Wang, *Transmission bandpass guided-mode resonance filters.* Appl. Opt, 1995. **34**(35): p. 8106–8109.

113. Wang, S.S. and R. Magnusson, *Multilayer waveguide-grating filters.* Appl. Opt, 1995. **34**: p. 2414–2420.

114. Thurman, S.T. and G.M. Morris, *Controlling the spectral response in guided-mode resonance filter design.* Applied Optics, 2003. **42**(16): p. 3225-3233.

115. Liu, Z.S. and R. Magnusson, *Concept of Multiorder Multimode Resonant Optical Filters.* IEEE Photonics Technology Letters, 2002. **14**(8): p. 1091.

116. Tibuleac, S. and R. Magnusson, *Reflection and transmission guided-mode resonance filters.* J. Opt. Soc. Am. A, 1997. **14**: p. 1617–1626.

117. Jacob, D., *Dielectric Resonant Grating Structures For Narrow-band Filtering Applications*, in *School of Optics/CREOL*. 2001, University of Central Florida: Orlando.

118. Fano, U., *The Theory of Intensity Anomalies of Bending (in German).* Ann. Phys., 1938. **32**.

119. Fano, U., *The theory of anomalous diffraction gratings and of quasi-stationary waves on metallic surfaces (Sommerfeld's waves).* J. Opt. Soc. Am, 1941. **31**: p. 213–222.

120. Hessel, A. and A.A. Oliner, *A new theory of Wood's anomalies on optical gratings.* Appl. Opt, 1965. **4**(10): p. 1275.

121. Neviere, M., R. Petit, and M. Cadilhac, *About the theory of optical grating coupler-waveguide systems.* Optics Communications, 1973. **8**(2): p. 113-117.

122. Jacob, D., S. Dunn, and M.G. Moharam, *Normally incident resonant grating reflection filters for efficient narrowband spectral filtering of finite beams.* J. Opt. Soc. Am. A, 2001. **18**: p. 2109-2120.

123. Jacob, D.K., S.C. Dunn, and M.G. Moharam, *Resonant grating reflection filters for normally incident Gaussian beams.* Diffractive Optics and Micro-Optics, 2000: p. 23–25.

124. Jacob, D.K., S.C. Dunn, and M.G. Moharam, *Design considerations for narrow-band dielectric resonant grating reflection filters of finite length.* Journal of the Optical Society of America A, 2000. **17**(7): p. 1241-1249.

125. Lemarchand, F., *Etude et realisation de reseaux de diffraction pour le filtrage optique bande etroite*. 1999, Ecole Nationale Superieure de Physique de Marseille: Marseille, France.

126. Lemarchand, F., et al., *Study of the resonant behavior of waveguide gratings: increasing the angular tolerance of guided-mode filters.* J. Opt. A.: Pure and Appl. Opt., 1999. **1**: p. 545-551.

127. Sentenac, A. and A.L. Fehrembach, *Angular tolerant resonant grating filters under oblique incidence.* J. Opt. Soc. Am. A, 2005. **22**: p. 475-480.

128. Brundett, D.L., E.N. Glytsis, and T.K. Gaylord, *Normal-incidence guided-mode resonant grating filters: design and experimental demonstration.* Opt. Lett, 1998. **23**: p. 700-702.

129. Kikuta, H., H. Yoshida, and K. Iwata, *Ability and Limitation of Effective Medium Theory for Subwavelength Gratings.* Optical Review, 1995. **2**(2): p. 92-99.

130. Lalanne, P. and D. Lemercier-Lalanne, *Depth dependence of the effective properties of subwavelength gratings.* J. Opt. Soc. Am. A, 1997. **14**(2): p. 450–458.

131. Boonruang, S., A. Greenwell, and M.G. Moharam, *Multiline two-dimensional guided-mode resonant filters.* Applied Optics, 2006. **45**(22): p. 5740-5747.

132. Sauvan, C., et al., *Accurate modeling of line-defect photonic crystal waveguides.* Photonics Technology Letters, IEEE, 2003. **15**(9): p. 1243-1245.

133. Magnusson, R., et al., *Photonic devices enabled by waveguide-mode resonance effects in periodically modulated films.* Proc. SPIE, 2003. **5225**: p. 20-34.

134. Stenzel, O., *Resonant reflection and absorption in grating waveguide structures (Invited Paper)[5355-01].* Proceedings-SPIE The International Society for Optical Engineering, 2004. **5355**: p. 1-13.

135. Shin, D., et al., *Thin-film optical filters with diffractive elements and waveguides.* Optical Engineering (Bellingham, Washington), 1998. **37**(9): p. 2634-2646.

136. Bieber, A. and T. Brown, *Coupling anomalies in SimGen/Si/SiO2 waveguide systems.* Optics Express, 2002. **10**(20): p. 1139-1144.

137. Costa, R., A. Melloni, and M. Martinelli, *Bandpass resonant filters in photonic-crystal waveguides.* Photonics Technology Letters, IEEE, 2003. **15**(3): p. 401-403.

138. Lalanne, P., *Electromagnetic analysis of photonic crystal waveguides operatingabove the light cone.* Quantum Electronics, IEEE Journal of, 2002. **38**(7): p. 800-804.

139. Lalanne, P. and H. Benisty, *Out-of-plane losses of two-dimensional photonic crystals waveguides: Electromagnetic analysis.* Journal of Applied Physics, 2001. **89**(2): p. 1512-1514.

140. Lalanne, P. and A. Talneau, *Modal conversion with artificial materials for photonic-crystal waveguides.* Optics Express, 2002. **10**(8): p. 354-359.

141. Palamaru, M. and P. Lalanne, *Photonic crystal waveguides: Out-of-plane losses and adiabatic modal conversion.* Applied Physics Letters, 2001. **78**(11): p. 1466.

142. Tokushima, M., et al., *Lightwave propagation through a 120° sharply bent single-line-defect photonic crystal waveguide.* Applied Physics Letters, 2000. **76**(8): p. 952-954.

143. Grann, E.B., *Subwavelength Grating Structures for Artifiicial Media Applications*, in *School of Optics/CREOL*. 1995, University of Central Florida: Orlando.

144. Grann, E.B., M.G. Moharam, and D.A. Pommet, *Artificial uniaxial and biaxial dielectrics with use of two-dimensional subwavelength binary gratings.* J. Opt. Soc. Am. A, 1994. **11**(10): p. 2695-2703.

145. Grann, E.B. and J. David N. Sitter, *Integrated Narrowband Optical Filter Based on Embedded Subwavelength Resonant Grating Structures*. 2000, Lockheed Martin Energy Research Corporation: USA.

146. Tamir, T., ed. *Integrated Optics*. Topics in Applied Physics. Vol. 7. 1975, Springer-Verlag: New York.

147. Almeida, V.R., R.R. Panepucci, and M. Lipson, *Nanotaper for compact mode conversion.* Optics Letters, 2003. **28**(15): p. 1302-1304.

148. Felici, T.P. and D.F.G. Gallagher, *Improved waveguide structures derived from new rapid optimization techniques.* Proceedings of SPIE, 2003. **4986**: p. 375-385.

149. O'Daniel, J.K., et al., *Integrated wavelength stabilization of in-plane semiconductor lasers by use of a dual-grating reflector.* Optics Letters, 2006. **31**(2): p. 211-213.

150. Vaissie, L., et al., *High Efficiency Surface-Emitting Laser With Subwavelength Antireflection Structure.* Photonics Technology Letters, IEEE, 2005. **17**(4): p. 732-734.

151. Luyssaert, B., et al., *Efficient nonadiabatic planar waveguide tapers.* Journal of Lightwave Technology 2005. **23**(8): p. 2462-2468.

152. Johnson, E.G., et al., *Micro- and Nano-Optics in Surface Emitting Lasers*, in *Nanophotonics*. 2006, OSA: Uncasville, CT, USA.

153. Nakagawa, W. and Y. Fainman, *Tunable optical nanocavity based on modulation of near-field coupling between subwavelength periodic nanostructures.* Selected Topics in Quantum Electronics, IEEE Journal of, 2004. **10**(3): p. 478-483.

154. Dong, P. and A.G. Kirk, *Compact double-grating coupler between vertically stacked silicon-on-insulator waveguides.* Applied Optics, 2005. **44**(35): p. 7540-7547.

155. Lalanne, P. and J.P. Hugonin, *Bloch-wave engineering for high-Q, small-V microcavities.* Quantum Electronics, IEEE Journal of, 2003. **39**(11): p. 1430-1438.

156. Maes, B., P. Bienstman, and R. Baets, *Modeling of Kerr nonlinear photonic components with mode expansion.* Optical and Quantum Electronics, 2004. **36**(1): p. 15-24.

157. Neviere, M., E. Popov, and R. Reinisch, *Electromagnetic resonances in linear and nonlinear optics: phenomenological study of grating behavior through the poles and zeros of the scattering operator.* J. Opt. Soc. Am. A, 1995. **12**(3): p. 513–523.

158. Veronis, G., et al., *Coupled optical and electronic simulations of electrically pumped photonic-crystal-based light-emitting diodes.* Journal of Applied Physics, 2005. **97**(4): p. 44503-44503.

159. Chen, H.C., *Theory of Electromagnetic Waves: A Coordinate Free Approach*. 1983: McGraw-Hill.

160. Griffiths, D.J., *Introduction to Electrodynamics*. 1999: Prentice Hall.

161. Harrington, R.F., *Time-harmonic electromagnetic fields*. 1961: McGraw-Hill New York.

162. Boyd, J.P., *Chebyshev and Fourier Spectral Methods, 2nd edition (revised)*. 2001, Mineola, New York: Dover.

163. Li, L., *Use of Fourier series in the analysis of discontinuous periodic structures.* J. Opt. Soc. Am. A, 1996. **13**(1870): p. 1876.

164. Peng, S. and G.M. Morris, *Resonant scattering from two-dimensional gratings.* J. Opt. Soc. Am. A, 1996. **13**(5): p. 993.

165. Popov, E., M. Neviere, and N. Bonod, *Factorization of products of discontinuous functions applied to Fourier-Bessel basis.* Journal of the Optical Society of America A, 2004. **21**(1): p. 46-52.

166. Sauvan, C.H., P. Lalanne, and J.P. Hugonin, *Truncation rules for modelling discontinuities with Galerkin method in electromagnetic theory.* Optical and Quantum Electronics, 2004. **36**(1): p. 271-284.

167. Popov, E., *Light diffraction by relief gratings: a microscopic and macroscopic view*, in *Progress in Optics*, E. Wolf, Editor. 1993, Elsevier: Amsterdam. p. 139-187.

168. Popov, E. and M. Neviere, *Grating theory: new equations in Fourier space leading to fast converging results for TM polarization.* Journal of the Optical Society of America A, 2000. **17**(10): p. 1773-1784.

169. Popov, E. and M. Nevière, *Maxwell equations in Fourier space: fast-converging formulation for diffraction by arbitrary shaped, periodic, anisotropic media.* Journal of the Optical Society of America A, 2001. **18**(11): p. 2886-2894.

170. Papoulis, A., *Systems and Transforms with Applications in Optics*. 1968: McGraw-Hill.

171. Zhou, C. and L. Li, *Formulation of the Fourier modal method for symmetric crossed gratings in symmetric mountings.* Journal of Optics A: Pure and Applied Optics, 2004. **6**(1): p. 43-50.

172. *MATLAB (R) Central File Exchange*. [cited; Available from: http://www.mathworks.com/matlabcentral/.

173. *Geometric Bounding Toolbox*. [cited; Available from: http://www.sysbrain.com.

174. *CAMFR*. [cited; Available from: http://camfr.sourceforge.net/.